

Low Salinity Waterflooding: Effect of Fines Migration and Ion Type on Oil Recovery



Abdullah Al-Sarihi, BEng. (Hons), MEngSc.

Australian School of Petroleum and Energy Resources
Faculty of Engineering, Computer & Mathematical Sciences
The University of Adelaide

A thesis submitted for the degree of
Doctor of Philosophy (PhD)

October 2019

*To Brenda Vargas Murillo,
thank you for being in my life.*

Table of Contents

Abstract.....	i
Declaration.....	iv
Acknowledgements.....	v
Thesis by Publication.....	vii
1 Contextual Statement.....	1
1.1 Research Background.....	1
1.2 Research Objectives.....	4
1.3 Thesis Structure.....	5
1.4 How The Publications Are Related to The Thesis.....	8
1.5 References:.....	11
2 Literature Review.....	13
2.1 Introductory Background.....	13
2.2 Low Salinity Waterflooding in Sandstone.....	13
2.2.1 Properties of Water, Oil and Rock.....	13
2.3 Mechanisms of low salinity waterflooding.....	20
2.3.1 Ionic Exchange.....	20
2.3.2 pH Increase.....	21
2.3.3 Double Layer Expansion.....	22
2.3.4 Fines Migration.....	23
2.3.5 Osmosis.....	25
2.3.6 Salting-in.....	27
2.4 Low Salinity Waterflooding in Carbonates:.....	29
2.4.1 Surface Charge and Oil Adhesion.....	29
2.4.2 Ionic Exchange.....	30
2.4.3 Double Layer Expansion.....	33
2.4.4 Anhydrite Dissolution.....	34
2.5 Low Salinity Water Coreflooding.....	35
2.6 Conclusion of the Literature Review.....	37
2.7 References.....	39
3 Admissible Parameters For Two-Phase Coreflood And Welge-JBN Method.....	43
3.1 Admissible Parameters For Two-Phase Coreflood And Welge-JBN Method.....	44
3.2 Coreflood Planning Criteria For Relative Permeability Computation by Welge-JBN Method.....	88
4 Effects of Fines Migration on Enhanced Oil Recovery.....	96
4.1 Effects of Fines Migration on Residual Oil During Low-Salinity Waterflooding.....	97
4.2 Low-salinity Waterflooding in Non-Polar Oil.....	114
5 Fines Stabilisation by Ca Ions And Its Effect on LSW Injection.....	120
5.1 Fines Stabilisation by Ca Ions And Its Effect On LSW Injection.....	121
6 Conclusions and Recommendations.....	136
Appendix.....	140
Fines Migration as an EOR Method During Low Salinity waterflooding.....	140

Abstract

This is a PhD thesis by publication that includes six published papers, five of which are journal papers and one is a full manuscript conference paper. The goal of this thesis is to investigate the effect of low salinity waterflooding (LSW) and salt ion type on enhancing oil recovery, which is implemented to select LSW reservoir candidates for a Wintershall Holding project. In addition, another aim of this thesis is to design a set of criteria to plan two-phase corefloods to accurately determine relative permeability by using Welge-JBN method.

Low salinity water injection in oil fields has gained wide interest in the literature over the last two decades due to the fact that it is a cost-effective enhanced oil recovery technology. However, not only the mechanisms of LSW are not clearly understood, but there is some controversy around some LSW phenomena, especially fines migration, which is deemed to have the detrimental impact of formation damage in oil and gas reservoirs. This thesis focuses on the fines-migration mechanism of LSW and shows that it can be utilised to produce incremental oil using the induced formation damage in the reservoir.

This study shows that micro-scale sweep efficiency is improved during low salinity waterflooding by flux diversion, that is caused by fines detachment and migration. Initially, clay particles are attached to the rock surface by electrostatic forces caused by the initial high-salinity formation water that saturates the rock. In this work, it is shown that injecting low salinity brine into the rock causes clay particles to be detached due to the weakening of electrostatic forces. As a result, fines migration results in blockage of high permeability water channels during high salinity water injection and diversion of the water flux to thin pores where residual oil is trapped. The results indicate that residual oil saturation was

decreased by 5-18% in multiple low salinity coreflooding experiments with different salinity concentrations.

Another part of this study investigates the effect of brine ion type on fines migration and oil recovery during LSW. It is demonstrated that having divalent ions such as calcium in the initial formation water, and the water injected into the porous media (including LSW), aids to stabilise fines due to the strong affinity and adsorption of such ions on the clay and rock surface. Deionised water injection confirms this, as hydrogen ions cannot exchange with calcium ions. This is confirmed by the fact that there are no clay particles in the effluent solution, no rise in pressure drop across the samples, and no detection of desorbed calcium ions in the Ion Chromatography results.

Injection of low salinity sodium chloride solution, followed by deionised water flooding, induced desorption of the calcium ions, which then enabled clay particles to detach as a result of the weak electrostatic forces between clay and rock surface, that is caused by the sodium. This is important as it can be applied in controlling formation damage programs and preventing injectivity/production issues in oil and gas wells. Furthermore, enhanced oil recovery can also be achieved as proven by the incremental oil production observed when fines migration takes place in the two-phase flow tests due to the improved micro-scale sweep efficiency as explained above in the first part of the thesis.

Moreover, a new set of criteria for coreflooding parameters to model relative permeability, for the experimental tests performed in this study, is introduced in this thesis and can, also, be applied in any two-phase flow experiments. These criteria are essential as they are needed for valid determination of relative permeability by the Welge-JBN method. They fulfil the assumption of low capillary-viscous ratio to achieve a large-scale approximation

by optimising the core length and displacement rate. The numerical simulation results demonstrate that this ratio should not exceed 0.5 for the model to have valid relative permeability calculations by the Welge-JBN technique. The criteria include capillary number, precision of water-cut measurement, sampling period, and pressure measurement accuracy, which are critical to plan any coreflood tests to achieve accurate results.

Declaration

I certify that this work contains no material which has been accepted for the award of any other degree or diploma in my name, in any university or other tertiary institution and, to the best of my knowledge and belief, contains no material previously published or written by another person, except where due reference has been made in the text. In addition, I certify that no part of this work will, in the future, be used in a submission in my name, for any other degree or diploma in any university or other tertiary institution without the prior approval of the University of Adelaide and where applicable, any partner institution responsible for the joint-award of this degree.

I acknowledge that copyright of published works contained within this thesis resides with the copyright holder(s) of those works.

I also give permission for the digital version of my thesis to be made available on the web, via the University's digital research repository, the Library Search and also through web search engines, unless permission has been granted by the University to restrict access for a period of time.

I acknowledge the support I have received for my research through the provision of an Australian Government Research Training Program Scholarship.

Abdullah Al-Sarihi

Acknowledgements

Reaching this stage of finishing my PhD was definitely not done singlehandedly. First and foremost, I would like to thank my family for their patience and support during my studies. Thank you for your love and encouragement, I owe you a lot.

I would like to thank my supervisors Dr. Abbas Zeinijahromi and Prof. Pavel Bedrikovetsky for their constant support, guidance, and encouragement throughout my PhD studies. I would have never been able to accomplish this milestone without your assistance. I learnt a lot from you. I would also like to thank my co-supervisor Dr. Sara Borazjani for her guidance and advice.

I genuinely appreciate the time Dr. Themis Carageorgos put in to review this thesis. Thank you for the critical and constructive suggestions. Also, thank you for your support and guidance through all the stages of my PhD.

I would like to express my deep gratitude to Dr. Alex Badalyan for his help and support. I learnt so much from you during these 3 years. The results of my work would not have been achieved without your guidance.

Special thanks to Dr. Zhenjiang You who I co-authored two papers with - thank you for your great contribution and effort. Also, I would like to thank Thomas Russell for his cooperation in writing a paper about fines stabilisation. It was great working with you.

I am very grateful to have met and worked with my colleagues at the Australian School of Petroleum. Very special thanks to my close friend Gabriel Malgaresi for his support and encouragement to tackle the hardships of this PhD. Thank you for being a great friend. I learnt so much from you and you contributed positively to my life in many ways. I would also like to thank my

colleagues Abolfazl, Fengtao, Jack, Larissa, Michael, Mike, Monica, Reza, Roozbeh, Saurabh, Shahdad, Shuyan, Tamineh, and Yazan for the great time we had during this PhD.

My sincere gratitude goes to Dr. Rouhi Farajzadeh (Shell) for his support and encouragement to start this PhD. I appreciate your advice and help before and while I was doing this degree.

Lastly, thank you to the staff of the Australian School of Petroleum and Energy Resources for their help during my time at the school.

Thesis by Publication

Al-Sarihi, A., You, Z., Behr, A., Genolet, L., Kowollik, P., Zeinijahromi, A. and Bedrikovetsky, P., 2019. Admissible Parameters for Two-Phase Coreflood and Welge-JBN Method. *Transport in Porous Media*, pp.1-41.

Al-Sarihi, A., You, Z., Behr, A., Genolet, L., Kowollik, P., Zeinijahromi, A. and Bedrikovetsky, P., 2018. Coreflood Planning Criteria for Relative Permeability Computation by Welge-JBN Method. *The APPEA Journal*, 58(2), pp.664-668.

Al-Sarihi, A., Zeinijahromi, A., Genolet, L., Behr, A., Kowollik, P. and Bedrikovetsky, P., 2018. Effects of fines migration on residual oil during low-salinity waterflooding. *Energy & Fuels*, 32(8), pp.8296-8309.

Al-Sarihi, A., Zeinijahromi, A. and Bedrikovetsky, P., 2018. Low-salinity Waterflooding in Non-polar oil. *The APPEA Journal*, 58(2), pp.660-663.

Al-Sarihi, A., Russell, T., Bedrikovetsky, P. and Zeinijahromi, A., 2019. Fines Stabilization by Ca Ions and Its Effect on LSW Injection. *Energy & Fuels*, 33(11), pp.10775-10786.

Al-Sarihi, A., Zeinijahromi, A., Genolet, L., Behr, A., Kowollik, P. and Bedrikovetsky, P., 2018. Fines Migration as an EOR Method During Low Salinity Waterflooding. SPE Asia Pacific Oil and Gas Conference and Exhibition. Society of Petroleum Engineers.

1 Contextual Statement

1.1 Research Background

Enhanced oil recovery by low salinity waterflooding (LSW) has been intensively studied in the past two decades. However, the exact mechanism(s) of LSW that yields incremental oil production is still a debate (Morrow and Buckley 2011; Sheng 2014; Qiao et al. 2016). The mechanisms proposed in the literature include fines migration, ionic exchange, pH change, decreased contact angle and interfacial tension, and osmosis (RezaeiDoust et al. 2011; Al Shalabi et al. 2014; Mahani et al. 2015a; Fredriksen et al. 2016).

This thesis dissertation first starts by presenting, in papers 1 and 2 (Chapter 3), the development of a comprehensive set of criteria that is done for the first time and can be applied not only to perform the low salinity waterflooding experiments in this work, but also conventional coreflooding tests to enable accurate determination of relative permeability using Welge-JBN method.

Welge-JBN technique is used to determine relative phase permeabilities, which are vital functions in the determination of oil production performance (Welge 1952; Johnson et al. 1959; Jones and Roszelle 1978). At the core level, these functions are determined empirically from laboratory coreflooding experiments. This method has the advantage of calculating relative permeability at large range of saturations (Barenblatt et al. 1991; Johansen and James 2016; Kianinejad et al. 2016). Several ways of interpreting data to calculate relative permeability by JBN method were proposed. This includes exponential approximation of the water-cut curve (Civan and Donaldson 1989; Toth et al. 2001; Chen et al. 2016), polynomial approximation (Miller and Ramey Jr 1985), and analytical interpretation method

that reduces the numerical error in the numerical simulation technique (Cao et al. 2014; Cao et al. 2015).

However, applying Welge-JBN method in the core scale requires careful consideration of flow rate and core length to fulfil the validity of Buckley-Leverett large scale approximation, which states that capillary forces are negligible compared to viscous forces in the field scale (Barenblatt et al. 1991; Lake et al. 2014). This theoretical criterion is not always fulfilled in the reviewed literature data and, this could lead to erroneous and unrepresentative calculations of the relative permeability. In addition, coreflow parameters need to match the operational conditions of precise measurement of oil and water fractional volumes, pressure drop across the core sample, and the minimum sampling period required to generate enough data points on the fractional flow curve (Dos Santos et al. 1997; Hussain et al. 2010). Therefore, two theoretical criteria and four operational criteria are presented, and must be fulfilled to accurately determine fractional flow and relative permeability functions.

Another objective of this PhD is investigating the mechanism of fines migration as an enhanced oil recovery technology in papers 3 and 4 (Chapter 4). In addition, the effect of brine ion types such as monovalent and divalent ions on fines migration and stabilisation is discussed in paper 5 (Chapter 5). In this work, sodium chloride and calcium chloride were used. Another important parameter that was controlled is the wettability of the rock. Nonpolar mineral oil was used so that the weak Van der Waals forces induced by the chemical structure of this oil and the rock surface do not cause an oil-wet or mixed-wet surface, which ensures a water-wet surface. Controlling the wettability enables isolating fines migration from other LSW mechanisms that aim to alter wettability. Therefore, any effect of LSW on oil production in this case is due solely to fines detachment.

Fines migration occurs because of the detachment of clay particles from the rock surface which were initially attached to the rock surface by electrostatic forces in the presence of high salinity initial water saturation (Sarkar and Sharma 1990; Bedrikovetsky et al. 2011; Zeinijahromi et al. 2016). When low salinity water is injected into the reservoir, the chemical equilibrium of the saline water is disturbed as a result of mixing with the lower concentration brine and, thus, the electrostatic forces are weakened. This leads to fines detachment and then migration by the drag forces caused by the flowing water and oil (Zeinijahromi et al. 2011; Hussain et al. 2013).

Fines migration results in reduction of water relative permeability as detached clay particles block the pore throats of preferential water paths (Khilar et al. 1983; Khilar and Fogler 1998). This leads to flux diversion where the wetting phase moves into the thin un-swept pores in which residual oil ganglia is trapped. Therefore, water mobility is controlled and extra oil recovery is achieved (Lever and Dawe 1984; Hussain et al. 2013; Zou et al. 2018).

While the benefit of fines migration to improve oil recovery is published in papers 3 and 4, paper 5 focuses on inhibiting fines migration in the case of severe formation damage that can take place around the production or injection wells. This is important when fines migration is utilised to enhance oil recovery where complete formation damage can be avoided. Several studies demonstrated that different types of salt ions can have variable sensitivity on the rock surface. However, a comprehensive study on the effect of ion type on fines migration and oil recovery is not present.

Decreasing the concentration of divalent salt ions such as calcium in calcium chloride (CaCl_2) brine have negligible effect on detaching clay particles and, hence, fines migration. Therefore, permeability does not decline compared to

injecting the same concentration of monovalent salt ions such as sodium in sodium chloride (NaCl) brine (Khilar et al. 1983; Valdya and Fogler 1992). This shows the impact of the initial salt ion type that is present in the porous media, not only the injected brine. The paper compares fines stability during coreflooding by injection of NaCl and CaCl₂ brines in step-wise decreasing salinity concentration. Single phase as well as two phase coreflooding was performed on clay rich consolidated and unconsolidated (artificial) core samples. The impact on oil recovery is also studied in the paper. Two of the single phase tests were accompanied with ion chromatography to demonstrate the ionic exchange process between divalent and monovalent ions. Furthermore, non-polar mineral oil is used in the two phase flow experiments to rule out the impact of wettability alteration and focus only on fines migration as an enhanced oil recovery mechanism. To confirm no wettability change took place, Amott tests were executed on sister core samples with both polar (crude oil) and non-polar oil at different salinities range. The tests with non-polar oil showed a constant water-wet wettability index (1) during the different salinity injection stages. The Amott tests with polar oil showed a slight change towards a water-wet wettability index when the water salinity was switched from high to low.

1.2 Research Objectives

The study of this thesis has the following aims:

- a) Design a comprehensive criteria for the parameters needed in coreflooding experiments to fulfil Welge-JBN method in determining relative permeability.
- b) Apply the newly designed criteria in coreflood relative permeability determination.

- c) Investigate the effect of low-salinity-induced fines migration on enhanced oil recovery.
- d) Isolate fines migration from other low salinity waterflooding mechanisms and determine incremental oil production solely due to this technology.
- e) Determine the phenomenon of improving sweep efficiency by pore throat blockage through fines migration that can be applied in real oil fields.
- f) Study the ion type impact on fines migration and oil recovery.
- g) Investigate fines stabilization and inhibition in oil reservoirs.
- h) Determine the mechanism of calcium ions desorption from the rock surface due to low salinity waterflooding.

1.3 Thesis Structure

This is a PhD thesis by publication. Six papers are included in the thesis, five of which are journal papers and one is a conference paper (attached in the appendix). The PhD student is the first author in all of the papers.

Chapter 1 has the contextual statement, the structure of this thesis, and how the papers fulfil the aim of the thesis.

Chapter 2 provides a literature review and introductory background on low salinity waterflooding. It shows the several mechanisms believed to play a role in enhanced oil recovery during LSW.

Chapter	Title	Paper	Status
Chapter 3	Admissible parameters for two-phase coreflood and Welge-JBN method	1	Published
	Coreflood planning criteria for relative permeability computation by Welge-JBN method	2	Published
Chapter 4	Effects of fines migration on residual oil during low-salinity waterflooding	3	Published
	Low-salinity waterflooding in non-polar oil	4	Published
Chapter 5	Fines stabilisation by Ca ions and its effect on LSW injection	5	Published
Appendix	Fines migration as an EOR method during low salinity waterflooding	6	Published

Chapter 3 presents the designed criteria needed to perform the experiments mentioned in chapters 4 and 5, which are also applicable to conventional coreflooding experiments. The study concluded that there are six important criteria that need to be fulfilled simultaneously, in order to accurately apply the Welge-JBN method to determine relative permeability during coreflooding. The two theoretical criteria include capillary number and capillary-viscous ratio. The four operational criteria are water-cut precision measurement, pressure drop precision measurement, number of effluent samples required, the minimum time needed for the effluent samples to construct the fractional flow curve. Numerical simulation and experimental work was performed in this study. The numerical simulation was done on different capillary-viscous ratios to determine the maximum ratio that can be applied to ensure the validity of Welge-JBN method, which fulfil the large scale approximation of Buckley-Leverett model. This was achieved by comparing relative permeability generated numerically for different capillary-viscous ratios with that determined by Welge-JBN analytically. The experimental work was performed based on the criteria and matched both, the Welge-JBN and the numerical simulation methods. The results illustrate that capillary pressure does not influence the fractional flow and relative permeability for capillary-viscous ratios under 0.5. Also, the required displacement rate and core length can be determined using these criteria, while ensuring the fulfilment of all the assumptions needed for the Welge-JBN method.

Chapter 4 includes two papers that investigate the effect of solely fines migration on oil recovery where wettability alteration mechanism was successfully excluded by the use of non-polar oil in water-wet Berea rock samples. The study was also conducted on low clay Bentheimer core samples as well as clean sand artificial core samples. The results show that at the presence of high

clay content, fines migration is significant during low salinity waterflooding and residual oil saturation was reduced by 5-18% as a result. Low-clay and clean sand cores show no fines migration and, therefore, no extra oil was produced during low salinity waterflooding. The main conclusion from this chapter is that the higher the clay content, the higher is the residual oil saturation reduction.

Chapter 6 focuses on fines stabilization with the injection of calcium chloride into clay-rich cores to control and mitigate the detrimental effects of formation damage in oil fields during low salinity waterflooding. This is important for the decreased well injectivity and productivity when a low salinity waterflooding scheme is implemented. The study investigates alternating sodium and calcium ions' concentration and its impact on clay particle detachment and oil production improvement. Both naturally consolidated and artificial core samples were tested in single and two phase fluid flow schemes. The results show no significant fines migration taking place when low salinity calcium chloride is injected in cores are initially saturated with high salinity calcium chloride. Further injection of deionized water still did not show any signs of fines migration. After switching to sodium chloride, significant particle concentration was measured in the effluent solution accompanied by high pressure drop across the cores. This indicates kinetic desorption of calcium ions, which are replaced by sodium ions as can be inferred from the ion chromatography results. Additionally, incremental oil production was obtained as a result of fines migration after sodium chloride injection, which was followed by another fresh water flush as well. This shows the importance of ion type to control the formation damage needed to enhance oil recovery and to prevent any severe impacts of fines migration on well injectivity/productivity.

The paper '*Fines migration as an EOR method during low salinity waterflooding*' in the appendix was presented in the Asia Pacific Oil and Gas Conference and Exhibition (APOGCE) in 2018 and the content of the paper is a continuation of the work done in chapter three.

1.4 How The Publications Are Related to The Thesis

The papers in Chapter 3 introduce, for the first time, a comprehensive criteria that are required during two-phase coreflooding (presented in chapters 4, 5, and the appendix) to apply Welge-JBN method to calculate relative permeability. This criteria can, also, be applied in any other two-phase flow corefloods. The papers reported the maximum capillary-viscous ratio that can be used for large-scale Buckley-Leverett model, in order to accurately calculate relative permeability by fulfilling the assumption of negligible capillary pressure effect. In total, it proposes two theoretical and four operational criteria that are needed to fulfil the parameters of the Welge-JBN method. This criteria fulfils the other aims of the thesis by introducing essential and universal parameters such as capillary-viscous ratio and capillary number, which need to be fulfilled simultaneously for the two-phase relative permeability corefloods conducted during this PhD. These criteria are also applicable universally.

The paper '*Effects of fines migration on residual oil during low-salinity waterflooding*' in Chapter 4 presents a study on the impact of the fines migration mechanism on enhancing oil recovery by microscale flux diversion. Double coreflooding was performed with high salinity and low salinity water injection followed by tertiary piecewise decreasing salinity waterflooding. The experimental results show that simultaneous fines production, permeability

decline, and residual oil reduction take place when low salinity water is injected. Water-wetness was kept throughout the high salinity and low salinity water injection, meaning wettability alteration had no contribution to the LSW effect. Moreover, this work shows a proportional relationship between clay content and the decrease in the residual oil saturation. As the clay content increases in the reservoir, the higher the formation damage and, hence, the higher the reduction of the residual oil saturation. Therefore, this paper fulfils the aim of identifying fines migration as a low salinity mechanism to improve oil recovery and excludes other mechanisms' contribution to the incremental oil produced.

The paper 'Low-salinity waterflooding in non-polar oil' in Chapter 4 is a continuation of the work done on the first paper and confirms its results.

After confirming that microscale flux diversion phenomenon is the driving mechanism in fines migration to enhance oil recovery in the papers presented in Chapter 5, the paper titled 'Fines stabilisation by Ca ions and its effect on LSW injection' investigates how the salt ion type can impact both fines detachment and stabilisation. The work was conducted by injecting calcium chloride, ranging from high to low salinity and then fresh water, followed by sodium chloride and finally by fresh water. The results indicate a dependency of fines migration on salt ion type. When calcium chloride in varying salinity concentrations is injected into core samples initially saturated with CaCl_2 , clay particles remain attached to the rock surface and no fines migration takes place, even when fresh water is injected afterwards. That means Ca ions are strongly attached to the rock surface and significantly large pore volumes of fresh water need to be injected to desorb these ions from the rock surface. This procedure enables stabilising clay in the reservoir to avoid formation damage in production/injection wells in oil and gas fields. On the other hand, when sodium chloride is injected after the calcium chloride

displacement, calcium ions desorb as they are exchanged with sodium ions, which then leads to fines detachment and migration. This happens after the second fresh water injection due to the weakened electrostatic forces between clay and the rock surface, at the presence of sodium ions. Additionally, reduction of residual oil saturation is observed when fines migration takes place which indicates sweep efficiency improvement as mentioned in papers 3 and 4. Therefore, this paper fulfils the objective of determining the ion type dependency that could cause either fines detachment or stabilization, depending on the objective of the low salinity waterflooding scheme in oil and gas fields.

The paper in the appendix titled 'Fines migration as an EOR method during low salinity waterflooding' is a continuation of the papers in chapter four and was presented in the Asia Pacific Oil and Gas Conference and Exhibition - SPE in 2018.

1.5 References:

- Al Shalabi, E.W., Sepehrnoori, K., Delshad, M.: Mechanisms behind low salinity water injection in carbonate reservoirs. *Fuel* **121**, 11-19 (2014)
- Barenblatt, G., Entov, V., Ryzhik, V.: Theory of Fluid Flows through Natural Rocks. In. Kluwer, (1991)
- Bedrikovetsky, P., Siqueira, F.D., Furtado, C.A., Souza, A.L.S.: Modified particle detachment model for colloidal transport in porous media. *Trans. Porous Media* **86**(2), 353-383 (2011)
- Cao, J., James, L.A., Johansen, T.E.: Determination of two phase relative permeability from core floods with constant pressure boundaries. In: Society of Core Analysis Symposium, Avignon, France 2014
- Cao, J., Liu, X., James, L., Johansen, T.: Analytical Interpretation Methods for Dynamic Immiscible Core Flooding at Constant Differential Pressure. In: Society of Core Analysis Symposium, St. John's Newfoundland and Labrador, Canada 2015, pp. 16-21
- Chen, X., Kianinejad, A., DiCarlo, D.A.: An extended JBN method of determining unsteady-state two-phase relative permeability. *Water Resources Research* **52**(10), 8374-8383 (2016)
- Civan, F., Donaldson, E.: Relative permeability from unsteady-state displacements with capillary pressure included. *SPE Form. Eval.* **4**(02), 189-193 (1989)
- Dos Santos, R.L., Bedrikovetsky, P., Holleben, C.R.: Optimal Design and Planning for Laboratory Corefloods. In: Latin American and Caribbean Petroleum Engineering Conference 1997. Society of Petroleum Engineers
- Fredriksen, S.B., Rognmo, A.U., Fernø, M.A.: Pore-Scale Mechanisms During Low Salinity Waterflooding: Water Diffusion and Osmosis for Oil Mobilization, 2016/4/20/
- Hussain, F., Cinar, Y., Bedrikovetsky, P.G.: Comparison of methods for drainage relative permeability estimation from displacement tests. In: SPE improved oil recovery symposium 2010. Society of Petroleum Engineers
- Hussain, F., Zeinijahromi, A., Bedrikovetsky, P., Badalyan, A., Carageorgos, T., Cinar, Y.: An experimental study of improved oil recovery through fines-assisted waterflooding. *J. Pet. Sci. Eng.* **109**, 187-197 (2013)
- Johansen, T.E., James, L.A.: Solution of multi-component, two-phase Riemann problems with constant pressure boundaries. *Journal of Engineering Mathematics* **96**(1), 23-35 (2016)
- Johnson, E., Bossler, D., Bossler, V.: Calculation of relative permeability from displacement experiments. (1959)
- Jones, S., Roszelle, W.: Graphical techniques for determining relative permeability from displacement experiments. *J. Pet. Technol.* **30**(05), 807-817 (1978)
- Khilar, K.C., Fogler, H.S.: Migrations of fines in porous media, vol. 12. Springer Science & Business Media, (1998)
- Khilar, K.C., Fogler, H.S., Ahluwalia, J.: Sandstone water sensitivity: existence of a critical rate of salinity decrease for particle capture. *Chem. Eng. Sci.* **38**(5), 789-800 (1983)
- Kianinejad, A., Chen, X., DiCarlo, D.A.: Direct measurement of relative permeability in rocks from unsteady-state saturation profiles. *Advances in water resources* **94**, 1-10 (2016)
- Lake, L.W., Johns, R., Rossen, W.R., Pope, G.A.: Fundamentals of enhanced oil recovery. (2014)
- Lever, A., Dawe, R.A.: Water-sensitivity and migration of fines in the hopeman sandstone. *J. Pet. Geo.* **7**(1), 97-107 (1984)
- Mahani, H., Berg, S., Ilic, D., Bartels, W.-B., Joekar-Niasar, V.: Kinetics of low-salinity-flooding effect. *SPE J* **20**(01), 8-20 (2015)

- Miller, M.A., Ramey Jr, H.: Effect of temperature on oil/water relative permeabilities of unconsolidated and consolidated sands. *Society of Petroleum Engineers Journal* **25**(06), 945-953 (1985)
- Morrow, N., Buckley, J.: Improved oil recovery by low-salinity waterflooding. *J. Pet. Technol.* **63**(05), 106-112 (2011)
- Qiao, C., Johns, R., Li, L.: Modeling low-salinity waterflooding in chalk and limestone reservoirs. *Energy Fuels* **30**(2), 884-895 (2016)
- RezaeiDoust, A., Puntervold, T., Austad, T.: Chemical Verification of the EOR Mechanism by Using Low Saline/Smart Water in Sandstone. *Energy Fuels* **25**(5), 2151-2162 (2011). doi:10.1021/ef200215y
- Sarkar, A.K., Sharma, M.M.: Fines migration in two-phase flow. *J. Pet. Technol.* **42**(05), 646-652 (1990)
- Sheng, J.J.: Critical review of low-salinity waterflooding. *J. Pet. Sci. Eng.* **120**, 216-224 (2014). doi:10.1016/j.petrol.2014.05.026
- Toth, J., Bodi, T., Szucs, P., Civan, F.: Direct determination of relative permeability from nonsteady-state constant pressure and rate displacements. In: *SPE Production and Operations Symposium 2001*. Society of Petroleum Engineers
- Valdya, R., Fogler, H.: Fines migration and formation damage: influence of pH and ion exchange. *SPE production engineering* **7**(04), 325-330 (1992)
- Welge, H.J.: A simplified method for computing oil recovery by gas or water drive. *J. Pet. Technol.* **4**(04), 91-98 (1952)
- Zeinijahromi, A., Farajzadeh, R., Bruining, J.H., Bedrikovetsky, P.: Effect of fines migration on oil-water relative permeability during two-phase flow in porous media. *Fuel* **176**, 222-236 (2016)
- Zeinijahromi, A., Lemon, P., Bedrikovetsky, P.: Effects of induced fines migration on water cut during waterflooding. *J. Pet. Sci. Eng.* **78**(3-4), 609-617 (2011)
- Zou, S., Hussain, F., Arns, J.-y., Guo, Z., Arns, C.H.: Computation of Relative Permeability From In-Situ Imaged Fluid Distributions at the Pore Scale. *SPE J* **23**(03), 737-749 (2018)

2 Literature Review

2.1 Introductory Background

Hydrocarbon extraction is essential to sustain the global demand of energy. Initially, oil is produced from the reservoir by natural pressure depletion. This is a primary oil production mechanism. As the subsurface pressure decreases, other technologies are applied to provide enough pressure to mobilize oil towards the surface. Water injection to displace oil in the reservoir is one of these techniques. It is a secondary mechanism. Recent studies showed even more oil can be produced if the salinity of the injected water is lowered or manipulated (Zhang and Morrow 2006; Berg 2010; Fernø et al. 2011).

However, the mechanism of low salinity water flooding is not fully understood. Various hypothesis and mechanisms have been proposed in the literature. They concluded that low salinity effect is only seen when the crude oil has polar components and clay should also be present in the case of sandstone (Lager et al. 2008a; Austad et al. 2010; Nasralla and Nasr-El-Din 2011). In addition, modelling of the low salinity techniques such as ionic exchange has not received enough attention in the literature, especially in carbonate reservoirs.

2.2 Low Salinity Waterflooding in Sandstone

2.2.1 Properties of Water, Oil and Rock

- Water

Connate water in the porous media contains several ions that contribute to its salinity. It includes monovalent ions (such as Na^+ , K^+ , Cl^- , etc.) and divalent ions (such as Mg^{2+} , Ca^{2+} , SO_4^{2-} , etc.) (Van Cappellen et al. 1993).

- Oil

Oil is composed of polar and nonpolar components. Acid and base numbers, mgKOH/g, (AN and BN, respectively) are used to determine the polarity of crude oil and they are wetting parameters for the rock surfaces. Carboxyl group, RCOO⁻, is a main acidic component of crude oil and it can be mostly seen in heavy oil where high concentration of resin and asphaltene fractions exist. Basic compounds such as cyclic nitrogen components NH⁺, are determined by the basic number. Depending on the rock surface charge and the concentration of the charged crude oil components, the wettability of reservoirs can be determined. For example, having a high AN means a high concentration of acidic components and that can make positive rock surface such as carbonate strongly oil-wet. Therefore, oil recovery becomes low in such reservoir conditions. Non-polar oil, on the other hand, does not have charged components (Austad 2013; Brady et al. 2015).

- Rock

In sandstones, low salinity effect is seen when the rock contains clay (Austad et al. 2010). Clay is present in sandstones in few percentages whereas the majority of the rock is quartz (SiO₂) (De Velde Harsenhorst 2014). Layers of alumio-silicates are stacked on top of each other forming clay, which are present in the form of SiO₄ tetrahedrons and Al₂((OH)₆)_n or ((Fe/Mg)₃(OH)₆)_n. There are two types of clays; 1:1 where there is one octahedral sheet and one tetrahedral sheet, 2:1 where there is one tetrahedral sheet between two octahedral sheets (Hughes et al. 2010). The following schematic represents the arrangement of type 1:1.

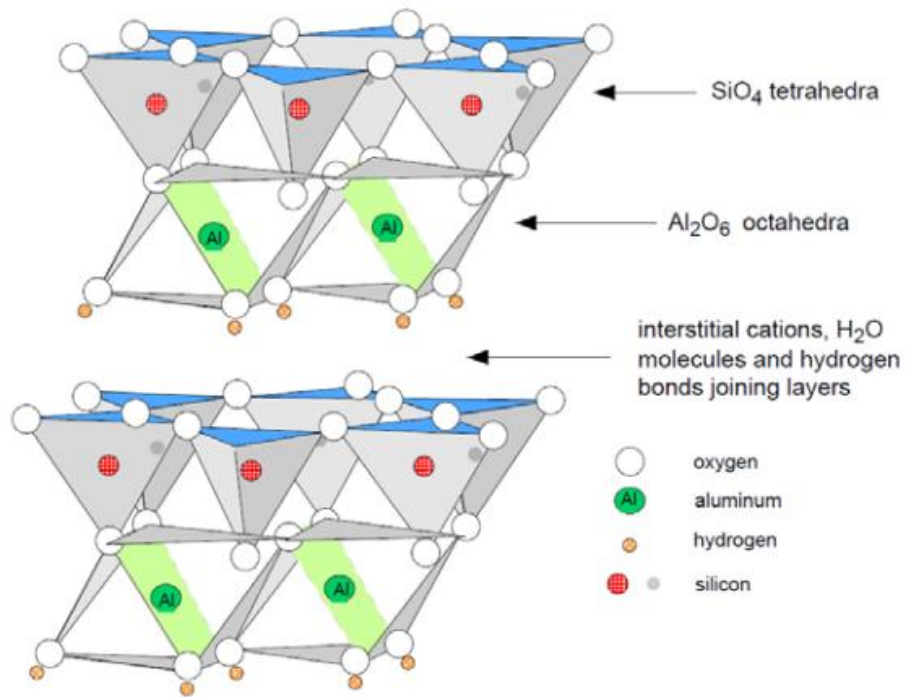


Figure 1: Type 1:1 clay arrangement (Hughes et al. 2010)

Type 1:1 clays bind to each other by direct adhesion through the positive hydrogen ions (from the OH^- group in AlOH^-) into SiO_2^- groups from different clay layers. Because of the strong bond, this kind of clay does not swell. Kaolinite is one of these clays. Type 2:1 binds with other clay layers through interlayer ions, like potassium, or water molecules. That is due to the repulsion between these layers. Therefore, swelling can occur in such clay types since repulsion between layers can increase the thickness of the interlayer for Illite and montmorillonite (De Velde Harsenhorst 2014).

2.2.1.1 Adsorption of oil on the rock surface

- Clay Surface Charge

Clay acquires its surface charge in two ways; structural permanent charge and pH dependent charge. A permanent negative charge on the surface can occur

due to the exchange of some ions due to weathering such as replacement of Si^{4+} by Al^{3+} in the tetrahedral sheets. This phenomenon creates a deficiency in positive charge and thus produces a negatively charged site. Substitution of such ions occurs mainly in 2:1 type minerals (Velde and Meunier 2008).

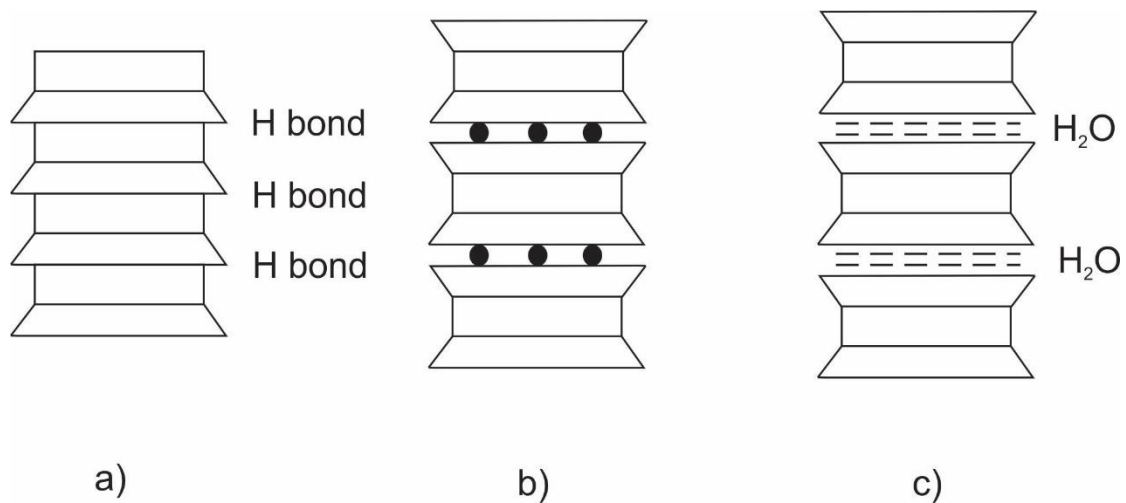
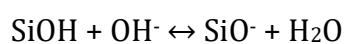


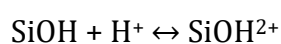
Figure 2: a) Kaolinite, b) Illite, and c) Montmorillonite

pH induced charge happens because silica (Si) has a point of zero charge at $\text{pH} = 2$ and Aluminium (Al) has this point at $\text{pH} = 8$. The difference in these points indicates that the two metals do not have equal protonation, which can result in varying surface charge at a given pH.

In addition, high pH makes the clay surface negative due to the abundance of OH^- which reacts with SiOH according to:



Low pH increases the concentration of H^+ and results in a positive surface charge according to: (Pevear and Eslinger 1988; Velde and Meunier 2008; De Velde Harsenhorst 2014)



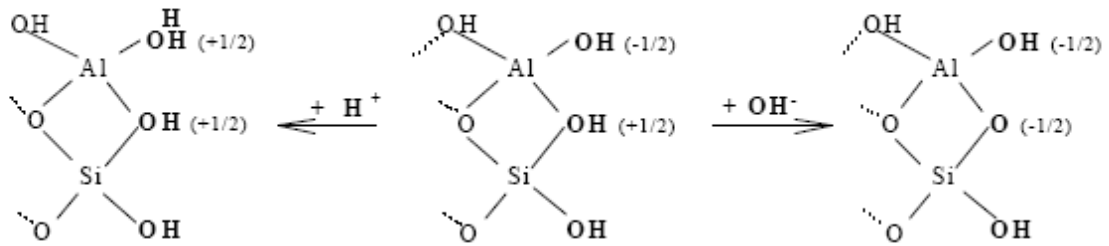


Figure 3: pH effect on the charge of clay surface in low pH medium (left), intermediate pH medium (centre) and high pH medium (right) (Sparks 2003)

- Oil Adsorption

Non-polar oil adsorbs on the rock surface through Van der Waals forces because there are no charged components in this oil to bond via other forms (Lager et al. 2008b). Regarding polar oil, Burgos et al. (2002) tested the adsorption of basic oil components from quinoline on kaolinite and montmorillonite. They observed a higher adsorption on montmorillonite than kaolinite as the former is a 2:1 clay type with larger negatively charged surface area. In addition, they noticed that pH plays a role in the amount of adsorbed compounds. As pH of the solution decreases, more quinoline attaches to the clay. That is because low pH produces protonated quinoline components (from H⁺) which results in attachment of these components due to the high adsorption affinity of hydrogen to clay surface.

At pH higher than 5, kaolinite has very low adsorption capacity, whereas montmorillonite can still absorb more components at pH = 7. When pH reaches 4 the highest rate of adsorption is achieved on these two clays. Below pH =4, H⁺ competes with the protonated quinoline to settle on the negative sites and can even replace these protonated compounds (Austad et al. 2010).

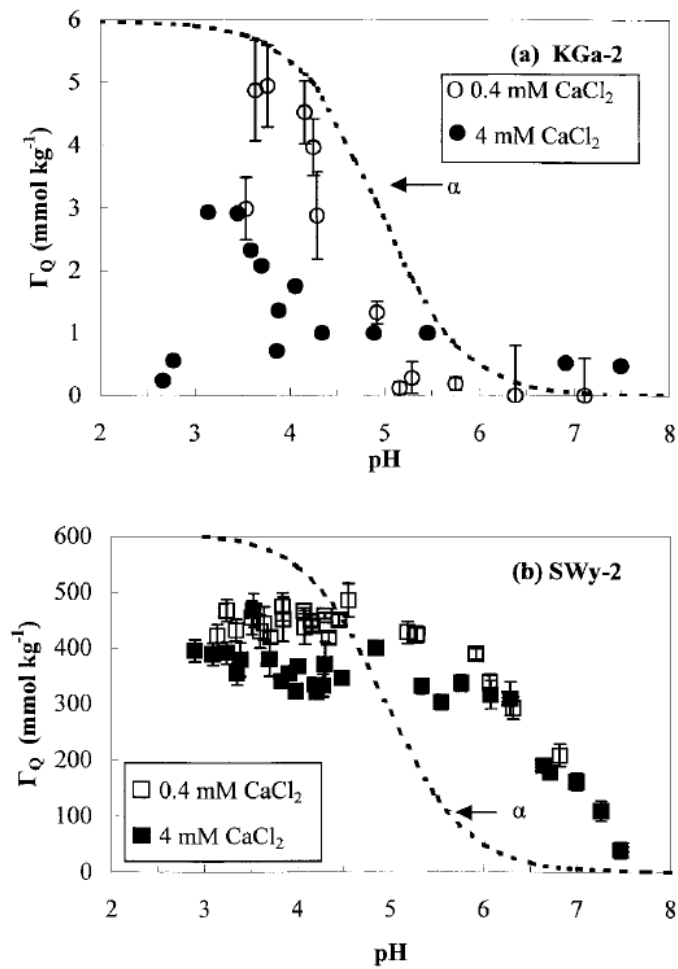


Figure 4: Adsorption of quinoline on (a) kaolinite and (b) montmorillonite (Burgos et al. 2002)

Acids follow basic components in how they adsorb on clay surfaces. pH also plays a role in the amount of acidic components attached on the negatively charged clays. As pH decreases more adsorption takes place (Austad et al. 2010).

At pH values of 4-5, the amount of non-dissociated acids rises. Carboxylic material such as RCOOH adsorbs through hydrogen bonds as shown in figure 5. These bonds are similar to the dimeric acid complex connection (right hand side of figure 5) (Austad et al. 2010).

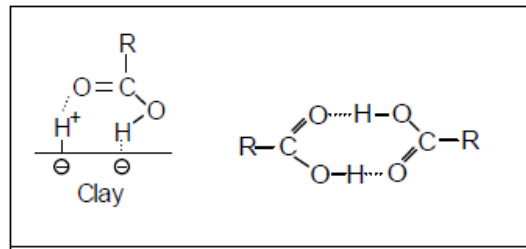


Figure 5: Acid adsorption on clay via hydrogen bond- similar to dimeric acid bonding (right hand side) (Austad et al. 2010)

Bonding mechanisms of oil on the rock surface are categorized into cation exchange, ionic bridging, ligand exchange and Van der Waals forces, which are considered as the main bonds (Myint and Firoozabadi 2015). Cation exchange adsorption takes place as quaternized nitrogen or heterocyclic ring replaces an initially adsorbed metallic cation on the clay surface. When a polar oil component attaches to an exchangeable cation already adsorbed on the clay surface it forms a cation bridging bond. Ligand bond occurs when a carboxylic component connects with a multivalent cation forming organo-metallic complexes. This is considered stronger than cation bridging and cation exchange (Lager et al. 2008a; Wang et al. 2013; Cotterill 2014). Other bonding systems are protonation, anion exchange, water bridging and hydrogen bonding. It is worthwhile mentioning that polar oil can also attach directly on the rock surface (Lager et al. 2008a). The main bonds are illustrated in figure 6.

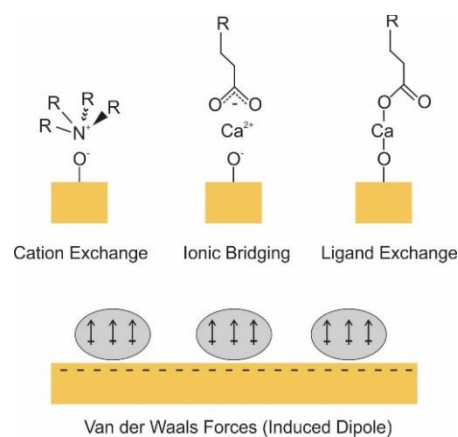


Figure 6: Main bonding systems of oil components on rock surface (Cotterill 2014)

2.3 Mechanisms of low salinity waterflooding

2.3.1 Ionic Exchange

According to the bonding mechanisms mentioned above, multicomponent ion exchange in low salinity occurs at the clay surface where the directly adsorbed organic compounds and organo-metallic complexes are displaced by the invading ions (Lager et al. 2008b; Ligthelm et al. 2009; Brady and Krumhansl 2012; Borazjani et al. 2019). The following figure shows an example of this ionic exchange.

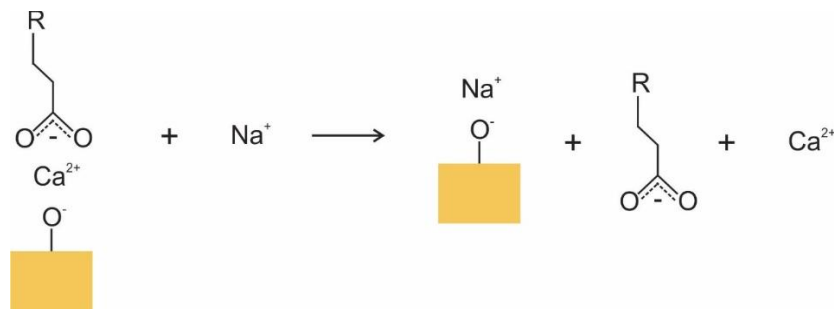
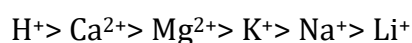


Figure 7: Multicomponent ion exchange between sodium and an organo-metallic complex formed by calcium (Cotterill 2014)

Austad et al. (2010) also proposed a mechanism that includes exchanging of ions to desorb oil component complexes. As the cation exchange capacity (CEC) of clay allows multivalent ions such as Ca^{2+} to adsorb on its surface, injecting low salinity water can disturb this equilibrium. An invading water with less concentrated multivalent ions leads to proton, H^+ from the water molecule, to replace the calcium ion due to its higher affinity to clay surface than calcium according to:



This causes the water molecule to split, leaving a free OH⁻ which reacts with the hydrogen ion that is attached to the oil component with a hydrogen bond. As a consequence of this ion exchange, the oil component is released from the clay surface because the bonding between the oil complex and the surface is weak. This is shown in figure 8 for both basic and acidic oil components.

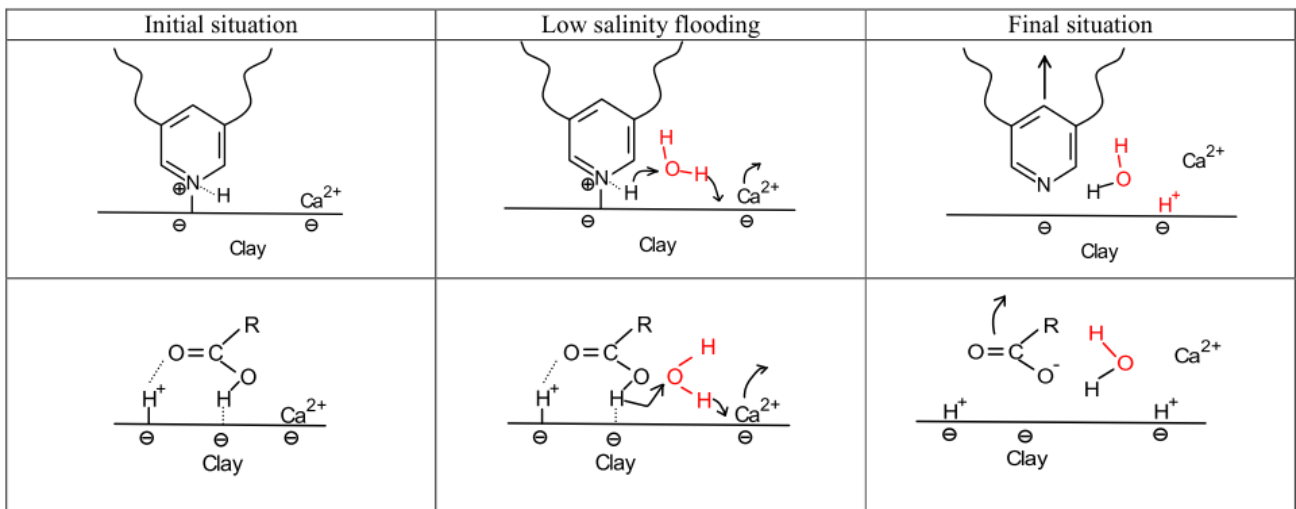
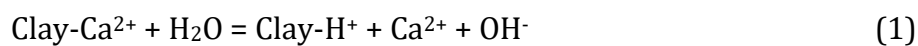


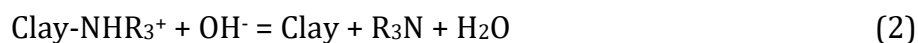
Figure 8: Basic oil component desorption (upper) and acidic component desorption during the ion exchange of hydrogen and the multivalent ion on the clay surface (Austad et al. 2010)

2.3.2 pH Increase

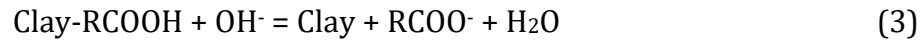
The proton exchange in the previous section is explained according to the following reactions:



For the basic component:



And for the acidic component:



From the first reaction, the production of OH^- increases pH and this is believed to be another mechanism of low salinity water flooding. Producing OH^- creates an alkaline environment because it reacts with H^+ that is connecting the oil compound with the clay to form water and hence release oil as shown in reactions 2 and 3 (Austad et al. 2010; RezaeiDoust et al. 2011; Aksulu et al. 2012).

Another explanation for the increasing pH to cause incremental oil recovery by low salinity is related to the low interfacial tension between oil and water. As pH increases, organic acids form in-situ surfactants which reduce the interfacial tension between oil and water. Oil/water or water/oil emulsions can be generated because of the low interfacial tension which can aid to better the water sweep efficiency (Zhang and Morrow 2006; Sheng 2014).

Also, Valdya, Fogler (1992) noticed a relationship between high pH values and fines migration. As pH increase, more fines are released because more negative charge is seen (as shown in the zeta potential measurement) which leads to more repulsion with the rock surface. This could also explain the incremental oil recovery by fines mobilization as will be mentioned in the fines migration section.

2.3.3 Double Layer Expansion

Electrical double layer is created by the accumulation of charged ions on oppositely charged surface (Israelachvili 2011). The negatively charged clay

surface attracts positive ions such as Na^+ and Ca^{2+} as shown in figure 9. As the ionic strength increases (higher salinity) the double layer becomes thinner and vice versa. In addition, divalent ions make the layer thin as well as the double positive charge covers more of the negative clay surface (Hughes et al. 2010).

The thin layer caused by high salinity brine suppresses the negatively charged clay by reducing the electrostatic repulsive forces between the clay-clay, clay-water and the water-oil interfaces. When the salinity of water is reduced, the chemical equilibrium is disturbed and hence the ions move away from the clay surface. That results in expansion of the double layer caused by increasing the repulsive forces between clay-water and also water-oil as well as clay-clay. Water film becomes thicker and more stable. Therefore, the surface becomes more water wet and extra oil is desorbed (Ligthelm et al. 2009; Nasralla and Nasr-El-Din 2011; Liu et al. 2007).

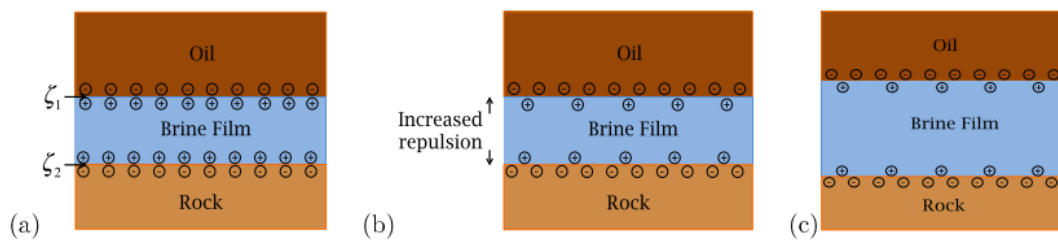


Figure 9: Expansion of the electric double layer, EDL, between clay-water and water-oil interfaces (Myint and Firoozabadi 2015); a) high salinity formation water is present; b) low salinity water injection initiates repulsion between oil and rock surface; c) complete separation of oil from surface

2.3.4 Fines Migration

When high salinity water is present in a porous media, the clay is stable and in equilibrium because there is a balance between colloidal forces and capillary forces. Colloidal forces include attractive and repulsive forces that depend on the

Van der Waals and electrostatic forces according to the DLVO theory (Israelachvili 2011).

When low salinity water is injected, the repulsive forces increase and the double layer expands. This leads clay particles to mobilize in the porous rock and to be produced in the effluent. As polar oil is attached to the clay surface, it is transferred with the fines as they are released as shown in figure 10 (Fogden et al. 2011). Also, such particles can block the large pores by straining (Zeinijahromi et al. 2012) which can reduce water permeability and hence enhance water mobility by reducing channelling and fingering effects. This results in better sweep efficiency (Hussain et al. 2013). Figure 11 demonstrates the straining effect of particles.

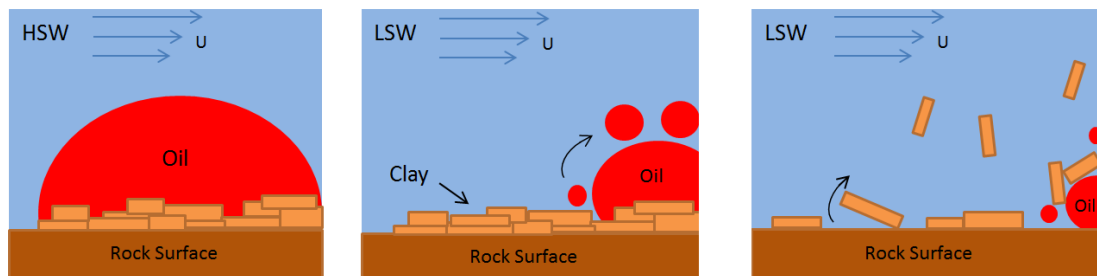


Figure 10: Oil recovery by fines migration

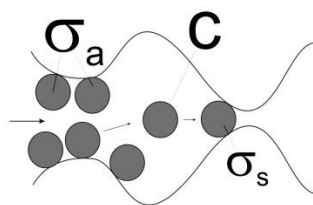


Figure 11: Particle straining in a pore throat as fines are mobilized (Zeinijahromi et al. 2012)

2.3.5 Osmosis

In low salinity water flooding, osmosis theory is believed to act as following. At initial conditions, connate water (high salinity) is present along with the oil phase in the rock. As low salinity water is introduced to this system, equilibrium in the water phase is disturbed because of the difference in water molecules concentration between the high and low salinity brines. That is also because in the high salinity water, there are more free ions that are not attached to water molecules. The difference in concentrations makes low salinity brine to have a higher chemical potential (high water molecule concentration) than the high salinity water. This encourages water molecules to transfer towards low chemical potential zone (high salinity) (Fredriksen et al. 2016).

Because the oil phase exists between the high and low salinity brines, it acts as a semi-permeable membrane that allows pure water (no ions) to transport through it towards the high salinity water to reach equilibrium in water molecules concentration of both brines. Water molecules move towards high salinity brine until it reaches the osmotic pressure, which is the pressure needed to stop the flow of water molecules from the low salinity region (Sandengen et al. 2016).

The water phase on the high salinity region expands as a consequence of water flow from the low salinity region. This expansion can lead to displacement of the oil that is attached to it. In the case of water-in-oil emulsions, water volume increases in the emulsion which results in expelling the oil phase that surrounds it (Fredriksen et al. 2016; Sandengen et al. 2016).

The increase in pressure in the high salinity water due to the movement of the molecules from the low salinity water is called osmotic pressure. It was described by Fritz, Marine (1983) as:

$$\pi = \frac{RT}{V} \ln\left(\frac{a_1}{a_{11}}\right)$$

Where π is the osmotic pressure, R is the gas constant (0.082 [liter.atm]/[g-mol.K]), T is temperature (K), V is molar volume (liter/g-mol), a_1 is the water activity of low salinity brine and a_{11} is the water activity of high salinity brine. Water activity is measured on a scale from 0 to 1, where 0 represents no water molecules and 1 represents all water molecules. Because pure water has activity of 1, the above equation is written as:

$$\pi = -\frac{RT}{V} \ln(a_{11})$$

Chemical potential of water is the work done or energy exerted when water molecules react or move. It depends on the concentration of water molecules (mole fraction) and the mean free energy of water. Therefore, osmosis causes water molecules to do work. That means there needs to be difference in chemical potential of water on both sides of the semi-permeable membrane for the molecules to transport. Low salinity brine has higher potential than high salinity brine and, hence, water molecules move from low to high salinity brine through the membrane (Schmid et al. 2014).

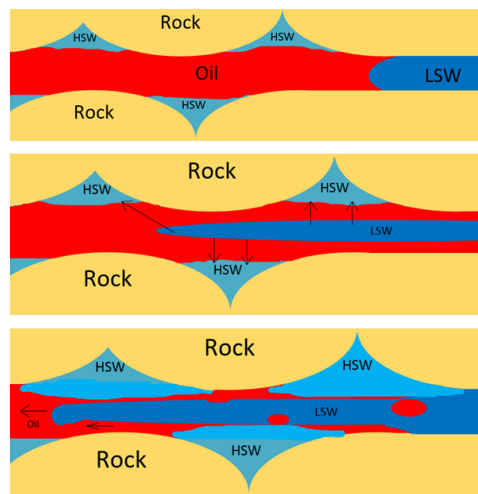


Figure 102: Osmosis through oil phase in cavities

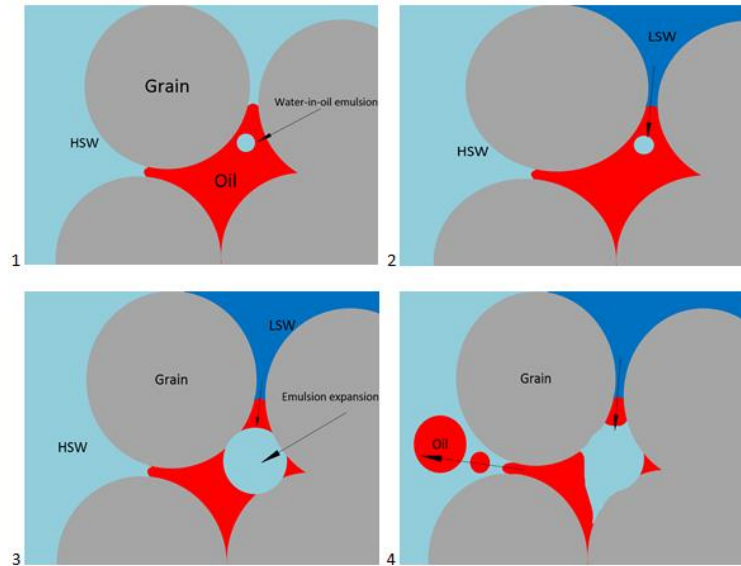


Figure 13: Osmosis through oil phase in an isolated pore

2.3.6 Salting-in

RezaeiDoust et al. (2009) referred to the salting-in/ salting out phenomena to explain the low salinity effect. Polar organic components are soluble in water as hydrogen bonds are formed with the hydrophobic part of the organic compound making water structures. Salt ions such as Ca^{2+} and Na^+ have the ability to break these water structures around the organic molecules. Therefore, as the salinity increases, the solubility of polar compounds is reduced. On the other hand, when the salinity is lowered, the breaking effect of the ions is diminished and that improves the solubility of polar oil in water. This is called the salting-in effect. It improves oil recovery by mobilizing polar components in the aqueous phase.

2.3.6.1 Other Wettability Alteration Mechanisms

Along with the mechanisms of double layer expansion, pH increase and ionic exchange to change the wettability of a rock surface to more water, there are

also other theories explaining wettability alteration. Sohrabi et al. (2015) did some experiments on micromodels with crude oil as well as coreflooding and spontaneous imbibition. They related low salinity effect to the formation of micelles which they called micro dispersions in the oil phase. This dispersion results from reforming the natural active surfactants from the oil by low salinity water. They detach the initially adsorbed active surface compounds on the rock surface, which yields a more water wet surface. This is illustrated in figure 14.

Moreover, Hassenkam et al. (2014) did a nanoscale test to study the effect of low salinity on wettability alteration. They performed an atomic force microscopy (AFM) on core samples with carboxylic acids at different injection salinities. Their results showed a decline in the adhesion forces between the acids and the quartz surface when low salinity brine (1500 ppm) is introduced in the rock. This could be another reason for the wettability alteration and, therefore, the oil recovery enhancement. They also concluded that the decrease in adhesion forces occurs at salinity of 5000-8000 ppm or below, which agrees with the previous studies that there is an approximate threshold of low salinity waterflooding effect at a salinity of around 5000 ppm (Al-Shalabi and Sepehrnoori 2016).

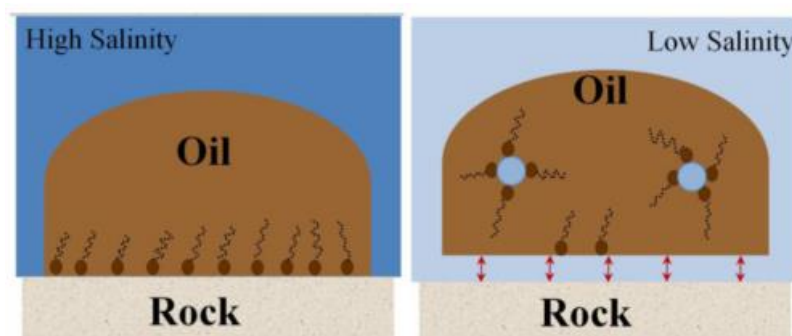
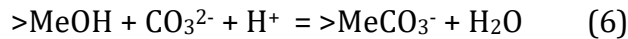
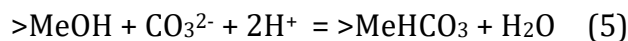
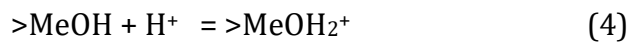
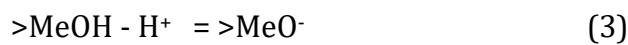
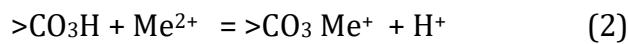


Figure 14: Wettability alteration by forming water micro-dispersions in the presence of low salinity water (Sohrabi et al. 2015)

2.4 Low Salinity Waterflooding in Carbonates:

2.4.1 Surface Charge and Oil Adhesion

Carbonate rock's chemical structure consists mainly of calcite (CaCO_3), dolomite ($\text{CaMg}(\text{CO}_3)_2$) or CaSO_4 (anhydrite). The charge on the surface is influenced by the pH of the aqueous phase and it is controlled by the following reactions:



> is the solid part of the rock and Me stands for metal ions such as Ca and Mg. As can be seen from the reactions above, there can be positive, negative or no charge. The pH at which there is no charge is called isoelectric point and for carbonate it is around 8-9. Because the actual pH of the aqueous phase in the reservoir is less than 8, the equilibrium of the above reactions is disturbed. Reaction (4) is the most dominant and it moves to the right at lower pH values, resulting in a positive charge on the carbonate surface (Van Cappellen et al. 1993; Pokrovsky et al. 1998).

It is important to emphasize that the surface of carbonate has a positive charge as well as negative, but the positive one dominates. The surface is illustrated in figure 15 as stated by Mahani et al. (2016a). Polar oil compounds

adsorb on the surface by the electrostatic attraction between oppositely charged oil/surface components (Brady et al. 2012) (figure 16).

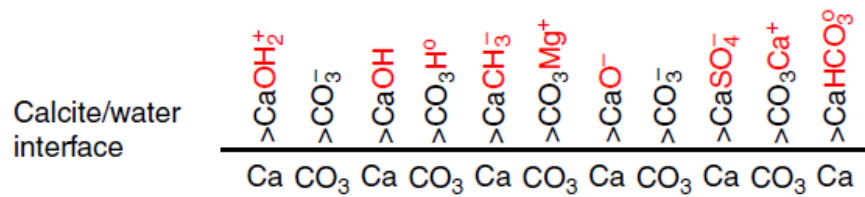


Figure 15: Carbonate surface components and charge (Mahani et al. 2016b)

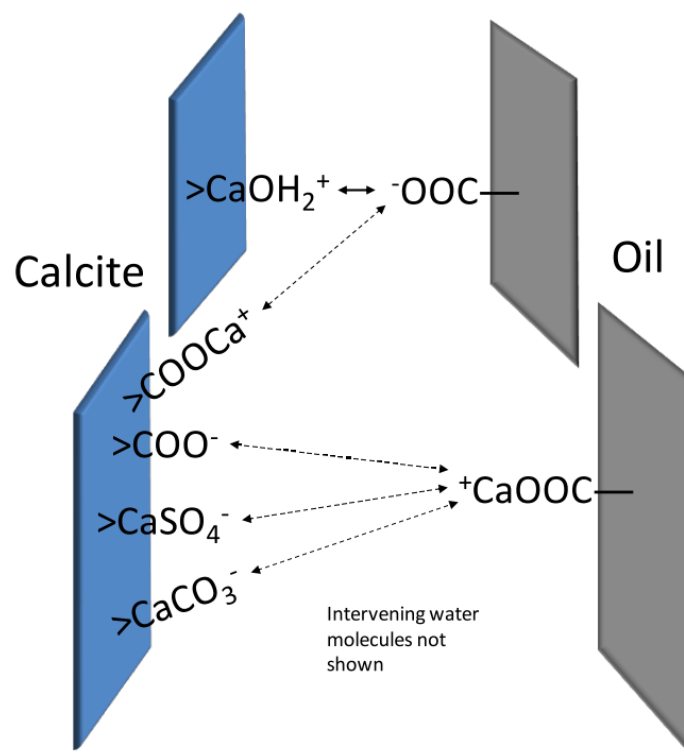


Figure 16: Polar oil adsorption on calcite surface (Brady et al. 2012)

2.4.2 Ionic Exchange

RezaeiDoust et al. (2009) and Standnes, Austad (2003) explained the ionic exchange mechanism in carbonates as shown in figure 17 A (where temperature is less than 70° C) as follows: Oil is attached to $>Ca^+$ (that is on the surface). It forms

$[>Ca^+ \text{RCOO}]$. SO_4^{2-} concentration is increased in the injected water. As SO_4^{2-} approaches the carbonate surface and reaches closer to the $>Ca^+$, it adds a negative charge on the carbonate surface. This negative charge attracts Ca^{2+} , which is also injected with the water. As the injected Ca^{2+} reaches the negative charge (caused by SO_4^{2-}) it repulses with $>Ca^+$. The repulsion results in $[Ca^{2+} \text{RCOO}]$ to depart the surface.

In figure 17 B (where temperature is greater than $70^\circ C$) the mechanism is as follows: Oil is attached to $>Ca^+$ (that is on the surface), where it forms $[>Ca^+ \text{RCOO}]$. As SO_4^{2-} approaches the carbonate surface and closer to the $>Ca^+$, it adds a negative charge on the carbonate surface. This negative charge attracts Mg^{2+} that is added in the injection water. At high temperatures, Mg^{2+} is able to replace Ca^{2+} . As Mg^{2+} attaches to the surface, Ca^{2+} departs along with the oil as $[Ca^{2+} \text{RCOO}]$. Another advantage for the reactions at this temperature is that it prevents the interaction of Ca^{2+} with SO_4^{2-} to form $CaSO_4$ because Mg^{2+} replaces Ca^{2+} at high temperatures.

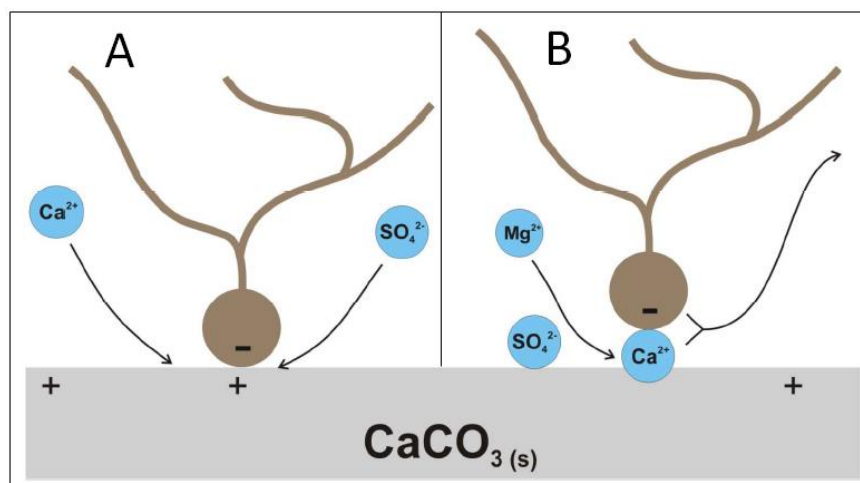


Figure 17: Ion exchange to desorb oil from the carbonate surface (RezaeiDoust et al. 2009)

It is also believed that adding SO_4^{2-} is enough to create a negative surface that can change the wettability to less oil wet. The negative sulphate ion is attracted to the positively charged surface. It encourages repulsion with oil that was originally attached on the surface due to the opposite charges. That results in releasing it from the surface as shown in figure 18 (Austad 2013).

An increase in the negative charge by adding SO_4^{2-} was also observed when measuring zeta potential of a carbonate surface (Mahani et al. 2015b). Zeta potential measures the charge of a surface. Their electrokinetic study illustrated that regardless of the carbonate rock type, zeta potential tends to become more negative as the water salinity is changed from formation water to sea water and diluted sea water but spiked with SO_4^{2-} . They also noticed a more negative surface charge as pH is decreased as shown in figure 19.

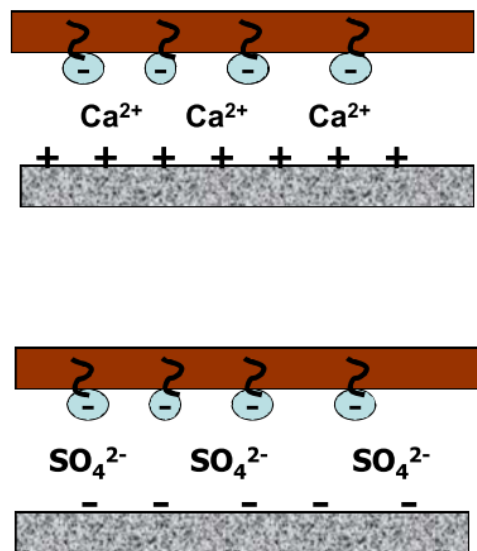


Figure 18: Negative surface charged created by SO_4^{2-} that causes repulsion with the negatively charged oil (Austad 2013)

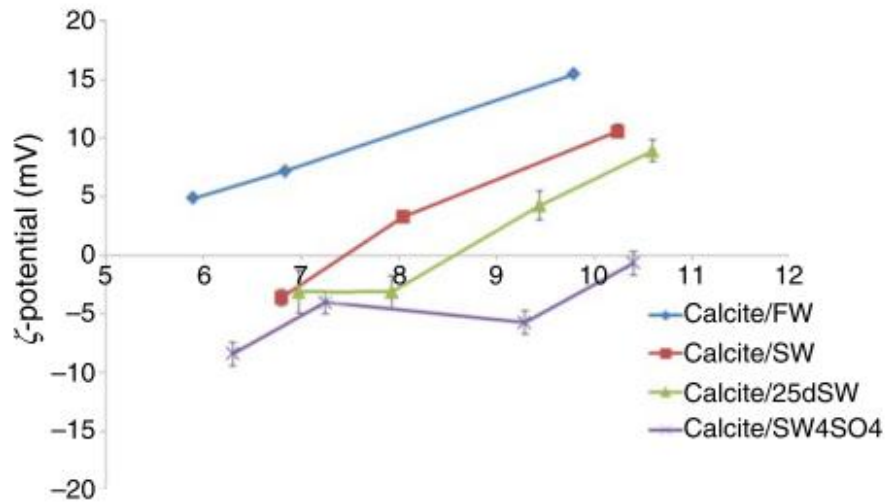


Figure 19: Negative charge increases as pH decreases with different salinities (Mahani et al. 2016b)

2.4.3 Double Layer Expansion

Figure 20 shows that at high concentration of Na^+ and Cl^- (high salinity), the surface of the rock is covered with monovalent ions. This causes difficulty for SO_4^{2-} and Ca^{2+} to penetrate to the calcite surface due to the accumulation of ions on the surface. As the concentration of NaCl is reduced and the double layer expands, SO_4^{2-} and Ca^{2+} find their way to the surface much easier, assisting the ionic exchange process to release oil (Austad 2013).

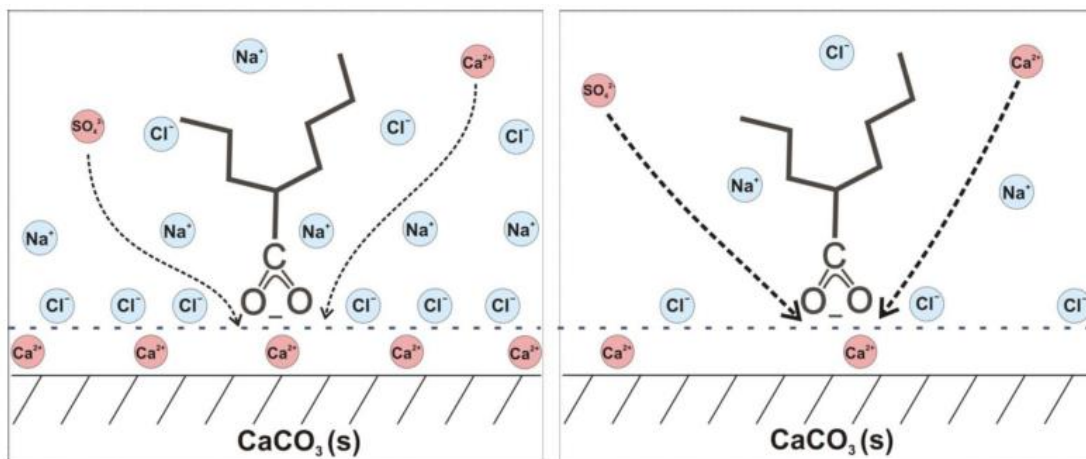
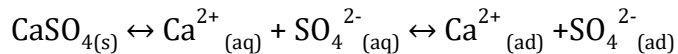


Figure 20: Reducing the ionic strength provides easier path for SO_4^{2-} and Ca^{2+} to penetrate to the surface and exchange ions (Austad 2013)

2.4.4 Anhydrite Dissolution

Anhydrite (CaSO_4) dissolution to enhance oil recovery by low salinity is another mechanism proposed by Austad et al. (2015). Figure 21 shows that high salinity water keeps the following reaction in equilibrium:



$\text{CaSO}_{4(s)}$ (in the rock) does not dissociate because there are enough $\text{Ca}^{2+}_{(aq)}$ and $\text{SO}_4^{2-}_{(aq)}$ in the water phase so the reaction is in equilibrium.

When water salinity is reduced, the reaction equilibrium is disturbed. Therefore, $\text{CaSO}_{4(s)}$ starts to dissociate from the rock in order to reach equilibrium again. That provides SO_4^{2-} to attach on the positive rock surface (as there are still positive sites because not all the rock dissociates). SO_4^{2-} repulses with the negatively charged oil and therefore oil leaves the surface. Also as the rock dissociates, the dissolved parts can take the oil that is attached to them and become mobile (Austad et al. 2015).

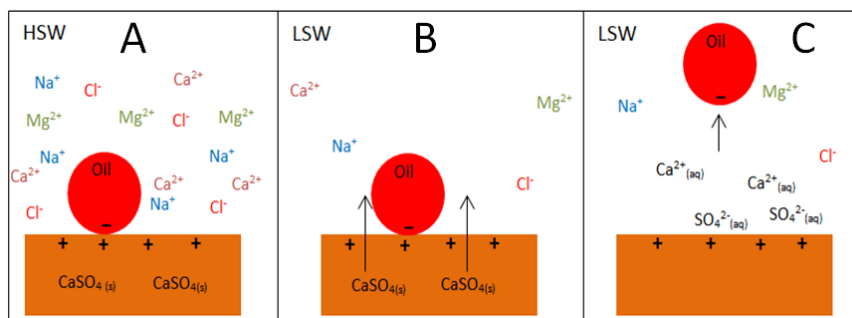


Figure 21: Anhydrite dissolution as a result of low salinity water injection; A) high salinity waterflooding; B) low salinity water injection; C) complete separation of oil from rock surface due to low salinity water injection

2.5 Low Salinity Water Coreflooding

Laboratory coreflooding has been an important tool in the oil and gas industry to test technologies on reservoir (or outcrop) core samples before applying them in the field and to also investigate scientific theories in the laboratory. Oil recovery and relative permeability, which are important parameters for reservoir simulation, can be obtained from coreflooding (Toth et al. 1984; Odeh et al. 1985; Lake et al. 2014). Waerflooding is generally tested by what is called two phase coreflooding, which refers to injecting two different fluids (oil and water) into the core sample. This can take place simultaneously or by displacing one phase that is already saturating the core sample by another (McPhee et al. 2015). Low salinity water coreflooding is done by injecting low concentration of brine into a core sample in either secondary mode (low salinity water displaces the oil that is fully saturating the core in the presence of connate water) or in tertiary mode (low salinity water injection in a core that has already been flooded with high salinity water where residual oil is present) (Hussain et al. 2013, Nasralla et al. 2018).

In this study, a set of necessary criteria were developed not only to perform low salinity coreflooding but to also be applied in conventional coreflooding procedures. This criteria is important to model low salinity waterflooding, and conventional waterflooding in general, in order to obtain accurate relative permeability data to assess the mobility of oil and water in the process of optimising and enhancing oil recovery. Welge-JBN method is one of the most sophisticated techniques that have been applied, since the past century, to calculate relative permeability from laboratory coreflooding (Welge 1952; Johnson et al. 1959; Toth et al. 1984). Therefore, the accuracy of performing

coreflood tests is vital to determine valid relative permeability data. To be able to correctly apply the Welge-JBN method to calculate relative permeability, it is necessary to fulfil the Buckley-Leverett assumption of having negligible capillary pressure in the large scale approximation of Rapoport-Leas system as per the following equation (Rapoport and Leas 1953):

$$\frac{\partial s}{\partial t_D} + \frac{\partial f(s)}{\partial x_D} = \varepsilon_c \frac{\partial}{\partial x_D} \left(-k_{ro}(s) f(s) J'(s) \frac{\partial s}{\partial x_D} \right)$$

Where s is the saturation, f is fractional flow, x_D is the dimensionless distance, t_D is the dimensionless time, ε_c is the capillary-viscous ratio, k_{ro} is the oil relative permeability, J' is derivative of the capillary function.

(Note: the full derivation of the model to calculate relative permeability is presented in the paper 'Admissible Parameters for Two-Phase Coreflood and Welge-JBN Method' in chapter 3)

In Buckley-Leverett solution, the above equation reduces to (Buckley and Leverett 1942):

$$\frac{\partial s}{\partial t_D} + \frac{\partial f(s)}{\partial x_D} = 0$$

This can be achieved when the capillary-viscous ratio (ε_c), which measures the dominance of capillary forces over the viscous forces, is considerably small. Core length and displacing velocity play a big role in determining the capillary-viscous ratio according to the following equation (Bedrikovetsky 2013):

$$\varepsilon_c = \frac{\sigma \sqrt{k \phi}}{\mu_o L U}$$

Where σ is the interfacial tension, k is the permeability, ϕ is the porosity, μ_o is the oil viscosity, L is the core length, and U is the displacing velocity. This relationship can be applied to determine the minimum flow rate used in a coreflood for any core length.

Capillary number ($N_c = \frac{U \mu_w}{\sigma}$) (Bedrikovetsky 2013), on the other hand, can be used to determine the maximum flow rate in a coreflood. Those two criteria, as well as other operational criteria such as number of effluent samples needed to construct the fractional flow have not received attention in the literature and they were developed in this study before applying them to conduct the low salinity coreflooding experiments presented in this thesis.

2.6 Conclusion of the Literature Review

Although the literature review covered the currently known low salinity mechanisms in sandstone and carbonate rocks, this thesis focuses on understanding and determining how exactly fines migration enhances oil production. In previous LSW studies, improved oil recovery was attributed to a combined effect of fines migration and other mechanisms such as ionic exchange because most studies were performed using crude oil and multivalent salt ions. Clay detachment along with the crude oil that is attached to it (due to its polar nature) during LSW is widely explained in the literature as the reason for the fines migration effect on enhancing oil recovery. Micro-scale diversion of water flux has not received much attention.

This study, on the other hand, fills the gap and explains how micro-scale flux diversion is a major reason for the improved sweep efficiency during LSW by isolating fines migration from other mechanisms with the use of non-polar oil

and monovalent salt ions that induce clay detachment at low brine concentration. In addition, fines migration is perceived as detrimental as it can cause formation damage in the field and, thus, it is not used as an enhanced oil recovery method. In this research, it is shown that fines migration can improve oil recovery in some experiments without detrimental and complete formation damage.

Divalent ions, such as calcium, have been used in low salinity waterflooding where less clay particles detachment was observed. In this study, this phenomenon is applied to stabilise fines migration when monovalent and divalent ions are alternated to enhance oil recovery, which has not been discussed in the literature. In this research, a strong hysteretic behaviour of mutual adsorption-desorption of Ca and Na ions is observed, which has not been explained in the literature previously.

In addition, criteria of laboratory coreflooding to accurately determine relative permeability using Welge-JBN method have not been discussed in literature. In this work, the admissible parameters required for this method were developed, not only for the low salinity coreflooding but for conventional laboratory waterflooding tests. This includes two theoretical criteria namely capillary-viscous ratio and capillary number; and four operational criteria which are precision of pressure measurement, effluent sampling period, minimum number of samples for the fractional flow curve, and precision of water-cut measurements.

As can be seen from the literature review, the objectives of this thesis have not been met, despite the valuable research that has been done in this area so far.

2.7 References

- Aksulu, H., Håmsø, D., Strand, S., Puntervold, T., Austad, T.: Evaluation of Low-Salinity Enhanced Oil Recovery Effects in Sandstone: Effects of the Temperature and pH Gradient. *Energy Fuels* **26**(6), 3497-3503 (2012). doi:10.1021/ef300162n
- Al-Shalabi, E.W., Sepehrnoori, K.: A comprehensive review of low salinity/engineered water injections and their applications in sandstone and carbonate rocks. *J. Pet. Sci. Eng.* **139**, 137-161 (2016)
- Al Shalabi, E.W., Sepehrnoori, K., Delshad, M.: Mechanisms behind low salinity water injection in carbonate reservoirs. *Fuel* **121**, 11-19 (2014)
- Austad, T.: Water-Based EOR in Carbonates and Sandstones: New Chemical Understanding of the EOR Potential Using Smart Water. *Enhanced Oil Recovery Field Case Studies*, 301-335 (2013)
- Austad, T., Rezaeidoust, A., Puntervold, T.: Chemical Mechanism of Low Salinity Water Flooding in Sandstone Reservoirs, 2010/1/1/
- Austad, T., Shariatpanahi, S.F., Strand, S., Aksulu, H., Puntervold, T.: Low Salinity EOR Effects in Limestone Reservoir Cores Containing Anhydrite: A Discussion of the Chemical Mechanism. *Energy Fuels* **29**(11), 6903-6911 (2015)
- Barenblatt, G., Entov, V., Ryzhik, V.: Theory of Fluid Flows through Natural Rocks. In. Kluwer, (1991)
- Bedrikovetsky, P., Siqueira, F.D., Furtado, C.A., Souza, A.L.S.: Modified particle detachment model for colloidal transport in porous media. *Trans. Porous Media* **86**(2), 353-383 (2011)
- Bedrikovetsky, P.: Mathematical theory of oil and gas recovery: with applications to ex-USSR oil and gas fields, vol. 4. Springer Science & Business Media, (2013)
- Berg, S., A. W. Cense, E. Jansen and K. Bakker: Direct Experimental Evidence of Wettability Modification by Low Salinity Petrophysics **51**(5), 314-322 (2010)
- Borazjani, S., Behr, A., Genolet, L., Kowollik, P., Bedrikovetsky, P.: Ion-Exchange Inverse Problem for Low-Salinity Coreflooding. *Trans. Porous Media* **128**(2), 571-611 (2019)
- Brady, P.V., Krumhansl, J.L.: A surface complexation model of oil-brine-sandstone interfaces at 100° C: Low salinity waterflooding. *J. Pet. Sci. Eng.* **81**, 171-176 (2012)
- Brady, P.V., Krumhansl, J.L., Mariner, P.E.: Surface Complexation Modeling for Improved Oil Recovery, 2012/1/1/
- Brady, P.V., Morrow, N.R., Fogden, A., Deniz, V., Loahardjo, N., Winoto: Electrostatics and the Low Salinity Effect in Sandstone Reservoirs. *Energy & Fuels* **29**(2), 666-677 (2015). doi:10.1021/ef502474a
- Buckley, S.E., Leverett, M.: Mechanism of fluid displacement in sands. *Transactions of the AIME* **146**(01), 107-116 (1942)
- Burgos, W.D., Pisutpaisal, N., Mazzarese, M.C., Chorover, J.: Adsorption of quinoline to kaolinite and montmorillonite. *Environmental engineering science* **19**(2), 59-68 (2002)
- Cao, J., James, L.A., Johansen, T.E.: Determination of two phase relative permeability from core floods with constant pressure boundaries. In: Society of Core Analysis Symposium, Avignon, France 2014
- Cao, J., Liu, X., James, L., Johansen, T.: Analytical Interpretation Methods for Dynamic Immiscible Core Flooding at Constant Differential Pressure. In: Society of Core Analysis Symposium, St. John's Newfoundland and Labrador, Canada 2015, pp. 16-21
- Chen, X., Kianinejad, A., DiCarlo, D.A.: An extended JBN method of determining unsteady-state two-phase relative permeability. *Water Resources Research* **52**(10), 8374-8383 (2016)
- Civan, F., Donaldson, E.: Relative permeability from unsteady-state displacements with capillary pressure included. *SPE Form. Eval.* **4**(02), 189-193 (1989)
- Cotterill, S.: Low Salinity Effects on Oil Recovery. (2014)
- De Velde Harsenhorst, R.: Electrokinetics in Low Salinity Waterflooding. TU Delft, Delft University of Technology (2014)
- Dos Santos, R.L., Bedrikovetsky, P., Holleben, C.R.: Optimal Design and Planning for Laboratory Corefloods. In: Latin American and Caribbean Petroleum Engineering Conference 1997. Society of Petroleum Engineers
- Fernø, M.A., Grønnsdal, R., Åsheim, J., Nyheim, A., Berge, M., Graue, A.: Use of Sulfate for Water Based Enhanced Oil Recovery during Spontaneous Imbibition in Chalk. *Energy Fuels* **25**(4), 1697-1706 (2011). doi:10.1021/ef200136w
- Fogden, A., Kumar, M., Morrow, N.R., Buckley, J.S.: Mobilization of Fine Particles during Flooding of Sandstones and Possible Relations to Enhanced Oil Recovery. *Energy Fuels* **25**(4), 1605-1616 (2011). doi:10.1021/ef101572n

- Fredriksen, S.B., Rognmo, A.U., Fernø, M.A.: Pore-Scale Mechanisms During Low Salinity Waterflooding: Water Diffusion and Osmosis for Oil Mobilization, 2016/4/20/
- Fritz, S.J., Marine, I.W.: Experimental support for a predictive osmotic model of clay membranes. *Geochimica et Cosmochimica Acta* **47**(8), 1515-1522 (1983)
- Hassenkam, T., Andersson, M., Hilner, E., Matthiesen, J., Dobberschutz, S., Dalby, K.N., Bovet, N., Stipp, S.L.S., Salino, P., Reddick, C.: A fast alternative to core plug tests for optimising injection water salinity for EOR. In: SPE Improved Oil Recovery Symposium 2014. Society of Petroleum Engineers
- Hughes, D., Larsen, S., Wright, R.: Review of Low Salinity Water Flooding. Department of Energy and Climate Change, 1-33 (2010)
- Hussain, F., Cinar, Y., Bedrikovetsky, P.G.: Comparison of methods for drainage relative permeability estimation from displacement tests. In: SPE improved oil recovery symposium 2010. Society of Petroleum Engineers
- Hussain, F., Zeinijahromi, A., Bedrikovetsky, P., Badalyan, A., Carageorgos, T., Cinar, Y.: An experimental study of improved oil recovery through fines-assisted waterflooding. *J. Pet. Sci. Eng.* **109**, 187-197 (2013)
- Israelachvili, J.N.: Intermolecular and surface forces: revised third edition. Academic press, (2011)
- Johansen, T.E., James, L.A.: Solution of multi-component, two-phase Riemann problems with constant pressure boundaries. *Journal of Engineering Mathematics* **96**(1), 23-35 (2016)
- Johnson, E., Bossler, D., Bossler, V.: Calculation of relative permeability from displacement experiments. (1959)
- Jones, S., Roszelle, W.: Graphical techniques for determining relative permeability from displacement experiments. *J. Pet. Technol.* **30**(05), 807-817 (1978)
- Khilar, K.C., Fogler, H.S.: Migrations of fines in porous media, vol. 12. Springer Science & Business Media, (1998)
- Khilar, K.C., Fogler, H.S., Ahluwalia, J.: Sandstone water sensitivity: existence of a critical rate of salinity decrease for particle capture. *Chem. Eng. Sci.* **38**(5), 789-800 (1983)
- Kianinejad, A., Chen, X., DiCarlo, D.A.: Direct measurement of relative permeability in rocks from unsteady-state saturation profiles. *Advances in water resources* **94**, 1-10 (2016)
- Lager, A., Webb, K., Black, C., Singleton, M., Sorbie, K.: Low Salinity Oil Recovery-An Experimental Investigation. *Petrophysics* **49** (2008a)
- Lager, A., Webb, K.J., Collins, I.R., Richmond, D.M.: LoSal Enhanced Oil Recovery: Evidence of Enhanced Oil Recovery at the Reservoir Scale, 2008/1/1/
- Lake, L.W., Johns, R., Rossen, W.R., Pope, G.A.: Fundamentals of enhanced oil recovery. (2014)
- Lever, A., Dawe, R.A.: Water-sensitivity and migration of fines in the hopeman sandstone. *J. Pet. Geo.* **7**(1), 97-107 (1984)
- Ligthelm, D.J., Gronsveld, J., Hofman, J., Brussee, N., Marcelis, F., van der Linde, H.: Novel Waterflooding Strategy By Manipulation Of Injection Brine Composition, 2009/1/1/
- Liu, Q., Dong, M., Asghari, K., Tu, Y.: Wettability alteration by magnesium ion binding in heavy oil/brine/chemical/sand systems—Analysis of electrostatic forces. *J. Pet. Sci. Eng.* **59**(1), 147-156 (2007)
- Mahani, H., Berg, S., Ilic, D., Bartels, W.-B., Joekar-Niasar, V.: Kinetics of low-salinity-flooding effect. *SPE J* **20**(01), 8-20 (2015a)
- Mahani, H., Keya, A.L., Berg, S., Bartels, W.-B., Nasralla, R., Rossen, W.R.: Insights into the Mechanism of Wettability Alteration by Low-Salinity Flooding (LSF) in Carbonates. *Energy Fuels* **29**(3), 1352-1367 (2015b). doi:10.1021/ef5023847
- Mahani, H., Keya, A.L., Berg, S., Nasralla, R.: Electrokinetics of Carbonate/Brine Interface in Low-Salinity Waterflooding: Effect of Brine Salinity, Composition, Rock Type, and pH on ζ -Potential and a Surface-Complexation Model. (2016a). doi:10.2118/181745-PA
- Mahani, H., Keya, A.L., Berg, S., Nasralla, R.: Electrokinetics of Carbonate/Brine Interface in Low-Salinity Waterflooding: Effect of Brine Salinity, Composition, Rock Type, and pH on ζ -Potential and a Surface-Complexation Model. *SPE J* (2016b)
- McPhee, C., Reed, J., Zubizarreta, I.: Core Analysis: A Best Practice Guide, vol. 64. Elsevier, (2015)
- Miller, M.A., Ramey Jr, H.: Effect of temperature on oil/water relative permeabilities of unconsolidated and consolidated sands. *Society of Petroleum Engineers Journal* **25**(06), 945-953 (1985)
- Morrow, N., Buckley, J.: Improved oil recovery by low-salinity waterflooding. *J. Pet. Technol.* **63**(05), 106-112 (2011)
- Myint, P.C., Firoozabadi, A.: Thin liquid films in improved oil recovery from low-salinity brine. *Current Opinion in Colloid & Interface Science* **20**(2), 105-114 (2015). doi:10.1016/j.cocis.2015.03.002

- Nasralla, R.A., Nasr-El-Din, H.A.: Impact of Electrical Surface Charges and Cation Exchange on Oil Recovery by Low Salinity Water, 2011/1/1
- Nasralla, R.A., Mahani, H., van der Linde, H.A., Marcelis, F.H., Masalmeh, S.K., Sergienko, E., Brussee, N.J., Pieterse, S.G., Basu, S.: Low Salinity Waterflooding for a carbonate reservoir: Experimental evaluation and numerical interpretation. *J. Pet. Sci. Eng.* **164**, 640-654 (2018)
- Odeh, A., Dotson, B.: A method for reducing the rate effect on oil and water relative permeabilities calculated from dynamic displacement data. *J. Pet. Technol.* **37**(11), 2,051-052,058 (1985)
- Pevear, D., Eslinger, E.: Clay minerals for petroleum geologists and engineers. SEPM Tulsa, OK (1988)
- Pokrovsky, O., Schott, J., Thomas, F., Mielczarski, J.: Surface speciation of Ca and Mg carbonate minerals in aqueous solutions: A combined potentiometric, electrokinetic, and DRIFT surface spectroscopy approach. *Min. Mag. A* **62**, 1196-1197 (1998)
- Qiao, C., Johns, R., Li, L.: Modeling low-salinity waterflooding in chalk and limestone reservoirs. *Energy Fuels* **30**(2), 884-895 (2016)
- Rapoport, L., Leas, W.: Properties of linear waterfloods. *J. Pet. Technol.* **5**(05), 139-148 (1953)
- RezaeiDoust, A., Puntervold, T., Austad, T.: Chemical Verification of the EOR Mechanism by Using Low Saline/Smart Water in Sandstone. *Energy Fuels* **25**(5), 2151-2162 (2011). doi:10.1021/ef200215y
- RezaeiDoust, A., Puntervold, T., Strand, S., Austad, T.: Smart Water as Wettability Modifier in Carbonate and Sandstone: A Discussion of Similarities/Differences in the Chemical Mechanisms. *Energy Fuels* **23**(9), 4479-4485 (2009). doi:10.1021/ef900185q
- Sandengen, K., Kristoffersen, A., Melhuus, K., Jøsang, L.O.: Osmosis as Mechanism for Low-Salinity Enhanced Oil Recovery. (2016). doi:10.2118/179741-PA
- Sarkar, A.K., Sharma, M.M.: Fines migration in two-phase flow. *J. Pet. Technol.* **42**(05), 646-652 (1990)
- Schmid, K., Gross, J., Helmig, R.: Chemical osmosis in two-phase flow and salinity-dependent capillary pressures in rocks with microporosity. *Water Resources Research* **50**(2), 763-789 (2014)
- Sheng, J.J.: Critical review of low-salinity waterflooding. *J. Pet. Sci. Eng.* **120**, 216-224 (2014). doi:10.1016/j.petrol.2014.05.026
- Sohrabi, M., Mahzari, P., Farzaneh, S., Mills, J., Tsois, P., Ireland, S.: Novel insights into mechanisms of oil recovery by low salinity water injection. In: SPE Middle East Oil & Gas Show and Conference 2015. Society of Petroleum Engineers
- Sparks, D.L.: Environmental soil chemistry. Academic press, (2003)
- Standnes, D.C., Austad, T.: Wettability alteration in carbonates: Interaction between cationic surfactant and carboxylates as a key factor in wettability alteration from oil-wet to water-wet conditions. *Colloids and Surfaces A: Physicochemical and Engineering Aspects* **216**(1), 243-259 (2003)
- Tao, T., Watson, A.: Accuracy of JBN estimates of relative permeability: part 2-algorithms. *Society of Petroleum Engineers Journal* **24**(02), 215-223 (1984)
- Toth, J., Bodi, T., Szucs, P., Civan, F.: Direct determination of relative permeability from nonsteady-state constant pressure and rate displacements. In: SPE Production and Operations Symposium 2001. Society of Petroleum Engineers
- Valdya, R., Fogler, H.: Fines migration and formation damage: influence of pH and ion exchange. *SPE production engineering* **7**(04), 325-330 (1992)
- Van Cappellen, P., Charlet, L., Stumm, W., Wersin, P.: A surface complexation model of the carbonate mineral-aqueous solution interface. *Geochimica et Cosmochimica Acta* **57**(15), 3505-3518 (1993)
- Velde, B.B., Meunier, A.: The origin of clay minerals in soils and weathered rocks. Springer Science & Business Media, (2008)
- Wang, X., Lee, S.Y., Miller, K., Welbourn, R., Stocker, I., Clarke, S., Casford, M., Gutfreund, P., Skoda, M.W.: Cation bridging studied by specular neutron reflection. *Langmuir : the ACS journal of surfaces and colloids* **29**(18), 5520-5527 (2013). doi:10.1021/la400767u
- Welge, H.J.: A simplified method for computing oil recovery by gas or water drive. *J. Pet. Technol.* **4**(04), 91-98 (1952)
- Zeinijahromi, A., Farajzadeh, R., Bruining, J.H., Bedrikovetsky, P.: Effect of fines migration on oil-water relative permeability during two-phase flow in porous media. *Fuel* **176**, 222-236 (2016)
- Zeinijahromi, A., Lemon, P., Bedrikovetsky, P.: Effects of induced fines migration on water cut during waterflooding. *J. Pet. Sci. Eng.* **78**(3-4), 609-617 (2011)

- Zeinjahromi, A., Vaz, A., Bedrikovetsky, P.: Well impairment by fines migration in gas fields. *J. Pet. Sci. Eng.* **88**, 125-135 (2012)
- Zhang, Y., Morrow, N.R.: Comparison of secondary and tertiary recovery with change in injection brine composition for crude-oil/sandstone combinations. In: *SPE/DOE Symposium on Improved Oil Recovery 2006*. Society of Petroleum Engineers
- Zou, S., Hussain, F., Arns, J.-y., Guo, Z., Arns, C.H.: Computation of Relative Permeability From In-Situ Imaged Fluid Distributions at the Pore Scale. *SPE J* **23**(03), 737-749 (2018)

3 Admissible Parameters for Two-Phase Coreflood and Welge-JBN Method

This chapter presents two papers on the developed criteria for the Welge-JBN method to obtain relative permeability. The admissible parameters developed in this study are applied to conduct the coreflood experiments presented in Chapters 4 and 5.

The paper 'Admissible Parameters for Two-Phase Coreflood and Welge-JBN Method' in section 3.1 has a comprehensive study that explains the theoretical details of the criteria thoroughly with three coreflood tests that differ in oil viscosity and core length. The paper 'Coreflood Planning Criteria for Relative Permeability Computation by Welge-JBN Method' in section 3.2 is a peer-reviewed extended abstract and it presents the criteria briefly with one laboratory coreflood results where the criteria was applied. It was written at the early stage of the criteria development and, therefore, the paper in sections 3.1 is more comprehensive and thorough of this particular study. The order of the papers in the chapter is based on the quantity of work done in each paper.

3.1 Admissible Parameters for Two-Phase Coreflood and Welge-JBN Method

Al-Sarhi, A., You, Z., Genolet, L., Behr, A., Kowollik, P., Zeinjahromi, A., and Bedrikovetsky, P., published 11/2019

Journal of Transport in Porous Media

Statement of Authorship

Title of Paper	Admissible parameters for two-phase corefood and Welge-JBN method
Publication Status	<input type="checkbox"/> Published <input type="checkbox"/> Accepted for Publication <input checked="" type="checkbox"/> Submitted for Publication <input type="checkbox"/> Unpublished and Unsubmitted work written in manuscript style
Publication Details	A. Al-Sarhi, Z. You, L. Genolet, A. Behr, P. Kowolik, A. Zeinjahromi, and P. Bedrikovetsky, Admissible parameters for two-phase corefood and Welge-JBN method, Journal of Transport in Porous Media

Principal Author

Name of Principal Author (Candidate)	Abdullah Al-Sarhi		
Contribution to the Paper	Literature review, experimental work, analysis of results, writing the manuscript.		
Overall percentage (%)	70%		
Certification:	This paper reports on original research I conducted during the period of my Higher Degree by Research candidature and is not subject to any obligations or contractual agreements with a third party that would constrain its inclusion in this thesis. I am the primary author of this paper.		
Signature		Date	17/9/2019

Co-Author Contributions

By signing the Statement of Authorship, each author certifies that:

- i. the candidate's stated contribution to the publication is accurate (as detailed above);
- ii. permission is granted for the candidate to include the publication in the thesis; and
- iii. the sum of all co-author contributions is equal to 100% less the candidate's stated contribution.

Name of Co-Author	Zhenjiang You		
Contribution to the Paper	Numerical simulation, review of manuscript		
Signature		Date	12/9/19

Name of Co-Author	Luis Genolet		
Contribution to the Paper	Support in analysis of results		
Signature		Date	10.09.2019

Please cut and paste additional co-author panels here as required.

Name of Co-Author	Aron Behr		
Contribution to the Paper	Support in analysis of results		
Signature		Date	11/9/19

Name of Co-Author	Patrick Kowolik		
Contribution to the Paper	Support in analysis of results		
Signature		Date	10/9/19

Name of Co-Author	Abbas Zeinijahromi		
Contribution to the Paper	Model formulation, review manuscript		
Signature		Date	17/09/19

Name of Co-Author	Pavel Bedrkiovetsky		
Contribution to the Paper	Model formulation, review of manuscript		
Signature		Date	17/09/19



Admissible Parameters for Two-Phase Coreflood and Welge–JBN Method

A. Al-Sarhi¹ · Z. You³ · A. Behr² · L. Genolet² · P. Kowollik² · A. Zeinijahromi¹ · P. Bedrikovetsky¹

Received: 28 March 2019 / Accepted: 8 November 2019
© Springer Nature B.V. 2019

Abstract

The Welge–JBN method for determining relative permeability from unsteady-state waterflood test is commonly used for two-phase flows in porous media. We discuss the theoretical criteria that limits application of the basic Buckley–Leverett model and Welge–JBN method and the operational criteria of the accuracy of measurements during core waterflood tests. The objective is determination of the waterflood test parameters (core length, flow velocity and effluent sampling frequency) that fulfil the theoretical and operational criteria. The overall set of criteria results in five inequalities in three-dimensional Euclidian space of these parameters. For known rock and fluid properties, a formula for minimum core length to fulfil Welge–JBN criteria is derived. For cases where the core length is given, formulae for test's flow velocity and sampling period are provided to satisfy the test admissibility conditions. The application of the proposed methodology is illustrated by two coreflood tests.

Keywords Relative permeability · Two-phase flow · Welge–JBN method · Coreflood parameters · Mathematical model · Laboratory waterflooding test

List of Symbols

f_k	Fractional flow during steady-state
f_{\min}	Minimum measured value of fractional flow
J	Capillary J -function
k	Permeability (m^2)
K_r	Relative permeability
K_{rowi}	Relative permeability of oil at initial water saturation
K_{rwor}	Relative permeability of water at residual oil saturation
L	Core length (m)
l_g	Oil ganglion length (m)
N_c	Capillary number

✉ P. Bedrikovetsky
pavel.bedrikovetski@adelaide.edu.au

¹ Australian School of Petroleum, The University of Adelaide, Adelaide 5000, Australia

² Wintershall Holding GmbH, EOT/R, Friedrich-Ebert Str. 160, 34119 Kassel, Germany

³ The University of Queensland, Brisbane, QLD 4072, Australia

N_{\min}	Minimum number of samples
n_o	Corey's oil exponent
n_w	Corey's water exponent
P_c	Capillary pressure (Pa)
p	Pressure (Pa)
p_{\min}	Minimum measured pressure (Pa)
P	Dimensionless pressure
q_w	Water mass rate per unit area for linear flow ($\text{kg}/\text{m}^2 \text{ s}$)
R	Radius (m)
r	Pore throat radius
s	Water saturation
t	Time
s_f	Frontal saturation during waterflooding
S_{or}	Residual oil saturation
S_{wi}	Connate water saturation
U	Velocity
V_{\min}	Minimum distinguishable volume
x	Distance (m)
x_D	Dimensionless distance

Greek Letters

ε_c	Capillary–viscous ratio
ε_w	Water-cut measurement accuracy
ε_p	Pressure drop accuracy
ε_s	Sampling period accuracy
Δt	Sampling period
σ	Interfacial tension (N/m)
ϕ	Porosity
μ	Viscosity (Pa s)
ρ	Density (kg/m^3)
σ	Interfacial tension (N/m)
θ	Macroscopic contact angle
λ	Total mobility
ξ	Self-similar coordinate

Subscripts

c	Capillary
m	Maximum for velocity and for core length at maximum velocity
min	Minimum
w	Water
o	Oil
i	Initial
D	Dimensionless

Abbreviations

BL	Buckley–Leverett
BTC	Breakthrough curve
PDC	Pressure drop curve

RL	Rapoport–Leas
SS	Steady-state
USS	Unsteady-state

1 Introduction

Relative phase permeabilities are the main functions that determine oil recovery. At the core scale, these functions are empirical and are determined from laboratory waterflooding of the cores. The Welge–JBN method is used to determine relative permeabilities from the coreflood data (Welge 1952; Johnson et al. 1959; Jones and Roszelle 1978). The advantage of this method is that it allows determining relative permeability for a wide range of saturations during a single displacement of gas/oil by water.

Currently, petroleum industry and research widely use the Welge–JBN method for determining relative permeability in artificial and natural reservoir cores, for oil–water and gas–water fluids (Cao et al. 2014; Abbas 2016; Chen et al. 2016; Kianinejad et al. 2016). Civan and Donaldson (1989) and Toth et al. (2001, 2002) suggested exponential approximation of water-cut curve after the production of the transition zone, in order to perform the Welge–JBN calculations. Miller and Ramey Jr (1985) proposed polynomial approximation. Based on analytical model by Johansen and James (2016), Cao et al. (2014, 2015) presented an analytical interpretation method of JBN data, which eliminates the need of using numerical differentiation and, therefore, reduces the overall numerical error. Promising recent developments of JBN include measurements of rates and pressure in intermediate core point (Chen et al. 2016) and using gravity drainage in vertical core (Kianinejad et al. 2016).

The alternative to the Welge–JBN method is regularisation of the inverse solution by using the minimisation algorithm for a least-squares objective function (Sigmund and McCaffery 1979; Richmond and Watsons 1990). Both methods can be combined with the upscaling results from the sub-core scale (Arns et al. 2003; Adler 1995, 2013; Hussain et al. 2014; Zou et al. 2018; Rabinovich 2017, 2018; Arns and Adler 2018).

However, applications of the Welge–JBN method are restricted—the coreflood parameters (core length and flow rate) must fulfil the validity conditions of Buckley–Leverett (BL) model, which originates the Welge–JBN method (Barenblatt et al. 1991; Lake et al. 2014). Besides, the coreflood parameters must duplicate the operational conditions of precise measurements of oil and water rates and pressure drop across the core during the test (Torsæter and Abtahi 2003; Badalyan et al. 2012; McPhee et al. 2015). These theoretical and operational criteria are fundamental to the planning and designing of the laboratory coreflood test.

The *theoretical criterion* to ensure that the residual oil saturation is independent of the flow velocity is (Barenblatt et al. 1991; Lake et al. 2014):

$$N_c = \frac{U \mu_w}{\sigma} \leq 10^{-5} \sim 10^{-4} \quad (1)$$

where N_c is the capillary number; U is the velocity, μ_w is the water viscosity and σ is the interfacial tension. However, the overall relative permeability curves can be velocity dependent even at lower bound $N_c = 10^{-5}$ (Odeh and Dotson 1985; Rabinovich 2018). Therefore, the recommended velocity for determining relative permeability is the reservoir velocity (Dake 1983). The criterion (1) corresponds to the dominance of capillary pressure

over the viscous pressure drop at the pore scale. In Sect. 2.3 we derive this criterion from the condition of oil droplet immobility in the pore loop under typical reservoir velocities.

The N_c interval given by Eq. (1) is more typical for water-wet systems, which are the focus of this work. The alternative estimates for oil-wet and mixed-wet rocks are presented further in Sect. 6.

Another theoretical criterion is negligible capillary pressure if compared with the pressure drop across the core (Barenblatt et al. 1991; Bedrikovetsky 2013):

$$\varepsilon_c = \frac{\sigma \sqrt{k \phi}}{\mu_o L U} \ll 1 \quad (2)$$

Here ε_c is the capillary–viscous ratio, k is the permeability, ϕ is the porosity, and L is the core length. Core length L enters denominator of the ratio (2), so the assumption restricts application of the Welge–JBN method in short cores (Barenblatt et al. 1991; Adler 1995; Honarpour et al. 1986).

The *operational criteria* include precision of measurements for pressure, sample volume for each phase and the necessary number of samples taken during one pore volume injected (PVI) (Honarpour et al. 1986; Torsæter and Abtahi 2003; Badalyan et al. 2012; McPhee et al. 2015; Rabinovich 2017).

The objective of this study is determination of operational parameters for laboratory waterflood test that determine the relative permeability; the parameters must fulfil the theoretical criteria for application of Welge–JBN methods and the operational criteria for the precise measurements.

The laboratory corefloods must simultaneously fulfil all the theoretical and operational criteria. The laboratory waterflood planning based on the system of inequalities for theoretical and operational criteria was attempted by Dos Santos et al. (1997). That paper considered the theoretical criteria and the operational criteria for pressure measurement precision, minimum sampling time and minimum volume for produced fluid. However, the required number of samples during 1 PVI and the precision of water-cut measurements had not been considered. Hussain et al. (2010, 2012, 2013) followed the methodology proposed by Dos Santos et al. (1997) but suggested that it is impossible to satisfy all the criteria simultaneously.

The theoretical and operational criteria are mutually dependent, i.e. they form a system of inequalities. For example, the flow rate that is high enough to be measured with necessary accuracy provides small capillary–viscous ratio (2) that contradicts the capillary number condition (1). Small flow rate may cause small sample volume and low pressure drop that contradicts the measurement precision conditions. An injection rate can be increased for large sample period, which decreases the number of points taken during one PVI. As a result, the coreflood parameters must fulfil a system of inequalities for theoretical and operational criteria. In a multidimensional space of coreflood parameters, each criterion provides a domain given by an inequality. Each test parameter point that falls into the intersection of all domains provides flow rate, core length and sampling frequency where all the criteria are fulfilled. Determination of laboratory waterflood parameters fulfilling the theoretical and operational criteria is *not available*.

The present paper accounts for a system of two theoretical and four operational criteria for laboratory waterflooding. The solution of system of six inequalities determines a 3D domain in the space of velocity, rate and sampling period where all theoretical and operational criteria are fulfilled. It was discovered that if the capillary–viscous ratio does

not exceed 0.3–0.5, the effect of capillary pressure on relative permeability determined by the Welge–JBN method can be neglected. In addition, the results showed that the minimum core length, which satisfies six criteria, is fully determined by two theoretical criteria. Besides, the pressure precision criterion is weaker than capillary–viscous ratio criterion for the common coreflood conditions and, therefore, can be neglected. For practical planning of two-phase coreflooding, the system of six inequalities defines the core length, flow rate and sampling period.

The structure of the paper is as follows. Section 2 presents BL model for one-dimensional (1D) waterflooding as well as *two* consequent theoretical criteria of capillary number and capillary–viscous ratio; the detailed mathematical derivations are present in “Appendixes A–E”. Section 3 derives *four* operational criteria of the measurements precision during coreflooding. Section 4 formulates the combined system of *six* inequalities for theoretical and operational criteria and describes the corresponding domain in three-dimensional space of velocity, rate and sampling period. Section 5 presents the laboratory set-up for unsteady-state waterflood test and two examples of planned coreflood based upon the solution of the system of inequalities. Section 6 discusses the applications of the system of inequalities for practical planning and design of corefloods.

2 Criteria for Validity of the Mathematical Model for Two-Phase Immiscible Flow

This section presents the analytical model for waterflooding while neglecting capillary pressure, and an exact solution for inverse problem of determining relative permeability from coreflood data (Sect. 2.1 and “Appendixes A–E”). The inverse solution is then applied to the numerical data from the waterflood model that accounts for capillary pressure, mimicking the coreflood data treatment (Sect. 2.2). Section 2.3 derives the capillary number criterion (1), representing the validity of the relative permeability concept, from the condition of residual oil drop immobility under typical reservoir velocities. Section 2.4 combines two criteria for large-scale approximation of basic equations for two-phase immiscible flow in porous media.

2.1 Analytical Model for 1D Waterflood and Inverse Solutions

The one-dimensional two-phase immiscible displacement of incompressible liquids in porous media is described by the BL system. It consists of equations for volumetric balance for water (A.2), the modified Darcy’s law for the total two-phase flux (A.1) and the expression for capillary pressure (A.4) (Buckley and Leverett 1942; Rapoport and Leas 1953; Lake et al. 2014). The governing Rapoport–Leas (RL) system (A.9, A.10) contains the dimensionless group for capillary–viscous ratio ϵ_c (2, A.8) that is the ratio between the average capillary pressure and the pressure drop across the core at the beginning of the displacement.

In large-scale approximation, where the length scale L is large enough to achieve inequality (2), Eqs. (A.9, A.10) degenerate into Eqs. (B.1, B.2). The 1-D BL solution for the displacement of oil by water is self-similar, i.e. saturation $s(x_D, t_D)$ as an unknown function depends only on one dimensionless group $\xi = x_D/t_D$, $s(x_D, t_D) = s(\xi)$. The solution is given by Eq. (B.4).

The BL solution is the zero-order approximation for the RL system’s (A.9, A.10) solution with respect to small parameter ϵ_c . The first-order approximation is obtained by the method of matched asymptotic expansions (Barenblatt et al. 1991; Bedrikovetsky 2013).

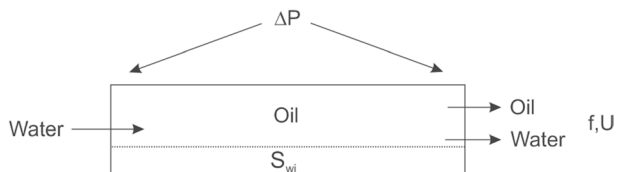
Figure 1 shows the schematic for laboratory coreflood. Water and oil volumetric fluxes are measured at the effluent along with the pressure drop across the core. The Welge–JBN method (derived in “Appendixes C and D”) determines relative permeability functions for water and oil from those measurements.

The saturation profiles across the overall core are shown in Fig. 2a, b at moments 1 and 2 before the breakthrough and at moment 3 after the breakthrough. Barenblatt et al. (1991) reproduces those profiles based on the asymptotic solution for 1D waterflood accounting for capillary pressure term. Large-scale solution (B.4) corresponds to the dotted curves in Fig. 2a and black curves in Fig. 2b. The continuous curves in Fig. 2a and blue and red curves presented in Fig. 2b are the solutions of Eqs. (A.9, A.10) for $\epsilon_c > 0$. Schematic in Fig. 2a shows that before the breakthrough, large-scale solution (B.4) is matched by the capillary pressure stabilised zone. After the breakthrough, solution (B.4) is matched with the capillary pressure end effect. Pressures in water and oil phases are continuous across the core outlet; therefore, the capillary pressure is continuous too. The capillary pressure is zero downstream the outlet, so it is zero downstream also. This results in boundary condition (A.13) of zero capillary pressure. Figure 2a, b considers water–wet case, where the condition of zero capillary pressure yields residual oil saturation at the effluent. Effluent saturation is equal to the connate water saturation in oil–wet case; the condition $s = S_{wi}$ holds in oil-wet cores during the overall displacement process. Thicknesses of two capillary zones have the order of magnitude of ϵ_c .

The numerical solutions presented in Fig. 2b for $\epsilon_c = 0, 0.5$ and 1.0 (black, blue and red curves, respectively) at the moments 0.05, 0.15 and 0.30 PVI also exhibit the stabilised and end-effect zones with thickness ϵ_c . The other parameters used in the simulation are listed in the first rows of Tables 1 and 2. The higher is the capillary–viscous ratio the faster is the water breakthrough, and the larger water volume accumulates near the core outlet.

Figure 2c demonstrates the match between the large-scale BL solution and the capillary pressure boundary layers at the breakthrough curve (BTC) $f(x_D = 1, t_D)$. The dashed curve corresponds to solution of RL Eqs. (A.9, A.10) that accounts for capillary pressure, and the solid curve shows its large-scale approximation by solution (B.4). The capillary pressure in Eq. (A.9) smoothes the shock in solution (B.4). This transition zone with thickness ϵ_c is produced during the period ϵ_c/D PVI, where D is the waterfront speed. The solid and dashed curves coincide after the transition zone production. As it follows from the volumetric balance given by Eq. (A.2), the overall deviation between the continuous and dashed curves is zero (see grey area in Fig. 2c).

Fig. 1 Schematic of unsteady-state waterflood test for relative permeability determination



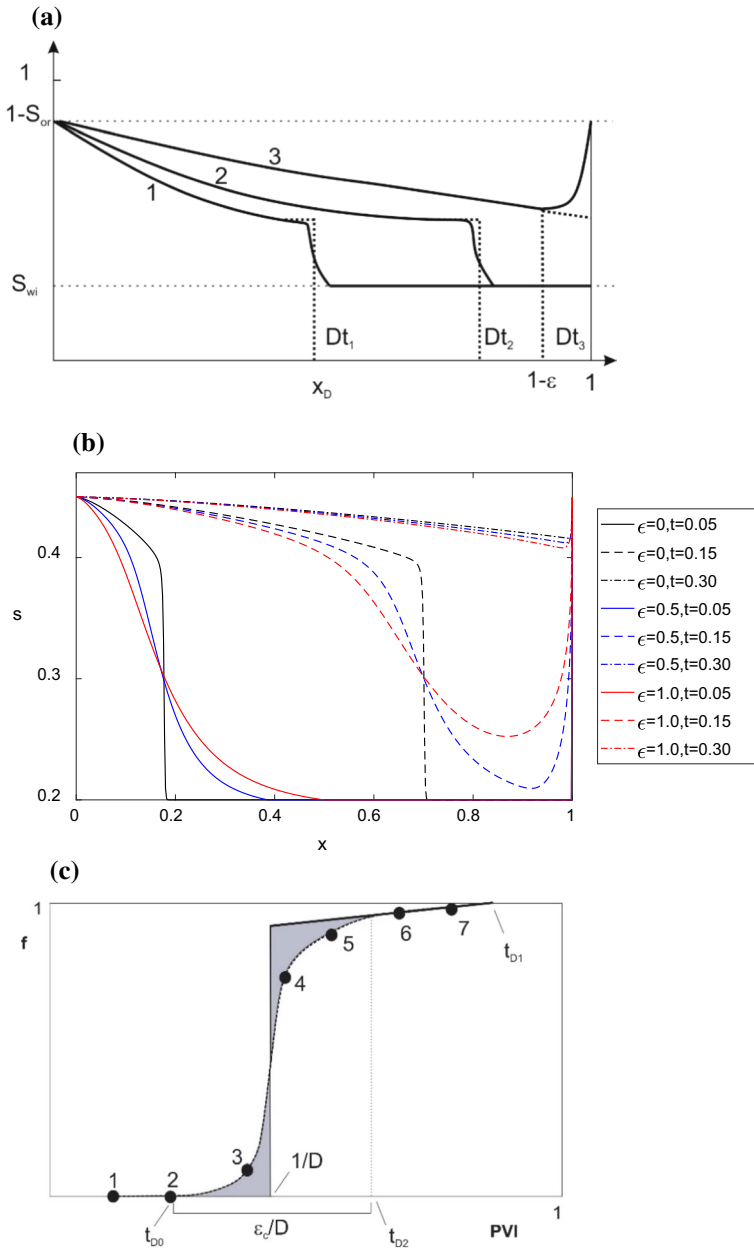


Fig. 2 Effects of capillary pressure on saturation profile and water cut: **a** schematic of matching Buckley–Leverett saturation profile with capillary transition zone before the breakthrough and with end-effect zone after the breakthrough, **b** the numerical modelling exhibits capillary transition and end-effect zones, **c** effects of capillary pressure on water-cut history

Table 1 Corey parameters for three synthetic cases of coreflood tests

	S_{wi}	S_{or}	K_{rowi}	K_{rwor}	n_w	n_o
Test 1	0.33	0.35	0.70	0.04	1.20	1.65
Test 2	0.34	0.45	0.52	0.06	1.30	1.90
Test 3	0.33	0.55	0.95	0.04	1.20	1.65

Table 2 Rock and fluid properties for three synthetic cases of coreflood tests

	k (m ²)	U (m/s)	μ_o (Pa s)	μ_w (Pa s)	σ (N/m)	ϕ	θ	L (m)	R (m)
Test 1	3×10^{-14}	3×10^{-6}	0.005	0.00095	0.03	0.18	0°	0.12	0.019
Test 2	4×10^{-14}	4×10^{-6}	0.0015	0.00095	0.03	0.22	0°	0.05	0.019
Test 3	3×10^{-14}	3×10^{-6}	0.05	0.00095	0.03	0.18	0°	0.12	0.019

2.2 Effects of Capillary Pressure on Welge–JBN–Generated Relative Permeability

The Welge’s method determines the fractional flow function $f(s)$ from the water cut $f(t_D, x_D=1)$ at the outlet $x_D=1$ (“Appendix C”). The JBN’s method calculates total mobility ratio using the pressure drop data $\Delta p(t_D)$ (“Appendix D”). Both methods solve the inverse problems for Eqs. (B.1, B.2) and determine two functions of relative permeability, provided the core length is large enough to fulfil the large-scale approximation condition (2), i.e. it is assumed that $\varepsilon_c=0$. However, the available core lengths are often limited and restricted to few centimetres; hence, the coreflood data correspond to nonzero values of capillary–viscous ratio ε_c . Consequently, in this section we use numerical solution of the problem (A.9–A.13) to mimic the coreflood data.

We can determine the effects of ε_c on relative permeability as calculated by Welge–JBN formulae (D.3) from numerical solution of Eqs. (A.9, A.10). The procedure starts with assumed relative permeability curves for water and oil as an input (solid black line in Fig. 4e, f). The numerical solution is then used to calculate pressure drop curve (PDC) across the core $\Delta p(t_D)$ (Fig. 4b) and produced water cut $f(t_D, x_D=1)$ for different capillary–viscous ratios ε_c (Fig. 4a). The simulated $\Delta p(t_D)$ and $f(t_D, x_D=1)$ are then used to recalculate relative permeability curves (dashed lines in Fig. 4e, f) using Welge–JBN. Then we analyse the deviation between the input relative permeability curves and the relative permeability curves obtained from the inverse problem. The measure of the deviation is the coefficient of determination R^2 . The procedure determines the maximum value of ε_c where the Welge–JBN method is valid.

The complete system of governing RL equations (A.9, A.10) subject to initial and boundary conditions (A.11–A.13) is solved numerically using the finite-difference method (Aziz and Settari 1979). A second-order central difference scheme is applied to spatial derivatives. At each time step, the saturation Eq. (A.9) is solved using the Runge–Kutta method. The time step is taken as $\Delta t_D=2 \times 10^{-4}$ PVI, and the length interval $\Delta x_D=2 \times 10^{-3}$. The Courant number is $\Delta t_D/\Delta x_D=0.1 < 1$, which indicates that the finite-difference scheme is stable (Chen 2007). After the saturation profiles $s(x_D, t_D)$ are obtained, the pressure distribution $p(x_D, t_D)$ is determined from Eq. (A.10) for the obtained saturation distribution. The results of numerical modelling for coreflooding are presented in Figs. 3, 4 and 5.

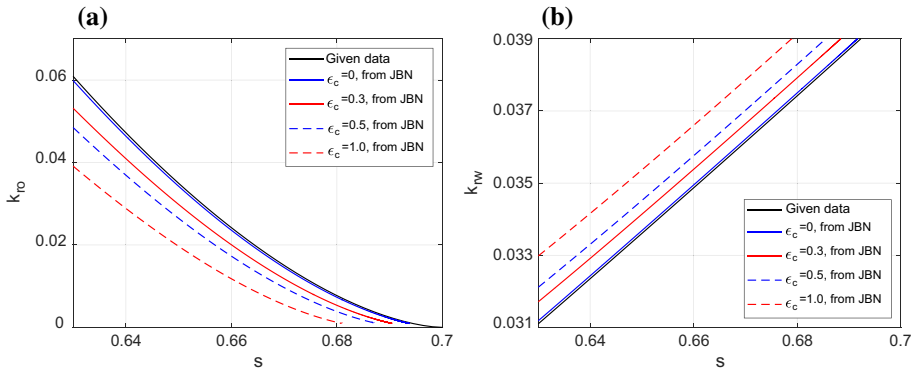


Fig. 3 Effects of capillary–viscous ratio on Welge’s and JBN data for Berea core ($k=30$ mD, $\mu_o=5$ cp, $L=0.12$ m): **a** zoom for relative permeability for oil as calculated by JBN method, **b** zoom for relative permeability for water as calculated by JBN method

The relative permeability is given by Corey formulae. Table 1 shows six Corey parameters for two coreflood Tests 1 and 2 that are discussed further in the text in Sect. 5; the results are presented in Figs. 3 and 4, respectively. The data of Test 3 in Table 1 correspond to a numerical example of heavy oil displacement (Fig. 5). Table 2 lists the rock and fluid properties used in the simulation. The simulation data presented in Figs. 3, 4, and 5 correspond to second, third and fourth lines in Tables 1 and 2, respectively.

In Figs. 3, 4 and 5, the continuous blue and red curves and blue and red dashed curves correspond to $\epsilon_c=0, 0.3, 0.5$, and 1.0 , respectively. Figures 4a, b and 5a, b show that the capillary pressure in RL Eq. (A.9) smoothes the water-cut jump and increases pressure drop before the breakthrough. Figure 4c shows that the large-scale solution for the S-shaped fractional flow curve (typical for oil viscosity 1.5 cp) contains a shock where Welge–JBN method provides the relative permeabilities from the frontal shock saturation ($S_f=0$) to $1 - S_{or}$. Figure 5c shows the convex fractional flow curve, which corresponds to continuous solution $\xi = x_D/t_D$, $s(x_D, t_D) = s(\xi)$ under heavy oil with viscosity of 50 cp. Here the inverse Welge–JBN method determines the relative permeability for the overall saturation interval from S_{wi} to $1 - S_{or}$. Figures 4d and 5d present relative permeability as calculated by Welge–JBN method from breakthrough data for four different values of $\epsilon_c=0, 0.3, 0.5$, and 1.0 ; Figs. 3a, b, 4e, f, 5e, f, present zoom of the relative permeability at short saturation intervals.

An increase in capillary–viscous ratio causes an increase in relative permeability for water and decrease in relative permeability for oil, which are determined by Welge–JBN method. For $\epsilon_c=0.5$, the variation between the original relative permeability and that calculated by Welge–JBN method is negligible ($R^2=0.83$ – 0.99 , column five in Table 3). For $\epsilon_c=0.3$, the accuracy for determination of relative permeability as calculated by Welge–JBN method is high ($R^2=0.93$ – 0.99 , column four in Table 3).

The accuracy of the above-mentioned numerical results is presented in Fig. 6 for $\epsilon_c=0, 0.3, 0.5$ and 1.0 for three coreflood cases presented in Figs. 3, 4 and 5. The plots allow calculating the critical value of capillary–viscous ratio that provides a given accuracy R^2 for determination of the relative permeability. The effect of capillary–viscous

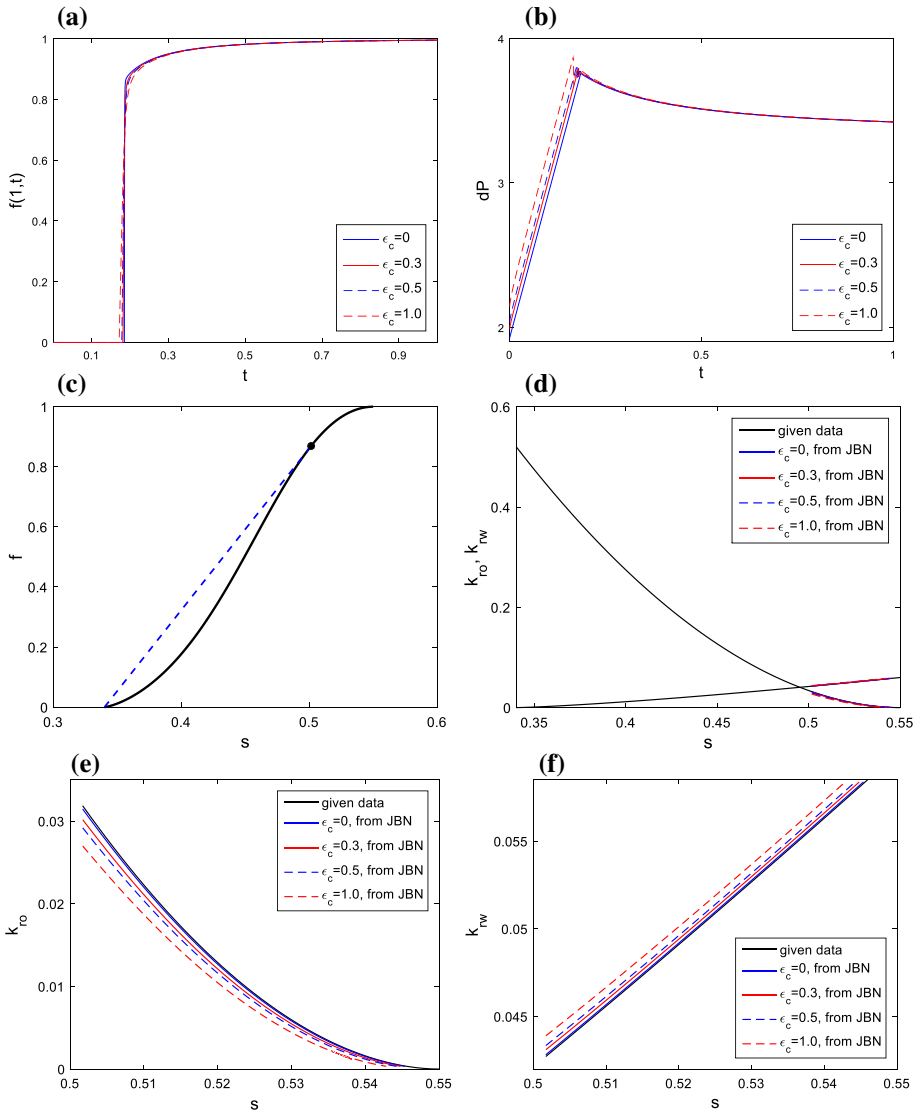


Fig. 4 Effects of capillary–viscous ratio on Welge’s and JBN data for Berea core ($k=40$ mD, $\mu_o=1.5$ cp and $L=0.05$ m): **a** water cut at the effluent for different capillary–viscous ratios, **b** pressure drop across the core, **c** fractional flow curve as calculated by Welge’s method, **d** relative permeability as calculated by JBN method, **e** zoom for relative permeability for oil, **f** zoom for relative permeability for water

ratio on relative permeability for $\epsilon_c < 0.5$ is negligibly small, which validates Welge–JBN method for corefloods where the capillary–viscous ratio does not exceed 0.5. Further in this work, the criterion of capillary–viscous ratio is based on the value $\epsilon_c = 0.5$.

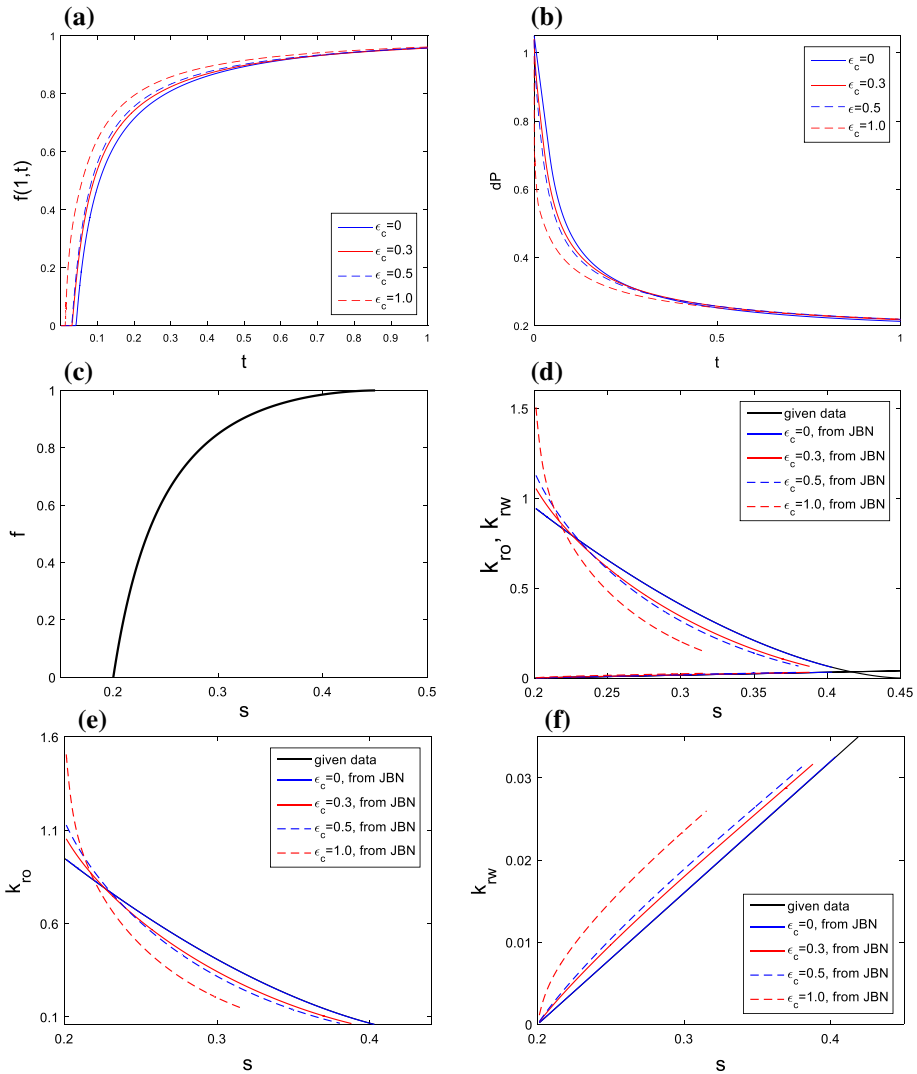


Fig. 5 Effects of capillary–viscous ratio on Welge’s and JBN data for heavy oil (50 cp) and Berea core ($k=30$ mD, $L=0.12$ m): **a** water cut in the effluent for different capillary–viscous ratios, **b** pressure drop across the core, **c** fractional flow curve as calculated by Welge’s method, **d** relative permeability as calculated by JBN method, **e** zoom for relative permeability for oil, **f** zoom for relative permeability for water

2.3 Capillary Number Criterion

In this section, we derive the capillary number criterion (1) from the condition of immobility of the residual oil drop in the pore loop (Fig. 7) (Chatzis et al. 1983; Barenblatt et al. 1991; Lake et al. 2014). The capillary number is the ratio between the viscous and capillary forces on pore scale. Capillary force dominance over the viscous force

Table 3 Accuracy of relative permeability determination for different capillary–viscous ratios

ϵ_c	0	0.3	0.5	1.0
Test 1				
R^2 for K_{ro} (s)	0.9995	0.9264	0.8262	0.5055
R^2 for K_{rw} (s)	0.9996	0.9428	0.8541	0.5122
Test 2				
R^2 for K_{ro} (s)	0.9995	0.9929	0.9814	0.9347
R^2 for K_{rw} (s)	0.9997	0.9962	0.9893	0.9586
Test 3				
R^2 for K_{ro} (s)	0.9993	0.9702	0.9388	0.5397
R^2 for K_{rw} (s)	1.0000	0.9794	0.9554	0.6351

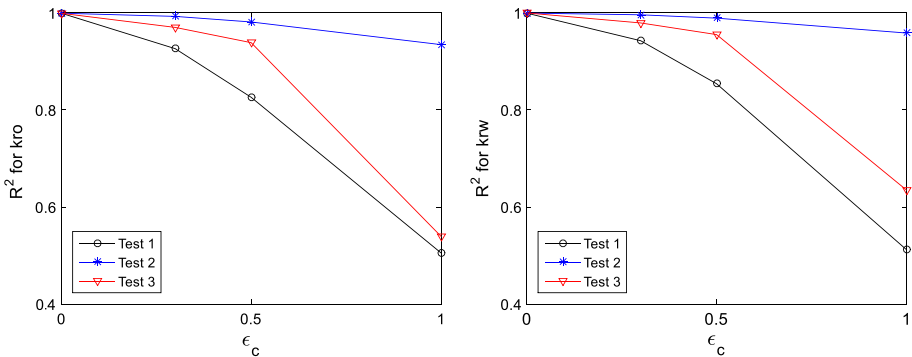
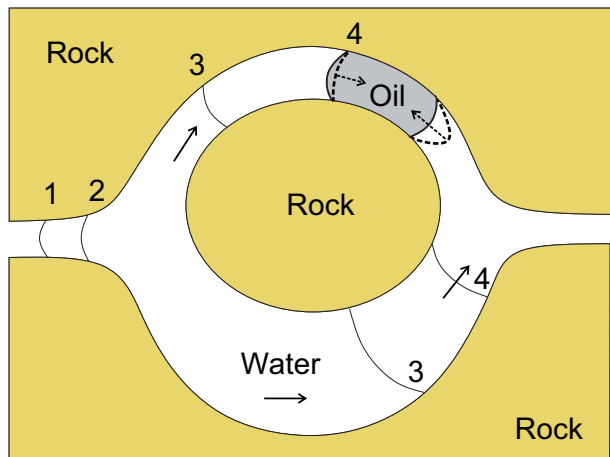


Fig. 6 Accuracy of relative permeability determination from numerical “coreflood” data for different values of capillary–viscous ratio

Fig. 7 Entrapment of oil droplet in thick pore and the bypassing water—the drop immobility condition (adapted from Chatziz et al. 1983)



provides the velocity interval where the concept of saturation-dependent relative permeability is valid i.e. the relative permeability is independent of flow velocity.

The dominance interval for capillary number presented by inequality (1) is taken from the desaturation curves. The interval for maximum capillary numbers in Eq. (1)

corresponds to the N_c values in desaturation curve $S_{or} = S_{or}(N_c)$, where the residual oil saturation is independent of the capillary number. This criterion can be obtained as a condition of immobility of a drop of non-wetting phase at the corresponding flow rates, i.e. where the pressure drop exerted on the trapped oil droplet is equilibrated by the capillary force (Fig. 7):

$$\Delta p \Big|_{l_g} = l_g \frac{\partial p}{\partial x} = l_g \frac{U \mu_w}{k} < \sigma \cos \theta \left(\frac{1}{r_+} - \frac{1}{r_-} \right) \approx \frac{\sigma}{5 \sqrt{k/\phi}} \tag{3}$$

$$N_c = \frac{U \mu_w}{\sigma} < \frac{\sqrt{k\phi}}{5 l_g}$$

Here Δp is the pressure drop, p is the pressure, x is the distance, l_g is the oil ganglion length, θ is contact angle, and r_- and r_+ are the pore throat radii ahead and behind the oil ganglion, respectively. Typical value for the difference between reciprocal radii in Eq. (3) is reciprocal to pore throat radius given by Eq. (F.4). We consider water-wet sandstone where $\cos\theta = 1$.

Figure 7 shows positions of water–oil meniscus in three moments where the moment 3 corresponds to the oil ganglion entrapment. Force balance between viscous and capillary forces is given by Eq. (3) resulting in the inequality (1). Here the right-hand side values correspond to typical values of permeability, porosity and the oil ganglion length. Considering $\cos\theta = 0.1$ for mixed-wet carbonates changes the interval (1) for critical capillary number to 10^{-4} – 10^{-3} .

2.4 Capillary–Viscous Ratio Criterion

Following the numerical results shown in Figs. 3, 4 and 5, we define the condition for large-scale approximation as:

$$\varepsilon_c = \frac{\sigma \sqrt{k\phi}}{\mu_o L U} \leq 0.5 \rightarrow LU \geq \frac{\sigma \sqrt{k\phi}}{0.5 \mu_o} \tag{4}$$

The maximum admissible velocity to fulfil $N_c = 10^{-5}$, as it follows from inequality (1), is (Dos Santos et al. 1997)

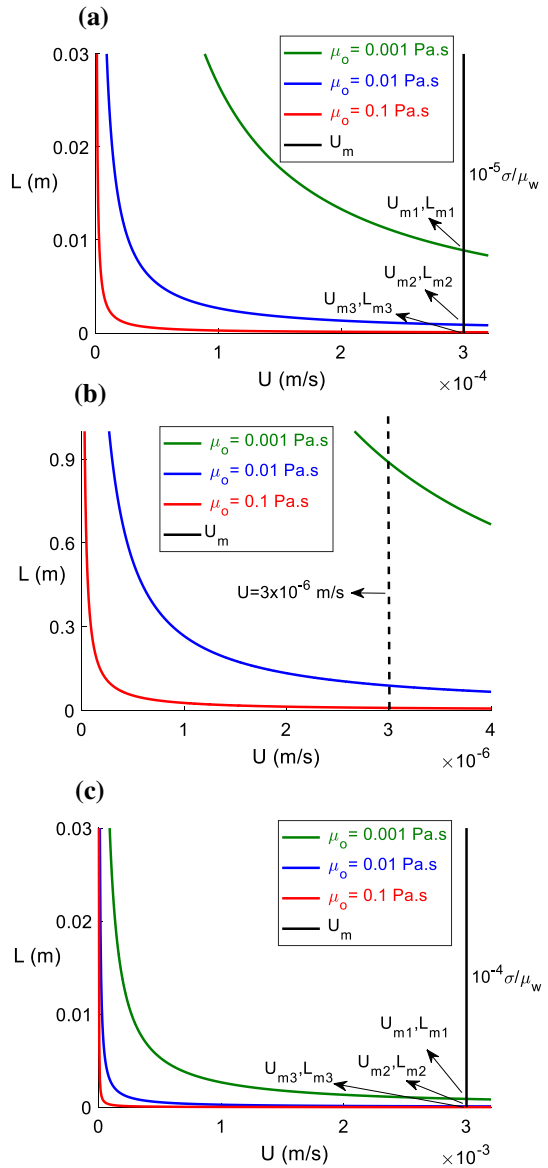
$$U_m = 10^{-5} \frac{\sigma}{\mu_w} \tag{5}$$

The minimum admissible core length is obtained from Eqs. (4) and (5):

$$L_m = \frac{\sigma \sqrt{k\phi}}{0.5 \mu_o U_m} = 2 \times 10^5 \frac{\mu_w}{\mu_o} \sqrt{k\phi} \tag{6}$$

Figure 8 shows the admissible domains restricted by conditions (1) and (4) in (U, L) plane for three maximum values of capillary number, which are typical for the desaturation curves (Barenblatt et al. 1991; Lake et al. 2014). The intersection points of hyperbolas,

Fig. 8 The capillary number and capillary–viscous ratio restrictions on flow rate U and core length L for different oil viscosities and maximum capillary numbers: **a** admissible domain in (U, L) plane for maximum capillary number $N_c = 10^{-5}$, **b** zoom around velocity $U = 3 \times 10^{-6}$ m/s, **c** admissible domain in (U, L) plane for maximum capillary number $N_c = 10^{-4}$



given by Eq. (4), with vertical straight lines (1), give the minimum core lengths L_m and the corresponding velocity U_m , where the conditions (1) and (4) are fulfilled.

Figure 8a corresponds to maximum capillary number $N_c = 10^{-5}$. Figure 8b shows the domain for maximum $N_c = 10^{-4}$. The plots are constructed for three values of oil viscosity. Other parameters used are: $k = 1 \times 10^{-14}$ m² (10 mD), $\phi = 0.2$, $\mu_w = 0.001$ Pa s, and $\sigma = 0.03$ N/m. The minimum core length to fulfil $N_c \leq 10^{-5}$ is 0.015, 0.016 and 0.02 m for oil viscosities $\mu_o = 0.1, 0.01$ and 0.001 Pa s, respectively. For $N_c \leq 10^{-4}$ the minimum

core length to fulfil conditions (1, 4) is shown to be less than 0.01 m for all the cases mentioned earlier (Fig. 8b).

Typically for permeability between 10^{-16} and 10^{-14} m² (0.1–10 mD), porosity from 0.07 to 0.4, oil viscosity from 0.001 to 1 Pa s and water viscosity of 0.001 Pa s, the minimum core length L_m to fulfil conditions (1, 4) varies from 5.3×10^{-7} to 0.01 m. Thus, for typical core lengths in industry (between 0.03 and 0.07 m) the condition $L > L_m$ always holds.

3 Operational Criteria for Laboratory Coreflood

In this section, we present four criteria for laboratory waterflooding of a core, saturated by oil. This includes criteria for the pressure precision (Sect. 3.1), the number of samples (Sect. 3.2), the water-cut precision (Sect. 3.3) and the sampling period (Sect. 3.4).

3.1 Precision of Pressure Measurements

Pressure drop measurement precision is determined by the half-scale of the pressure transducers (Fig. 1). For precise measurements, the pressure drop across the core must exceed the half-scale p_{min} :

$$\begin{aligned} \Delta p &\geq p_{min} \\ \epsilon_p &= \frac{\Delta p}{p_{min}} \geq 1 \end{aligned} \tag{7}$$

Let the minimum of total mobility $\lambda(s)$ over the saturation interval $[S_{wi}, 1 - S_{or}]$ be λ_{min} , so the following inequality is fulfilled:

$$\lambda(s) \geq \lambda_{min} \tag{8}$$

The lower estimate of the flux becomes

$$U = k \frac{\lambda(s)}{\mu_0} \frac{\Delta p}{L} \geq \frac{k \lambda_{min}}{\mu_0} \frac{p_{min}}{L}, \tag{9}$$

which corresponds to the following inequality, determining the domain above the hyperbola in plane (U, L) :

$$UL \geq \frac{k \lambda_{min} p_{min}}{\mu_0} \tag{10}$$

Let us compare the positions of the hyperbolas for capillary–viscous ratio and pressure drop precision, given by Eqs. (4) and (10), respectively. The pressure drop precision is the weak criterion if compared with capillary–viscous ratio criterion if

$$\frac{\sigma \sqrt{k \Phi}}{0.5 \mu_o} \geq \frac{k \lambda_{min} p_{min}}{\mu_0} \tag{11}$$

yielding the following restriction for pore size in the rock, r_p :

$$r_p = 5 \sqrt{k / \Phi} \leq \frac{10 \sigma}{\lambda_{min} p_{min}}. \tag{12}$$

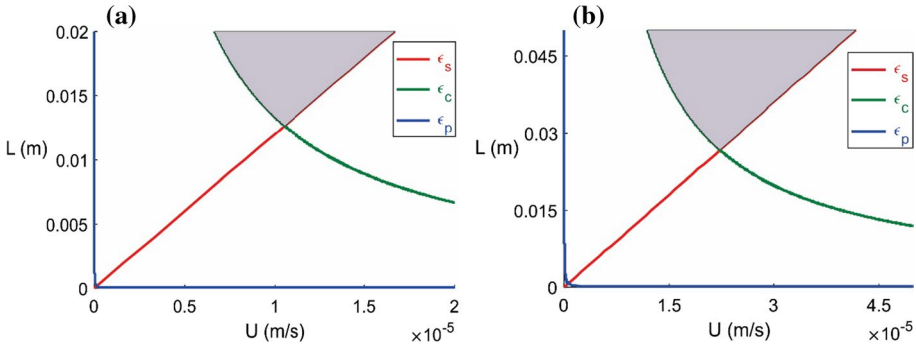


Fig. 9 Restrictions for precision of sampling duration (ϵ_s), pressure measurement (ϵ_p) and capillary–viscous ratio, ϵ_c : **a** $k = 10^{-14} \text{ m}^2$, **b** $k = 2 \times 10^{-13} \text{ m}^2$

Formula (12) for mean pore radius is presented in “Appendix F”. From Eq. (12) follows the inequality for rock permeability

$$k \leq \phi \left(\frac{2\sigma}{\lambda_{\min} p_{\min}} \right)^2 \tag{13}$$

Let us estimate minimum value for right-hand side of inequality (13). For minimum values of $\sigma = 0.01 \text{ N/m}$ and porosity $\phi = 0.1$, and for maximum values $\lambda_{\min} = 1.0$ and $p_{\min} = 200 \text{ Pa}$, the right-hand side of inequality (13) is equal to 10^{-9} m^2 (10^3 D), which highly exceeds the permeability of real cores. Thus, the assumption that the pressure precision is a weak parameter can be accepted for all real cores. Therefore, the pressure precision criterion can always be neglected.

The admissibility domain for criteria ϵ_c and ϵ_p is shown in Fig. 9. The parameters used are: $\Delta t = 30 \text{ s}$, $N_{\min} = 7$, $V_{\min} = 5 \times 10^{-8} \text{ m}^3$, $p_{\min} = 40 \text{ Pa}$, $f_{\min} = 0.1$, $\sigma = 0.03 \text{ N/m}$, $R = 0.019 \text{ m}$, $\phi = 0.20$ and $\mu_o = 0.02 \text{ Pa s}$. In both cases of low and high permeability (Fig. 9a, b, respectively), the hyperbola that corresponds to pressure precision measurements and given by inequality (10) is located below the hyperbola for capillary–viscous ratio (4), i.e. ϵ_p criterion can be waived. Figure 9 corresponds to cross section $\Delta t = \text{const}$ of the 3D domain defined by inequalities (1, 4, 18) and presented in Fig. 10a.

The upper limitations on the pore pressure and overburden are set for the fragile or soft rocks. The estimate (13) shows that these limitations do not affect the pressure drop precision criterion ϵ_p .

3.2 Number of Samples During One PVI

Consider the number of water-cut measurements that should be obtained at the effluent for capturing the S-shape of the fractional flow curve. Figure 2c shows water-cut curve corresponding to the large-scale BL model (B.1, B.2) and the RL model (A.9, A.10) that accounts for capillary pressure (solid and dashed curves, respectively). The deviation period corresponds to production of the transition zone and has an order of magnitude of ϵ_c/D , where D is the dimensionless velocity of the saturation front given by Eq. (B.4) (Barenblatt et al. 1991). After the breakthrough for $t_D > 1/D$, the water-cut curve is convex and increases monotonically. Following Civan and Donaldson (1989) and Toth et al. (2001,

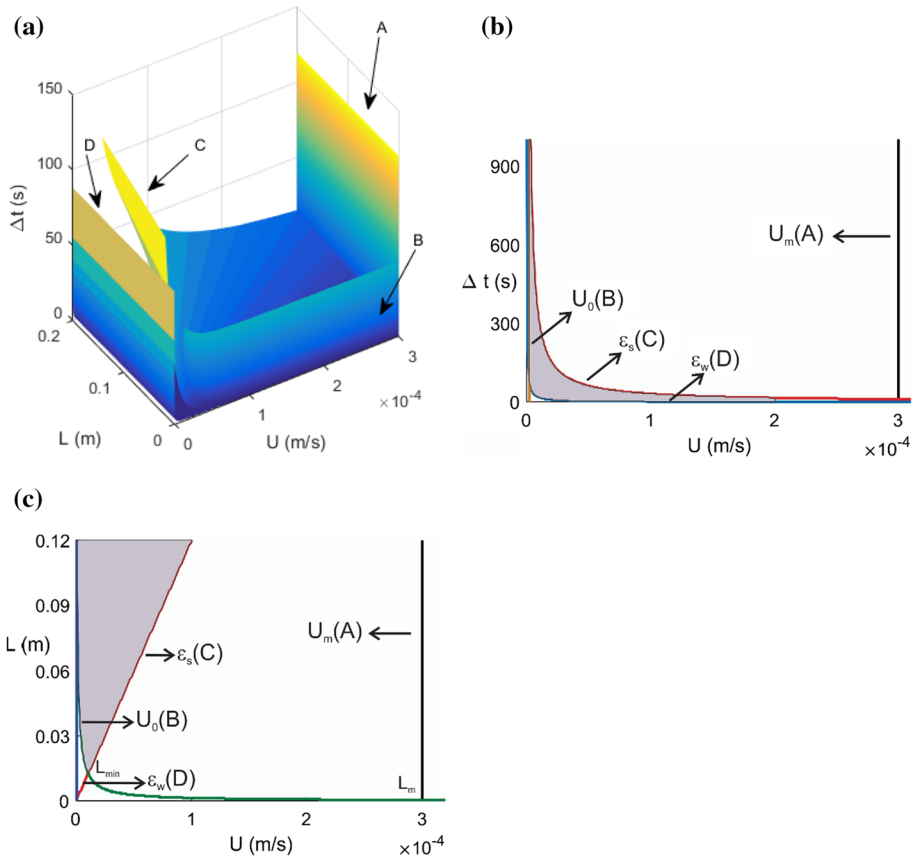


Fig. 10 Three-dimensional domain for system of five inequalities: **a** three-dimensional image of the domain in coordinates $(U, L, \Delta t)$, **b** the domain projection in plane $(U, \Delta t)$, **c** the domain projection in plane (U, L)

2002), we use the exponential approximation of water-cut curve after the production of the transition zone; the analytical expressions allow performing the Welge–JBN calculations, given by Eqs. (C.5) and (D.2). Considering that water cut tends to one with time tending to infinity, it is necessary to measure at least two values outside the $\epsilon_c D^{-1}$ -long interval after the breakthrough. These are points 6 and 7 in Fig. 2c.

The sequence for constructing the BL BTC is as follows:

- (a) plotting a smooth curve through the experimental data points between $f=0$ at $t_D = t_{D0}$ and $f=1$ at $t_D = t_{D1}$ such that the area underneath the curve is equal to the water volume V_{01} injected during this time period (Fig. 2c)

$$V_{01} = \int_{t_{D0}}^{t_{D1}} f(t) dt$$

- (b) calculation of the capillary–viscous ratio ϵ_c , which has an order of magnitude of the thickness of capillary transient zone;

- (c) calculation of end-point saturations S_{wi} and S_{or} from the volumetric balance during the coreflood, and the corresponding end-point relative permeabilities K_{rowi} and K_{rwor} from the pressure drops at the beginning and at the end of the displacement;
- (d) taking typical Corey powers n_w and n_o , calculate fractional flow function and the water-front velocity D ;
- (e) adding the duration of the transition period ε_c/D to the moment t_{D0} will provide the time after which the BL solution is valid;
- (f) approximation of the BTC at $t_D > t_{D2}$ by an exponential curve and extrapolation of this curve into the interval $[t_{D0}, t_{D2}]$;
- (g) identification of the shock position in the BL solution $1/D$ such that the area between the BL and experimental BTCs to the right of the shock is equal to the area under the BTC to the left of the shock;
- (h) approximation of the pressure drop data by the PDC, which is straight line before the breakthrough and exponent afterwards.

The transitional zone thickness can be calculated from the travelling wave solution of the Rapoport–Leas (RL) equation (A.9). Preliminary calculation of the water-front velocity D also assumes a priori knowledge of Corey powers n_w and n_o . The calculations (a)–(f) can be repeated after determination of the relative permeability by the Welge–JBN method.

Provided the dashed curve extrapolates the large-scale water-cut values from points 6 and 7, and the continuous S-shaped curve of measured water-cut values is given, the volume balance condition determines unique values for the breakthrough moment $1/D$ and the breakthrough water cut $f(1/D)$.

The breakthrough moment cannot be measured directly; the points 1 and 2 correspond to before-the-breakthrough period. A few points define the form of the BTC between points 2 and 6. Figure 2c shows how three intermediate points 3, 4 and 5 determine the form of S-shape BTC. It allows determining the shock-front position $t_D = 1/D$. Thus, the estimated minimum number of measured points for the conditions of the above-mentioned example is $N_{min} = 7$.

Therefore, the number of samples to be collected during 1 PVI must exceed $N_{min} + 1$:

$$\frac{\pi R^2 L \phi}{U \pi R^2 \Delta t} \geq N_{min} + 1 \tag{14}$$

where Δt is the sample collection duration, R is the core radius and $N_{min} + 1$ is the minimum number of samples.

Inequality (14) restricts a domain in three-dimensional space with coordinates $(U, L, \Delta t)$:

$$\Delta t \leq \frac{\phi}{N_{min} + 1} \frac{L}{U} \tag{15}$$

Further in the text, we call inequality (15) the number-of-samples criterion.

3.3 Sample Volume for Precise Water-Cut Measurements

Let us express the condition for precise measurement of volumes of both phases collected in a single sample, as inequalities for three variable coreflood parameters U, L , and Δt .

The half-scale of volume in a burette V_{min} is known. Volume V_{min} of each phase should be visibly distinguished. Volume of either phase in the burette must exceed V_{min} :

$$U\pi R^2\Delta t \geq f_{\min} V_{\min} \tag{16}$$

yielding

$$U\Delta t \geq \frac{f_{\min} V_{\min}}{\pi R^2} \tag{17}$$

Here f_{\min} is the minimum measured fractional flow value, which determines the water-cut measurement accuracy.

The restrictive surface for inequality (17) is a cylinder with sides parallel to axis L and the base given by hyperbola in plane $(U, \Delta t)$.

For our tests, the value $f_{\min}=0.05$ is chosen.

Further in the text, we call inequality (17) the f -precision criterion.

Let us determine the conditions of compatibility for the number-of-samples and f -precision criteria. Inequalities (15) and (17) determine lower and upper bounds for sampling duration:

$$\frac{f_{\min} V_{\min}}{\pi R^2 U} \leq \Delta t \leq \frac{\phi}{N_{\min} + 1} \frac{L}{U} \tag{18}$$

The upper bound in inequalities (18) exceeds the lower bound if

$$\frac{f_{\min} V_{\min}}{\pi R^2} \leq \frac{\phi L}{N_{\min} + 1} \tag{19}$$

yielding the lower bound for core length:

$$L \geq \frac{f_{\min} V_{\min} (N_{\min} + 1)}{\pi R^2 \phi} \tag{20}$$

Maximum right-hand side of inequality (20) is reached for $f_{\min}=0.1$, $V_{\min}=2.5 \times 10^{-7} \text{ m}^3$, $N_{\min}=7$, $R=0.02 \text{ m}$ and $\phi=0.1$, leading to $L=2 \times 10^{-3} \text{ m}$. The reservoir cores available in the industry are always longer than this value, which fulfils inequality (20). Therefore, the criteria for the number of samples and f -precision are always compatible.

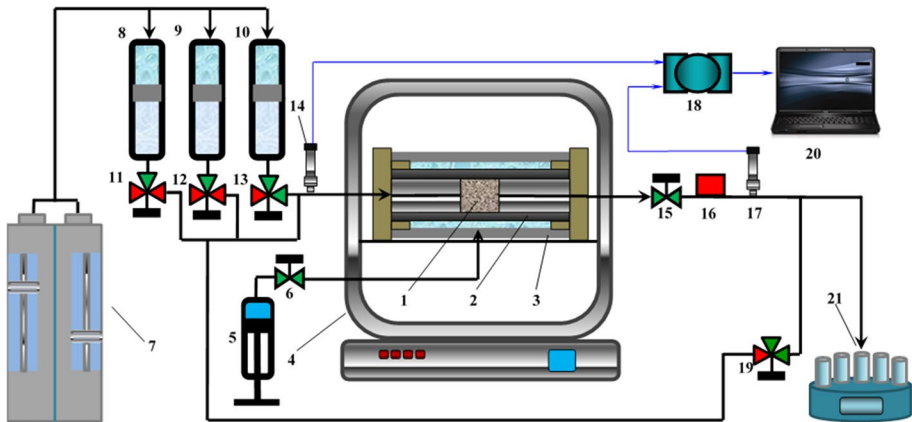


Fig. 11 Set-up for laboratory waterflood

Water-cut measurements must be essentially precise at water breakthrough under small water fractions in oil, and during the late waterflooding under small oil fractions in water. The visual observations here may be rather inaccurate, and other methods for quantification may be required. Katika et al. (2016) consider four methods for quantification of small amounts of oil in water: image analysis, ultraviolet spectroscopy, low-field nuclear magnetic resonance spectrometry, and liquid scintillation counting. All four methods provide the high-accuracy reproducible results.

3.4 Sampling Period

For the laboratory set-up presented in Figs. 1 and 11, the duration of the sampling period Δt is determined by the minimum rotation time of the automatic fraction collector, when a burette is replaced with another one at the core outlet (Dos Santos et al. 1997):

$$\Delta t \geq \Delta t_{\min} \quad (21)$$

Here Δt_{\min} is the minimum duration for sample collection. For the set-up presented in Fig. 11, $\Delta t_{\min} = 1$ s, which is the typical value for most laboratory automatic fraction collectors.

The corresponding domain in three-dimensional space $(U, L, \Delta t)$ is located above the horizontal plane with height equal to Δt_{\min} .

4 Determining the Domain of Admissible Parameters $(U, L, \Delta t)$

In this section, we present the geometry of the two- and three-dimensional domains that represent the solution of the system of inequalities (1, 4, 18, 21).

4.1 Geometry of 3D Domain

Let us consider 3D domain (the geometric set of points) where five inequalities (1, 4, 18, 21) are fulfilled.

In Fig. 10c, the base (U, L) contains parabola (4) and straight line (1) that limits the velocity U . The admissible zone is defined by two inequalities (4, 5). In 3D space (Fig. 10a) with coordinates $(U, L, \Delta t)$, inequalities (4, 5) determine the cylinder with the above-mentioned base. The coordinates of the intersection point are U_m and L_m :

$$\left(10^{-5} \frac{\sigma}{\mu_w}, 2 \times 10^5 \frac{\mu_w}{\mu_o} \sqrt{k \Phi} \right) \quad (22)$$

The admissible points $(U, L, \Delta t)$ that fulfil the number-of-samples criterion (15) are located below the line-helix surface in Fig. 10a (Banchoff and Lovett 2016). Figure 10b, c shows the projections of 3D admissible domain onto planes $(U, \Delta t)$ and (U, L) , respectively. Above the straight lines $L/U = \text{const}$ in plane (U, L) , the surface “height” Δt is constant. Therefore, the surface consists of one-parametric family of horizontal straight lines, which are the rectilinear generators. The vertical axis Δt is the directing curve. The surface height above the line $L/U = 0$, which is L -axis, is zero. The surface height above the line $U/L = 0$, which is U -axis, is infinity. The height takes all intermediate values for

intermediate straight lines with $L/U = \text{const}$. Therefore, the projection of straight lines defined as $\Delta t = \text{const}$ rotates around the origin in plane (U, L) , where Δt increases monotonically from zero along the axis U up to infinity along axis L .

The domain is limited from below by a cylinder with sides parallel to axis L and base the hyperbola (17) in plane $(U, \Delta t)$, which reflect the f -precision criterion (Fig. 10).

The parameters used for calculation of the domain and admissible areas in Fig. 10 are: $N_{\min} = 7$, $V_{\min} = 5 \times 10^{-8} \text{ m}^3$, $f_{\min} = 0.1$. Other core parameters are presented in the first row of Table 2.

Joining inequalities (15) and (17) yields double inequality (18). The intersection of two surfaces corresponds to the following equality

$$\frac{f_{\min} V_{\min}}{\pi R^2 U} = \frac{\phi}{N_{\min} + 1} \frac{L}{U}, \text{ or } L = \frac{f_{\min} V_{\min} (N_{\min} + 1)}{\pi R^2 \phi} = L_0 \tag{23}$$

i.e. two surfaces intersect along the vertical plane $L = L_0$.

The maximum value of L_0 has been calculated at the end of Sect. 3.3. It is always smaller than reservoir core lengths used. Therefore, inequality (20) is always fulfilled, i.e. the parabolic cylinder is located below the line-helix surface (Fig. 10).

4.2 Determining Minimum Admissible Core Length L

The minimum admissible core length L is given by the following lemma.

Lemma *For any solution of system (5, 15, 17, 21), $L \geq L_m$.*

Proof Consider the solution of system (5, 15, 17, 21) for constant L . The admissible area is limited by inequalities (18) in plane $(U, \Delta t)$, which is the area between two hyperbolas in Fig. 10b. It is also limited by two vertical lines $U < U_m$ and capillary–viscous criterion (4)

$$U_0 = \frac{\sigma \sqrt{k} \phi}{0.5 \mu_o L} \leq U \leq U_m = 10^{-5} \frac{\sigma}{\mu_w} \tag{24}$$

The admissible area forms a curvilinear parallelogram (Fig. 10b).

With decreasing of L , the lower bound in inequality (24) moves to the right, and the upper bound in inequality (18) moves down. The lower and upper bounds in inequality (24) coincide at $L = L_m$, where $U = U_m$. The admissible domain degenerates into a vertical interval between two hyperbolas (18):

$$L = L_m, \quad U = U_m, \quad \Delta t_{\min} = \frac{f_{\min} V_{\min}}{\pi R^2 U_m} \leq \Delta t \leq \frac{\phi}{N_{\min} + 1} \frac{L_m}{U_m} \tag{25}$$

Therefore, $L = L_m$ is the minimum L -value in 3D domain, which proves the lemma.

Thus, in 3D space, the domain is always located behind the vertical plane $L = L_m$.

As it is shown in Sect. 3.3, the number-of-samples criterion provides the upper bound while the f -precision criterion yields the lower bound $L = L_{\min}$:

$$L_{\min} = \sqrt{\frac{\sigma \Delta t (N_{\min} + 1)}{0.5 \mu_o}} \sqrt{\frac{k}{\phi}} \tag{26}$$

which is obtained by intersection between the ϵ_c -hyperbola and the number-of-samples straight line (Fig. 10c).

Maximum sampling period Δt_0 is determined by intersection of hyperbola given by number-of-sample criterion (15) with straight line $U=U_0$, where U_0 is determined from maximum capillary–viscous ratio, Eq. (24)

$$\Delta t_0 = \frac{0.5\mu_o L^2}{\sigma(N_{\min} + 1)} \sqrt{\frac{\phi}{k}} \tag{27}$$

The intersection of the hyperbola given by the number-of-sample criterion (15) with straight line $U=U_m$ determines sampling period Δt_1

$$\Delta t_1 = \frac{10^5 \mu_w \phi L}{\sigma(N_{\min} + 1)} \tag{28}$$

The intersection of the hyperbola given by the f -precision criterion (17) with straight line $U=U_m$ determines sampling period Δt_{\min} given by Eq. (25). □

Figure 12a shows the admissible areas in plane $(U, \Delta t)$. The admissible areas are filled with grey. The parameters are presented in Table 2. The calculated results for Test 1 are: $L_m=0.001$ m, $L_{\min}=0.04$ m, $U_m=3 \times 10^{-4}$ m/s (85 ft/day), $U_0=1.7 \times 10^{-6}$ m/s (0.48 ft/day), $\Delta t_{\min}=0.29$ s, $\Delta t_0=2562$ s, $\Delta t_1=36$ s. The working velocity can be chosen from

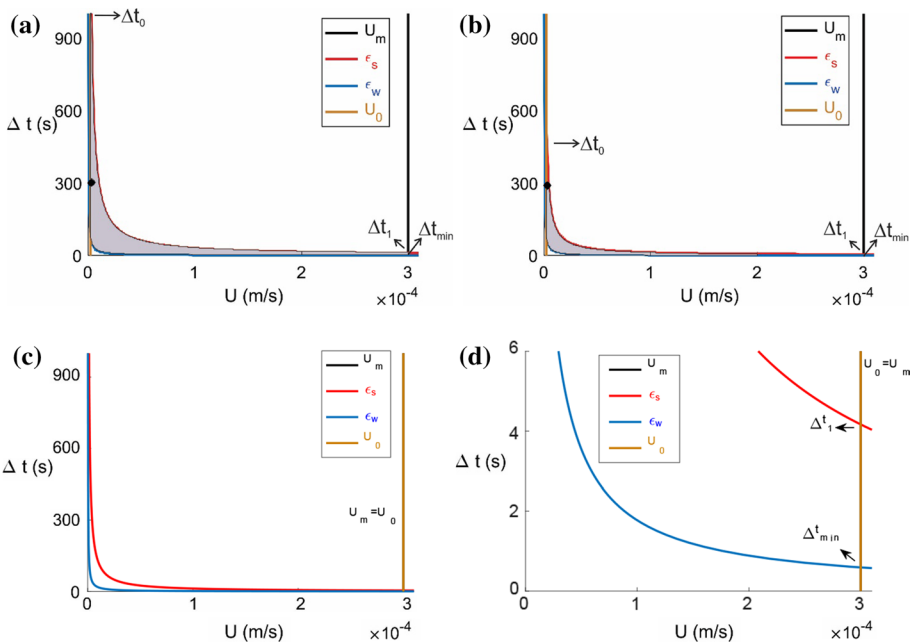


Fig. 12 Four restrictions for coreflood with given core length and admissible domain in plane $(U, \Delta t)$: **a** conditions of Test 1, **b** conditions of Test 2, **c** the case where $L=L_{\min}$, **d** zoom for small sampling periods

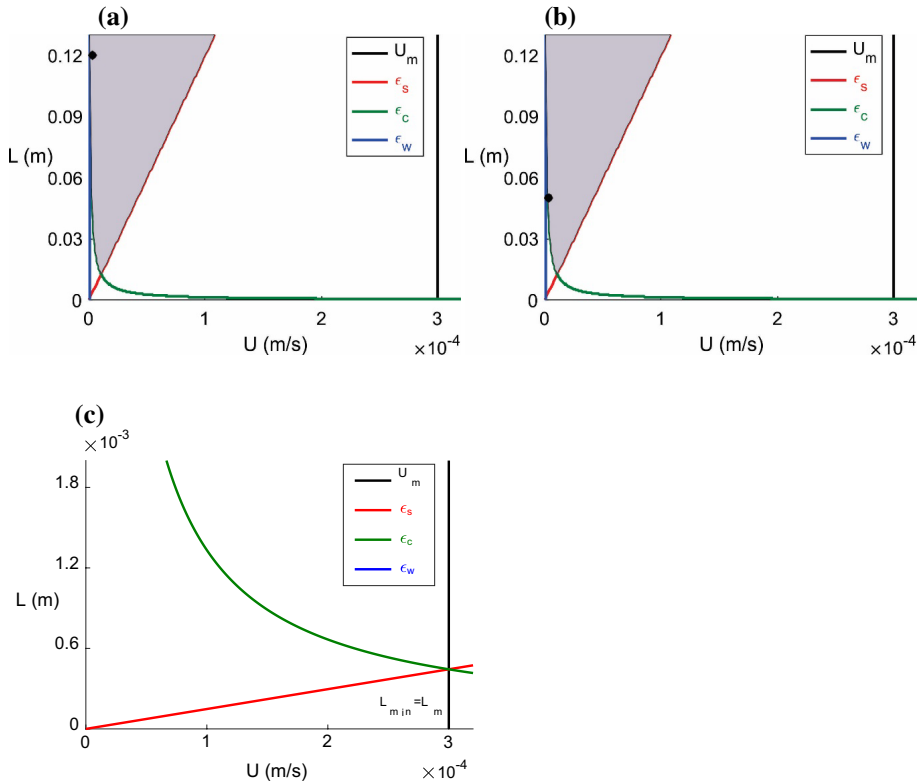


Fig. 13 Four restrictions for coreflood with fixed sampling period and admissible domain in plane (U, L) : **a** conditions of Test 1, **b** conditions of Test 2, **c** the case corresponding to minimum sampling period of the domain $\Delta t = \Delta t_{min}$

1.7×10^{-6} m/s (0.48 ft/day) to 3×10^{-4} m/s (85 ft/day); the sampling period can be selected from 0.29 to 2562 s. The velocity and sampling period selected for Test 1 are shown by a solid point with coordinates $U = 3 \times 10^{-6}$ m/s (0.85 ft/day) and $\Delta t = 300$ s.

The calculated results for Test 2 are: $L_m = 0.004$ m, $L_{min} = 0.04$ m, $U_m = 3 \times 10^{-4}$ m/s (85 ft/day), $U_0 = 2.5 \times 10^{-6}$ m/s (0.7 ft/day), $\Delta t_{min} = 0.29$ s, $\Delta t_0 = 444$ s, $\Delta t_1 = 50$ s (Fig. 12b). The velocity and sampling period selected for Test 2 are shown by a solid point with coordinates $U = 4 \times 10^{-6}$ m/s (1.1 ft/day) and $\Delta t = 290$ s.

Figure 12c, d corresponds to $L = L_m$, where U_0 becomes equal to U_m , and the admissible curvilinear rectangular degenerates into vertical interval $[\Delta t_{min}, \Delta t_1]$ with $U = U_m$.

4.3 Determining Minimum Sampling Time Δt_{min}

Horizontal cross sections of the domain correspond to constant values of Δt . Figure 13 shows the admissible area in plane (U, L) . Here the green parabolas correspond to ϵ_c criterion, the vertical black line expresses N_c criterion, the red straight line corresponds to number-of-sample criterion, ϵ_s (15), and the vertical blue line corresponds to f-precision criterion, ϵ_w . Because the vertical blue line is characterised by the equality of Eq. (17), Eq. (25) leads to

$U\Delta t = U_m \Delta t_{\min}$. From inequality $\Delta t \geq \Delta t_{\min}$, follows that $U \leq U_m$, i.e. the vertical blue line always lays to the left of black line (Fig. 13c).

As sampling time Δt decreases, the slope of the red straight line decreases, and the blue line moves to the right. The red line crosses point (U_m, L_m) for sampling time Δt_m , given by Eq. (25). At $\Delta t = \Delta t_{\min}$, abscissa of the blue line is equal to U_m , i.e. $U = U_m$.

As a result, the lowest point of the domain corresponds to $\Delta t = \Delta t_{\min}$.

Let us compare the values of Δt and Δt_{\min} . The minimum value of Δt_{\min} corresponds to $f_{\min} = 0.05$, $V_{\min} = 0.05 \times 10^{-6} \text{ m}^3$, $\sigma = 0.05 \text{ N/m}$, $\mu_o = 0.001 \text{ Pa s}$, and is equal to 0.0044 s . The maximum value of Δt_{\min} corresponds to $f_{\min} = 0.2$, $V_{\min} = 0.25 \times 10^{-6} \text{ m}^3$, $\sigma = 0.01 \text{ N/m}$, $\mu_o = 0.1 \text{ Pa s}$ and is equal to 44 s .

Therefore, the lowest point of the domain Δt can be higher than the minimum and lower than the maximum sampling period Δt_{\min} .

Figure 13a, b presents the admissible domain for conditions of Tests 1 and 2; the corresponding data are given in Table 2 and Sect. 5. Sampling times have already been selected from admissible zones in Fig. 12a, b and are 300 s and 290 s, respectively. The minimum core lengths for both tests are almost equal (0.05 m and 0.04 m for two cores, respectively), and the corresponding velocity is $3 \times 10^{-6} \text{ m/s}$. Solid points inside admissible domains correspond to flow rates used in both corefloods.

Figure 13c shows the parameters of the lowest domain sampling period: $L_m = 5 \times 10^{-4} \text{ m}$, $U = U_m = 3 \times 10^{-4} \text{ m/s}$ (85 ft/day), $\Delta t = \Delta t_{\min} = 0.29 \text{ s}$.

4.4 Admissible Velocity and Sampling Time for a Given Core Length

Let us discuss the system of inequalities (5, 15, 17, 21) for a given core length L . After fixing L , the system of inequalities becomes two-dimensional (Fig. 10b). The capillary number and capillary–viscous ratio criteria yield inequality (5). The upper boundary is equal to U_m . We denote the lower boundary as U_0 . The admissible area in plane $(U, \Delta t)$ is located between two vertical straight line (Fig. 12).

The criteria for number of samples and f -precision yield inequalities (18), which can be transformed to the following

$$\frac{f_{\min} V_{\min}}{\pi R^2} \leq U\Delta t \leq \frac{\phi L}{N_{\min} + 1} \tag{29}$$

The admissible area in Fig. 12 is located between two hyperbolas (29). The working velocity and sampling time are selected from the admissible area.

5 Laboratory Study

In this section, we present the laboratory set-up and equipment (Sect. 5.1) and the coreflooding methodology (Sect. 5.2). We show the examples of two coreflood planning by applying the theoretical and operational criteria (Sect. 5.3) and the results of those tests (Sect. 5.4).

5.1 Laboratory Set-up

Figure 11 shows the schematic of waterflooding set-up. A core plug (1) is inserted inside a 1.5" in diameter Viton sleeve (2). A Hassler-type coreholder (3) accommodates the sleeve

and the core holder is then placed in an oven (4). A manual piston pressure generator (5) is used to apply overburden pressure by compressing distilled water. QUIZIX high-precision pump (7) is used to inject brine to the core, and separating vessels (8–10) are used to inject oil to the core. Inlet and outlet pressures in the core holder are measured by pressure transmitter (18). Back-pressure regulator (16) keeps 500 psi of pressure at core outlet. Pressure and rate data are recorded in real time. Effluent samples are collected using automatic fraction collector (21).

Table 2 shows the properties of two Berea sandstone cores used for waterflooding tests. The injected and formation water are identical and obtained by dissolution of 35,000 ppm NaCl in fresh Milli-Q water. The oil phase is synthetic mineral (non-polar) oil.

5.2 Study Methodology

The core was put under vacuum for 1 day and then saturated by water to ensure that 100% water saturation was achieved. The coreflood test was performed following the standard procedures. First, 10 pore volumes of the brine (formation water) is injected to measure absolute permeability. Then, oil is injected at constant flow rate for the primary drainage until no water production is observed (S_{wi} is achieved) followed by 2-weeks ageing. Imbibition test is then performed by formation water injection at constant flow rate until S_{or} .

The overall rate, produced water rate and pressure drop across the core are measured during the coreflood test. The precision criteria for those measurements are formulated in the next section.

5.3 Laboratory Waterflood Planning Examples

In this section, we present two examples of planning the coreflooding including performing the test and relative permeability calculations using Welge–JBN method. Table 2 presents the parameters of these two tests. In order to determine the waterflood test parameters L , U and Δt , the following steps must be undertaken.

Minimum core length First we present the calculations of the minimum core length. Consider the case where rock and fluid properties of the reservoir (permeability, porosity, interfacial tension, contact angle) are known and it is necessary to determine minimum core length L , injection rate U and minimum sampling time Δt . The laboratory set-up for waterflooding tests is established (Fig. 11), so the half-scale p_{min} for pressure drop measurements, the number of samples during one PVI N_{min} , sample volume for precise watercut measurements V_{min} and sampling period Δt are known.

From Eq. (26) using $N_{min}=7$, and $\Delta t=30$ s for Test 1 (second row in Table 2), we obtain $L_{min}=0.04$ m.

For Test 2 (third row in Table 2), $N_{min}=7$, and $\Delta t=30$ s, $L_{min}=0.05$ m.

Flow Rate and Sampling Time Here we present the calculations of U and Δt , provided L is already known:

1. Calculate minimum velocity U_0 using Eq. (24);
2. Calculate maximum velocity U_m using Eq. (5);
3. Select a flow rate from the interval $[U_0, U_m]$;
4. Calculate minimum and maximum sampling time from inequalities (18);
5. Select a sampling time from the interval of the minimum and maximum Δt values.

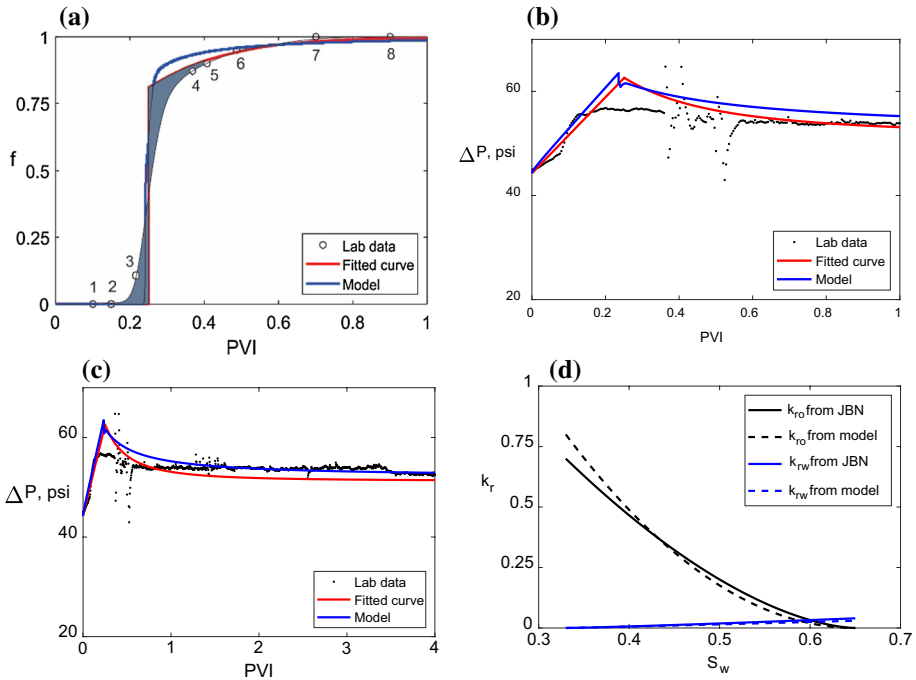


Fig. 14 Determination of relative permeability by Welge–JBN method for Test 1: **a** water-cut history, **b** pressure drop zoom around breakthrough, **c** pressure drop across the core, **d** relative permeability curves for water and oil

For Test 1, $V_{\min}=5 \times 10^{-8} \text{ m}^3$, and $N_{\min}=7$. The calculated minimum and maximum Darcy’s velocities are $1.7 \times 10^{-6} \text{ m/s}$ (0.48 ft/day) and $3 \times 10^{-4} \text{ m/s}$ (85 ft/day), respectively. The selected rate is $3 \times 10^{-6} \text{ m/s}$ (0.85 ft/day). The range of sampling time is $0.29 \leq \Delta t \leq 2562 \text{ s}$ and the selected Δt value is 300 s. The core length is fixed for Test 1 (Table 2), and the admissible area is presented in Fig. 12a. Inside the admissible area, we chose $U=3 \times 10^{-6} \text{ m/s}$ (0.85 ft/day) (black point) and $\Delta t=300 \text{ s}$ (red straight line, ϵ_s).

For Test 2, $V_{\min}=5 \times 10^{-8} \text{ m}^3$, and $N_{\min}=7$. The calculated minimum and maximum Darcy’s velocities are $2.5 \times 10^{-6} \text{ m/s}$ (0.7 ft/day) and $3 \times 10^{-4} \text{ m/s}$ (85 ft/day), respectively. The selected rate is $4 \times 10^{-6} \text{ m/s}$ (1.1 ft/day). The range of sampling time is $0.29 \leq \Delta t \leq 414 \text{ s}$, and the selected Δt value is 290 s.

5.4 Experimental Results

The results of two coreflood Tests 1 and 2—water cut at the effluent BTC and pressure drop across the core PDC—are shown in Figs. 14 and 15, respectively. In Test 1, core length is $L=0.12 \text{ m}$ and permeability is $3 \times 10^{-14} \text{ m}^2$ (30 mD). In Test 2, core length is $L=0.05 \text{ m}$ and permeability is $4 \times 10^{-14} \text{ m}^2$ (40 mD). Black dots in Figs. 14a–c and 15a–c correspond to measured data, exponential approximations are given by red curves, and blue curves reflect the modelling results.

Eight sampling points 1, 2...8 are shown in Fig. 14a. Here, water-cut history is shown until one PVI, afterwards $f=1$. Figure 14b shows pressure drop across the core. Zoom of

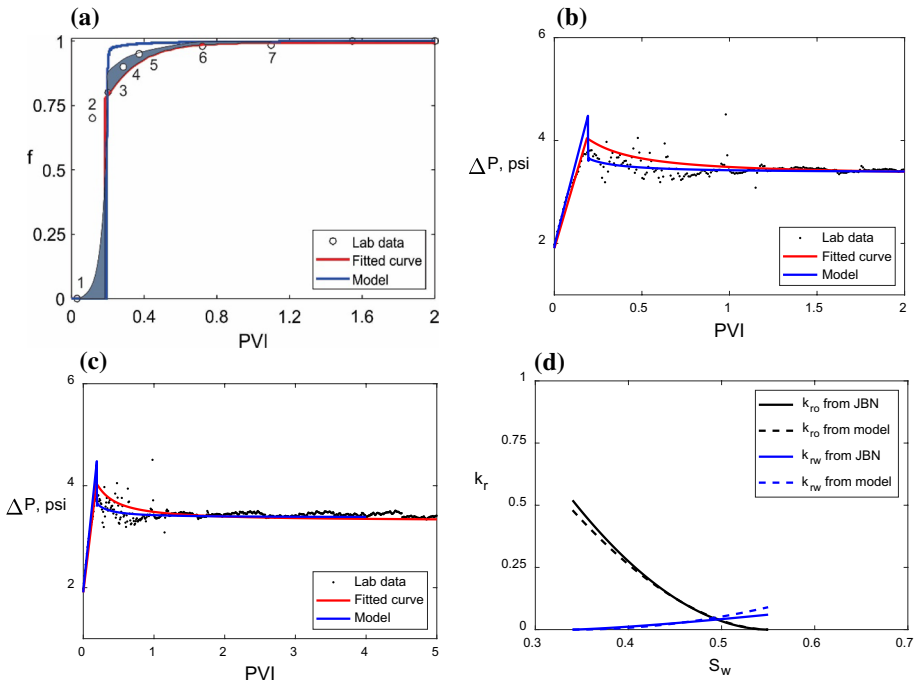


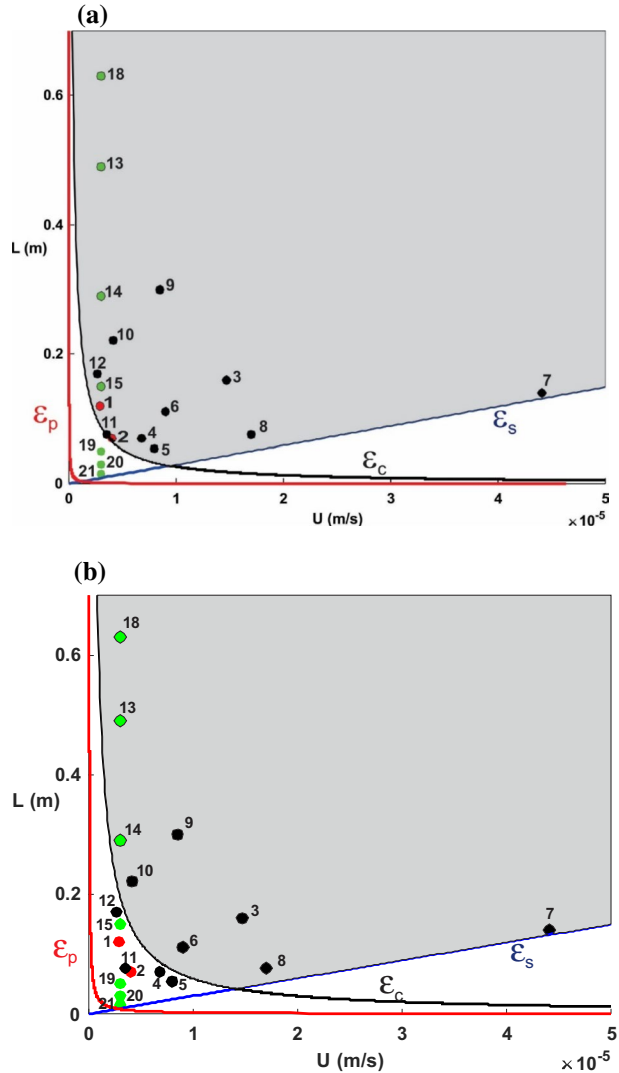
Fig. 15 Determination of relative permeability by Welge–JBN method for Test 2: **a** water-cut history, **b** pressure drop zoom around breakthrough, **c** pressure drop across the core, **d** relative permeability curves for water and oil

the pressure drop near to breakthrough time is shown in Fig. 14c. The BL BTC is obtained from the experimental data using the methodology proposed in Sect. 3.2. The BTCs and PDCs after the moment $1/D$ are approximated by exponents and are subject to explicit calculations by formulae (C.5) and (D.2, D.3). For Test 1, $\epsilon_c=0.3$. Figure 14d presents the obtained relative permeability. The corresponding Corey parameters are presented in Table 1 (Test 1).

Analogous results for Test 2 are presented in Fig. 15 and in Table 1. The admissible area is shown in Fig. 13b. The test parameters are determined as $U=4 \times 10^{-6}$ m/s (1.1 ft/day) and $\Delta t=290$ s. For the second test, $\epsilon_c=0.25$. The values of coefficient of determination R^2 presented in Table 3 indicate close agreement between the measured and modelled data. Specifically for value of capillary–viscous ratio 0.3 for Test 1, the R^2 values are 0.97 and 0.83 for K_{r_o} and K_{r_w} , respectively. For Test 2, where capillary–viscous ratio 0.25, the R^2 values for K_{r_o} and K_{r_w} are 0.99 and 0.85, respectively.

Let us compare the results of the proposed method of determining L and U with the routine practice. Figure 16a presents the admissible area for conditions of Test 1. Red points correspond to Tests 1 and 2 performed in this work. Black points correspond to tests 3, 4...12 from the literature; the corresponding references are presented in Table 4. Green points 13...21 correspond to numerical experiments performed in Sect. 2.2. All laboratory points 1, 2, 3...12 belong to admissible area. However, this result depends on the conditions of the concrete coreflood. Conditions in Fig. 16b differs from those in Fig. 16a by permeability value. As a result, points 1, 2, 4, 5, 11, and 12 are outside the admissible area.

Fig. 16 Parameters for 12 laboratory and 7 mathematical experiments from those listed in Table 4: **a** rock and fluid properties are the same as Test 1, **b** increasing permeability from $k = 3 \times 10^{-14}$ to $k = 5 \times 10^{-14} \text{ m}^2$



6 Summary and Discussions

Six criteria are to be fulfilled during waterflooding in cores to assure that the laboratory data can be used to calculate relative permeability curves and are valid at large scale. The theoretical criteria for capillary number and capillary–viscous ratio determine the validity of the Welge–JBN method for determining relative permeability from coreflooding. Four other criteria reflect the operational limitations: precision of pressure measurements, number of samples taken during one PVI, precision of water-cut measurements and minimum sampling time.

Table 4 Examples of coreflood tests from the literature

Test	L (m)	U (m/s)	References
1	0.12	3.0×10^{-6}	Test 1
2	0.05	4.0×10^{-6}	Test 2
3	0.16	1.5×10^{-5}	Al Shalabi et al. (2013)
4	0.07	7.0×10^{-6}	Akin (2001)
5	0.05	8.0×10^{-6}	Hussain et al. (2013)
6	0.11	9.0×10^{-6}	Islam and Bentsen (1986)
7	0.14	4.4×10^{-5}	Kim and Lee (2017)
8	0.08	1.7×10^{-5}	Odeh and Dotson (1985)
9	0.30	8.5×10^{-6}	Pereira et al. (2014)
10	0.22	4.1×10^{-6}	Sigmund and McCaffery (1979)
11	0.08	3.5×10^{-6}	Tao and Watson (1984)
12	0.17	2.6×10^{-6}	Zeinijahromi et al. (2016)
13	0.49	3.0×10^{-6}	Simulation test $\varepsilon_c=0.3, \mu_o=5$ cp
14	0.29	3.0×10^{-6}	Simulation test $\varepsilon_c=0.5, \mu_o=5$ cp
15	0.15	3.0×10^{-6}	Simulation test $\varepsilon_c=1, \mu_o=5$ cp
16	2.08	3.0×10^{-6}	Simulation test $\varepsilon_c=0.3, \mu_o=1.5$ cp
17	1.25	3.0×10^{-6}	Simulation test $\varepsilon_c=0.5, \mu_o=1.5$ cp
18	0.63	3.0×10^{-6}	Simulation test $\varepsilon_c=1, \mu_o=1.5$ cp
19	0.05	3.0×10^{-6}	Simulation test $\varepsilon_c=0.3, \mu_o=50$ cp
20	0.03	3.0×10^{-6}	Simulation test $\varepsilon_c=0.5, \mu_o=50$ cp
21	0.015	3.0×10^{-6}	Simulation test $\varepsilon_c=1, \mu_o=50$ cp

6.1 Maximum Capillary Number

The majority of desaturation curves “start” at $N_c=10^{-5}$, so the maximum capillary number can be assumed 10^{-5} , which corresponds to flow velocity given by Eq. (5) having an order of magnitude 10^{-4} – 10^{-5} m/s (28–3 ft/day) (Barenblatt et al. 2003; Lake et al. 2014). However, recent works suggest the relative permeability velocity dependence at lower rates (Perrin et al. 2009; Kuo et al. 2010; Krause 2012; Krause and Benson 2015; Kuo and Benson 2015). Besides, the general recommendation is to use reservoir velocity for waterflood tests, which can be one order of magnitude lower than that given by Eq. (5) and by the system of inequalities (1, 4, 18, 21) (Dake 1983). Indeed, more frequent coreflood velocity, as it follows from Fig. 16, is $U=3 \times 10^{-6}$ m/s (0.85 ft/day). The minimum core lengths calculated for this velocity are shown in Fig. 8b.

The inference that flow velocities of the order of magnitude 10^{-4} – 10^{-5} m/s (28–3 ft/day) fulfil the theoretical and operational criteria is extremely attractive, because it allows for significant acceleration of the corefloods. However, using high flow rates during corefloods requires significant experimental verification. For the velocity $U=3 \times 10^{-6}$ m/s (0.85 ft/day), the minimum core length are 0.009, 0.089, and 0.89 m for oil viscosities $\mu_o=0.1, 0.01, \text{ and } 0.001$ Pa s, respectively (Fig. 8). So, for the case of low- and medium-viscosity oil, the capillary–viscous ratio criterion cannot be fulfilled (usually 8–9-cm-long reservoir cores are unavailable, only outcrop cores are available at these lengths).

An inference that flow velocities of the order of magnitude 10^{-4} – 10^{-5} m/s (28–3 ft/day) fulfil the theoretical and operational criteria is important for relative permeability studies near to well vicinity, related to well injectivity issues.

Desaturation curves for different cores show that the maximum capillary number, where S_{or} is velocity-independent can vary from 10^{-6} to 10^{-4} (Barenblatt et al. 1991; Lake et al. 2014). Usually, this number is unavailable during coreflood planning, which makes it difficult to determine maximum admissible velocity for a given coreflood test. The Barenblatt's non-equilibrium theory for two-phase displacement could be considered as an alternative approach (Barenblatt et al. 1991, 2003). It contains the dispersivity parameter, also known as the correlation radius or typical size of micro-heterogeneity, which can be known a posteriori for various deposition environments. Besides, the criteria for minimum lengths of stabilised and end-effect zones can substitute the criteria of capillary number and capillary–viscous ratio (Bedrikovetsky 2013). Those lengths tend to infinity for high and low injection rates, yielding an optimal velocity where the lengths are minimum. The optimal velocity can minimise the effects of non-equilibrium and capillary pressure on the results of Welge–JBN calculations.

Another way around the velocity dependence of relative permeability is its recalculation from low-velocity region to that of high-velocity, and vice versa, by the upscaling from the sub-core scale (Arns et al. 2003, 2009; Arns and Adler 2018; Rabinovich et al. 2016). Saturation-dependent relative permeability is obtained at different scales under viscous or gravity domination (Adler and Thovert 1999; Adler 2013; Arns et al. 2009; Arns and Adler 2018).

6.2 Capillary–Viscous Ratio

The criterion of large-scale approximation requires negligibly small capillary–viscous ratio. Numerical calculations of two-phase flow with capillary pressure show that the value of capillary–viscous ratio 0.3–0.5 provides relative permeability determination with high accuracy (Figs. 3, 4, 5, 6).

Figures 3b and 4b show pressure drop curves versus PVI for different values of capillary–viscous ratio. If compared with BL solution, the term of capillary pressure yields: (a) increase in pressure drop before the breakthrough; (b) earlier breakthrough time and (c) abrupt decrease in the pressure drop after the breakthrough. Yet, capillary pressure has almost no effect on pressure drop after the breakthrough.

In the definition of capillary–viscous ratio (2), the end-point value of relative permeability for oil K_{rowi} can be included. In this case, K_{ro} (s) becomes normalised by dividing relative permeability for both phases by K_{rowi} . This is reasonable, since the normalisation keeps the fractional flow term in Eq. (B.1) intact, yielding the same inverse solution for $\varepsilon_c = 0$. The critical value for capillary–viscous ratio, which provides given accuracy of the inverse solution, depends on relative permeability. Scaling of relative permeabilities and capillary–viscous ratio by the factor K_{rowi} decreases the number of empirical constants by one. For example, for Corey relative permeability, the critical value for ε_c depends on six constants, while the product $\varepsilon_c \times K_{rowi}$ after the normalisation depends on five constants. Therefore, the range of variation for the critical value of the product $\varepsilon_c \times K_{rowi}$ is supposed to be smaller than the range for ε_c . The systematic implementation of this idea would determine the empirical formula for the critical value of the product $\varepsilon_c \times K_{rowi}$ versus normalised Corey parameters for relative permeability and capillary pressure, and of viscosity ratio.

6.3 Operational Criteria

The capillary pressure usually exceeds the pressure measurement precision. Thus, for conventional coreflood conditions, neglecting the capillary pressure automatically yields pressure measurements with necessary accuracy, i.e. the criterion for precision of pressure measurements can be ignored. Therefore, the system of five inequalities must be solved to fulfil the theoretical and operational criteria during laboratory waterflooding.

The criteria for the number of samples and f -precision are always compatible for cores exceeding 0.01 m.

6.4 System of Five Inequalities

The lowest point Δt_{\min} of 3D domain in space $(U, L, \Delta t)$ can be located above or below the horizontal plane $\Delta t = \Delta t_{\min}$, which determines the minimum sampling period.

The admissible 3D domain is an intersection of four areas: cylinder with the base in (U, L) plane, another cylinder with the base in $(U, \Delta t)$ plane, half-space $\Delta t > \Delta t_{\min}$ and the area below the line-helix surface.

The minimum core length, corresponding given velocity and sampling frequency, is expressed by explicit formulae (5, 6).

6.5 Practical Coreflood Planning

The system of five inequalities can be solved numerically using software Maple (Maplesoft™ 2019) with built-in solver for system of inequalities. Another way of solution is MATLAB (MathWorks® 2019) using Meshgrid and Surf commands for 3D problems; minimum core length L can be found using the Optimization Tool with Minimax Optimization function (Zhou et al. 2017). The domain obtained by solution of the system (1, 4, 18, 21) in 3D space $(L, U, \Delta t)$ provides the admissible parameters for the laboratory waterflood.

6.6 Oil–Wet and Mixed-Wet Cases

In the current analysis in the paper, the upper capillary number is assumed 10^{-4} which can be more appropriate for water-wet or weakly oil-wet systems, i.e. mostly sandstone rocks with low or moderate clay content. In oil-wet systems, which are typically carbonates, the horizontal plateau of the desaturation curve can extend to 10^{-3} (Barenblatt et al. 1991; Lake et al. 2014). One way around is introduction of cosine of the contact angle θ as a multiplier to interfacial tension σ in basic Eqs. (A.1)–(A.13). Here the contact angle is macroscopic measure of wettability. Consequently, the term $\sigma \times \cos\theta$ appears in theoretical criteria (1) and (2). The planning and design of oil-wet and mixed-wet corefloods can be performed using the presented analysis for dimensionless theoretical and operational inequalities by changing the interfacial tension σ to the product $\sigma \times \cos\theta$.

Wettability alteration yields change of the interfacial tension σ to the product $\sigma \times \cos\theta$ in the outlet boundary condition (A.13). It changes the saturation distribution in the capillary

end-effect zone (Barenblatt et al. 1991; Hussain et al. 2013) and the capillary pressure effect on the pressure drop during coreflooding.

6.7 Admissible Criteria for Steady-State Coreflood

The present paper primarily addresses the unsteady-state (USS) technique which is commonly used for determination of relative permeability. However, the technique has a major drawback providing the values of relative permeability in a narrow saturation range in the interval $[S_f, 1 - S_{or}]$ after the water breakthrough. The advantage of the steady-state (SS) test is that it provides the full-range relative permeability curves for the interval $[S_{wi}, 1 - S_{or}]$, yet the SS procedure is more time-consuming (Virnovsky and Guo 1995; Sorop et al. 2015).

The data treatment for SS tests is based on the same mathematical model (A.9, 10) as USS tests (Virnovsky and Guo 1995; Virnovsky et al. 1998). Therefore, the theoretical criteria (1) and (2) must be fulfilled during SS tests. The operational criteria should include precision of pressure measurements, like in Sect. 3.1, sample volume for precise water-cut measurements, like in Sect. 3.3. The operational criterion for number of steady states is different from that presented in Sect. 3.2, because the stabilised fractional flow values (f_1, f_2, \dots, f_N) are fully controlled and set in advance for SS tests, while they are defined by oil and water production for each sample collected during USS tests. Another operational criterion is that for accepted value f_{k0} for the stabilised fractional flow, so that $f_k - f_{k0} < \delta, k = 1, 2 \dots N, \delta \ll 1$. The detailed description of the operational criteria for SS method of relative permeability determination is a topic of forthcoming work.

6.8 Generalisations

The methodology for determining laboratory waterflood parameters $\Delta t, L$ and U is developed for typical laboratory set-up presented in Fig. 11. Different set-ups result in different set of operational criteria and various admissible domains. For example, automatic online separator can highly increase the accuracy of water-cut measurements. However, presently the fraction collector is still widely used in laboratory measurements, which imposes the above-mentioned restrictions on the sample volumes, affecting the working rate, and sampling frequency. Another reason for discussing the set-up with periodical sample collection in this paper is that the next work considers smart and low-salinity waterflood with measurements of effluent ion concentrations, where the ion composition must be determined for every sample of the produced aqueous solution (Farajzadeh et al. 2015, 2017; Borazjani et al. 2017, 2019).

Recent advances in CT tomography and X-ray methods promoted numerical solution of the inverse problem to address the limitations of the inverse analytical solution (C.5, D.2, D.3). In particular, using in situ saturation monitoring with X-rays or CT, one can account for the capillary pressure in the determination of relative permeability functions. Sorop et al. (2015), Nasralla et al. (2018) and Bartels et al. (2019) presented the examples of such studies. Using in situ saturation monitoring, it is possible to exclude end effect and distinguish the saturation interval where the Welge–JBN data are valid. Also, the saturation profile allows determining capillary pressure $P_c(s)$ at some saturations.

The effect of gravity segregation on laboratory waterflooding can be neglected. Yet, the criterion of gravity–viscous ratio must be accounted for in immiscible gas flooding, where the

difference between water and gas densities is significantly higher than that for water and oil (Dos Santos et al. 1997).

The proposed method for laboratory waterflood planning by solving system of inequalities, derived from the limitation of mathematical model and of measurement precision, can be extended to multiphase–multicomponent flows. The governing system contains mass balance equations for each component in two (or three) phases and accounts for the component dispersion (diffusion), non-equilibrium sorption and interface mass transfer (Barenblatt et al. 1991; Farajzadeh et al. 2013, 2015; Lake et al. 2014). In this case, the additional theoretical inequalities include dimensionless groups for diffusion of components, for non-equilibrium of sorption, and component distribution between phases, etc. The extra operational criterion is the precision of breakthrough concentration measurements.

7 Conclusions

Simultaneous considerations of dimensionless groups from the theory of two-phase immiscible flow in porous media along with required precision of laboratory measurements during coreflooding yield the following conclusions:

1. Two criteria of capillary number and capillary–viscous ratio are the theoretical requirements defining areas of validity for the Welge–JBN method.
2. For capillary–viscous ratio below 0.3–0.5, capillary pressure almost does not affect the curves of fractional flow and relative permeability, obtained by the Welge–JBN method.
3. Four operational criteria include those for pressure precision, number of samples, f -precision and minimum sampling period.
4. For common precisions of pressure measurements and permeability values, the pressure precision criterion can be neglected.
5. The theoretical and operational criteria correspond to the system of 5 inequalities.
6. The system of all inequalities can be solved graphically in the Euclidian 3D space “velocity–core length–sampling time”.
7. The minimum core length, where the above-mentioned 5 criteria can be fulfilled, is equal to L_m , which depends on rock permeability and porosity only. The corresponding flow velocity to be carried out during the coreflooding is equal to U_m , which is fully determined by IFT and oil viscosity.
8. For given fluid and rock properties, 3D solution determines core length, operating/operational velocity and the sample collection period.
9. For given core length, 2D solution determines operating/operational velocity and the sample collection period.

Acknowledgements The paper is dedicated to the memory of Eng. C. Holleben (Petrobras) who initiated the work by Dos Santos et al. (1997). The authors are grateful to Dr. A. Badalyan (The University of Adelaide) for fruitful discussions. Deep gratitude is due to Profs. M. Lurie and A. Kurbanov (Moscow Oil–Gas Gubkin University), who introduced PB to waterflood mathematics.

Appendix A: Mathematical Model for Two-Phase Immiscible Displacement

Following Rapoport and Leas (1953), Barenblatt et al. (1991), Lake et al. (2014), here we present the mathematical model for two-phase flow of immiscible incompressible fluids in porous media. The modified Darcy's law expresses the momentum balance for each phase

$$u_w = -\frac{kk_{rw}(s)}{\mu_w} \frac{\partial P_w}{\partial x} \quad u_o = -\frac{kk_{ro}(s)}{\mu_o} \frac{\partial P_o}{\partial x} \quad (\text{A.1})$$

where k is the permeability, u_w and u_o are the water and oil velocities, respectively, K_{rw} and K_{ro} are the relative permeability for water and oil, s is the saturation, μ_w and μ_o are the viscosity for water and oil and P_w and P_o are the phase pressures in water and oil.

Volumetric balance for water is:

$$\phi \frac{\partial s}{\partial t} + \frac{\partial u_w}{\partial x} = 0 \quad (\text{A.2})$$

Here ϕ is the porosity.

The total flux conservation follows from incompressibility of both phases:

$$u_w + u_o = U(t) \quad (\text{A.3})$$

where U is the total velocity.

The difference between phase pressures is equal to capillary pressure

$$P_o - P_w = P_c(s) = \frac{\sigma \cos \theta}{\sqrt{(k/\phi)}} J(s) \quad (\text{A.4})$$

Here P_c is the capillary pressure, σ is the interfacial tension, θ is the contact angle, and J is the capillary function.

Substituting Darcy's law for both phases (1, 2) into the expression (4) for the total flux, expressing pressure in oil from Eq. (5) and also substituting it into Eq. (4) yield

$$U = -k \left(\frac{k_{rw}(s)}{\mu_w} + \frac{k_{ro}(s)}{\mu_o} \right) \frac{\partial P_w}{\partial x} - \frac{kk_{ro}(s)}{\mu_o} \frac{\sigma \cos \theta}{\sqrt{(k/\phi)}} \frac{\partial J(s)}{\partial x} \quad (\text{A.5})$$

Expressing pressure gradient in water and substituting it into Eq. (1) yields

$$u_w = Uf(s) + \frac{kk_{ro}(s)}{\mu_o} \frac{\sigma \cos \theta}{\sqrt{(k/\phi)}} \left(\frac{\partial J(s)}{\partial x} \right) f(s), \quad f(s) = \left(1 + \frac{k_{ro}(s)\mu_w}{k_{rw}(s)\mu_o} \right)^{-1} \quad (\text{A.6})$$

where f is the fractional flow for water.

Substituting expression for water flux (A.6) into volume balance equation for water (A.2) results in one equations for unknown saturation $s(x, t)$:

$$\phi \frac{\partial s}{\partial t} + U \frac{\partial f(s)}{\partial x} = -\frac{\partial}{\partial x} \left[\frac{kk_{ro}(s)}{\mu_o} \frac{\sigma \cos \theta}{\sqrt{(k/\phi)}} \left(\frac{\partial J(s)}{\partial x} \right) \right] \quad (\text{A.7})$$

Introduce the following dimensionless variables and parameters:

$$x_D = \frac{x}{L}, \quad t_D = \frac{1}{\phi L} \int_0^t U(y)dy, \quad P = \frac{kp}{\mu_o UL}, \quad \epsilon_c = \frac{\sigma \cos \theta \sqrt{k\phi}}{\mu_o UL} \tag{A.8}$$

Here x_D is the dimensionless distance, L is the core length, t_D is the dimensionless time, P is the dimensionless pressure, and ϵ_c is the capillary-viscous ratio.

Equations (A.5, A.7) become

$$\frac{\partial s}{\partial t_D} + \frac{\partial f(s)}{\partial x_D} = \epsilon_c \frac{\partial}{\partial x_D} \left(-k_{ro}(s)f(s)J'(s) \frac{\partial s}{\partial x_D} \right), \quad f(s) = \left(1 + \frac{k_{ro}(s)\mu_w}{k_{rw}(s)\mu_o} \right)^{-1} \tag{A.9}$$

$$1 = -\frac{k\lambda(s)}{LU} \frac{\partial P}{\partial x_D} - \epsilon_c k_{ro}(s) \frac{\partial J(s)}{\partial x_D}, \quad \lambda(s) = \frac{k_{rw}(s)\mu_o}{\mu_w} + k_{ro}(s) \tag{A.10}$$

Here $\lambda(s)$ is the total mobility of two phases.

Equations (A.1) and (A.3) are decoupled, which means that the saturation distribution during the displacement $s(x_D, t_D)$ is determined from Eq. (A.1). Afterwards, the pressure distribution $p(x_D, t_D)$ is determined from Eq. (A.2) for the obtained saturation distribution.

Water flux in continuity Eq. (A.1) consists on the advective and capillary components, defined by Eq. (A.9).

The core is initially saturated with oil and connate water, i.e. the initial condition for Eq. (A.1) is:

$$t_D = 0: \quad s = S_{wi} \tag{A.11}$$

Here S_{wi} is the initial water saturation.

Only water flows through the inlet cross section, so the boundary condition at the inlet of the core is:

$$x_D = 0: \quad f - \epsilon_c k_{ro} f J'(s) \frac{\partial s}{\partial x_D} = 1 \tag{A.12}$$

The boundary condition at the core outlet after the breakthrough is given by the condition of continuity of pressures in the both phases across the outlet interface, from which follows the continuity of the capillary pressure also. At the right-hand side of the core outlet, we assume a segregated flow regime, so the capillary pressure is zero. Therefore, the capillary pressure is zero behind the core outlet too. Thus, the boundary condition at the outlet of the core corresponds to zero capillary pressure:

$$x_D = 1: \quad J(s) = 0 \tag{A.13}$$

and the outlet saturation after the breakthrough is equal to its maximum value $s^0 = 1 - S_{or}$. Here S_{or} is the residual oil saturation.

Appendix B: Large-Scale Approximation of the Buckley–Leverett Equations

For small values of ε_c , one can neglect terms with ε_c in right-hand sides of Eqs. (A.9, A.10):

$$\frac{\partial s}{\partial t_D} + \frac{\partial f(s)}{\partial x_D} = 0 \tag{B.1}$$

$$1 = -\frac{k\lambda(s)}{LU} \frac{\partial P}{\partial x_D} \tag{B.2}$$

For this case, fractional flow function $f(s)$ is the ratio between the water flux and the total flux.

Approaching $\varepsilon_c > 0$ in the boundary condition (A.6), we obtain:

$$x_D = 0: \quad f = 1 \tag{B.3}$$

The solution $s(x_D, t_D)$ of the 1 – D capillary–pressure–free displacement problem (B.1), (A.5)–(A.7) is self-similar, depending only on the group $\xi = x_D/t_D$, i.e. $s(x_D, t_D) = s(\xi)$:

$$s(x_D, t_D) = \begin{cases} 1 - S_{or}, & 0 < \frac{x_D}{t_D} < D_{or} = f'(1 - S_{or}) \\ \frac{x_D}{t_D} = f'(s), & D_{or} < \frac{x_D}{t_D} < D = f'(S_f) = \frac{(S_f)}{S_f - S_{wi}} \\ S_{wi}, & D < \frac{x_D}{t_D} < \infty \end{cases} \tag{B.4}$$

The self-similarity of the solution is the only information which is required for inverse problem to have exact solution (see). In two following sections exact shape of $s(x_D, t_D)$ will not be used, and only the fact of self-similarity will be exploited.

Appendix C: Welge’s Method for Determination of Fractional Flow Function

Let us discuss how to determine the fractional flow function $f(s)$ from the water-cut history $f(1, t_D)$ measured during the coreflood.

Let us integrate Eq. (B.1) over the region Δ on the plane (x_D, t_D) which is limited by the triangle $\partial\Delta: (0, 0) \rightarrow (1, 0) \rightarrow (1, t_D) \rightarrow (0, 0)$ and apply the Green’s formula (Bedrikovetsky 2013):

$$0 = \iint_{\Delta} \left(\frac{\partial s}{\partial t_D} + \frac{\partial f}{\partial x_D} \right) dx_D dt_D = \oint_{\partial\Delta} f dt_D - s dx_D \tag{C.1}$$

Let us calculate the contour integral in (C.1) over the sides of triangle $\partial\Delta$:

$$(0, 0) \rightarrow (1, t_D): \quad 0 \times 0 + (-s_i \times 1) = -s_i \tag{C.2}$$

$$(1, 0) \rightarrow (1, t_D): \quad \int_0^{t_D} f(1, \tau) d\tau - s \times 0 \tag{C.3}$$

$$(0, 0) \rightarrow (1, t_D): f(s(1/t_D)) - s(1/t_D)f'_s(s) \tag{C.4}$$

Substituting the expressions for the integrals over the sides of the triangle (C.2–C.4) into Eq. (C.1), we obtain the expression for the saturation on the core outlet:

$$s(1, t_D) = s_i + f(1, t_D) t_D - \int_0^{t_D} f(1, t) dt \tag{C.5}$$

Corresponding the saturation values, calculated by (C.5), to the water-cut values, which have been measured at the same moments, we obtain the dependence $f=f(s)$.

Appendix D: JBN Method for Determination of Relative Permeability

Following the works by Johnson et al. (1959) and Jones and Roszelle (1978), let us calculate the pressure drop on the core during the waterflood:

$$\Delta p(t_D) = \int_0^1 \left(-\frac{\partial p}{\partial x_D} \right) dx_D = \frac{UL}{k} \int_0^1 \frac{dx_D}{\lambda(s)} = \frac{UL t_D}{k} \int_0^{1/t_D} \frac{d\xi}{\lambda(s)} \tag{D.1}$$

Expressing the integral from (D.1) and taking its derivative with respect to the upper limit, we obtain the explicit expression for the total mobility

$$\lambda = \frac{d}{d\xi} \left(\frac{k \Delta p(\xi) \xi}{UL} \right), \quad \xi = \frac{1}{t_D} \tag{D.2}$$

Corresponding the values of total mobility calculated by (D.2) to the values of saturations calculated by (C.5) for the coherent moments, we obtain the dependence $\lambda=\lambda(s)$.

From the expression for the fractional flow function (A.9), the formulae for determination of relative permeabilities for both phases are:

$$k_{rw} = f \lambda \mu_w; \quad k_{ro} = (1 - f) \lambda \mu_o \tag{D.3}$$

It is important to emphasise that formulae (C.5) and (D.2), (D.3) deliver the solution $f=f(s)$ and $\lambda=\lambda(s)$ only for saturations which are realised during the displacement process. In the case of the displacement of oil with the connate water by water, the method provides with the fractional flow function and total mobility only for saturations higher than the frontal saturation s_f and below the s^0 and also in the initial point S_{wi} .

Appendix E: Determination of the Frontal Saturation and Displacement Velocity from the Waterless Period Data

Let us calculate the pressure drop on the core, as in (D.1), but for the moment before the breakthrough. Acting by analogy to Eq. (D.1), we obtain

$$\Delta p(t_D) = \frac{UL}{k} \left(t_D \int_0^D \frac{d\xi}{\lambda(s)} + \frac{1 - D t_D}{\lambda(s_i)} \right) \tag{E.1}$$

where initial saturation s_i can exceed connate water saturation S_{wi} .

Let us transform Eq. (E.1) to the form

$$\frac{k \Delta p (t_D)}{UL} = T \left(\int_0^D \frac{d\xi}{\lambda(s)} - \frac{D}{\lambda(s_i)} \right) + \frac{1}{\lambda(s_i)} \quad (\text{E.2})$$

Equation (E.2) gives the straight line versus t_D . The free constant in it is determined by the total mobility before the flood, which is known from the initial saturation process. The slope of the line together with the condition that the velocity D is the tangent of the fractional flow curve in the frontal saturation point makes it possible to determine the slope D and the frontal saturation s_f . The slope of the pressure drop as defined by Eq. (E.2) and calculated from the measured data is an additional information for relative permeability tuning from the coreflood data.

Appendix F: Determination of Pore Throat Radius from Permeability and Porosity

Following Barenblatt et al. (1991), here we derive permeability and porosity for cubic lattice with the tube radius r and the bond length l . One cube is adjacent to 12 bonds and one bond belongs to four cubes, so each cube includes three bonds. The porosity is equal to

$$\phi = 3 \frac{\pi r^2 l}{l^3} \quad (\text{F.1})$$

Flow through a cube side corresponds to flow through a single tube. Comparing Darcy and Poiseuille laws

$$U = \frac{k \Delta p}{\mu l} = \frac{1}{l^2} \frac{\pi r^4}{8\mu} \frac{\Delta p}{l}, \quad (\text{F.2})$$

we obtain the formula for permeability

$$k = \frac{\pi r^4}{8l^2} \quad (\text{F.3})$$

From Eqs. (F.1) and (F.3) follows the expression for pore throat radius r

$$r = \sqrt{\frac{24k}{\phi}}. \quad (\text{F.4})$$

References

- Abbas, M.: An extension of Johnson, Bossler and Neumann JBN method for calculating relative permeabilities. In: SPE Annual Technical Conference and Exhibition 2016. Society of Petroleum Engineers (2016)
- Adler, P.M.: *Multiphase Flow in Porous Media*. Springer, Amsterdam (1995)
- Adler, P.: *Porous Media: Geometry and Transports*. Elsevier, Amsterdam (2013)

- Adler, P.M., Thovert, J.-F.: *Fractures and Fracture Networks*, pp. 103–162. Springer, Berlin (1999)
- Akin, S.: Estimation of fracture relative permeabilities from unsteady state corefloods. *J. Pet. Sci. Eng.* **30**(1), 1–14 (2001)
- Al Shalabi, E.W., Sephehnoori, K., Delshad, M.: Mechanisms behind low salinity water flooding in carbonate reservoirs. In: *SPE Western Regional & AAPG Pacific Section Meeting 2013 Joint Technical Conference 2013*. Society of Petroleum Engineers (2013)
- Arns, C., Adler, P.: Fast Laplace solver approach to pore-scale permeability. *Phys. Rev. E* **97**(2), 023303 (2018)
- Arns, J.-Y., Arns, C.H., Sheppard, A.P., Sok, R.M., Knackstedt, M.A., Pinczewski, W.V.: Relative permeability from tomographic images; effect of correlated heterogeneity. *J. Pet. Sci. Eng.* **39**(3–4), 247–259 (2003)
- Arns, C., Knackstedt, M., Mecke, K.: Boolean reconstructions of complex materials: integral geometric approach. *Phys. Rev. E* **80**(5), 051303 (2009)
- Aziz, K., Settari, A.: *Petroleum Reservoir Simulation*. Applied Science Publ. Ltd., London (1979)
- Badalyan, A., Carageorgos, T., Bedrikovetsky, P., You, Z., Zeinijahromi, A., Aji, K.: Critical analysis of uncertainties during particle filtration. *Rev. Sci. Instrum.* **83**(9), 095106 (2012)
- Banchoff, T.F., Lovett, S.T.: *Differential Geometry of Curves and Surfaces*. Chapman and Hall/CRC, London (2016)
- Barenblatt, G., Entov, V., Ryzhik, V.: *Theory of Fluid Flows Through Natural Rocks*. Kluwer, Dordrecht (1991)
- Barenblatt, G., Patzek, T.W., Silin, D.: The mathematical model of nonequilibrium effects in water–oil displacement. *SPE J.* **8**(04), 409–416 (2003)
- Bartels, W.-B., Mahani, H., Berg, S., Hassanizadeh, S.: Literature review of low salinity waterflooding from a length and time scale perspective. *Fuel* **236**, 338–353 (2019)
- Bedrikovetsky, P.: *Mathematical Theory of Oil and Gas Recovery: With Applications to Ex-USSR Oil and Gas Fields*, vol. 4. Springer, Berlin (2013)
- Borazjani, S., Behr, A., Genolet, L., Van Der Net, A., Bedrikovetsky, P.: Effects of fines migration on low-salinity waterflooding: analytical modelling. *Trans. Porous Media* **116**(1), 213–249 (2017)
- Borazjani, S., Behr, A., Genolet, L., Kowollik, P., Bedrikovetsky, P.: Ion-exchange inverse problem for low-salinity coreflooding. *Trans. Porous Media* **128**(2), 571–611 (2019)
- Buckley, S.E., Leverett, M.: Mechanism of fluid displacement in sands. *Trans. AIME* **146**(01), 107–116 (1942)
- Cao, J., James, L.A., Johansen, T.E.: Determination of two phase relative permeability from core floods with constant pressure boundaries. In: *Society of Core Analysis Symposium*, Avignon, France (2014)
- Cao, J., Liu, X., James, L., Johansen, T.: Analytical interpretation methods for dynamic immiscible core flooding at constant differential pressure. In: *Society of Core Analysis Symposium*, St. John's Newfoundland and Labrador, Canada, pp. 16–21 (2015)
- Chatzis, I., Morrow, N.R., Lim, H.T.: Magnitude and detailed structure of residual oil saturation. *Soc. Pet. Eng. J.* **23**(02), 311–326 (1983)
- Chen, Z.: *Reservoir Simulation: Mathematical Techniques in Oil Recovery*, vol. 77. SIAM, Philadelphia (2007)
- Chen, X., Kianinejad, A., DiCarlo, D.A.: An extended JBN method of determining unsteady-state two-phase relative permeability. *Water Resour. Res.* **52**(10), 8374–8383 (2016)
- Civan, F., Donaldson, E.: Relative permeability from unsteady-state displacements with capillary pressure included. *SPE Form. Eval.* **4**(02), 189–193 (1989)
- Dake, L.P.: *Fundamentals of Reservoir Engineering*, vol. 8. Elsevier, Amsterdam (1983)
- Dos Santos, R.L., Bedrikovetsky, P., Holleben, C.R.: Optimal design and planning for laboratory corefloods. In: *Latin American and Caribbean Petroleum Engineering Conference*. Society of Petroleum Engineers (1997)
- Farajzadeh, R., Ameri, A., Faber, M.J., Van Batenburg, D.W., Boersma, D.M., Bruining, J.: Effect of continuous, trapped, and flowing gas on performance of Alkaline Surfactant Polymer (ASP) flooding. *Ind. Eng. Chem. Res.* **52**(38), 13839–13848 (2013)
- Farajzadeh, R., Lotfollahi, M., Eftekhari, A., Rossen, W., Hirasaki, G.: Effect of permeability on implicit-texture foam model parameters and the limiting capillary pressure. *Energy Fuels* **29**(5), 3011–3018 (2015)
- Farajzadeh, R., Guo, H., van Winden, J., Bruining, J.: Cation exchange in the presence of oil in porous media. *ACS Earth Space Chem.* **1**(2), 101–112 (2017)
- Honarpour, M., Koederitz, F., Herbert, A.: *Relative permeability of petroleum reservoirs*. CRC Press, United States (1986)

- Hussain, F., Cinar, Y., Bedrikovetsky, P.G.: Comparison of methods for drainage relative permeability estimation from displacement tests. In: SPE Improved Oil Recovery Symposium. Society of Petroleum Engineers (2010)
- Hussain, F., Cinar, Y., Bedrikovetsky, P.: A semi-analytical model for two phase immiscible flow in porous media honouring capillary pressure. *Trans. Porous Media* **92**(1), 187–212 (2012)
- Hussain, F., Zeinijahromi, A., Bedrikovetsky, P., Badalyan, A., Carageorgos, T., Cinar, Y.: An experimental study of improved oil recovery through fines-assisted waterflooding. *J. Pet. Sci. Eng.* **109**, 187–197 (2013)
- Hussain, F., Pinczewski, W.V., Cinar, Y., Arns, J.-Y., Arns, C., Turner, M.: Computation of relative permeability from imaged fluid distributions at the pore scale. *Trans. Porous Media* **104**(1), 91–107 (2014)
- Islam, M.R., Bentsen, R.: A dynamic method for measuring relative permeability. *J. Can. Pet. Technol.* **25**(01), 39–50 (1986)
- Johansen, T.E., James, L.A.: Solution of multi-component, two-phase Riemann problems with constant pressure boundaries. *J. Eng. Math.* **96**(1), 23–35 (2016)
- Johnson, E., Bossler, D., Bossler, V.: Calculation of relative permeability from displacement experiments (1959)
- Jones, S., Roszelle, W.: Graphical techniques for determining relative permeability from displacement experiments. *J. Pet. Technol.* **30**(05), 807–817 (1978)
- Katika, K., Ahkami, M., Fosbøl, P.L., Halim, A.Y., Shapiro, A., Thomsen, K., Xiarchos, I., Fabricius, I.L.: Comparative analysis of experimental methods for quantification of small amounts of oil in water. *J. Pet. Sci. Eng.* **147**, 459–467 (2016)
- Kianinejad, A., Chen, X., DiCarlo, D.A.: Direct measurement of relative permeability in rocks from unsteady-state saturation profiles. *Adv. Water Resour.* **94**, 1–10 (2016)
- Kim, C., Lee, J.: Experimental study on the variation of relative permeability due to clay minerals in low salinity water-flooding. *J. Pet. Sci. Eng.* **151**, 292–304 (2017)
- Krause, M.: Modeling and investigation of the influence of capillary heterogeneity on relative permeability. In: SPE Annual Technical Conference and Exhibition. Society of Petroleum Engineers (2012)
- Krause, M.H., Benson, S.M.: Accurate determination of characteristic relative permeability curves. *Adv. Water Resour.* **83**, 376–388 (2015)
- Kuo, C.-W., Benson, S.M.: Numerical and analytical study of effects of small scale heterogeneity on CO₂/brine multiphase flow system in horizontal coreflows. *Adv. Water Resour.* **79**, 1–17 (2015)
- Kuo C.-w., Perrin J.-C., Benson, S.M.: Effect of gravity, flow rate, and small scale heterogeneity on multiphase flow of CO₂ and brine. In: SPE Western Regional Meeting. Society of Petroleum Engineers (2010)
- Lake, L.W., Johns, R., Rossen, W.R., Pope, G.A.: Fundamentals of enhanced oil recovery (2014)
- Maplesoft™: Solver for a system of inequalities. <https://www.maplesoft.com/support/help/maple/view.aspx?path=Task/SolveInequality> (2019). Accessed 10 March 2019
- MathWorks®: Meshgrid, Surf Commands <https://au.mathworks.com/products/matlab.html> (2019). Accessed 10 March 2019
- McPhee, C., Reed, J., Zubizarreta, I.: Core Analysis: A Best Practice Guide, vol. 64. Elsevier, Amsterdam (2015)
- Miller, M.A., Ramey Jr., H.: Effect of temperature on oil/water relative permeabilities of unconsolidated and consolidated sands. *Soc. Pet. Eng. J.* **25**(06), 945–953 (1985)
- Nasralla, R.A., Mahani, H., van der Linde, H.A., Marcelis, F.H., Masalmeh, S.K., Sergienko, E., Brussee, N.J., Pieterse, S.G., Basu, S.: Low salinity waterflooding for a carbonate reservoir: experimental evaluation and numerical interpretation. *J. Pet. Sci. Eng.* **164**, 640–654 (2018)
- Odeh, A., Dotson, B.: A method for reducing the rate effect on oil and water relative permeabilities calculated from dynamic displacement data. *J. Pet. Technol.* **37**(11), 2051–052058 (1985)
- Pereira, B.M.F., Shahverdi, H., Sohrabi, M.: Refinement of relative permeability measurements by accounting for viscous fingering in coreflood experiments. In: SPE Annual Technical Conference and Exhibition. Society of Petroleum Engineers (2014)
- Perrin, J.-C., Krause, M., Kuo, C.-W., Miljkovic, L., Charoba, E., Benson, S.M.: Core-scale experimental study of relative permeability properties of CO₂ and brine in reservoir rocks. *Energy Proc.* **1**(1), 3515–3522 (2009)
- Rabinovich, A.: Estimation of sub-core permeability statistical properties from coreflooding data. *Adv. Water Resour.* **108**, 113–124 (2017)
- Rabinovich, A.: Analytical corrections to core relative permeability for low-flow-rate simulation. *SPE J.* (2018)
- Rabinovich, A., Li, B., Durlofsky, L.J.: Analytical approximations for effective relative permeability in the capillary limit. *Water Resour. Res.* **52**(10), 7645–7667 (2016)

- Rapoport, L., Leas, W.: Properties of linear waterfloods. *J. Pet. Technol.* **5**(05), 139–148 (1953)
- Richmond, P., Watsons, A.: Estimation of multiphase flow functions from displacement experiments. *SPE Reserv. Eng.* **5**(01), 121–127 (1990)
- Sigmund, P., McCaffery, F.: An improved unsteady-state procedure for determining the relative-permeability characteristics of heterogeneous porous media (includes associated papers 8028 and 8777). *Soc. Pet. Eng. J.* **19**(01), 15–28 (1979)
- Sorop, T.G., Masalmeh, S.K., Suijkerbuijk, B.M.J.M., van der Linde, H.A., Mahani, H., Brussee, N.J., Marcelis, F.A.H.M., Coorn, A. Relative Permeability Measurements to Quantify the Low Salinity Flooding Effect at Field Scale (2015)
- Tao, T., Watson, A.: Accuracy of JBN estimates of relative permeability: part 2-algorithms. *Soc. Pet. Eng. J.* **24**(02), 215–223 (1984)
- Torsæter, O., Abtahi, M.: *Experimental Reservoir Engineering Laboratory Workbook*. Department of Petroleum Engineering and Applied Geophysics, Norwegian University of Science and Technology (NTNU), Trondheim (2003)
- Toth, J., Bodi, T., Szucs, P., Civan, F.: Direct determination of relative permeability from nonsteady-state constant pressure and rate displacements. In: *SPE Production and Operations Symposium*. Society of Petroleum Engineers (2001)
- Toth, J., Bodi, T., Szucs, P., Civan, F.: Convenient formulae for determination of relative permeability from unsteady-state fluid displacements in core plugs. *J. Pet. Sci. Eng.* **36**(1–2), 33–44 (2002)
- Virnovsky, G., Guo, Y.: Relative permeability and capillary pressure concurrently determined from steady-state flow experiments. In: *IOR 1995-8th European Symposium on Improved Oil Recovery* (1995)
- Virnovsky, G., Vatne, K., Skjaeveland, S., Lohne, A.: Implementation of multirate technique to measure relative permeabilities accounting. In: *SPE Annual Technical Conference and Exhibition*. Society of Petroleum Engineers (1998)
- Welge, H.J.: A simplified method for computing oil recovery by gas or water drive. *J. Pet. Technol.* **4**(04), 91–98 (1952)
- Zeinijahromi, A., Farajzadeh, R., Bruining, J.H., Bedrikovetsky, P.: Effect of fines migration on oil–water relative permeability during two-phase flow in porous media. *Fuel* **176**, 222–236 (2016)
- Zhou, K., Hou, J., Fu, H., Wei, B., Liu, Y.: Estimation of relative permeability curves using an improved Levenberg–Marquardt method with simultaneous perturbation Jacobian approximation. *J. Hydrol.* **544**, 604–612 (2017)
- Zou, S., Hussain, F., Arns, J.-Y., Guo, Z., Arns, C.H.: Computation of relative permeability from in situ imaged fluid distributions at the pore scale. *SPE J.* **23**(03), 737–749 (2018)

3.2 Coreflood Planning Criteria for Relative Permeability Computation by Welge-JBN Method

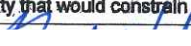
Al-Sarihi, A., You, Z., Genolet, L., Behr, A., Kowolik, P., Zeinjahromi, A., and Bedrikovetsky, P., published 05/2018

APPEA Journal

Statement of Authorship

Title of Paper	Corefood planning criteria for relative permeability computation by Welge-JBN method		
Publication Status	<input checked="" type="checkbox"/> Published	<input type="checkbox"/> Accepted for Publication	
	<input type="checkbox"/> Submitted for Publication	<input type="checkbox"/> Unpublished and Unsubmitted work written in manuscript style	
Publication Details	A. Al-Sarhi, Z. You, L. Genolet, A. Behr, P. Kowollik, A. Zeinjahromi, and P. Bedrikovetsky, 2018. Corefood planning criteria for relative permeability computation by Welge-JBN method. APPEA Journal		


Principal Author

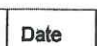
Name of Principal Author (Candidate)	Abdullah Al-Sarhi		
Contribution to the Paper	Literature review, experimental work, analysis of results, writing the manuscript.		
Overall percentage (%)	70%		
Certification:	This paper reports on original research I conducted during the period of my Higher Degree by Research candidature and is not subject to any obligations or contractual agreements with a third party that would constrain its inclusion in this thesis. I am the primary author of this paper.		
Signature		Date	17/9/2019

Co-Author Contributions

By signing the Statement of Authorship, each author certifies that:

- i. the candidate's stated contribution to the publication is accurate (as detailed above);
- ii. permission is granted for the candidate to include the publication in the thesis; and
- iii. the sum of all co-author contributions is equal to 100% less the candidate's stated contribution.

Name of Co-Author	Zhenjiang You		
Contribution to the Paper	Numerical simulation, review of manuscript		
Signature		Date	12/9/19

Name of Co-Author	Luis Genolet		
Contribution to the Paper	Support in analysis of results		
Signature		Date	10.03.2019

Please cut and paste additional co-author panels here as required.

Name of Co-Author	Aron Behr		
Contribution to the Paper	Support in analysis of results		
Signature		Date	11/9/19

Name of Co-Author	Patrick Kowolik		
Contribution to the Paper	Support in analysis of results		
Signature		Date	10/9/19

Name of Co-Author	Abbas Zeinjahromi		
Contribution to the Paper	Model formulation, review manuscript		
Signature		Date	17/09/2019

Name of Co-Author	Pavel Bedrkiovetsky		
Contribution to the Paper	Model formulation, review of manuscript		
Signature		Date	17/09/19

Coreflood planning criteria for relative permeability computation by Welge-JBN method

A. Al-Sarhi^{A,C}, Z. You^A, A. Behr^B, L. Genolet^B, P. Kowollik^B, A. Zeinijahromi^A and P. Bedrikovetsky^A

^AAustralian School of Petroleum, The University of Adelaide, Adelaide, SA 5005, Australia.

^BWintershall Holding GmbH, EOT/R, Friedrich-Ebert Str. 160, 34119 Kassel, Germany.

^CCorresponding author. Email: abdullah.sarhi@adelaide.edu.au

Abstract. Relative permeability computation is extensively applied in petroleum engineering through the Welge-JBN's method in unsteady-state corefloods. The purpose of this work is to determine admissible coreflood parameters that could limit the application of the Welge-JBN method. These parameters are presented through theoretical and operational criteria. The theoretical criteria include capillary number and capillary–viscous ratio. The operational criteria consist of measurement precision for pressure, volume sampling for either of phases, water cut measurement precision, and number of samples taken during one pore volume injected. The minimum core length and fluid displacement velocity for specific rock and fluid properties could be determined through these criteria. A laboratory coreflood example was performed using the proposed parameters.

Keywords: core length, flow velocity, waterflooding.

Accepted 27 February 2018, published online 28 May 2018

Introduction

Relative permeabilities are important functions for oil recovery determination. Welge-JBN's method is applied to calculate relative permeabilities from unsteady-state laboratory corefloods. However, in order to apply this method, core length and displacement velocity need to satisfy the Buckley-Leverett model (Lake 1989; Barenblatt *et al.* 1991).

This paper presents a system of two theoretical and four operational criteria that must be fulfilled simultaneously during coreflooding because they are interdependent. For instance, a small capillary–viscous ratio can be achieved with high displacement velocity but this high velocity can fail the capillary number criterion. On the other hand, a small velocity can give low pressure drop and small sampling volume but it can decrease the measurement precision of the water cut criterion. Thus, this study aims to provide the parameters necessary to calculate flow rate based on the core length given (or vice versa), where all the criteria can be satisfied. In addition, the capillary–viscous ratio is used in this study to numerically match the large scale Buckley-Leverett solution with the capillary pressure boundary layers, where this ratio plays a pivotal role in the matching accuracy.

Theoretical criteria

Capillary number criterion

The ratio of the viscous forces over the capillary pressure forces on the pore scale represents the capillary number. It shows that residual oil saturation is independent of flow rate (Lake 1989):

$$N_c = \frac{U \mu_w}{\sigma} \leq 10^{-5} \sim 10^{-4} \quad (1)$$

Here U is the velocity, μ_w is the water viscosity, and σ is the interfacial tension.

Flow rate can affect the relative permeability at $N_c = 10^{-5}$ and, reservoir velocity is suggested to be used in coreflooding (Dake 1983). Therefore:

$$U \leq 10^{-5} \frac{\sigma}{\mu_w} \quad (2)$$

Capillary–viscous ratio

Capillary pressure should be negligible compared to pressure drop across the core and it must be small to satisfy the large scale approximation of the Buckley-Leverett system (Bedrikovetsky 1993):

$$\varepsilon_c = \frac{\sigma \sqrt{k \phi}}{\mu_o L U} \ll 1 \quad (3)$$

where k is the permeability, ϕ is the porosity, and L is the core length.

Operational criteria

Pressure measurement precision criterion

Pressure drop across the core needs to be higher than the half-scale pressure of the transducers in order to calculate end point permeabilities accurately. Usually, relative permeability at connate water is close to the minimum of total mobility $\lambda(s)$, i.e. for the bulk of saturation interval $[s_{wi}, 1-s_{or}]$ the following inequality is fulfilled:

$$\lambda(s) \geq k_{rowi} \quad (4)$$

Here k_{rowi} is the oil relative permeability at initial water saturation. Applying Darcy's law, the velocity is:

$$U = k \frac{\lambda(s) \Delta p}{\mu_o L} \geq \frac{k k_{rowi} \Delta p_m}{\mu_o L}, \quad (5)$$

Where Δp is pressure drop and Δp_m is the half-scale pressure drop.

Number of samples criterion

To account for the S-shape breakthrough curve where exponential approximation can be made (Civan and Donaldson 1989), a minimum number of samples need to be collected:

$$\frac{\pi R^2 L \phi}{U \pi R^2 \Delta t} \geq N_m + 1 \quad (6)$$

where Δt is the sample-collection duration, R is the core radius and N_m is the minimum number of samples.

Precise measurement of water cut criterion

Oil and water collected in a single sample should be more than the half-scale volume of burette, V_m , multiplied by the minimum fractional flow value, f_m to accurately distinguish the phases for the water-cut curve:

$$U \pi R^2 \Delta t \geq f_m V_m \quad (7)$$

Sampling period criterion

There is a minimum collection time of effluent volumes needed in an experimental setup to meet the above-mentioned criteria:

$$\Delta t \geq \Delta t_{min} \quad (8)$$

Here Δt_{min} is minimum duration for sample collection.

Discussion

Six criteria need to be fulfilled to give accurate calculations of relative permeability by Welge-JBN's method. For the capillary-viscous ratio, calculations show that $\varepsilon_c \leq 0.5$ gives an almost negligible capillary pressure effect and shows the smallest discrepancy between the relative permeabilities calculated by the Welge-JBN method and numerical simulation as can be seen in Fig. 1. R^2 , the coefficient of determination, is 0.98. Table 1 presents the parameters of the core used in the calculations.

Regarding capillary number criteria, most desaturation curves begin at $N_c = 10^{-5}$, so the maximum capillary number can be assumed to be 10^{-5} , which corresponds to flow velocity having an order of magnitude 10^{-4} – 10^{-5} m/s which fulfils the theoretical and operational criteria.

For conventional coreflood conditions, neglecting the capillary pressure automatically yields pressure measurements with the necessary accuracy, so the criterion for precision of pressure measurements can be waived.

Figure 2 shows the admissible 3D domain, which is an intersection of four areas: a cylinder with the base in the (U, L) -plane, another cylinder with the base in the $(U, \Delta t)$ -plane, and the half-space $\Delta t > \Delta t_{min}$. A represents the velocity at maximum capillary number, B represents the minimum velocity based on the sampling period and water cut precision criteria, C indicates the sampling volume plane, and D is the water cut precision plane. As this domain ensures the satisfaction of the inequalities of the criteria (both theoretical and operational), the core length should be higher than the minimum length induced from the intersection of capillary-viscous, sampling time and, fractional flow precision planes. Also, the flow rate can be

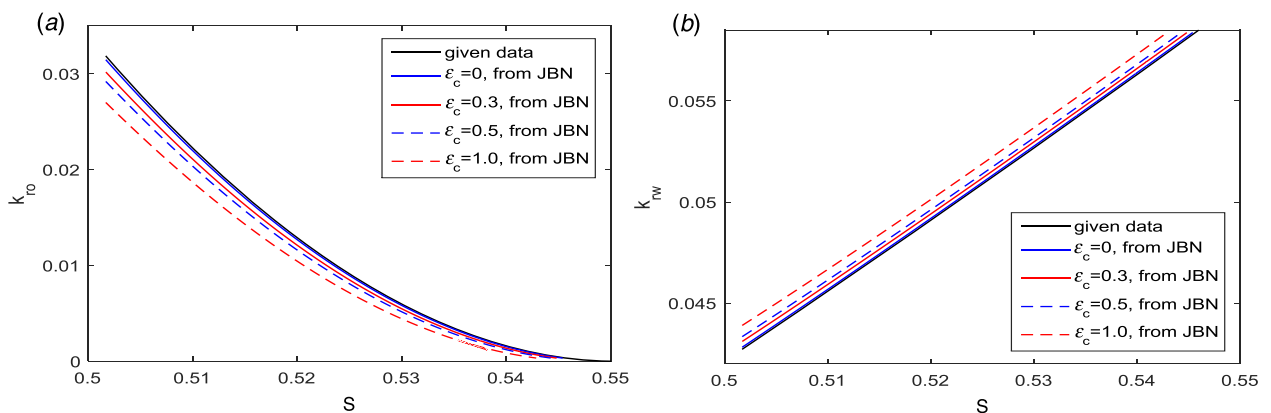
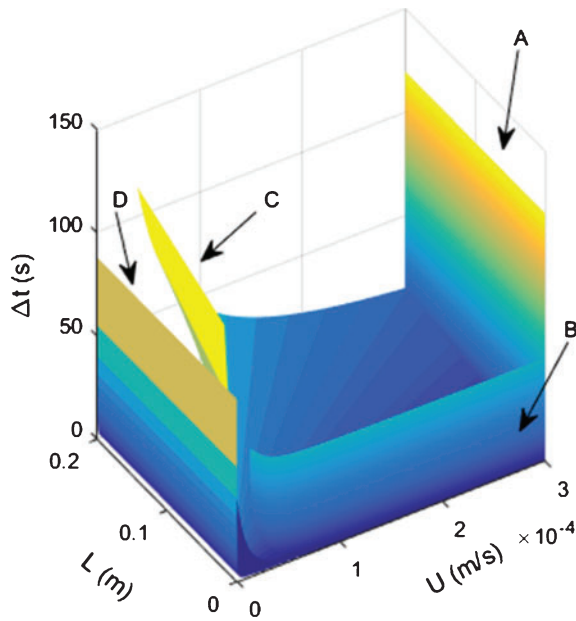


Fig. 1. Effects of capillary-viscous ratio on the accuracy of relative permeabilities using the Welge-JBN and numerical simulation (properties of the core is outlined in Table 1); (a) oil relative permeability and (b) water relative permeability.

Table 1. Corey parameters and rock/fluid properties of the coreflood example

S_{wi}	S_{or}	ϕ	k, m^2	k_{rowi}	k_{rwor}	n_w	n_o
0.34	0.45	0.22	4×10^{-14}	0.52	0.06	1.3	1.9

**Fig. 2.** Three-dimensional domain for system of five inequalities: three-dimensional image of the domain in coordinates $(U, L, \Delta t)$.

determined, if the core length is given, between planes B and C. The parameters used for calculation of this example of the domain and admissible areas in Fig. 2 are: $N_m = 7$, $V_m = 5 \times 10^{-8} \text{ m}^3$, $f_m = 0.1$.

Conclusions

The two criteria, capillary number and capillary–viscous ratio, are the theoretical requirements for the validity of the Welge-JBN method. For a capillary–viscous ratio below 0.5, capillary pressure almost does not affect the curves of relative permeability as obtained by the Welge-JBN method. Four operational criteria include pressure-precision, number-of-samples, fractional flow precision, and minimum sampling period. For common precisions of pressure measurements and permeability values, the pressure-precision criterion can be waived. The system of all inequalities can be solved graphically in a 3D space, which can determine velocity, core length and sampling time. The minimum core length, where the above-mentioned criteria can be fulfilled, depends on rock permeability and porosity only. The corresponding flow velocity to be carried out during the coreflooding is determined by interfacial tension and oil viscosity.

Conflicts of interest

The authors declare there are no conflicts of interest that could influence this work.

References

- Barenblatt, G. I., Entov, V. M., and Ryzhik, V. M. (1991): 'Theory of Fluids Flows through Natural Rocks', Kluwer Academic Publishers, Dordrecht, Boston, London.
- Bedrikovetsky, P. G. (1993): *Mathematical Theory of Oil and Gas Recovery (With applications to the development of the ex-USSR oil and gas-condensate reservoirs)*. Kluwer Academic Publishers, London, Boston, Dordrecht.
- Civan, F., and Donaldson, E. C. (1989). Relative permeability from unsteady-state displacement with capillary pressure included. *SPE Formation Evaluation* 4(2), 189–193. doi:10.2118/16200-PA
- Dake, L.P. (1983): 'Fundamentals of Reservoir Engineering', Elsevier Science & Technology.
- Lake, L. W. (1989): 'Enhanced Oil Recovery'. Prentice Hall, Englewood Cliffs, NY.

The authors



Abdullah Al-Sarihi is a PhD candidate in the Australian School of Petroleum at the University of Adelaide, Australia. He received his BEng and MSc degrees in petroleum engineering both from the University of New South Wales.



Dr Zhenjiang You is a senior researcher in the Australian School of Petroleum at the University of Adelaide, Australia. Dr You received his BEng degree in engineering mechanics and PhD degree in fluid mechanics, both from Zhejiang University.



Dr Aron Behr was awarded his PhD in Fluid Mechanics from Moscow Gubkin Oil-Gas University. Previously, he was a professor at Ukhta University (Russia) and a senior scientist at Freiberg University (Germany). Currently he is a senior petroleum engineer at Wintershall (Germany).



Dr Luis Genolet was awarded his PhD in chemical engineering. He was a chief scientist at Intevep Research (Venezuela). Currently he is a senior chemical engineer at Wintershall (Germany).



Patrick Kowollik has both a BSc and an MSc in petroleum engineering. Presently, he is a PhD student and trainee at Wintershall (Germany).



Dr Abbas Zeinijahromi is a Senior Lecturer in Petroleum Engineering at the Australian School of Petroleum, the University of Adelaide. Abbas holds a PhD in Petroleum engineering from the University of Adelaide, M.Sc. in Reservoir Engineering and B.Sc. in Production Engineering.



Prof. Pavel Bedrikovetsky is a professor and Chair in Petroleum Engineering at the Australian School of Petroleum in the University of Adelaide. He is also a senior staff consultant to Petrobras. He holds BEng and MSc degrees in applied mathematics, a PhD degree in fluid mechanics, and a DSc degree in reservoir engineering, all from Moscow Gubkin Petroleum University.

4 Effects of Fines Migration on Enhanced oil Recovery

This chapter has two papers published on the area of enhancing oil recovery by fines migration. The paper 'Effects of Fines Migration on Residual oil During Low-Salinity Waterflooding' in section 4.1 has nine coreflood tests, two of which are single-phase and the rest are two-phase. The paper investigates the theory of micro-scale flux diversion and how it reduces water permeability to improve sweep efficiency. The tests were performed on Berea (high clay content), Bentheimer (low clay content), and artificial cores (clean sand) to test the theory. The paper 'Low-salinity Waterflooding in Non-Polar oil' in section 4.2 is a peer-reviewed extended abstract and it also tests the same theory but it was conducted on only one Berea core sample and one artificial clean sand core sample. The order of the papers in the chapter is based on the quantity of work done in each paper.

4.1 Effects of Fines Migration on Residual oil During Low-Salinity Waterflooding

Al-Sarihi, A., Zeinjahromi, A., Genolet, L., Behr, A., Kowollik, P. and Bedrikovetsky, P., published 07/2018

Journal of Energy&Fuels

Statement of Authorship

Title of Paper	Effects of fines migration on residual oil during low-salinity waterflooding
Publication Status	<input checked="" type="checkbox"/> Published <input type="checkbox"/> Accepted for Publication <input type="checkbox"/> Submitted for Publication <input type="checkbox"/> Unpublished and Unsubmitted work written in manuscript style
Publication Details	A. Al-Sarihi, A. Zeinjahromi, L. Genolet, A. Behr, P. Kowollik, and P. Bedrikovetsky, 2018, Effects of fines migration on residual oil during low-salinity waterflooding, Journal of Energy&Fuels

Principal Author

Name of Principal Author (Candidate)	Abdullah Al-Sarihi			
Contribution to the Paper	Literature review, experimental work, analysis of results, writing the manuscript.			
Overall percentage (%)	70%			
Certification:	This paper reports on original research I conducted during the period of my Higher Degree by Research candidature and is not subject to any obligations or contractual agreements with a third party that would constrain its inclusion in this thesis. I am the primary author of this paper.			
Signature	<table border="1"> <tr> <td></td> <td>Date</td> <td>17/9/2019</td> </tr> </table>		Date	17/9/2019
	Date	17/9/2019		

Co-Author Contributions

By signing the Statement of Authorship, each author certifies that:

- i. the candidate's stated contribution to the publication is accurate (as detailed above);
- ii. permission is granted for the candidate to include the publication in the thesis; and
- iii. the sum of all co-author contributions is equal to 100% less the candidate's stated contribution.

Name of Co-Author	Abbas Zeinjahromi			
Contribution to the Paper	Support in analysis of results, methodology writing, review manuscript			
Signature	<table border="1"> <tr> <td></td> <td>Date</td> <td>17/09/19</td> </tr> </table>		Date	17/09/19
	Date	17/09/19		

Name of Co-Author	Luis Genolet			
Contribution to the Paper	Support in analysis of results			
Signature	<table border="1"> <tr> <td></td> <td>Date</td> <td>10.09.2019</td> </tr> </table>		Date	10.09.2019
	Date	10.09.2019		

Please cut and paste additional co-author panels here as required.

Name of Co-Author	Aron Behr		
Contribution to the Paper	Support in analysis of results		
Signature		Date	11/9/19

Name of Co-Author	Patrick Kowollik		
Contribution to the Paper	Support in analysis of results		
Signature		Date	10/9/19

Name of Co-Author	Pavel Bedrkiovetsky		
Contribution to the Paper	Support in analysis of results, literature review, review of manuscript		
Signature		Date	17/09/19

Effects of Fines Migration on Residual Oil during Low-Salinity Waterflooding

A. Al-Sarhi,[†] A. Zeinijahromi,^{*,†,‡} L. Genolet,[‡] A. Behr,[‡] P. Kowollik,[‡] and P. Bedrikovetsky[†]

[†]Australian School of Petroleum, The University of Adelaide, Adelaide SA 5005, Australia

[‡]Wintershall Holding GmbH, Friedrich-Ebert St. 160, 34119 Kassel, Germany

ABSTRACT: A novel mechanism of residual oil reduction during low-salinity water flooding by induced fines migration and consequent permeability damage is discovered. Dry corefloods (without oil) with piecewise-constant decreasing salinity are conducted to verify the presence of movable fines that yield permeability decrease. Sequential two-phase coreflood tests are performed using the displacement of nonpolar oil by high-salinity water, followed by full resaturation of the core by nonpolar oil and low-salinity waterflooding. The test then continued in tertiary mode, in which brines of decreasing salinity were injected in the presence of residual oil. Four Berea cores with high clay content, one Bentheimer core with low clay content, and two artificial cores with no clay content were used for two-phase waterflooding experiments. Reduction in permeability for water, fines production, and reduction in residual oil saturation accompanied the abrupt salinity decrease in all tests. This effect is attributed to fines mobilization that is due to salinity decrease, followed by fines migration and straining in thin pore throats that resulted in local hydraulic resistance and consequent pore-scale flux diversion, yielding S_{or} reduction. The S_{or} dependencies of the induced formation damage are derived from five series of laboratory tests. All the laboratory tests confirmed the proposed S_{or} reduction mechanism by fines-assisted low-salinity waterflooding.

INTRODUCTION

Finding which factors cause enhanced oil recovery (EOR) during low-salinity waterflooding (LSW) in sandstone is of great interest in applied reservoir engineering. The EOR mechanisms of low-salinity waterflooding have been summarized in Qiao and Johns,¹ Mahani et al.,² Morrow and Buckley,³ Sheng,⁴ Al Shalabi et al.,⁵ Mahani et al.,⁶ Al-Shalabi and Sepehrnoori,⁷ RezaeiDoust et al.,⁸ and Afekare and Radonjic.⁹ The incomplete list includes decreased contact angle and interfacial tension,^{3,6,10–21} ion exchange between injected water and reservoir clays,^{22–28} and fines migration.^{29–43} The most controversial of these factors is fines migration. Some have found that EOR during low-salinity coreflooding was not accompanied by fines migration,^{3,10,11,42} whereas others found that it was.^{32,36} Significant fines production has not been observed during successful field tests on low-salinity water injection.^{3,4,39} However, insignificant fines production during low-salinity waterflood in which residual oil saturation (S_{or}) decreases can be explained by pressure drop increase, permeability decline, and significant fines straining and size exclusion in the rock.^{44–51} Yet, sizable decrease in water relative permeability at residual oil ($K_{r,wor}$) during low-salinity water injection due to capillary phenomena has never been distinguished from that due to fines migration, straining, and flux diversion.

The clay fines are attached to the rock surface by electrostatic forces and are mobilized by viscous drag forces.^{15,23,26–28,46,47,52} When the torques of the electrostatic and drag forces offset, attached fines are in mechanical equilibrium, thereby satisfying the so-called maximum retention function, which is a function of flow velocity, salinity, pH,^{46–48} and saturation.^{33–36,38,39} Lifting of attached fines by

oil–water menisci is modeled by the dynamics of the surface, separating oil and water.^{53–57}

Fines migration yields significant reduction in water relative permeability during LSW or during oil production after water breakthrough in the production well.^{12,23,30–32,44–51} Those effects yield mobility control during LSW, with consequent sweep efficiency enhancement.^{33,34,38,39} Decrease in relative permeability for water as salinity decreases, observed in refs 3–7, 9–11, 17, and 36 improves the oil-displacement dynamics on the core scale.^{34,35}

Decrease in residual oil due to capillary and ionic exchange effects of LSW has been extensively studied,^{3–7,9} whereas the effects of fines migration on S_{or} have not.

The current paper fills the gap by comprehensive experimental investigation of the role of fines in residual oil reduction during low-salinity water displacement of nonpolar-oil. Tests using brines with different salinities were performed on cores containing high, low, and no movable clay fines to investigate the role of fines mobilization in incremental recovery. We propose a novel S_{or} -reduction mechanism for low-salinity waterflooding with mobilization, migration, and straining of fine clay particles. The laboratory tests confirm the mechanism of reduced residual oil by microscale pressure gradient increase and flux diversion due to strained clay fines.

LABORATORY STUDY

This section describes properties of rock and fluids that were used in this study, the methodology, and purpose of the tests.

Received: May 21, 2018

Revised: July 18, 2018

Published: July 19, 2018

Table 1. Core Properties

	Berea (single-phase)	Bentheimer (single-phase)	Berea 1 (two-phase)	Berea 2 (two-phase)	Berea 3 (two-phase)	Berea 4 (two-phase)	Bentheimer (two-phase)
K , mD	40.8	1006	38.7	28	26	30.2	1370
ϕ	0.21	0.23	0.18	0.19	0.18	0.18	0.23
length, cm	5.70	6.0	11.86	12.06	11.90	12.07	10.90
diameter, cm	3.80	3.80	3.81	3.81	3.80	3.80	3.80

Materials. Natural Core Plugs. Five Berea and two Bentheimer sandstone core plugs were drilled from a single block of Berea and a single block of Bentheimer sandstone. “One Berea and one Bentheimer” core were used for single-phase tests and “four Berea and one Bentheimer” cores were used for two-phase tests. The core plugs were cut using a water-cooled saw to a diameter of 3.8 cm and then dried before the tests.

Berea and Bentheimer sandstone were chosen because of their contrasting clay concentration: Berea sandstone contains a significant concentration of movable clay particles, while the concentration of clay particles in Bentheimer sandstone is very small. XRD mineralogy analysis of these cores is shown in Table 2.

Table 2. X-ray Diffraction (XRD) Analyses of Core Samples

	Berea 1% (w/w)	Berea 2% (w/w)	Bentheimer % (w/w)
quartz	83.4	81.5	94
K-feldspar	5.5	5.4	2.8
plagioclase	3.5	3.5	0
kaolinite	3.6	3.8	1.7
illite	4	5.8	1.6
anhydrite	0	0	0

Synthetic Artificial Core Plugs. Silica grains (99% silica, SIBELCO 50N) were used to create a clay-free unconsolidated core plug. Prior to preparing the samples, the sand was washed and sieved to grain size of 70–260 μm . The silica grains were fully saturated with 0.6 M brine, poured in a Viton sleeve, and then installed in a standard Hassler type core holder. The Viton sleeve was wrapped in three layers of masking, paper-based expandable tape, to prevent bulging of the sample during compaction and thereby ensure a constant diameter along the core. Axial and radial confining pressures were then applied to achieve maximum compaction.

Brine. Synthetic brines were prepared by dissolving a desired amount of NaCl (35 g/L for 0.6 M, 17.5 g/L for 0.3 M, 6 g/L for 0.1 M, 3 g/L for 0.05 M, 1.5 g/L for 0.025 M, and 0.75 g/L for 0.01 M) in Milli-Q water. Prior to the tests, the concentration of solid particles in the solution was measured and used as the background particle concentration in the calculations. We will refer to 0.6 M brine as high-salinity (HS) water or “formation water”, and 0.05 M brine as low-salinity (LS) water.

Oil. Nonpolar oil (Paraffin oil, Light 15 LR, Chem-Supply) with viscosity of 20 cP at 25 $^{\circ}\text{C}$ was used in all tests.

Methodology. Two types of coreflood tests (single-phase and sequential two-phase tests) were performed to study the effect of brine salinity on fines mobilization and core permeability, and to evaluate their effect on recovery of nonpolar oil (S_{or}). In addition, an Amott test was performed to assess the effect of salinity on the wettability index (WI).

Prior to performing the tests, each core plug was dried, weighed, and fully saturated with HS 0.6 M brine under vacuum. The saturated plug was installed in a standard Hassler type core holder and subjected to 1000 psi confining pressure. A dome backpressure regulator was used to maintain a constant 500 psi pressure at the core outlet. The core permeabilities were measured by creating a constant flow of HS brine using a high pressure, pulse-free syringe pump (Quizix Q6000 precision pump). Three Yokogawa differential pressure transmitters recorded online pressure data (inlet, outlet, and differential pressure). A GE Healthcare Frac-920 fraction

collector was used to continuously collect samples of the produced fluid. The concentration of solid particles in the effluent was measured using a PAMAS SVSS particle counter with a particle size range of 1–200 μm .

Single-Phase (Dry) Coreflood Test. Single-phase core floods were performed to determine whether the in situ clay particles were movable and to evaluate the degree of permeability damage they would cause at different brine salinities. These tests were performed under a constant flow rate with piecewise-constant decreasing injected brine salinity using the following procedure:

- I. Injection of HS 0.6 M NaCl synthetic brine at constant flow rate of 0.2 mL/min (Darcy velocity of 3×10^{-6} m/s) until permeability stabilization.
- II. Repeating step I with brine salinities of 0.3, 0.1, 0.05, and 0.01 M.

The produced fluid was sampled continuously to measure the solid concentration, pH, and salinity of the effluent fluid.

Sequential Two-Phase Test. The two-phase core floods were conducted to study the effects of brine salinity on S_{or} and to investigate the mechanism of incremental recovery. Sequential drainages and imbibitions (HS \rightarrow Nonpolar Oil \rightarrow HS \rightarrow Nonpolar Oil \rightarrow LS) were conducted to compare S_{or} after HS and LS waterfloods. This was followed by piecewise-decreasing injected brine salinity in the presence of residual oil (LS \rightarrow Piecewise-Decreasing Salinity). The following procedure was used:

- I. Injection of HS (0.6 M NaCl) synthetic brine at a constant flow rate of 0.2 mL/min until permeability stabilization.
- II. Displacing the HS brine with nonpolar oil at a constant flow rate until initial water saturation $S_{\text{wi}}^{\text{HS}}$ is achieved (no more water production occurs).
- III. Displacing the nonpolar oil with HS brine at a constant flow rate until remaining oil saturation $S_{\text{or}}^{\text{HS}}$ is obtained (no more oil is produced).
- IV. Displacing the HS brine with nonpolar oil at a constant flow rate until initial water saturation $S_{\text{wi}}^{\text{LS}}$ is obtained.
- V. Displacing the nonpolar oil with LS (0.05 M NaCl) brine at a constant flow rate until remaining oil saturation $S_{\text{or}}^{\text{LS}}$ is obtained.
- VI. Injection of 0.025 M NaCl synthetic brine at constant flow rate until pressure is stabilized and no more oil is produced.
- VII. Repeating step VI with 0.01 M, and then with deionized water (DI).

DI water was used here and not in the single-phase test as formation damage was expected to be less with 0.01 M in the presence of S_{or} . The produced fluid was sampled continuously to measure oil and water volumes, pH, salinity, and the solid concentration of the effluent.

Amott Test. Macroscopic mean wettability of the Berea Sandstone to HS, LS, and DI water was measured using an Amott test. The Amott tests were carried out using other sister cores drilled from the same Berea block and were performed according to the following procedure:

- I. Full saturation of the core plugs with HS water under vacuum ($S_{\text{w}} = 100\%$).
- II. Forced (coreflood) displacement of the HS brine with nonpolar oil at a constant flow rate.
- III. Spontaneous imbibition by submerging the core plugs in HS brine in an Amott cell.

- IV. Forced coreflood displacement of the remaining oil with HS brine at a constant flow rate.
- V. Spontaneous drainage by submerging the core in nonpolar oil in an Amott cell.
- VI. Forced coreflood displacement of the remaining water with nonpolar oil.
- VII. Calculation of the wettability index

$$WI = \frac{V_{osp}}{V_{ot}} - \frac{V_{wsp}}{V_{wt}} \quad (1)$$

where V_{osp} is the volume of oil displaced spontaneously, V_{ot} is the total volume of oil displaced by imbibition and forced displacement, V_{wsp} is the volume of water displaced spontaneously, and V_{wt} is the total volume of water displaced by drainage and forced displacement.

VIII. Repeating steps II to VII for LS.

IX. Repeating steps II to VII for DI.

All spontaneous imbibition and drainage experiments were performed under an All Faces Open (AFO) boundary condition.

EXPERIMENTAL RESULTS

This section describes the results of single-phase tests performed on the one Berea sandstone and one Bentheimer sandstone cores and two-phase corefloods performed on the four Berea sandstone, one Bentheimer sandstone, and two artificial unconsolidated core plugs. We measured pressure drop, accumulated oil production, fines production, produced fluid salinity and pH, and wettability and carried out energy dispersive X-ray spectrometry (EDX) with a scanning electron microscope (SEM).

Berea Sister Gray. Five core plugs (one 5.7 cm and four ~12 cm) were drilled from a block of Berea Sister Gray. X-ray diffraction (XRD) analyses of these samples showed a composition of quartz (81–83%), nonswelling kaolinite and illite clays (7–10%), and other minerals, as shown in Table 2.

Single-Phase (Dry) Test. The 5.7 cm plug was used in the single-phase core flood test with piecewise-constant salinity decrease. The core permeability, pH, and fines concentration in the effluent fluid at different salinities is shown in Figure 1a,b. Decreasing the NaCl concentration had a significant effect on the permeability of the core plugs, and core permeability decreased as the salinity of the injected brines was reduced. The extent of permeability reduction and produced particle concentration varied for each salt concentration. The initial core permeability slightly decreased and stabilized at 35 mD after 80 PVI of HS water (0.6 M). This was accompanied by production of a small volume of solid fines at the core effluent. Further reduction of brine salinity to 0.3 M had no significant effect on permeability reduction or fines production. Noticeable formation damage and fines production were observed when the salinity of the injected brine was reduced to 0.1 M brine, followed by 0.05 M brine, resulting in permeability decrease to 24 and 20 mD, respectively. Simultaneous production of fine particles at the effluent implies that the permeability reduction was likely due to clay particle mobilization. SEM-EDX analysis of the produced fines was performed to characterize their mineral composition (Figure 2a,b). Pulse height analysis of EDX suggested that the produced fines were kaolinite and illite. The observed particles were the mobilized particles, which were not captured by the porous medium and were able to reach the core outlet. A substantial decrease of permeability down to 0.14 mD was measured upon injection of 0.01 M brine, which was accompanied by production of a large volume of solid

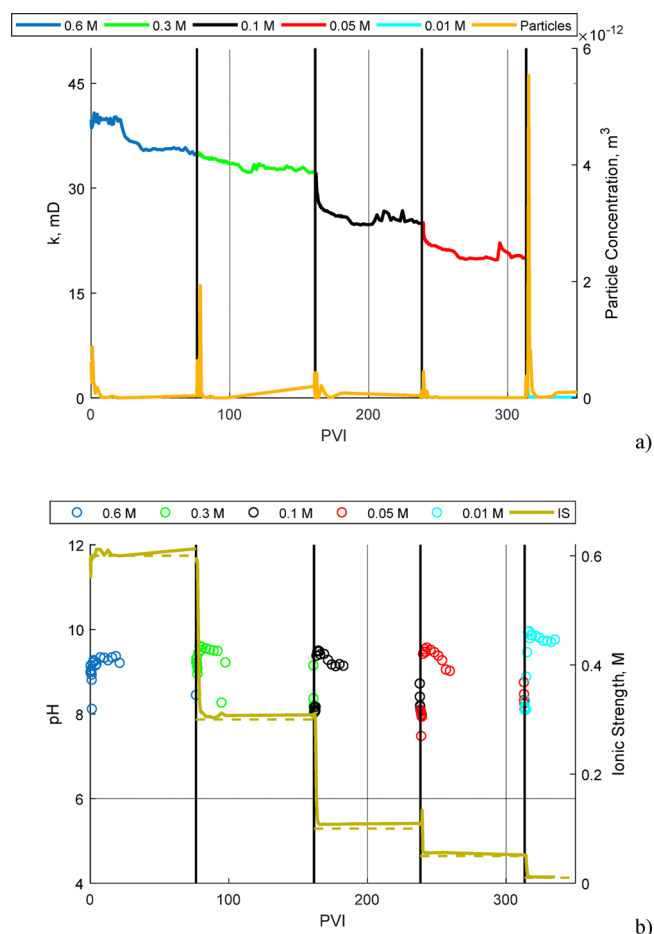


Figure 1. Berea sample used for the single-phase test: (a) Permeability reduction and produced fines concentration during piecewise decreasing of injected brine salinity; (b) pH and IS of the effluent fluid.

particles at the effluent. This was consistent with fines mobilization being the mechanism for permeability reduction.

The analysis of the produced fluid showed that only 1% of the movable clay particles (kaolinite and illite) were removed. Hence, deconsolidation of the core after detachment of 0.001 of the rock was not expected. In addition, the cores were inspected after the flooding test, and there was no sign of weakening. SEM-EDX results (Figure 2) also showed that the produced particles were mostly clay particles and no sand grains were detected at the effluent.

Figure 1b shows that the IS of the produced fluid (solid line) stabilized quickly at the value of injected brine IS (dashed line) after 2–3 PVI. The produced pH increased abruptly after each salinity change and then dropped gradually to the value higher than injection brine pH after ~10 PVI.

Sequential Two-Phase Tests. Four core plugs with similar properties (Table 1) from a block of Berea sandstone were trimmed to a diameter of 3.8 cm and a length of ~12 cm. Two-phase flow tests using core samples 1, 2, 3, and 4 were performed to study the effect of the salinity of the displacing brine on S_{or} . Sequential displacements with HS ($S_w = 100\%$) → Drainage 1 with Nonpolar oil (S_{wi}^{HS}) → HS (S_{or}^{HS}) → Drainage 2 with Nonpolar oil (S_{wi}^{LS}) → LS (S_{or}^{LS}) → Tertiary recovery (piecewise-decreasing salinity) were performed.

To be able to compare oil recoveries, the core has to be at the same initial condition (S_{wi}) before oil displacement by HS

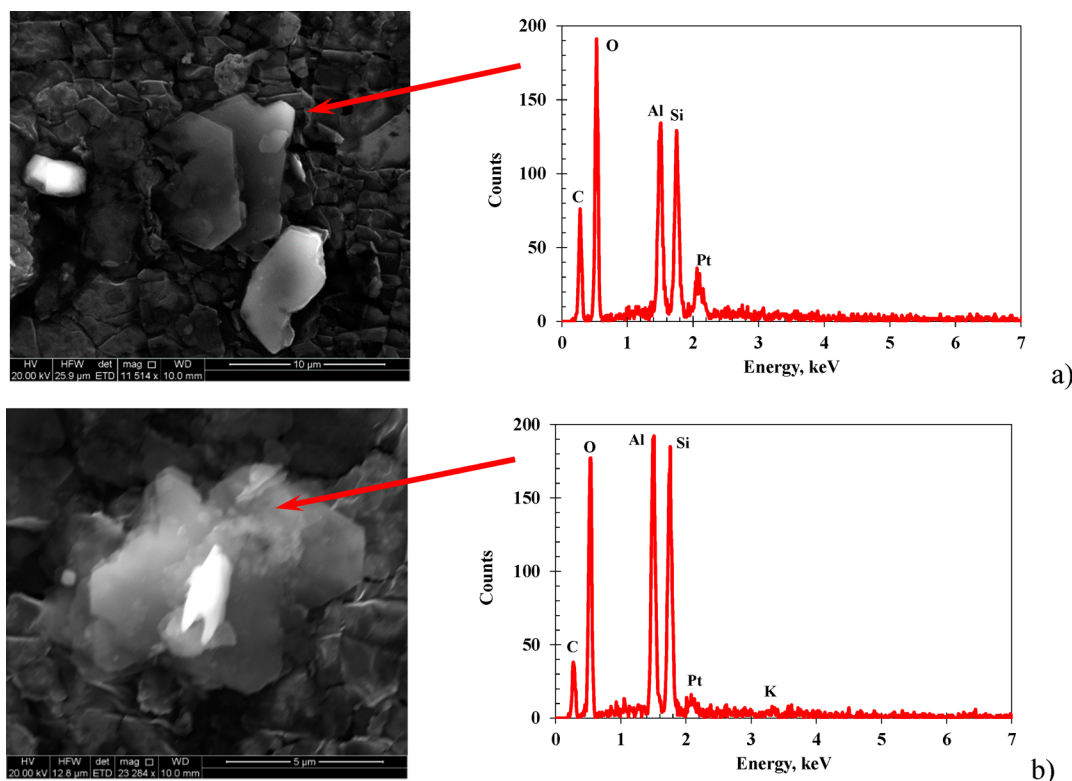


Figure 2. Single-phase (dry) coreflood on Berea sandstone: (a) SEM-EDX of produced fines collected at the core effluent showing kaolinite; (b) SEM-EDX of produced fines collected showing illite.

and LS, i.e., $S_{wi}^{HS} = S_{wi}^{LS}$. Figure 3a shows the plot of pressure drop across Berea sample 1 during brine displacements by oil. Pressure drop across the core was stabilized at ~ 17 psi for both drainage displacement processes. In addition, volumetric measurement of water and oil showed that water saturation at the end of drainages 1 and 2 were 0.079 and 0.083, respectively, implying that similar initial water saturations ($S_{wi}^{HS} = S_{wi}^{LS}$) were established prior to injection of HS and LS into Berea 1. The calculated end point oil relative permeability was 0.94 for both drainages 1 and 2. The plot of pressure drop and cumulative oil production vs PVI for the displacement of oil with HS and LS is presented in Figure 3b. The pressure drop for displacement of oil with HS exhibited the typical shape as expected. Displacement of oil with viscosity 20 cP by 1 cP HS brine caused an increase in pressure drop to 38 psi before breakthrough time, followed by a pressure decline and stabilization at 36 psi after ~ 12 PVI. The oil displacement with LS resulted in a continuous increase of the pressure drop to 155 psi (~ 4 times the stabilized pressure for HS). Despite the difference in pressure drop behavior, no change in oil production was observed when oil was displaced by LS if compared to oil displacement by HS where the recovered oil was 0.32 PV for both HS and LS. Bump flooding (i.e., abrupt increase in the injection flow rate for limited period of time to produce capillary trapped water/oil^{58,59}) with a flow rate = 2 mL/min was performed at the end of oil displacement by HS and LS, which resulted in no extra oil production due to capillary end effect.

A tertiary recovery test was performed to evaluate the dependency of oil recovery on the NaCl concentration of the displacing brine, where LS was followed by piecewise injection of brines with constant salinity decrease (0.05 M brine, 0.025 M brine, 0.01 M brine, and DI water) at a constant rate. The

pressure drop and cumulative oil production in Berea 1 for different salinities are presented in Figure 3c. Injection of 0.025 and 0.01 M brines did not significantly increase pressure drop or extra oil recovery. Instant increase in pressure drop was observed upon injection of DI water. Pressure drop rose significantly to ~ 750 psi (~ 20 and ~ 5 times the stabilized pressure for HS and LS, respectively) accompanied by 0.41 PV extra oil production (S_{or} reduction from 0.6 to 0.51).

Figures 4–6 show that the results of the experiments performed on Berea samples 2, 3, and 4 were similar to that of Berea sample 1. These four core plugs had similar pressure drop and similar oil production when oil was displaced with HS brine, and likewise for displacement with LS brine. The pressure drop decreased during oil displacement with HS, whereas continuous increase of the pressure drop was observed when LS was injected. The incremental oil recovery was negligible during displacement of oil by LS if compared to HS (Table 3). Tertiary recovery tests also showed similar results: considerable reduction of the remaining oil saturation was observed only during corefloods with DI water for samples 2 and 4 when a sharp rise in pressure drop occurred. Berea sample 3 showed more plateaus than the other samples in pressure drop. This is possibly due to its lower S_{or} compared to Berea 1, 2, and 4. Hence, higher rock surface is accessible to injected LS, yielding to higher fines mobilization potential.

Figure 3e shows IS and pH of the produced fluid. One can see that the IS of the produced brine (solid line) became equal to the IS of the injected brine (dashed line) after a short period of time. The pH of the produced fluid increased sharply after oil displacement by LS and then dropped gradually and stabilizes at 8.1 (higher than injection brine pH). This was accompanied by a significant amount of produced fines at the outlet. Insignificant fines production and pH increase were

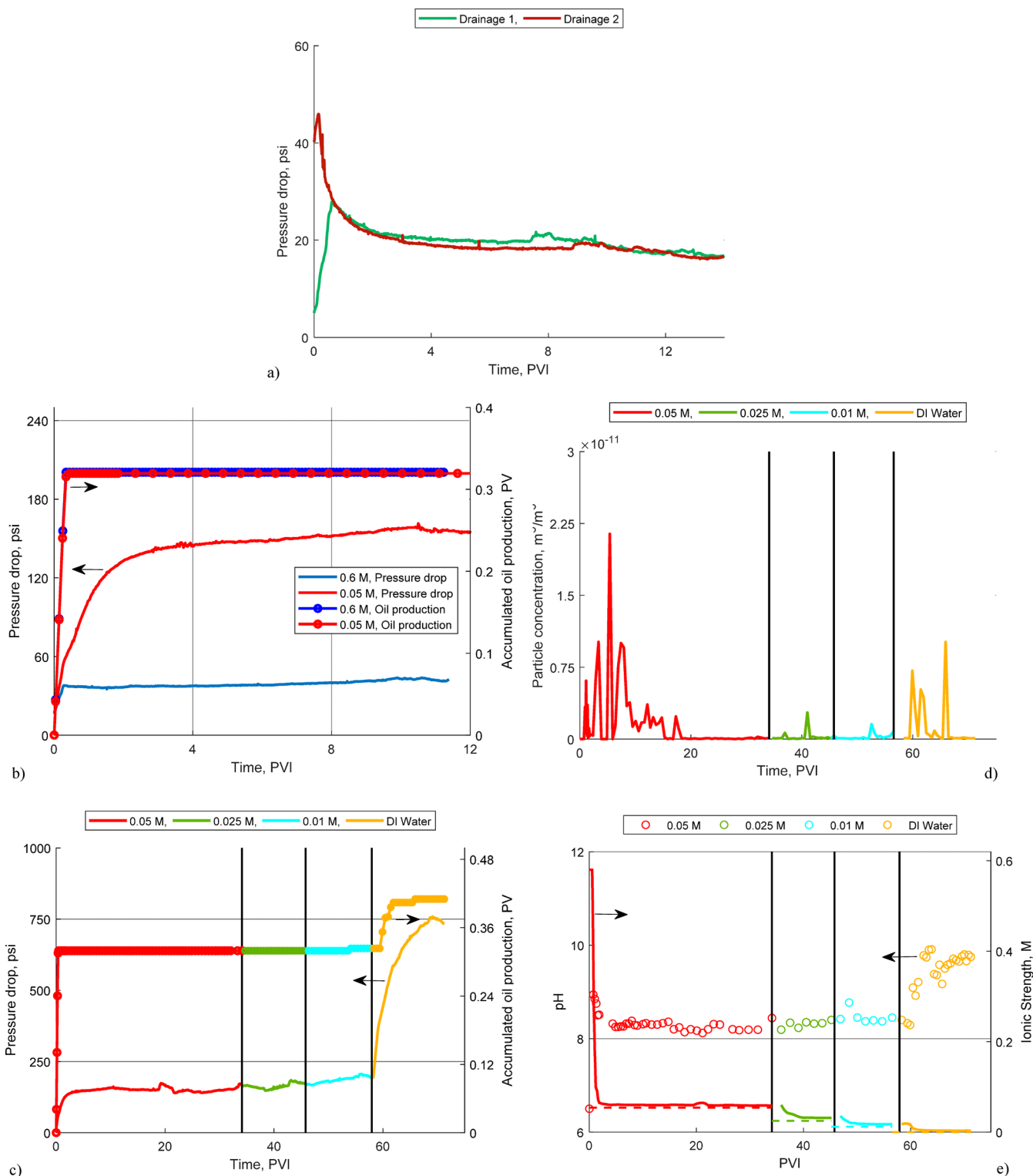


Figure 3. Sequential two-phase test on Berea core 1 with $k = 38.7$ mD and volumetric clay concentration $\sigma = 9.6\%$: (a) pressure drop during primary and secondary drainages; (b) oil production and pressure drop during HS and LS floods; (c) oil production and pressure drop during injection of brine with piecewise-constant decreasing salinity in the presence of residual oil; (d) volumetric breakthrough fines concentration during injection of brine with piecewise-constant decreasing salinity in a tertiary mode; (e) IS and pH of effluent brine.

observed during injection of 0.05 and 0.01 M brines. Upon injection of the DI water, the produced fluid pH increased significantly, accompanied by a noticeable amount of fines production.

Measurement of produced fines concentration was performed during the sequential two-phase test on Berea cores 1,

2, and 3. All cores showed similar behavior of fines production during the tertiary mode. Figure 5d presents the plot of the volume of produced fines vs PVI for different salinities in Berea 3. The reduction in brine salinity resulted in fines migration, and consequent increase in pressure drop was accompanied by extra oil recovery (Figure 5c). During tertiary recovery, a

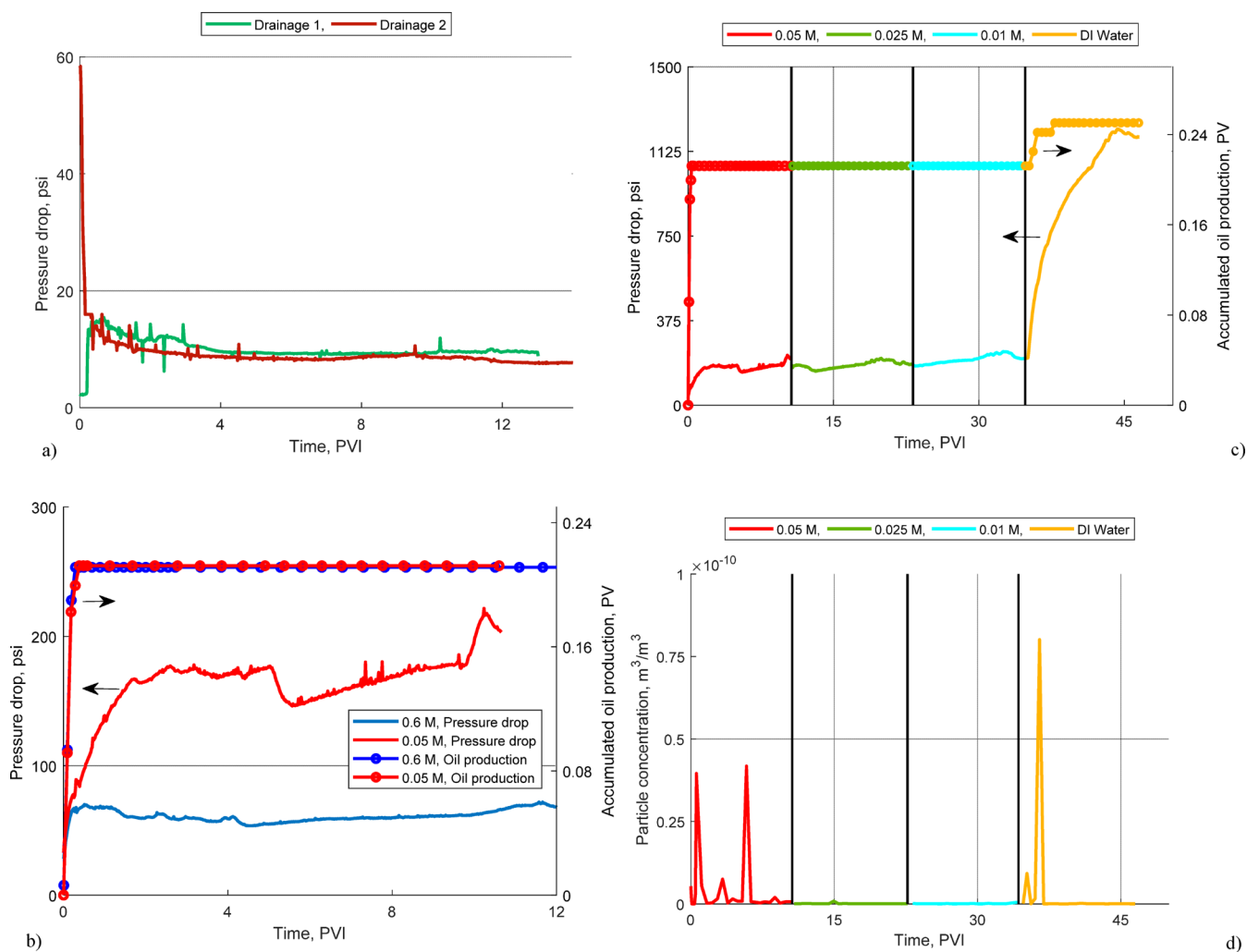


Figure 4. Sequential two-phase test on Berea core 2 with $k = 28$ mD: (a) pressure drop during primary and secondary drainage; (b) pressure drop during HS and LS; (c) oil production and pressure drop during injection of brine with piecewise-constant decreasing salinity in the presence of residual oil; (d) breakthrough fines concentration during injection of brine with piecewise-constant decreasing salinity in a tertiary mode.

negligible increase in pressure drop was observed when brine salinity was reduced from 0.05 to 0.025 M, which resulted in a small decrease of the remaining oil saturation from 0.41 to 0.39. Considerable extra oil (0.44 and 0.48 PV) was recovered when Berea core 3 was flushed with 0.01 M brine and DI water. As expected, this was accompanied by a significant rise in pressure drop (~ 15 and ~ 39 times the stabilized pressure drop for LS and HS, respectively) and large volume of produced fines, which is attributed to the role of fines mobilization in incremental oil recovery. Figures 3d and 4d show the production concentration of particles per PVI for Berea 1 and Berea 2 cores, respectively.

Bentheimer. Bentheimer sandstone was chosen due to its negligible clay content. An XRD analysis of the Bentheimer sample showed its composition to be 94% quartz and 3.3% kaolinite and illite clays (Table 2). The Bentheimer plug had permeability 1006 mD and porosity 23%, which are higher than those for the Berea cores. This is mainly due to lower clay content of the Bentheimer sample. A single-phase flow test was performed on the Bentheimer plug with diameter of 3.8 cm and a length of 6 cm. Figure 7 shows the plot of differential pressure across the core vs PVI for different salinities injected into the Bentheimer core plug. No significant formation

damage (permeability reduction) was observed when the core plug was flushed with 0.6 M (HS), 0.05 M (LS), 0.025 M, and 0.01 M brine. Injection of DI water caused ~ 1.7 times permeability decrease from 1006 mD down to 600 mD, which is much lower than that for the Berea sandstone (~ 380 times). The less severe damage (if compared with Berea) was expected because Bentheimer sandstone contains lower concentration of movable clays than does Berea sandstone.

The results of the sequential two-phase test on the Bentheimer plug are presented in Figure 8. The 11 cm long core was saturated with HS water and then brought to initial condition (drainage 1, $S_{wi}^{HS} = 0.12$) by injecting nonpolar to displace the HS brine. HS brine was then injected to displace the oil, until no oil production was observed ($S_{or}^{HS} = 0.4$). A second drainage was performed to re-initialize the core, prior to injection of LS brine. The drainage pressure drop measurements presented in Figure 8a show that the same initial condition was achieved: stabilized pressure at the end of drainages 1 and 2 were almost equal (~ 2.5 psi). The test was continued by injection of LS brine until no oil production was observed ($S_{or}^{LS} = 0.38$). The pressure drop during HS brine injection exhibited the typical shape as expected: an increase in pressure drop to 1.7 psi before breakthrough time, followed by

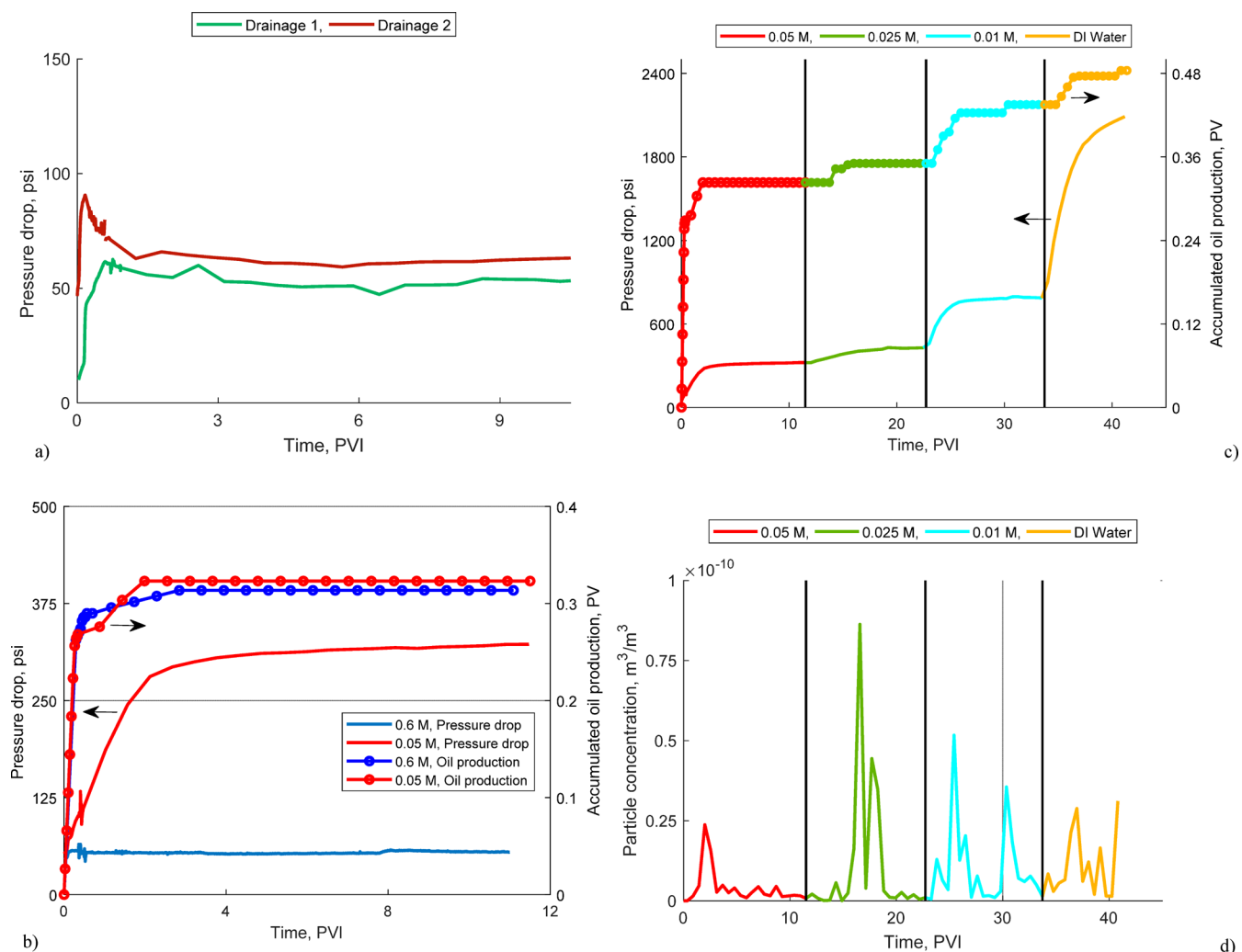


Figure 5. Sequential two-phase test on Berea core 3 with $k = 26$ mD: (a) pressure drop during primary and secondary drainage; (b) pressure drop during HS and LS; (c) oil production and pressure drop during injection of brine with piecewise-constant decreasing salinity in the presence of residual oil; (d) breakthrough fines concentration during injection of brine with piecewise-constant decreasing salinity in a tertiary mode.

a pressure decline and stabilization at 0.9 psi after ~ 8 PVI (Figure 8b). Similar pressure behavior was observed during displacement of oil with LS brine, which is consistent with the result of the single-phase flow, as no fines migration and formation damage were expected to occur. The ultimate oil recovery from injecting LS brine was not significantly different from that resulting from injecting HS brine. The insignificant reduction of S_{or} (3%) during LS (0.05M) injection for the Bentheimer core if compared with those for Berea tests can be explained by low initial clay concentration of the rocks (Table 2).

No extra oil was recovered during tertiary recovery test by 0.05 M, 0.025 M, 0.01 M, and DI water, and no significant increase in pressure drop across the core was observed (Figure 8c).

Unconsolidated Cores (Clean Sand). Sequential two-phase tests using artificial clay free porous medium were performed to create a baseline for evaluating the role of clay particles on recovery of nonpolar oil. Two artificial cores were prepared using only silica sand ranging with grain size from 70 to 260 μm .

The two-phase test on artificial core 1 exhibited the same pressure behavior during displacement of nonpolar oil with HS

and LS as well as the same volume of recovered oil (Figure 9a). In addition, no measurable oil production was observed during tertiary tests (Figure 9b).

The sequential two-phase core flood on artificial core 2 was performed using HS and DI water. Similar to the previous test on artificial core 1, the pressure behavior and oil production were similar for oil displacement by HS and DI water. This similar pressure behavior and oil recovery by HS and DI water was attributed to the absence of movable clay.

ANALYSIS OF THE RESULTS

The main effect of fines migration during low-salinity waterflooding is reduction of S_{or} due to local hydraulic resistance and consequent microscopic flux diversion. This flux diversion is induced by the size exclusion of mobilized fines in water-filled pores, and accompanied by permeability decrease and fines production at the effluent.

Berea Cores. Single-phase (dry) coreflood test with piecewise-constant decreasing salinity of Berea core exhibits a gradual permeability reduction with salinity variation from 0.6 to 0.01 M, and drastic decline in permeability at injected salinity 0.01 M (Figure 1a). The abrupt changes to water with lower salinity causes intensive production of fines, which

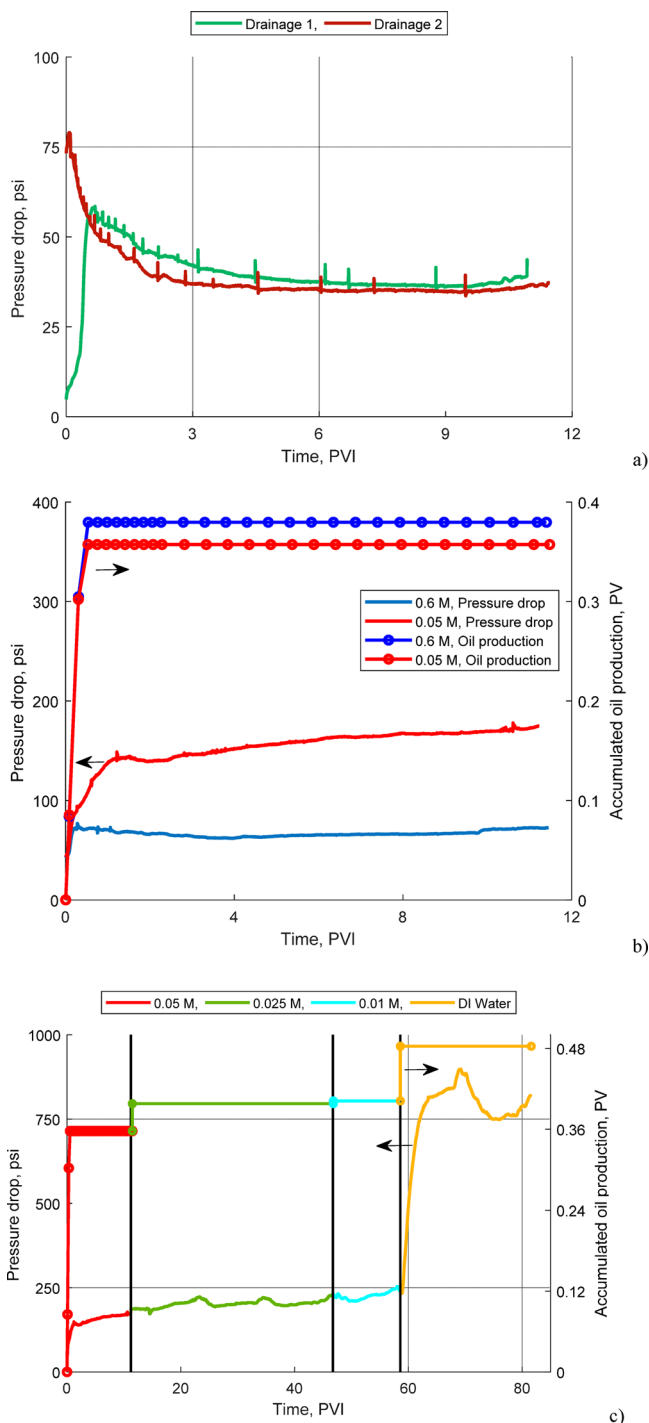


Figure 6. Sequential two-phase test on Berea core 4 with $k = 30.2$ mD and $\sigma = 7.6\%$: (a) pressure drop during primary and secondary drainage; (b) pressure drop during HS and LS; (c) oil production and pressure drop during injection of brine with piecewise-constant decreasing salinity in the presence of residual oil.

corresponds to the peaks in produced fine concentration. The higher is the permeability drop, the larger is the produced fines quantity. SEM-EDX of produced fines indicates kaolinite and illite clays as the mobilized fines during low-salinity water injection (Figure 2a,b). The test allows concluding that some part of the initial kaolinite and illite clays in the rock is movable and causes permeability decline.

Table 3. Results of Sequential Two-Phase Tests

	Berea 1	Berea 2	Berea 3	Berea 4	Bentheimer
$K_{r_{ow}}$ (Drainage 1)	0.94	0.27	0.69	0.96	0.38
S_{wi} (Drainage 1)	0.08	0.23	0.33	0.14	0.12
$K_{r_{wor}}$ (0.6 M)	0.04	0.025	0.034	0.02	0.05
S_{or} (0.6 M)	0.60	0.56	0.43	0.48	0.41
$K_{r_{ow}}$ (Drainage 2)	0.94	0.30	0.62	0.97	0.39
S_{wi} (Drainage 2)	0.08	0.22	0.26	0.15	0.15
$K_{r_{wor}}$ (0.05 M)	0.009	0.008	0.005	0.01	0.05
S_{or} (0.05 M)	0.60	0.55	0.41	0.49	0.38
$K_{r_{wor}}$ (0.025 M)	0.008	0.009	0.004	0.009	0.05
S_{or} (0.025 M)	0.60	0.55	0.39	0.45	0.38
$K_{r_{wor}}$ (0.01 M)	0.007	0.007	0.002	0.008	0.05
S_{or} (0.01 M)	0.60	0.55	0.30	0.44	0.38
$K_{r_{wor}}$ (DI water)	0.002	0.001	0.0009	0.002	0.05
S_{or} (DI water)	0.51	0.51	0.25	0.36	0.38

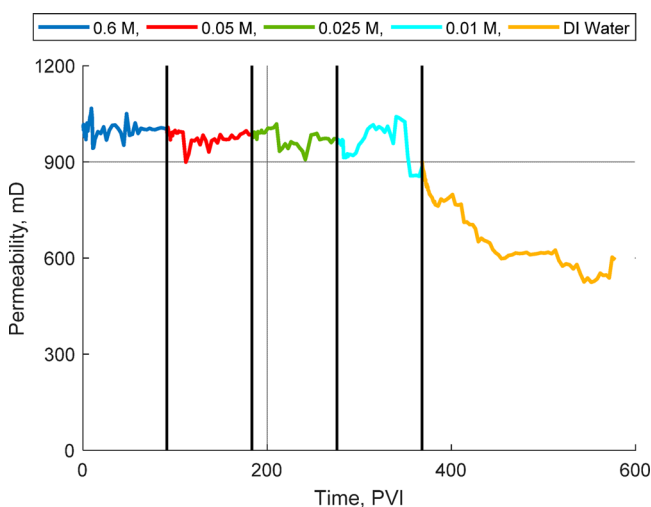


Figure 7. Single-phase test on Bentheimer core with $k = 1006$ mD and $\sigma = 3.3\%$: permeability reduction during piecewise decreasing of injected brine salinity.

The above-mentioned rock behavior is typical and is explained by weakening of electrostatic attraction between fines and the rock during salinity decrease, yielding mobilization of the attached fines by the viscous drag force.^{46–48} Migration and size exclusion of the mobilized fines in thin pores yield flux diversion with the trajectory tortuosity increase and consequent permeability reduction.^{44,45} Clay particles cover the pore walls, so the permeability increase due to particle detachment is significantly lower than that by further pore plugging. The same effects are expected in the presence of nonpolar oil.³⁰

Correlating pH and IS dynamics (Figure 1b) with breakthrough fines concentration (Figure 1a) supports the mechanism of fines mobilization and straining causing permeability decline during single-phase coreflood with piecewise-constant salinity decrease.

The pH initially rises at a time scale of 1 PVI after each injection of brine with lower salinity. This is due to fast desorption of Na^+ cations from clays and their substitution by hydrogen cations that results in decrease of hydrogen concentration in water and subsequent pH increase.⁶⁰ Then pH gradually decreases due to diffusion of low-pH connate water from dead-end pores to the transporting pores, while all

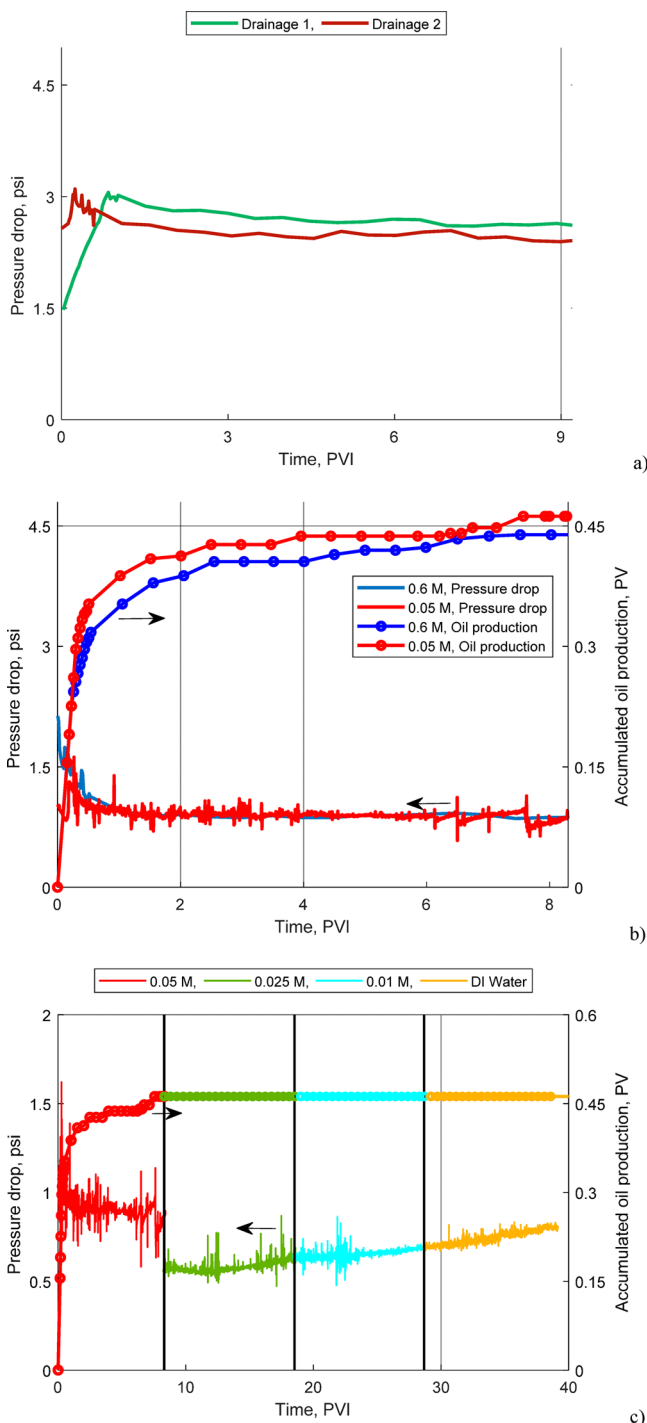


Figure 8. Sequential two-phase test on Bentheimer core with $k = 1370$ mD and $\sigma = 3.3\%$: (a) pressure drop during primary and secondary drainage; (b) pressure drop during HS and LS; (c) oil production and pressure drop during injection of brine with piecewise-constant decreasing salinity in the presence of residual oil.

vacant negative-charge sites on the rock surface are already filled by H^+ .

Three competitive processes govern pH variation after fast rise that follows the salinity alterations. First, ionic exchange on the kaolinite surface in stagnant zones and dead-end pores, yielding gradual pH increase. Second, production of particles during all stages of decreasing salinity. The clay detachment exposes new negatively charged surfaces, yielding extra H^+

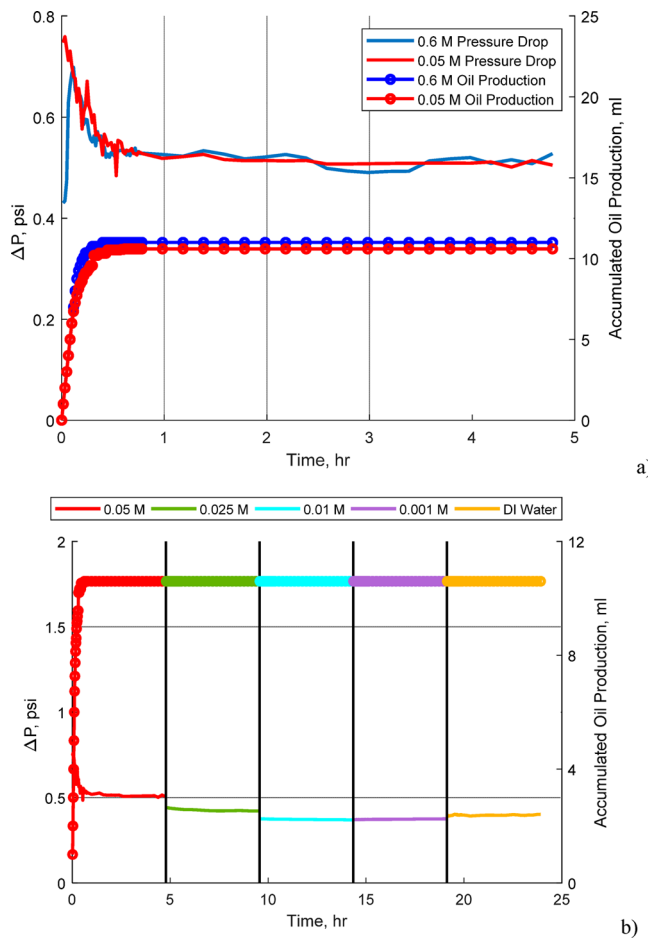


Figure 9. Sequential two-phase test on unconsolidated artificial clay-free core 1 with $k = 1623$ mD and no clays: (a) pressure drop and cumulative oil production during HS and LS; (b) cumulative oil production and pressure drop during injection of brine with piecewise-constant decreasing salinity.

adsorption on the surfaces and pH rise. The third process is the Brownian diffusion of low-pH water from dead-end pores to connected transporting pores. Decrease of pH at large times $t_D \gg 1$ PVI suggests that the process is diffusion-dominant.

The IS of the produced brine after 2–3 PVI stabilizes exactly at the salinity of the injected brine. This implies that no mineral dissolution occurs during the single-phase coreflood since the injected brine contains only NaCl.

Sequential primary drainage, primary imbibition by injection of HS formation water, resaturation by secondary drainage using the same HS water, secondary imbibition by injection of LS water, followed by injection of brine with piecewise-constant and decreasing salinity in the presence of residual oil, are performed on four Berea, one Bentheimer, and two artificial cores.

Full core resaturation and restoration of the “initial reservoir conditions” is controlled by connate water saturation S_{wi} and K_{rowi} after the primary and secondary drainages. Indeed, pressure drop during the primary and secondary drainages turns to the same limit (Figures 3a, 4a, 5a, and 6a). Oil mass balance exhibits the same connate water saturation after the primary and secondary drainages (Table 3).

Nonpolar oil is used in order to ensure full water wetting during salinity alteration from 0.6 M (seawater) until zero salinity during DI water injection. Constant wettability during

full-interval salinity alteration is confirmed by Amott tests (Table 4) where the wettability index remains close to one for

Table 4. Wettability Index from Amott Tests on Berea Sandstone Cores

	HS (0.6 M)	LS (0.05 M)	DI water
NaCl	0.98	0.99	0.97

the overall interval of salinity. So, water fills in all small crevices, cracks, and pores, where water mobility is extremely low; it explains the high relative permeability for oil in Table 3. Besides, no wettability alterations during salinity reduction allows excluding the osmotic effect of “thickening of water films”. Using nonpolar oil also allows separating fines-migration effects from capillary phenomena of EOR during LSW for polar oil with changing wettability during injected salinity decrease.

Usually waterflooding in fully water-wet cores yields the delayed water breakthrough due to filling of all thin pores, microfractures, and crevices accessible by the injected water during saturation increase and displacement of polar oil.⁶¹ However, the tests for four Berea cores show fast breakthrough, varying from 0.15 to 0.25 PVI. This effect is explained by complete water wetness for the case of nonpolar oil, which repels from the rock; all low-curvature-menisci pores and microfissures are filled by the formation water, which is not displaced by nonpolar oil during either primary or secondary drainage. Therefore, the injected water during both HS and LS waterfloods flows through conductive pores without diversion into the dead-end and thin pores, crevices, and microcracks, yielding fast breakthrough of the injected water.

Significant pressure drop increase during LS injection if compared with HS injection (Figures 3b, 4b, 5b, and 6b) is accompanied by fines production (Figures 3d, 4d, and 5d). Salinity decrease during LSW injection in a tertiary mode also exhibits simultaneous permeability decrease, fines production, and S_{or} reduction (Figures 3c, 4c, 5c, and 6c).

Fines production, permeability decline, and S_{or} reduction occur simultaneously. In the cores Berea 1, 2, and 4, it occurs at the lowest concentration or at DI water flooding (Figures 3c, 4c, and 6c). The Berea core 3 releases fines gradually with salinity variation from 0.05 M up to fresh water, so permeability and S_{or} decline occurs also gradually in the overall interval of salinity variation (Figure 5c).

Analysis of pH, IS, and fines production confirms the mechanism of fines release during injected water salinity decrease and permeability reduction in the presence of residual oil (Figure 3e). Fines mobilization and production occurs during injection of brine with salinity 0.05 M and DI water. Here, one can see the pH increase due to ionic exchange. Gradual increase of pH during injection of 0.05 M and DI water can be explained by ionic exchange and by the release of fines and new vacant sites on the surfaces of the rock and released fines.

Fines mobilization and production are not detected during flooding with 0.025 and 0.01 M; hence, the produced-fluid pH remains constant during these injections.

Bentheimer Core. Clay concentration in the Bentheimer core is significantly lower than in Berea (Figure 7). Consequently, the formation damage induced by fines migration is expected to be lower too. Indeed, the injection of water with piecewise-constant declining salinity yield

permeability decreases 1.7 times, while the permeability decreases 380 times for Berea cores.

During the sequential two-phase test, the pressure drop across the core almost does not change from HS (0.6 M) to LS (0.05 M) (Figure 8b) and S_{or} is also almost the same.

During tertiary mode (at S_{or}), permeability does not change significantly when salinity decreased from 0.6 M to DI water (Figure 8c). Consequently, S_{or} remained almost the same too.

Unconsolidated Cores. The pressure drop and production curves for 0.6 and 0.05 M are identical (Figure 9a). The same is observed in Figure 10 when injecting 0.6 M and DI water. Consequently, decrease in injected salinity from 0.6 M to DI water does not change S_{or} and permeability for water.

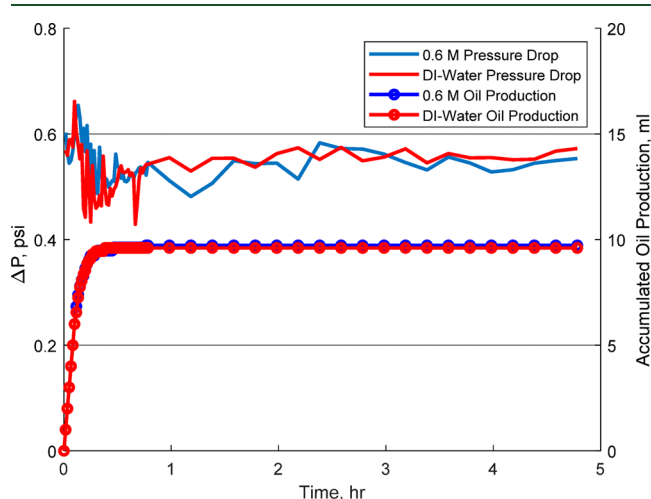


Figure 10. Two-phase test on unconsolidated artificial clay-free core 2 with $k = 1970$ mD: pressure drop and cumulative oil production during HS and DI water.

Figure 11a presents the change in residual oil saturation vs injected brine salinity for all coreflood tests. One can see that, for all consolidated cores (Berea and Bentheimer): (i) The lower is the injected salinity, the lower is the residual oil saturation. (ii) The S_{or} reduction is significant for high-clay-content Berea cores, and it is negligible for low-clay Bentheimer core. Figure 11b shows that reducing the brine salinity results in reduction of the absolute permeability and water phase permeability. Permeability reduction for low-clay-content Bentheimer core is significantly lower than that for Berea cores.

The formula for permeability decline due to increase of retained particle concentration is^{46–48,62}

$$k(\sigma) = \frac{k(0)}{1 + \beta\Delta\sigma} \quad (2)$$

where β is the formation damage coefficient, $k(\sigma)$ is the stabilized permeability after fines straining with concentration σ , $k(0)$ is the initial permeability, and $\Delta\sigma$ is the amount of strained particles during salinity alternation from 0.6 M to the injected water salinity. Table 3 presents the data on initial and stabilized relative permeability K_{rwo} allowing calculating the formation damage $\beta\Delta\sigma$, induced by straining of the mobilized fines.

Figure 12a,b presents the summary of S_{or} and K_{rwo} versus induced formation damage $\beta\Delta\sigma$ for all tests. The figure shows that the higher is the formation damage, the lower are the

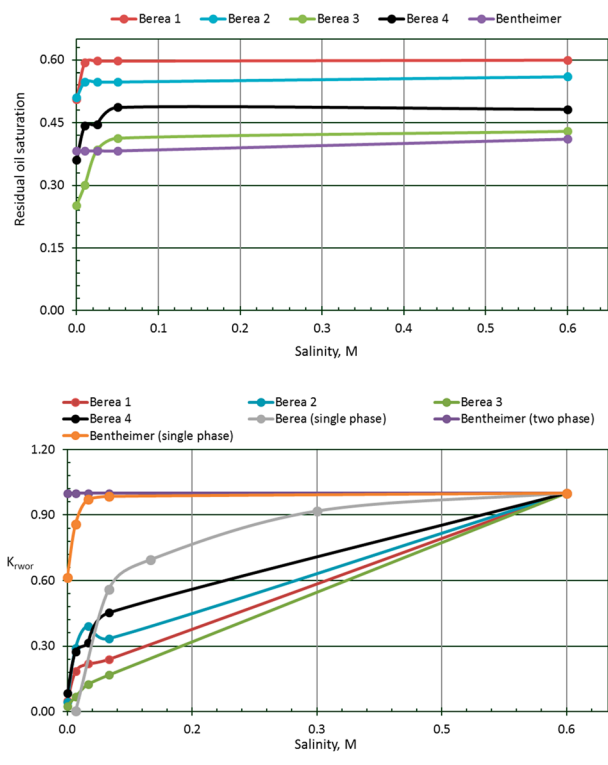


Figure 11. Effects of injected brine salinity on residual nonpolar oil: (a) decreasing of residual nonpolar oil saturation during piecewise-constant decreasing of brine salinity; (b) simultaneous K_{rwor} reduction.

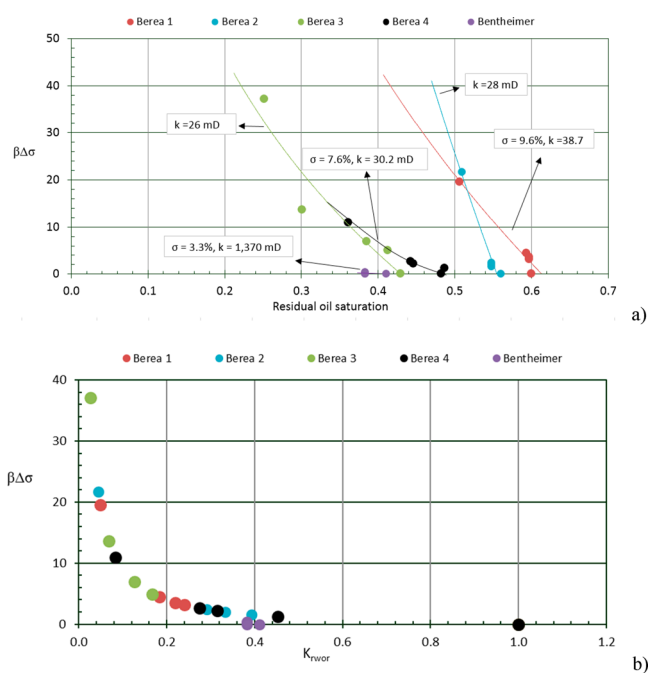


Figure 12. Effect of fines-migration formation damage $\beta\Delta\sigma$ on (a) residual oil saturation; (b) relative permeability for water at oil residual.

residual oil saturation and relative permeability for water at residual oil saturation. The K_{rwor} points from five tests with Berea and Bentheimer cores are located on a single curve (Figure 12b). The increase of the local pressure gradient in

water and consequent microscopic water flux diversion explain these phenomena (Figure 13).

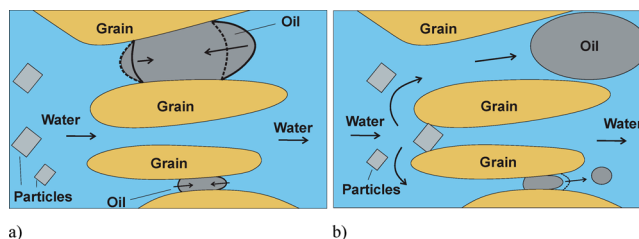


Figure 13. Schematic for local pressure gradient increase and flux diversion on the pore scale due to pore straining by migrating fines: (a) before straining; (b) after the straining.

Figure 13 presents the schematic of S_{or} reduction due to local hydraulic resistance imposed by strained fine particles. The microscopic flux diversion occurs due to plugging of the thin pores by the detached particles that results in the oil drop mobilization. Figure 13a shows two oil drops (residual oil) reside in the upper and lower pores and water flows through the middle pore. At the absence of bypassing water flow, both menisci of an oil droplet have the same curvature. Water causes flattening of the receded meniscus and makes the advanced meniscus more curvilinear. The advanced menisci curvatures are lower than the receded ones. The resulting capillary pressure opposes the viscous pressure drop across the droplet and provides a mechanical equilibrium for the droplet. Therefore, the resulting inner capillary pressure differences equilibrate the outer viscous pressure drop in moving water.

Figure 13b shows that pore blocking by the clay particles diverts the water flux into the pores with residual oil. Now the outer pressure drop exceeds the capillary pressure difference between the advanced and receded menisci, yielding mobilization of the oil drops. Therefore, the velocity increase causes the increase in viscous pressure drop that exceeds the maximum capillary pressure difference. This results in the displacement of the residual oil droplet.^{63,64} The upper oil drop is displaced completely and snap-off occurs with the lower oil drop.⁶⁴

The displacement is complete if the pressure in the oil droplet exceeds the “side” capillary pressure on the cylindrical droplet-pore surface; otherwise the snap-off occurs. The dimensionless capillary number $N_c = U\mu_w/\sigma$, where U is the water velocity, μ_w is the water viscosity, and σ is the water–oil interfacial tension, relates the viscous and capillary forces exerting on the residual oil droplet. The higher is the capillary number, the lower is the residual oil saturation. Therefore, desaturation curves $S_{or}(N_c)$ decline.^{63,65}

Pore plugging by fines migration usually causes hundreds times permeability reduction, which is explained by the increase of local hydraulic resistance in pore space (Figure 13b).^{30,44} Under the same flow rate, the appearance of local hydraulic resistance causes increase of the viscous pressure drop and full or partial displacement of the oil droplets. Sheng⁴ refers to S_{or} reduction due to plugging of some pores by migrating clays and silts as “improvement of the micro scale sweep efficiency”.

The S_{or} and K_{rwor} dependencies of formation damage, induced by fines migration (Figure 12), can be used as an input into reservoir simulators for fines-assisted LS injection.^{33–36,38–40,42,43,66}

The causal connection between S_{or} reduction and microscale flux diversion has also been discussed previously for permeability damage caused by other mechanisms associated with pore blockage as shown by Wang et al.,⁶⁷ Huh and Pope,⁶⁸ Bedrikovetsky,⁶¹ Mendez,⁶⁹ Bedrikovetsky et al.,⁷⁰ and Hwang and Sharma.⁷¹ This connection has been explained by local pressure gradient increase.

The effect of S_{or} reduction has also been observed during polymer flooding, where the adsorbed polymer induces some permeability damage. The effect was explained by viscous pressure-drop increase upon the trapped oil droplets, yielding their complete or partial removal as shown by Wang et al.,⁶⁷ Huh and Pope,⁶⁸ and Bedrikovetsky.⁶¹

S_{or} reduction during injection of water with solid or oily particles was also explained by particle capture and induced formation damage. Moreover, Sharma et al.¹¹ reformulated the capillary number in terms of pressure gradient, allowing using desaturation curves to determine S_{or} reduction due to formation damage.^{69–71} Permeability reduction with formation damage factor $\beta\Delta\sigma$ in eq 2 corresponds to an increase in capillary number $(1 + \beta\Delta\sigma)$ times, yielding the S_{or} reduction by $S_{or}(N_c) - S_{or}((1 + \beta\Delta\sigma) N_c)$.

DISCUSSION

Currently, LSW is considered as chemical EOR due to wettability alteration and the S_{or} reduction at core scale,^{1–17} and as mobility-control method due to formation damage induced by fines migration in the unswept zones at the reservoir scale.^{32–35,37,38} The present paper shows that fines-migration effect on S_{or} at core scale is also significant. Secondary and tertiary LS corefloods with nonpolar oil show a significant reduction of S_{or} due to microscale flux diversion caused by fines migration. This mechanism is different from S_{or} reduction caused by wettability alteration and other capillary phenomena, which might appear during displacement of polar oil.

Separation of wettability and formation-damage effects for LSW is difficult because both mechanisms are closely linked to the role of clays, in particular to clay wettability and fines release. Both effects yield S_{or} reduction at core scale. Kaolinite wettability prevents direct contact between clay and injected low-salinity water. However, change of wettability releases some oil films from the kaolinite surface, making it susceptible to fines release. Therefore, both physics phenomena are simultaneous and mutually related.

The lack of the separation of wettability-alteration and fines-migration effects prevents obtaining reliable laboratory-based modeling and upscaling that accounts for both effects. Nonetheless, separation of the wettability-change and permeability-damage effects has not been achieved in the lab tests so far. In particular, to the best of the authors' knowledge, no tests that separate the effects of wettability and fines migration are available.

In the current paper, we selected nonpolar oil in order to exclude the wettability effect; i.e., only fines migration causes S_{or} and K_{rwo} reduction. Quantitative evaluation of fines-migration effect on S_{or} for polar oils, and design of corresponding laboratory tests is a topic for future research.

CONCLUSIONS

Experimental study of residual nonpolar oil after fines-assisted low-salinity waterflooding allows drawing the following conclusions:

1. Simultaneous fines production, permeability decrease, and S_{or} reduction occur during water injection with piecewise-constant decreasing salinity, while complete water wetness is maintained during all stages of water injection.
2. The effect is explained by weakening of the "fine particle–rock" electrostatic attraction that results in release of fines with further straining and plugging of the water-filled pore. This causes flux diversion into pores containing oil ganglia, which yields the reduction in residual oil.
3. At the absence of fines migration, S_{or} reduction would cause some increase in relative permeability for water K_{rwo} . Under the conditions of the performed tests, fines straining is the only explanation of the observed reduction in K_{rwo} .
4. The lower is the injected water salinity, the higher is the fines production, the lower is the water phase permeability, and the lower is S_{or} .
5. The higher is the initial clay concentration in cores, the higher is S_{or} reduction during the salinity decrease.
6. The points of relative permeability of water at residual oil saturation versus formation damage factor are located on the same curve for all tests performed with Berea cores.

AUTHOR INFORMATION

Corresponding Author

*Tel.: +61-8 8313 8014. Fax: +61-8 8313 4345. E-mail: abbas.zeinijahromi@adelaide.edu.au.

ORCID

A. Zeinijahromi: 0000-0002-3088-6952

Notes

The authors declare no competing financial interest.

ACKNOWLEDGMENTS

Special thanks are due to Drs. A. Badalyan and L. Chequer for fruitful discussions (Australian School of Petroleum, University of Adelaide).

NOMENCLATURE

- k =permeability
 K_{rowi} =oil relative permeability at initial water saturation
 K_{rwo} =water relative permeability at residual oil saturation
 S_{or} =residual oil saturation
 S_{wc} =connate water saturation
 S_{wi} =initial water saturation
 v_{osp} =oil volume of spontaneous imbibition
 v_{ot} =total oil volume of spontaneous and forced imbibition
 v_{wsp} =water volume of spontaneous drainage
 v_{wt} =total water volume of spontaneous and forced drainage

Greek letters

- β =formation damage coefficient
 γ =salinity concentration
 σ =particle concentration
 $\Delta\sigma$ =strained particles concentration

Abbreviations

DI=deionized water
 EOR=enhanced oil recovery
 FW=fresh water
 HS=high-salinity water (0.6 M NaCl)
 IS=ionic strength
 LS=low-salinity water (0.05 M NaCl)
 LSW=low-salinity waterflooding
 M=molar
 PV=pore volume
 PVI=pore volume injected
 t_D =dimensionless time, PVI
 WI=wettability index

REFERENCES

- (1) Qiao, C.; Johns, R.; Li, L. Modeling low-salinity waterflooding in chalk and limestone reservoirs. *Energy Fuels* **2016**, *30* (2), 884–895.
- (2) Mahani, H.; Menezes, R.; Berg, S.; Fadili, A.; Nasralla, R.; Voskov, D.; Joekar-Niasar, V. Insights into the impact of temperature on the wettability alteration by low salinity in carbonate rocks. *Energy Fuels* **2017**, *31* (8), 7839–7853.
- (3) Morrow, N.; Buckley, J. Improved oil recovery by low-salinity waterflooding. *JPT, J. Pet. Technol.* **2011**, *63* (05), 106–112.
- (4) Sheng, J. J. Critical review of low-salinity waterflooding. *J. Pet. Sci. Eng.* **2014**, *120*, 216–224.
- (5) Al Shalabi, E. W.; Sepehrnoori, K.; Delshad, M. Mechanisms behind low salinity water injection in carbonate reservoirs. *Fuel* **2014**, *121*, 11–19.
- (6) Mahani, H.; Keya, A. L.; Berg, S.; Bartels, W.-B.; Nasralla, R.; Rossen, W. R. Insights into the Mechanism of Wettability Alteration by Low-Salinity Flooding (LSF) in Carbonates. *Energy Fuels* **2015**, *29* (3), 1352–1367.
- (7) Al-Shalabi, E. W.; Sepehrnoori, K. A comprehensive review of low salinity/engineered water injections and their applications in sandstone and carbonate rocks. *J. Pet. Sci. Eng.* **2016**, *139*, 137–161.
- (8) RezaeiDoust, A.; Puntervold, T.; Austad, T. Chemical Verification of the EOR Mechanism by Using Low Saline/Smart Water in Sandstone. *Energy Fuels* **2011**, *25* (5), 2151–2162.
- (9) Afekare, D. A.; Radonjic, M. From Mineral Surfaces and Coreflood Experiments to Reservoir Implementations: Comprehensive Review of Low-Salinity Water Flooding (LSWF). *Energy Fuels* **2017**, *31* (12), 13043–13062.
- (10) Tang, G.-Q.; Morrow, N. R. Influence of brine composition and fines migration on crude oil/brine/rock interactions and oil recovery. *J. Pet. Sci. Eng.* **1999**, *24* (2–4), 99–111.
- (11) Sharma, M.; Filoco, P. Effect of brine salinity and crude-oil properties on oil recovery and residual saturations. *SPE J.* **2000**, *5* (03), 293–300.
- (12) Schembre, J.; Tang, G.-Q.; Kovscek, A. Wettability alteration and oil recovery by water imbibition at elevated temperatures. *J. Pet. Sci. Eng.* **2006**, *52* (1–4), 131–148.
- (13) Lager, A.; Webb, K.; Black, C.; Singleton, M.; Sorbie, K. Low Salinity Oil Recovery-An Experimental Investigation. *Petrophysics* **2008**, *49*, 28–35.
- (14) Takahashi, S.; Kovscek, A. R. Wettability estimation of low-permeability, siliceous shale using surface forces. *J. Pet. Sci. Eng.* **2010**, *75* (1–2), 33–43.
- (15) Brady, P. V.; Morrow, N. R.; Fogden, A.; Deniz, V.; Loahardjo, N.; Winoto. Electrostatics and the low salinity effect in sandstone reservoirs. *Energy Fuels* **2015**, *29* (2), 666–677.
- (16) Mahani, H.; Berg, S.; Ilic, D.; Bartels, W.-B.; Joekar-Niasar, V. Kinetics of low-salinity-flooding effect. *SPE J.* **2015**, *20* (1), 8–20.
- (17) McMillan, M. D.; Rahnama, H.; Romiluy, J.; Kitty, F. J. Effect of exposure time and crude oil composition on low-salinity water flooding. *Fuel* **2016**, *185*, 263–272.
- (18) Dang, C.; Nghiem, L.; Nguyen, N.; Chen, Z.; Nguyen, Q. Mechanistic modeling of low salinity water flooding. *J. Pet. Sci. Eng.* **2016**, *146*, 191–209.
- (19) Khorsandi, S.; Qiao, C.; Johns, R. T. Displacement Efficiency for Low-Salinity Polymer Flooding Including Wettability Alteration. *SPE J.* **2017**, *22* (02), 417–430.
- (20) Boujelben, A.; McDougall, S.; Watson, M.; Bondino, I.; Agenet, N. Pore network modelling of low salinity water injection under unsteady-state flow conditions. *J. Pet. Sci. Eng.* **2018**, *165*, 462–476.
- (21) Zahid, A.; Shapiro, A.; Stenby, E. H.; Yan, W. Managing injected water composition to improve oil recovery: A case study of North Sea chalk reservoirs. *Energy Fuels* **2012**, *26* (6), 3407–3415.
- (22) Aghaeifar, Z.; Strand, S.; Austad, T.; Puntervold, T.; Aksulu, H.; Navratil, K.; Storås, S.; Håmsø, D. Influence of Formation Water Salinity/Composition on the Low-Salinity Enhanced Oil Recovery Effect in High-Temperature Sandstone Reservoirs. *Energy Fuels* **2015**, *29* (8), 4747–4754.
- (23) Civan, F. *Reservoir Formation Damage: Fundamentals, Modeling, Assessment, and Mitigation*; Gulf Publishing Company: Boston, 2007; Vol. 2.
- (24) RezaeiDoust, A.; Puntervold, T.; Strand, S.; Austad, T. Smart water as wettability modifier in carbonate and sandstone: A discussion of similarities/differences in the chemical mechanisms. *Energy Fuels* **2009**, *23* (9), 4479–4485.
- (25) Gillespie, M.; Kemp, S.; Vickers, B.; Waters, C.; Gowing, C. *Cation-exchange capacity (CEC) of selected lithologies from England Wales and Scotland*; Environment Agency: Bristol, U.K., 2001; Technical Report P2-222/TR.
- (26) Khilar, K. C.; Fogler, H. S. *Migrations of fines in porous media*; Kluwer Academic Publishers: Dordrecht, The Netherlands, 1998; Vol. 12.
- (27) Khilar, K. C.; Fogler, H. S.; Ahluwalia, J. Sandstone water sensitivity: existence of a critical rate of salinity decrease for particle capture. *Chem. Eng. Sci.* **1983**, *38* (5), 789–800.
- (28) Mohan, K. K.; Fogler, H. S.; Vaidya, R. N.; Reed, M. G. Water sensitivity of sandstones containing swelling and non-swelling clays. *Colloids Surf., A* **1993**, *73*, 237–254.
- (29) Torrijos, I. D. P.; Puntervold, T.; Strand, S.; Austad, T.; Abdullah, H. I.; Olsen, K. Experimental Study of the Response Time of the Low-Salinity Enhanced Oil Recovery Effect during Secondary and Tertiary Low-Salinity Waterflooding. *Energy Fuels* **2016**, *30* (6), 4733–4739.
- (30) Sarkar, A. K.; Sharma, M. M. Fines migration in two-phase flow. *JPT, J. Pet. Technol.* **1990**, *42* (05), 646–652.
- (31) Scheuerman, R. F.; Bergersen, B. M. Injection-water salinity, formation pretreatment, and well-operations fluid-selection guidelines. *JPT, J. Pet. Technol.* **1990**, *42* (07), 836–845.
- (32) Li, Y. Oil recovery by low salinity water injection into a reservoir: A new study of tertiary oil recovery mechanism. *Transp. Porous Media* **2011**, *90* (2), 333–362.
- (33) Zeinijahromi, A.; Lemon, P.; Bedrikovetsky, P. Effects of induced fines migration on water cut during waterflooding. *J. Pet. Sci. Eng.* **2011**, *78* (3–4), 609–617.
- (34) Yuan, H.; Shapiro, A. A. Induced migration of fines during waterflooding in communicating layer-cake reservoirs. *J. Pet. Sci. Eng.* **2011**, *78* (3–4), 618–626.
- (35) Zeinijahromi, A.; Nguyen, T. K. P.; Bedrikovetsky, P. Mathematical model for fines-migration-assisted waterflooding with induced formation damage. *SPE J.* **2013**, *18* (03), 518–533.
- (36) Hussain, F.; Zeinijahromi, A.; Bedrikovetsky, P.; Badalyan, A.; Carageorgos, T.; Cinar, Y. An experimental study of improved oil recovery through fines-assisted waterflooding. *J. Pet. Sci. Eng.* **2013**, *109*, 187–197.
- (37) Almada, P.; Pieterse, S.; Marcelis, A. H.; van Haasterecht, M.; Brussee, N.; van der Linde, H. Experimental investigation on the effects of very low salinity on Middle Eastern sandstone corefloods. In *SPE European Formation Damage Conference & Exhibition*, Noordwijk, The Netherlands, June 5–7, 2013; Society of Petroleum Engineers, 2013; SPE-165180-MS.

- (38) Zeinijahromi, A.; Al-Jassasi, H.; Begg, S.; Bedrikovetski, P. Improving sweep efficiency of edge-water drive reservoirs using induced formation damage. *J. Pet. Sci. Eng.* **2015**, *130*, 123–129.
- (39) Ahmetgareev, V.; Zeinijahromi, A.; Badalyan, A.; Khisamov, R.; Bedrikovetsky, P. Analysis of low salinity waterflooding in Bastrykskoye field. *Pet. Sci. Technol.* **2015**, *33* (5), 561–570.
- (40) Song, W.; Kovscek, A. R. Direct visualization of pore-scale fines migration and formation damage during low-salinity waterflooding. *J. Nat. Gas Sci. Eng.* **2016**, *34*, 1276–1283.
- (41) Demikhova, I. I.; Likhanova, N. V.; Perez, J. R. H.; Falcon, D. A. L.; Olivares-Xometl, O.; Berthier, A. E. M.; Lijanova, I. V. Emulsion flooding for enhanced oil recovery: Filtration model and numerical simulation. *J. Pet. Sci. Eng.* **2016**, *143*, 235–244.
- (42) Farajzadeh, R.; Guo, H.; van Winden, J.; Bruining, J. Cation exchange in the presence of oil in porous media. *ACS Earth Space Chem.* **2017**, *1* (2), 101–112.
- (43) Alhuraishawy, A. K.; Bai, B.; Wei, M.; Geng, J.; Pu, J. Mineral dissolution and fine migration effect on oil recovery factor by low-salinity water flooding in low-permeability sandstone reservoir. *Fuel* **2018**, *220*, 898–907.
- (44) Muecke, T. W. Formation fines and factors controlling their movement in porous media. *JPT, J. Pet. Technol.* **1979**, *31* (02), 144–150.
- (45) Lever, A.; Dawe, R. A. Water-sensitivity and migration of fines in the hopeman sandstone. *J. Pet. Geol.* **1984**, *7* (1), 97–107.
- (46) Bedrikovetsky, P.; Siqueira, F. D.; Furtado, C. A.; Souza, A. L. S. Modified particle detachment model for colloidal transport in porous media. *Transp. Porous Media* **2011**, *86* (2), 353–383.
- (47) Bedrikovetsky, P.; Zeinijahromi, A.; Siqueira, F. D.; Furtado, C. A.; de Souza, A. L. S. Particle detachment under velocity alternation during suspension transport in porous media. *Transp. Porous Media* **2012**, *91* (1), 173–197.
- (48) You, Z.; Bedrikovetsky, P.; Badalyan, A.; Hand, M. Particle mobilization in porous media: temperature effects on competing electrostatic and drag forces. *Geophys. Res. Lett.* **2015**, *42* (8), 2852–2860.
- (49) Yuan, B.; Wang, W. Using nanofluids to control fines migration for oil recovery: Nanofluids co-injection or nanofluids pre-flush?—A comprehensive answer. *Fuel* **2018**, *215*, 474–483.
- (50) Al-Yaseri, A.; Al Mukainah, H.; Lebedev, M.; Barifcani, A.; Iglauer, S. Impact of fines and rock wettability on reservoir formation damage. *Geophys. Prospect.* **2016**, *64* (4), 860–874.
- (51) Zhang, Y.; Lebedev, M.; Al-Yaseri, A.; Yu, H.; Nwdee, L. N.; Sarmadivaleh, M.; Barifcani, A.; Iglauer, S. Morphological evaluation of heterogeneous oolitic limestone under pressure and fluid flow using X-ray microtomography. *J. Appl. Geophys.* **2018**, *150*, 172–181.
- (52) Israelachvili, J. *Intermolecular and Surface Forces*; Academic Press: London, U.K, 1992; p 450.
- (53) Fogden, A.; Kumar, M.; Morrow, N. R.; Buckley, J. S. Mobilization of Fine Particles during Flooding of Sandstones and Possible Relations to Enhanced Oil Recovery. *Energy Fuels* **2011**, *25* (4), 1605–1616.
- (54) Shapiro, A. A. Two-phase immiscible flows in porous media: The Mesoscopic Maxwell–Stefan approach. *Transp. Porous Media* **2015**, *107* (2), 335–363.
- (55) Shapiro, A. A. Mechanics of the separating surface for a two-phase co-current flow in a porous medium. *Transp. Porous Media* **2016**, *112* (2), 489–517.
- (56) Huang, F.; Kang, Y.; You, L.; Li, X.; You, Z. Massive fines detachment induced by moving gas-water interfaces during early stage two-phase flow in coalbed methane reservoirs. *Fuel* **2018**, *222*, 193–206.
- (57) Shapiro, A. A. A Three-Dimensional Model of Two-Phase Flows in a Porous Medium Accounting for Motion of the Liquid–Liquid Interface. *Trans. Porous Media* **2018**, *122*, 713–744.
- (58) McPhee, C.; Reed, J.; Zubizarreta, I. *Core Analysis: A Best Practice Guide*; Elsevier: Amsterdam, 2015; Vol. 64.
- (59) Saeedi, A. *Experimental study of multiphase flow in porous media during CO₂ Geo-Sequestration processes*; Springer Theses; Springer Science & Business Media: Berlin, 2012.
- (60) Austad, T.; Rezaeidoust, A.; Puntervold, T. Chemical Mechanism of Low Salinity Water Flooding in Sandstone Reservoirs. In *SPE Improved Oil Recovery Symposium*, Tulsa, OK, April 24–28, 2010; Society of Petroleum Engineers, 2010; SPE-129767-MS.
- (61) Bedrikovetsky, P. *Mathematical Theory of Oil and Gas Recovery: With Applications to ex-USSR Oil and Gas Fields*; Springer Science +Business Media: Dordrecht, The Netherlands, 1993; Vol. 4.
- (62) Shutong, P.; Sharma, M. M. A model for predicting injectivity decline in water-injection wells. *SPE Form. Eval.* **1997**, *12* (03), 194–201.
- (63) Lake, L. W.; Johns, R. T.; Rossen, W. R.; Pope, G. A. *Fundamentals of Enhanced Oil Recovery*; Society of Petroleum Engineers: Richardson, TX, 2014.
- (64) Chen, M.; Rossen, W.; Yortsos, Y. C. The flow and displacement in porous media of fluids with yield stress. *Chem. Eng. Sci.* **2005**, *60* (15), 4183–4202.
- (65) Dullien, F. A. *Porous Media: Fluid Transport and Pore Structure*; Academic Press: Cambridge, MA, 2012.
- (66) Zeinijahromi, A.; Farajzadeh, R.; Bruining, J. H.; Bedrikovetsky, P. Effect of fines migration on oil–water relative permeability during two-phase flow in porous media. *Fuel* **2016**, *176*, 222–236.
- (67) Wang, D.; Cheng, J.; Yang, Q.; Wenchao, G.; Qun, L.; Chen, F. Viscous-elastic polymer can increase microscale displacement efficiency in cores. In *SPE Annual Technical Conference and Exhibition*, Dallas, TX, Oct 1–4, 2000; Society of Petroleum Engineers, 2000; SPE-63227-MS.
- (68) Huh, C.; Pope, G. A. Residual oil saturation from polymer floods: Laboratory measurements and theoretical interpretation. In *SPE Symposium on Improved Oil Recovery*, Tulsa, OK, April 20–23, 2008; Society of Petroleum Engineers, 2008; SPE-113417-MS.
- (69) del Carmen Mendez, Z. *Flow of dilute oil-in-water emulsions in porous media*; University of Texas at Austin: Austin, TX, 1999.
- (70) Bedrikovetsky, P.; Mackay, E. J.; Moraes, G. P.; Rosario, F. F.; Monteiro, R. P. Laboratory-based prediction of sulphate scaling damage. In *SPE International Oilfield Scale Symposium*, Aberdeen, U.K., May 31–June 1, 2006; Society of Petroleum Engineers, 2006; SPE-100611-MS.
- (71) Hwang, J.; Sharma, M. M. Generation and filtration of O/W emulsions under near-wellbore flow conditions during produced water re-injection. *J. Pet. Sci. Eng.* **2018**, *165*, 798–810.

4.2 Low-salinity Waterflooding in Non-polar oil

Al-Sarihi, A., Zeinjahromi, A., and Bedrikovetsky, P., published 05/2018

APPEA Journal

Statement of Authorship

Title of Paper	Low-salinity waterflooding in non-polar oil		
Publication Status	<input checked="" type="checkbox"/> Published	<input type="checkbox"/> Accepted for Publication	
	<input type="checkbox"/> Submitted for Publication	<input type="checkbox"/> Unpublished and Unsubmitted work written in manuscript style	
Publication Details	A. Al-Sarihi, A. Zeinjahromi, and P. Bedrikovetsky, 2018, Low-salinity waterflooding in non-polar oil, APPEA Journal		

Principal Author

Name of Principal Author (Candidate)	Abdullah Al-Sarihi		
Contribution to the Paper	Literature review, experimental work, analysis of results, writing the manuscript.		
Overall percentage (%)	80%		
Certification:	This paper reports on original research I conducted during the period of my Higher Degree by Research candidature and is not subject to any obligations or contractual agreements with a third party that would constrain its inclusion in this thesis. I am the primary author of this paper.		
Signature		Date	17/9/2019

Co-Author Contributions

By signing the Statement of Authorship, each author certifies that:

- i. the candidate's stated contribution to the publication is accurate (as detailed above);
- ii. permission is granted for the candidate to include the publication in the thesis; and
- iii. the sum of all co-author contributions is equal to 100% less the candidate's stated contribution.

Name of Co-Author	Abbas Zeinjahromi		
Contribution to the Paper	Support in analysis of results, review manuscript		
Signature		Date	17/09/19

Name of Co-Author	Pavel Bedrikovetsky		
Contribution to the Paper	Support in analysis of results, review of manuscript		
Signature		Date	17/09/19

Low-salinity waterflooding in non-polar oil

A. Al-Sarhi^{A,B}, A. Zeinijahromi^A and P. Bedrikovetsky^A

^AAustralian School of Petroleum, The University of Adelaide, Adelaide, SA 5005.

^BCorresponding author. Email: abdullah.sarhi@adelaide.edu.au

Abstract. Enhanced oil recovery by low-salinity waterflooding is considered to have positive results only when polar components exist in oil. This study shows that low-salinity brine can result in incremental recovery for non-polar oil through fines-assisted waterflooding. Despite the traditional view of fines migration that it should be avoided because of its detrimental effect on reservoir permeability, this work shows that permeability decline is a main mechanism in the low-salinity effect on non-polar oil. Laboratory coreflood tests were performed on a clay-rich Berea outcrop core and a clean sand core to investigate the effect of clay migration when the core is saturated with non-polar oil. The results show that fines migration reduces residual saturation by 18%. In addition, a decrease in the water volume production was observed due to the decrease in water relative permeability.

Keywords: EOR, fines migration, LSW, relative permeability.

Accepted 5 March 2018, published online 28 May 2018

Introduction

Low-salinity waterflooding (LSW) has been considered one of the most effective and low-cost enhanced oil recovery methods in recent years (Austad *et al.* 2010). However, the main mechanism of LSW is not yet clear. Several mechanisms have been proposed in the literature such as; fines migration, ionic exchange, double layer expansion and wettability alteration. Moreover, those mechanisms are claimed to have an effect on enhancing oil recovery only when polar oil components exist (Tang and Morrow 1999; Lager *et al.* 2008).

Fines migration has often been explained by the lifting, mobilising and subsequent plugging of pores by fine particles, which have been observed in numerous core flood tests with altered water composition (Sarkar and Sharma 1990; Khilar and Fogler 1998; Hussain *et al.* 2013; Zeinijahromi *et al.* 2016). In this study, we aim to study the effect of fines migration on oil production for non-polar oils.

Materials and methods

Rocks

A Berea sandstone core, with length of 12 cm and diameter of 3.8 cm, was used in this study. It has a permeability of 26 mD and porosity of 19%. The clay content of this core includes 5.5% K-feldspar, 3.5% plagioclase, 3.6% kaolinite and 4% illite.

The clean sand core has a length of 4.9 cm and diameter of 3.8 cm. The permeability is 1970 mD and porosity is 42%. There is no clay in the core.

Fluids

Different brine solutions with different salinity concentrations are prepared by dissolving the desired volume of NaCl in MilliQ water. The salinities used are: 0.6 M (as formation water), 0.05 M, 0.025 M, 0.01 M and 0 M (as low-salinity injection water).

Paraffin non-polar oil (Light 15 LR) from Chem-supply is used in the experiments.

Procedure

- The porosity of the cores is first measured by the weight method. The core is dried for 24 h at 60°C and it then undergoes vacuum pressure to remove any air in the pores. It is then saturated with 100% formation brine (0.6 M).
- Absolute permeability is measured by injected formation water through the core, where pressure drop is recorded and Darcy's law is applied to calculate permeability.
- Mineral oil is injected to saturate the core until initial water saturation, S_{wi} , is reached, which is calculated by mass balance.
- 10 pore volumes of high salinity water (0.6 M) are injected to displace oil until pressure drop across the core is stabilised. Residual oil saturation, S_{or} , is calculated.

- e) The core is re-saturated with oil until S_{wi} is restored and pressure drop across the core is stabilised.
- f) 10 pore volumes of 0.05 M low-salinity water are injected to displace the oil in the core and S_{or} is achieved.
- g) 10 pore volumes of each of 0.025 M are injected until no oil production is observed at the core outlet.
- h) Step 'g' is repeated for 0.01 M and fresh water.
- i) The effluent samples are processed to measure oil fraction and fine particles concentration.

Results and discussion

Fig. 1 shows oil production along with pressure drop during low-salinity water flooding for the Berea core. It can be seen that as the brine salinity decreases, pressure drop increases and incremental oil is recovered. Residual oil was reduced from 0.43 during HSW down to 0.25 during LSW.

On the other hand, pressure drop and oil production did not increase in the clean sand during LSW compared with HSW, as

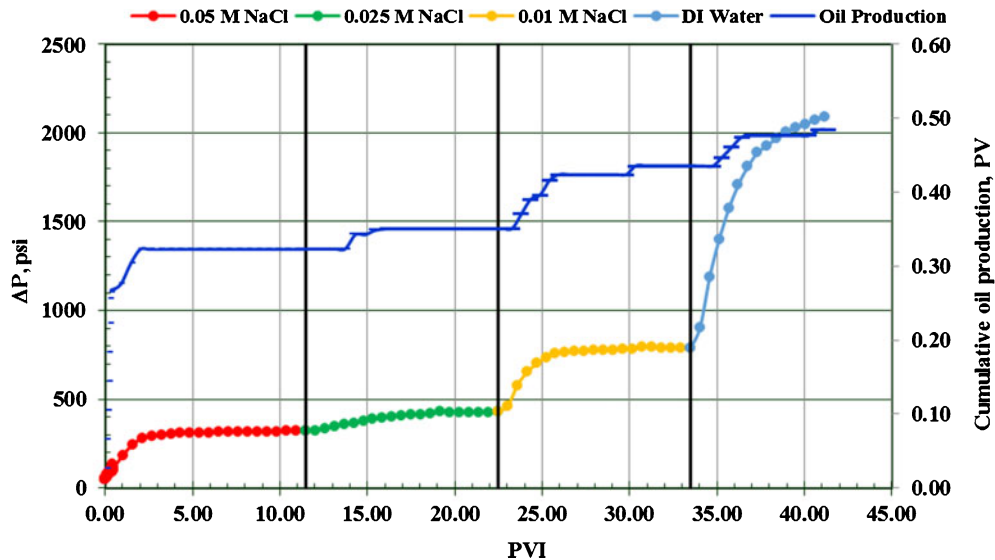


Fig. 1. Core I.a pressure drop and oil production during low-salinity waterflooding.

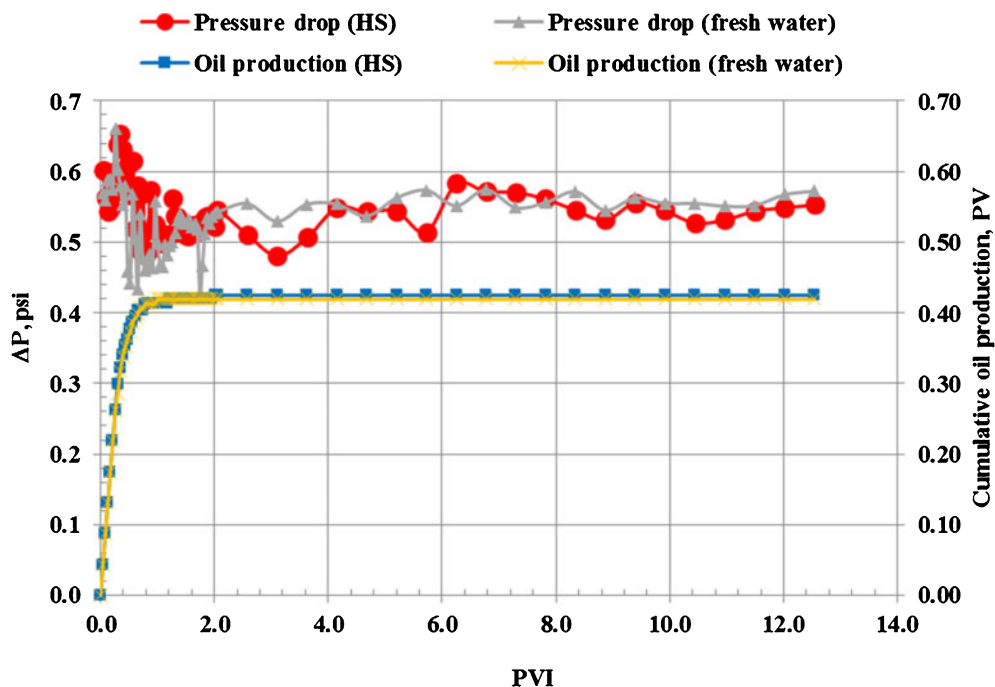


Fig. 2. Clean sand core pressure drop and oil production of HSW and DI-water injection.

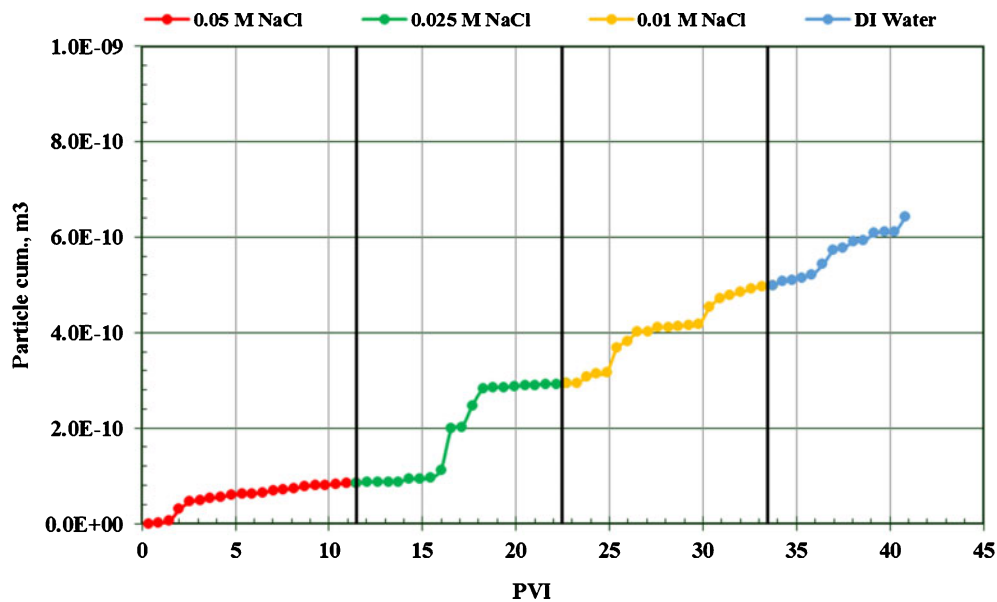


Fig. 3. Core 1.a fine particles production during low-salinity waterflooding.

shown in Fig. 2. This provides evidence that the migration of clay in the Berea core is the mechanism for enhancing oil production.

Fines migration occurs when the torque balance of the fine particles is disturbed. Drag and lifting forces form the detaching torque whereas electrostatic and gravitational forces form the attaching torque. The fine particles are attached to the rock surface when both torques are equal or when the attaching forces are stronger than the detaching ones. However, if the detaching torque exceeds that of the attaching one, then the particles are lifted and mobilised in the porous media (Hussain *et al.* 2013; Zeinijahromi *et al.* 2016). Decreasing the salinity of the injected water weakens the electrostatic forces because the repulsion between the particles and the rock surface increases due to the absence of positive ions (Na^+ in this study) which act as a bridge between (both negatively charged) rock surface and particles. Fig. 3 shows the increase in the concentration of particles produced with the decrease in salinity.

The detachment and mobilisation of particles causes plugging of pore throats in the Berea core, leading to increase in pressure drop and decline in water relative permeability (from 0.034 during HS to 0.001 during fresh water). This means the water flow is redirected into unswept zones in the rock. Therefore, the mobility of water is decreased and the micro-displacement efficiency is increased, leading to producing incremental oil from the unswept pores.

Conclusions

Injection of low-salinity water in Berea sandstone core resulted in residual oil saturation reduction of 18% when non-polar oil is used. The S_{or} reduction is accompanied by increase in pressure drop and fines production at the effluent. In addition, it is noticed that injection of low-salinity water in unconsolidated core (clean sand) had no effect on residual oil saturation and pressure drop. Extra oil production and fines migration occur simultaneously

showing that for non-polar oil, fines migration (clay mobilisation, pore blockages and flow diversion) is the mechanism of improved recovery at core scale.

Conflict of interest

The authors declare there are no conflicts of interest that could influence this work.

References

- Austad, T., Rezaeidoust, A., and Puntervold, T. (2010). Chemical mechanism of low salinity water flooding in sandstone reservoirs. In SPE improved oil recovery symposium. Society of Petroleum Engineers. doi:10.2118/129767-MS
- Hussain, F., Zeinijahromi, A., Bedrikovetsky, P., Badalyan, A., Carageorgos, T., and Cinar, Y. (2013). An experimental study of improved oil recovery through fines-assisted waterflooding. *Journal of Petroleum Science Engineering* **109**, 187–197. doi:10.1016/j.petrol.2013.08.031
- Khilar, K., and Fogler, H. (1998). 'Migrations of Fines in Porous Media.' (Kluwer Academic Publishers: Dordrecht/London/Boston)
- Lager, A., Webb, K. J., Black, C. J. J., Singleton, M., and Sorbie, K. S. (2008). Low salinity oil recovery – an experimental investigation. *Petrophysics* **49**(1), 28–35.
- Sarkar, A. K., and Sharma, M. M. (1990). Fines migration in two-phase flow. *SPE Journal of Petroleum Technology* **42**, 646–652. doi:10.2118/17437-PA
- Tang, G. Q., and Morrow, N. R. (1999). Influence of brine composition and fines migration on crude oil/brine/rock interactions and oil recovery. *Journal of Petroleum Science Engineering* **24**, 99–111. doi:10.1016/S0920-4105(99)00034-0
- Zeinijahromi, A., Farajzadeh, R., Bruining, J. H., and Bedrikovetsky, P. (2016). Effect of fines migration on oil–water relative permeability during two-phase flow in porous media. *Fuel* **176**, 222–236. doi:10.1016/j.fuel.2016.02.066

The authors



Abdullah Al-Sarihi is a PhD candidate in the Australian School of Petroleum at the University of Adelaide, Australia. He received his BEng and MSc degrees in petroleum engineering both from the University of New South Wales.



Dr Abbas Zeinjahromi is Senior Lecturer in Petroleum Engineering at the Australian School of Petroleum at the University of Adelaide. Abbas holds a PhD in Petroleum engineering from the University of Adelaide, MSc in Reservoir Engineering and BSc in Production Engineering.



Prof. Pavel Bedrikovetsky is a professor and Chair in Petroleum Engineering at the Australian School of Petroleum at the University of Adelaide. He is also a senior staff consultant to Petrobras. He holds BEng and MSc degrees in applied mathematics, a PhD degree in fluid mechanics, and a DSc degree in reservoir engineering, all from Moscow Gubkin Petroleum University.

5 Fines Stabilisation by Ca Ions and its Effect on LSW Injection

This chapter contains a paper published on the study of fines stability and shows hysteresis behaviour when alternating calcium and sodium ions in the injected water. It also shows how oil recovery is enhanced by micro-scale flux diversion (as explained in Chapter 4) after stabilising clay fines by treating the rock samples with calcium-rich brine.

5.1 Fines Stabilisation by Ca Ions and its Effect on LSW Injection

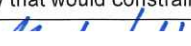
Al-Sarihi, A., Russell, T., Bedrikovetsky, P., and Zeinijahromi, A., published 10/2019

Journal of Energy&Fuels

Statement of Authorship

Title of Paper	Fines stabilisation by Ca ions and its effect on LSW injection
Publication Status	<input type="checkbox"/> Published <input type="checkbox"/> Accepted for Publication <input checked="" type="checkbox"/> Submitted for Publication <input type="checkbox"/> Unpublished and Unsubmitted work written in manuscript style
Publication Details	A. Al-Sarihi, T. Russell, P. Bedrikovetsky, and A. Zeinijahromi, Fines stabilisation by Ca ions and its effect on LSW injection, Journal of Energy&Fuels

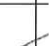
Principal Author


Name of Principal Author (Candidate)	Abdullah Al-Sarihi
Contribution to the Paper	Literature review, two-phase experiments, analysis of results, writing the manuscript.
Overall percentage (%)	65%
Certification:	This paper reports on original research I conducted during the period of my Higher Degree by Research candidature and is not subject to any obligations or contractual agreements with a third party that would constrain its inclusion in this thesis. I am the primary author of this paper.
Signature	
Date	17/9/2019

Co-Author Contributions

By signing the Statement of Authorship, each author certifies that:

- i. the candidate's stated contribution to the publication is accurate (as detailed above);
- ii. permission is granted for the candidate to include the publication in the thesis; and
- iii. the sum of all co-author contributions is equal to 100% less the candidate's stated contribution.

Name of Co-Author	Thomas Russell
Contribution to the Paper	Literature review, single-phase experiments, analysis of results, writing the manuscript.
Signature	
Date	09/09/2019

Name of Co-Author	Pavel Bedrikovetsky
Contribution to the Paper	Support in analysis of results, review of manuscript
Signature	
Date	17/09/19

Name of Co-Author	Abbas Zeinijahromi		
Contribution to the Paper	Support in analysis of results, review of manuscript		
Signature		Date	17/09/19

Fines Stabilization by Ca Ions and Its Effect on LSW Injection

A. Al-Sarhi,*^{ORCID} T. Russell, P. Bedrikovetsky, and A. Zeinjahromi^{ORCID}

Australian School of Petroleum, The University of Adelaide, Adelaide, SA 5005, Australia

ABSTRACT: Fines mobilization during the injection of low-salinity water yields a decrease in well injectivity and productivity but may cause an increase in the reservoir sweep efficiency during oilfield waterflooding. We investigate the stability of clay fines under the combined alteration of Na and Ca concentrations. Consequent injections of Ca and Na solutions in natural and engineered cores intercalated by deionized water (DIW) injections have been performed. Fines migration has not been observed during DIW injection after preflush by CaCl₂ solution; further consequent injection of NaCl and DIW yields a significant fines mobilization and permeability decline. The tests demonstrate a strong hysteretic behavior of mutual adsorption–desorption of Ca and Na cations on the reservoir clays and rock. The same phenomena have been observed in the presence of residual oil, where fines migration has been accompanied by incremental oil production.

INTRODUCTION

During fluid flow in subsurface reservoirs, small, naturally occurring particles can detach from the internal surface of the rock and become suspended in the flow.^{1–4} The resulting suspension flow forces particles through narrow crevices in the pore space, often resulting in particle capture, referred to here as straining. Straining restricts fluid flow through the pore spaces, causing a decrease in the rock permeability. The process in its entirety is referred to as fines migration and can have both positive and negative impacts on many industrial processes.^{1,2,5}

An understanding of fines migration has led to the insight that the permeability decline often originates in the detachment of in situ particles. The enhancement or mitigation of fines migration thus relies on controlling the conditions of particle detachment. Many studies have demonstrated that high fluid velocities,⁶ low fluid salinities,³ and high fluid pH⁷ are all effective at detaching particles. These factors are the primary explanation for why fines migration is often discussed in the context of low-salinity (LS) waterflooding projects, as these projects create conditions that favor particle detachment.

Several field studies have demonstrated that the permeability decline resulting from fines migration can have severe detrimental effects on injectivity^{8,9} and productivity^{10,11} during petroleum operations. Many operators will thus seek to inhibit fines detachment during these projects and often aim to increase salt concentrations in the injected water as a means to achieve this.

The role of fines migration during low-salinity waterflooding is not simply as a detriment to injection and production rates. While a myriad of mechanisms have been proposed to demonstrate why low-salinity water increases oil recovery,^{12–26} several studies have shown that fines migration can act as the mechanism for improved oil recovery during low-salinity waterflooding (LSW).^{27–29} Initially, the electrostatic forces attach the clay particles on the rock surface due to the abundance of salt ions that lower ζ -potential and the repulsive forces between clay fines and the rock surface, maintaining an equilibrium between the torques of electrostatic and drag (viscous) forces. When low-salinity brine is injected into

porous media, this equilibrium is disturbed and, as a result, clay particles are detached and mobilized by the drag forces caused by the displacing phase.^{1,12,30–35} Migration of fines leads to the aforementioned fines straining in the rock. As a result, water-permeable channels are plugged and the flow is directed toward unswept zones where residual oil is trapped.^{27,30,36–43} This microscale flux diversion causes a decline in water relative permeability and an increase in pressure drop, which improves microscopic sweep efficiency by mobility control, resulting in enhanced oil recovery.^{5,43–46}

In contrast with this enhancement of microscopic sweep efficiency, some simulation studies have demonstrated that by progressively damaging the fastest swept layers, fines migration can increase the reservoir scale sweep efficiency, thus unlocking additional reserves.⁴⁵

Due to the demonstrated effectiveness of fines migration in increasing both the microscopic and macroscopic sweep efficiencies, many low-salinity waterflooding projects aim to maximize particle detachment. Typically, this is achieved through minimization of the injected fluid salinity or by combining the low-salinity flood with alkaline solutions.

Despite the wealth of research on fines migration and the advent of new technologies designed to enhance or reduce it, several open problems remain regarding the nature of particle detachment. For instance, several studies have demonstrated that when different ions are used during initial core saturation, the cores show variable sensitivity to low-salinity water injection.^{47–49} These tests showed that decreasing the salinity of a CaCl₂ solution results in negligible changes in the permeability, whereas the same salinity decrease with a NaCl solution results in a significant permeability decline. Thus, the initiation of particle detachment is highly dependent on the cations that the rock has been exposed to previously, not solely on those in the solution during injection. Most injected fluids for low-salinity waterflooding projects are still designed on the basis that particle detachment is governed entirely by the

Received: August 12, 2019

Revised: October 15, 2019

Published: October 28, 2019

injected fluid. Thus, maximizing the benefit of these programmes by carefully controlling the ion composition will require an understanding of the impact of the observed history-dependent particle detachment.

The origin of this phenomenon as well as its dependence on ion valence and type remains unresolved.

In this work, we perform an experimental study to understand the phenomenon of clay fines stability under the environment of Ca and Na cations. Several coreflooding tests with CaCl₂ and NaCl solutions, both in single and two phase, are performed to investigate this phenomenon. We combine two of the single-phase tests with ion chromatography measurements to investigate the underlying ion exchange processes governing particle detachment. Such an investigation into the underlying processes during fines migration is not currently available in the literature. Based on the results of the tests, hysteresis in Ca²⁺ sorption is identified as the cause of the history-dependent sensitivity.

Despite the intensive current research on the influence of ion type on wettability alteration,^{2,17–23} a comprehensive study of the impact of this phenomenon on oil recovery is currently unavailable. In this study, we perform two-phase tests with nonpolar oil to avoid the impact of wettability changes and study the effect that ion-dependent fines migration can have on oil recovery.

LABORATORY STUDY

Materials. Natural Core Plugs. Three outcrop Berea sandstone core plugs were used in this study. One was used for the single-phase test and the rest for the two-phase tests. All cores were cut using a table saw cooled with a 3% KCl brine. Table 1 shows the properties of these cores.

Table 1. Properties of Berea Rock Samples

	Berea 1	Berea 2	Berea 3
permeability (mD)	120	40	21
porosity	0.19	0.19	0.19
length (cm)	5.05	12.10	12.05
diameter (cm)	3.80	3.80	3.80

Synthetic Core Plugs. Unconsolidated, artificial cores were prepared as part of this study to compare the effect of low-salinity water on clay particle (kaolinite) mobilization with natural core plugs. Artificially constructing cores results in a more homogeneous and reproducible rock with both controlled and consistent properties such as clay content and permeability.

The cores comprised silica sand and kaolinite. The sand used in this study has a silica content of >99% (brand 50N, SIBELCO, Australia). The sand was first sieved to constrain particle size, with a resulting mean diameter of 123 μm. Following sieving, the sand was washed sequentially in hexane, acetone, deionized water (DIW), 0.5 M HCl, and then deionized water. Washing of the sand in the last stage was repeated until the pH of the supernatant water returned to the pH of the natural deionized water. The sand was then dried at 60 °C for 24 h before use.

Analytical-grade kaolinite powder (Sigma-Aldrich, Australia) was used as the fines content of the cores. The mean diameter of the kaolinite was 2.064 μm. The kaolinite powder was first dried at 60 °C for 24 h before use.

The sand and kaolinite were first mixed dry and then suspended in 0.6 mol/L CaCl₂ solution before being placed into a Viton sleeve, which was then installed into a Hassler-type coreholder. The wet packing was performed under a side overburden pressure of 1000 psi.

A range of kaolinite mass content from 5 to 10% was chosen to emulate the kaolinite content of the Berea cores.

Brine. Aqueous solutions were prepared by dissolving NaCl (ChemSupply, 99.7% purity) or CaCl₂ (ChemSupply, 99% purity) into Milli-Q deionized water. All injected solutions were deaerated using a vacuum pump for at least 1 h to prevent dissolved air from entering the cores. All injected solutions had ionic strengths ranging between 0.6 M and that of deionized water. Salt concentrations given by M refer to the ionic strength of the solution in mol/L.

Oil. Mineral nonpolar paraffin oil (Light 15 LR from ChemSupply) with a viscosity of 20 cP at 25 °C was used in the two-phase tests.

Methodology. Figure 1 shows both a schematic and a photograph of the laboratory setup used in the experiment. The fluid was supplied by the pump (7) through the fluid cylinders (8–10) into the coreholder (3). Effluent samples were collected in a carousel (21), and differential pressure was measured using differential pressure transmitters (14,17). Detailed specifications of the equipment used are provided in the caption of the figure.

Four single-phase and two two-phase tests were performed in this study. Three of the single-phase tests were on unconsolidated cores and one on a Berea outcrop core (Berea 1). Both two-phase tests were done on Berea cores.

Prior to each test, the cores were dried at 60 °C for at least 24 h, deaerated under vacuum for the same period, and then saturated with 0.6 M CaCl₂ under vacuum. The cores were then installed in a Hassler-type coreholder, and a confining pressure of 1000 psi was applied to prevent annular flow between the core and the surrounding Viton sleeve. A backpressure of 500 psi was applied to keep a constant pressure at the outlet.

All tests were performed at constant room temperature.

Single-Phase Coreflooding Tests. The single-phase tests were performed to study the influence of solution ionic strength and injected composition on fines detachment and permeability.

Two unconsolidated cores of differing clay mass contents (7 and 10%) were used to test the influence of injected composition on fines detachment. Both pressure drop and outlet fines concentration measurements were used to detect the detachment and straining of particles. Different clay contents were used to provide more generality to the test results. Each test comprised saturating the cores with high-salinity CaCl₂ (0.6 M) and then injecting CaCl₂ solutions of progressively decreasing salinity to test the ionic strength dependence of particle stability with CaCl₂ solutions. This sequence ended with deionized water to identify whether the CaCl₂ had an influence on particle detachment even when not present in the injected solution. This was then followed with a 0.6 M high-salinity NaCl injection and then another deionized water injection. These were performed to determine whether the sensitivity of the cores to low-salinity water could be restored after the exposure to CaCl₂.

A third test on an unconsolidated 5% clay content core was performed using a similar procedure. One difference is that the sequential decrease in CaCl₂ ionic strength was substituted

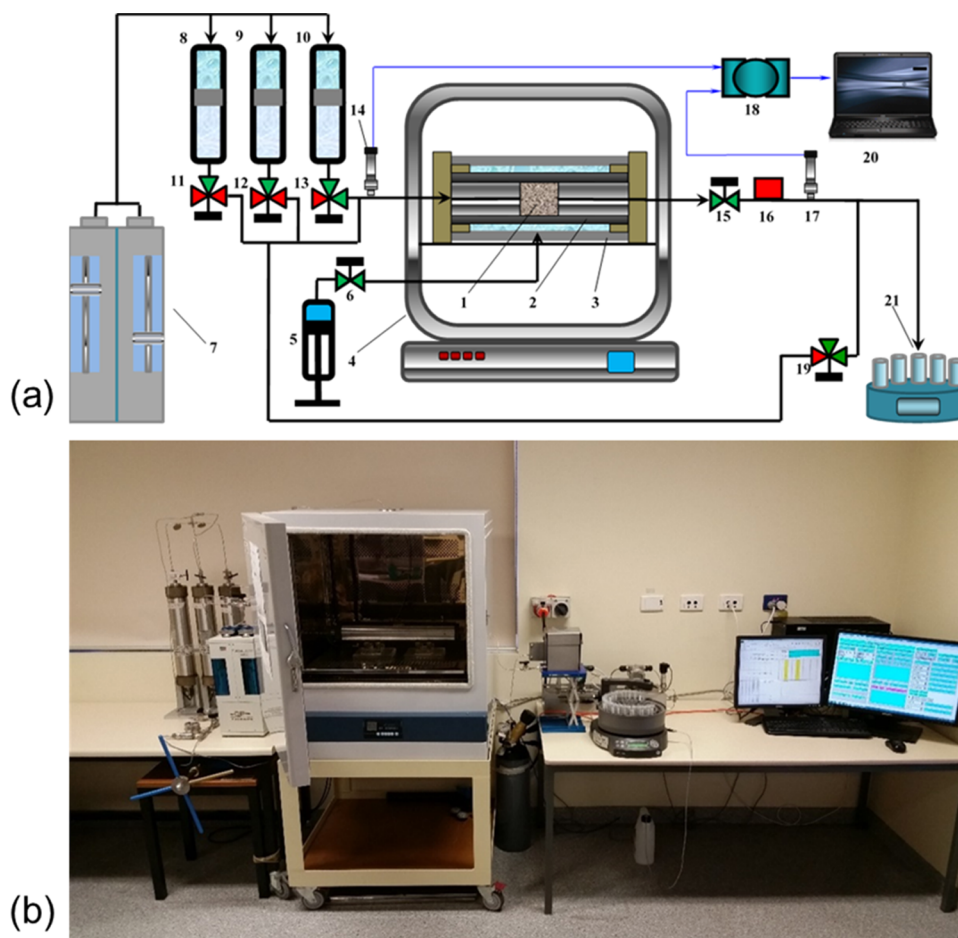


Figure 1. Laboratory setup used for two-phase coreflooding tests: (a) schematic and (b) photograph. (1) Core plug, (2) Viton sleeve, (3) Hassler-type coreholder, (4) oven to keep the temperature constant, (5) manual HiP piston pressure generator, (6) port switching valve, (7) Quizix Q6000 precision pump for two-phase tests (Prep-36, Scientific Systems pump used in the single-phase tests), (8–10) oil transfer vessels, (11–13) port switching valves, (14,17) absolute pressure transmitters, (15) port switching valve, (16) backpressure regulator, (18) ADAM-4019+ inlet data acquisition module, (19) port switching valve, (20) PC-based data acquisition system, and (21) GE Healthcare Frac-920 fractional collector.

with a direct decrease from high-salinity CaCl_2 to deionized water. In addition, ion chromatography measurements were performed on outlet samples to determine the Na^+ and Ca^{2+} concentrations separately. This test thus provided additional insight into the ion exchange mechanisms, as well as detecting fines detachment.

The last single-phase test was performed in the same manner as the 5% clay unconsolidated core but on a Berea outcrop core. While potentially less homogeneous, the Berea core is representative of many petroleum sandstone reservoirs and thus allows the results to be readily interpreted in the context of these systems.

During the single-phase tests, the brine solution was injected with a constant flow rate into the cores using a high-accuracy pump (Prep-36, Scientific Systems). The differential pressure across the core was measured using a series of four Yokogawa differential pressure transmitters. Having multiple differential pressure transmitters of varying sensitivities allowed the pressure across the core to be measured accurately over a wide range of differential pressures. Samples were collected at the outlet using a GE Healthcare Frac-920 fractional collector. All samples were processed using a POLA-2000 particle counter to determine the particle concentration and a Metrohm 930 ion chromatograph to determine the concentration of calcium and sodium ions.

The procedure of the single-phase test was as follows:

1. Injection of 0.6 M CaCl_2 at a low flow rate of 0.2 mL/min (superficial velocity 2.93×10^{-6} m/s) for a period of 24 h to achieve stable permeability. A lower flow rate is used to avoid particle detachment during permeability stabilization.
2. Sequential injection of 0.6 M CaCl_2 (and 0.3, 0.1, 0.05, 0.01, and 0.001 M CaCl_2 for the first two tests) and then deionized water at the test flow rate of 2 mL/min (superficial velocity 2.93×10^{-5} m/s). Each injection stage was performed until permeability had stabilized.
3. Injection of 0.6 M NaCl and then deionized water at the test flow rate of 2 mL/min (superficial velocity 2.93×10^{-5} m/s). Each injection stage was performed until permeability had stabilized.

Two-Phase Coreflooding Tests. The two-phase tests were conducted to determine the effect of calcium and sodium ions, both at high and low salinities, on the residual oil saturation (S_{or}).

The two-phase tests were performed on the Berea 2 and 3 cores.

The injected solutions were supplied using a pulse-free syringe pump (Quizix Q6000 precision pump). A dome backpressure regulator, supported by a nitrogen gas cylinder,

was used to maintain a constant outlet pressure of 500 psi. The pressure difference between the inlet and the outlet of the core was measured by Yokogawa (low pressure range) and Keller (high pressure range) pressure transducers. Darcy's law was applied to calculate the permeability of each core at the stabilized pressure drop along the cores. Outlet samples were collected in the same way as in the single-phase tests. Oil and water volumes were determined from the volumetric increments provided on the outlet samples. The particle concentration of the aqueous phase was measured using a POLA-2000 particle counter, with oil being removed from samples where necessary by syringe suction after centrifugation.

The procedure of the two-phase tests was as follows:

1. The core permeability was measured by injecting HS (high-salinity) 0.6 M CaCl_2 solution into the core at a constant rate of 0.2 ml/min (superficial velocity 2.93×10^{-6} m/s). This flow rate was used for the remainder of the test.
2. The first drainage displacement was performed by injecting nonpolar oil at the same constant rate until no more water was produced from the cores and the pressure drop stabilized, i.e., until the initial water saturation S_{wi} was obtained.
3. High-salinity waterflooding (HSW) was then performed by displacing oil with HS 0.6 M CaCl_2 brine until oil production stopped, indicating that the core was at residual oil saturation, S_{or} .
4. Another drainage stage was then performed to achieve the same initial condition (S_{wi}) before low-salinity waterflooding (LSW) took place by injecting low-salinity (LS) 0.05 M CaCl_2 to displace the oil.
5. Low-salinity waterflooding was then performed by injecting 0.05 M ionic strength CaCl_2 to displace the oil phase until residual oil was achieved.
6. Tertiary waterflooding with stepwise decreasing salinity of CaCl_2 brine was performed using solutions with ionic strengths of 0.025, 0.01 M, and deionized water (DIW). This step is important to provide insights into the impact of low-salinity CaCl_2 solutions on fines migration and oil recovery. Each injection continued until the pressure drop stabilized.
7. A 0.05 M NaCl solution was then injected followed by a DIW injection to investigate any effect of Na^+ ions on detaching Ca^{2+} and fines migration. Again, each stage was terminated only after the pressure drop had stabilized.

The oil and water volumes of all of the effluent samples as well as clay particle concentrations were measured immediately after sampling.

Two drainages have been performed to restore the S_{wi} conditions before LSW injection. The aim is to compare HSW and LSW injections for the identical reservoirs. Hysteresis between first and second drainage displacements can be significant. However, usually the difference between S_{wi} and K_{rowi} after first and second drainage displacements is insignificant.^{28,29} Table 3 shows very close agreement between the S_{wi} and K_{rowi} values for Berea 3 core and reasonable agreement for the Berea 2.

X-ray Diffraction (XRD) Study. To complement the coreflooding tests done on the Berea cores, an XRD study was performed on a cutting removed from the Berea core used

in the single-phase tests. The XRD analysis was conducted qualitatively using a Bruker D8 ADVANCE Powder X-ray diffractometer with a Cu-radiation source. The data was processed using Bruker DIFFRAC.EVA software and Crystallography Open Database reference patterns to identify mineral phases. The quantification of the mineralogy was calculated against an internal standard of zinc oxide at 10% using RockJock software.

EXPERIMENTAL RESULTS

Single-Phase Coreflooding Tests. The results of the tests on the 7 and 10% clay content cores are shown in Figures 2 and 3,

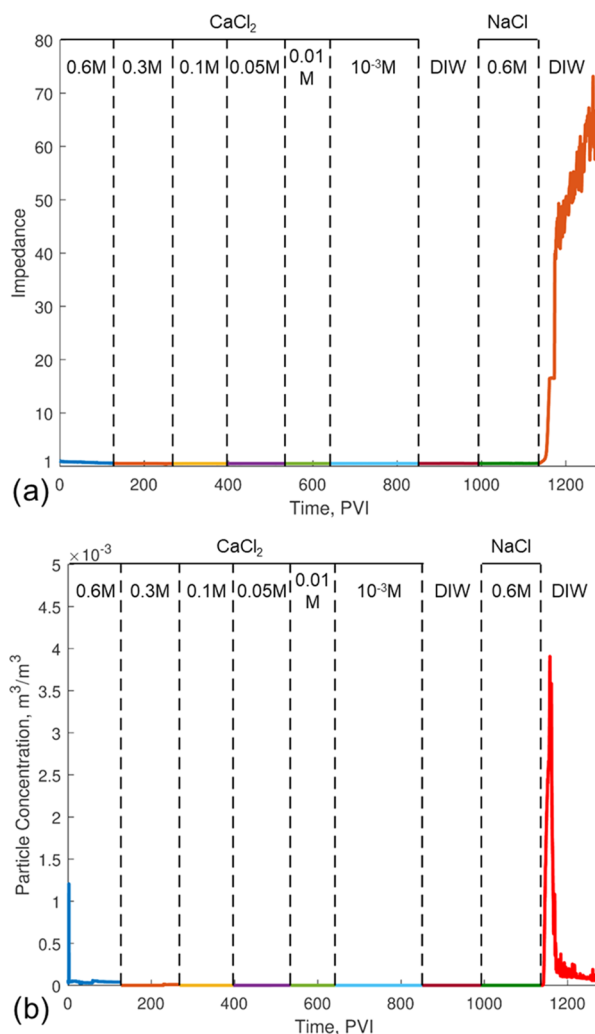


Figure 2. Single-phase test on unconsolidated sand-kaolinite core (7% kaolinite w/w, $k = 286$ mD): (a) normalized permeability, (b) outlet particle concentration.

respectively. Changes to the pressure drop of the cores are presented in a dimensionless form as the impedance, J

$$J = \frac{\Delta p}{\Delta p_0}$$

where Δp_0 is the stabilized initial pressure drop measured at the start of the test.

Unconsolidated Cores. Figure 2 shows the results from the test on the 7% clay content unconsolidated core. The undamaged permeability of the core was 286 mD, and the porosity was 0.386. Each injection stage lasted for at least 180 PVI. During the injection

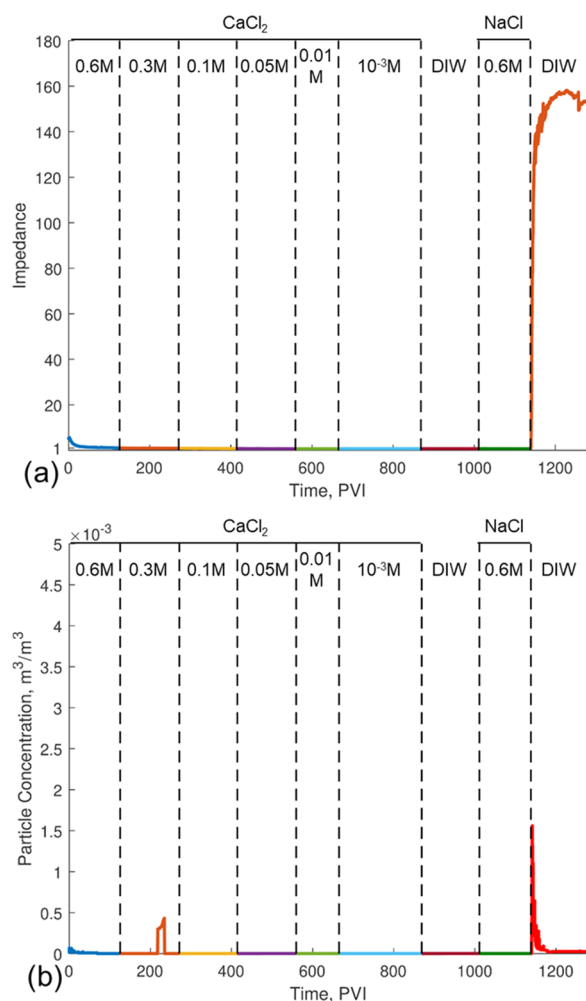


Figure 3. Single-phase test on unconsolidated sand-kaolinite core (10% kaolinite w/w, $k = 149$ mD): (a) normalized permeability, (b) outlet particle concentration.

of CaCl₂ solutions of decreasing salinity, including the first DIW injection stage, the pressure drop remains relatively constant. In addition to the negligible outlet particle concentration, this indicates a lack of fines detachment. A similar response is noted during the injection of 0.6 M NaCl, suggesting a lack of particle detachment. During the second deionized water injection, a significant rise in pressure drop and outlet particle concentration was observed, indicating that a substantial number of particles were detached due to the change in injected solution. The final value of impedance was 65.6, corresponding to a permeability of 4.36 mD.

Figure 3 presents the results from the next single-phase test, performed on the 10% clay unconsolidated core. The undamaged permeability of the core was 149 mD, and the porosity was 0.385. A relatively constant pressure drop and negligible outlet particle concentration during the CaCl₂ and the first DIW stages indicate no fines detachment during these injections, similar to the previous test. There is a noticeable exception in the outlet concentration during the 0.3 M CaCl₂ injection. This can be attributed to a slight desorption of Ca²⁺ ions, which leads to some attached particles being prone to detachment by the drag force. This persists during the NaCl injection. Fines migration is detected during the second deionized water injection, with a final stabilized impedance of 152, corresponding to a permeability of 0.98 mD.

Figure 4 presents the results of the 5% clay content unconsolidated core, with the additional ion chromatography results shown in Figure 4c. The initial permeability of the core was 537 mD, and the porosity was 0.366. A minor increase in the pressure drop is noted during the

first DIW injection, suggesting that some particles were detached. The NaCl injection shows no impact on the pressure drop. The second injection of DIW again shows indications of fines migration, with an increase of impedance to 1.7, with a final permeability of 358 mD.

The ion chromatography results in Figure 4c largely show that the injected solutions are being produced at the outlet. A careful examination of the Ca²⁺ concentration at the beginning of the NaCl injection, shown in Figure 4d, shows a noticeable peak in Ca²⁺ concentration, indicating a release of calcium ions during this injection stage that had not been desorbed during the first deionized water injection.

Berea Core. The results of the XRD study performed on Berea core 1 are presented in Table 2.

The results of the single-phase test on Berea 1 are presented in Figure 5. The initial permeability of the core was 120 mD. Qualitatively similar results are observed for both the pressure drop and outlet fines concentration, with indications of fines migration present only during the DIW injection after the NaCl stage. The final value of impedance was 3968, corresponding to a permeability of 0.03024 mD.

While showing some variation, the ion chromatography results again largely show the production of the injected solutions. The highlight of the NaCl injection stage shown in Figure 5d shows a significant peak in the Ca²⁺ concentration. This is in agreement with the 5% unconsolidated core test, indicating that the NaCl injection results in a desorption of some residual Ca²⁺ ions in the core.

Two-Phase Coreflooding Tests. In the two-phase coreflooding tests, the HSW and LSW effects of CaCl₂ brine on fines migration and oil recovery were compared in the secondary waterflooding processes (HSW after the first drainage and LSW after the second drainage) as well as in the tertiary waterflooding mode. To reach similar initial saturation conditions before HSW and LSW, oil was injected into the cores until the pressure drop stabilized at similar magnitudes for the first and second drainage displacements and no more oil was produced.

Berea 2. Figure 6a shows the pressure drop for these two oil displacements for Berea 2. In the first drainage displacement of HS CaCl₂ brine by nonpolar oil, the pressure drop increased to ~56 psi before the breakthrough and then decreased and stabilized at ~30 psi after injecting 8 pore volumes. In the second drainage displacement, the pressure drop increased to ~39 psi before the breakthrough and then stabilized at ~30 psi as well. The initial water saturations were 0.16 and 0.21 for the first and second drainages, respectively. The oil end-point relative permeabilities, K_{rowir} are 0.97 and 0.90, respectively.

Figure 6b shows the impedance and accumulated oil production for the secondary waterflooding by HS and LS CaCl₂ solutions. Each stage involved injecting 8 PV of the solution after the drainage displacement. The injection was stopped when the pressure drop stabilized and when no more oil was produced. At the start of the HSW, the initial pressure drop was ~28 psi. The impedance increased to ~2.1 before the breakthrough and then it dropped and stabilized at ~1.7. In the secondary LSW, the initial pressure drop was ~27 psi and the impedance increased to ~2.4 before breakthrough after which it dropped and stabilized at ~2. There is a slight difference in both impedance and oil recovery between the HSW and the LSW in the secondary mode. Oil production was 0.34 PV for the HSW and 0.38 for the LSW, as shown in Figure 6b, which could be due to the release of some fine particles during the LSW that slightly improved oil recovery. However, residual oil saturation for both displacements is 0.49, as shown in Table 3, which indicates that there is no significant effect of fines migration on oil recovery, unlike in the tertiary injection mode as discussed below.

Tertiary waterflooding was conducted to investigate the effect of CaCl₂ and NaCl brine ionic strength on fines migration and incremental oil recovery. The results of sequentially decreasing the injected CaCl₂ salinity down to DIW show no change in impedance (stable at ~1 with an initial pressure drop of ~27). Cumulative oil recovery also remains unaltered as shown in Figure 7a. The tertiary waterflooding was continued by injecting 0.05 M NaCl followed by DIW. Figure 7a shows that impedance increased significantly after the

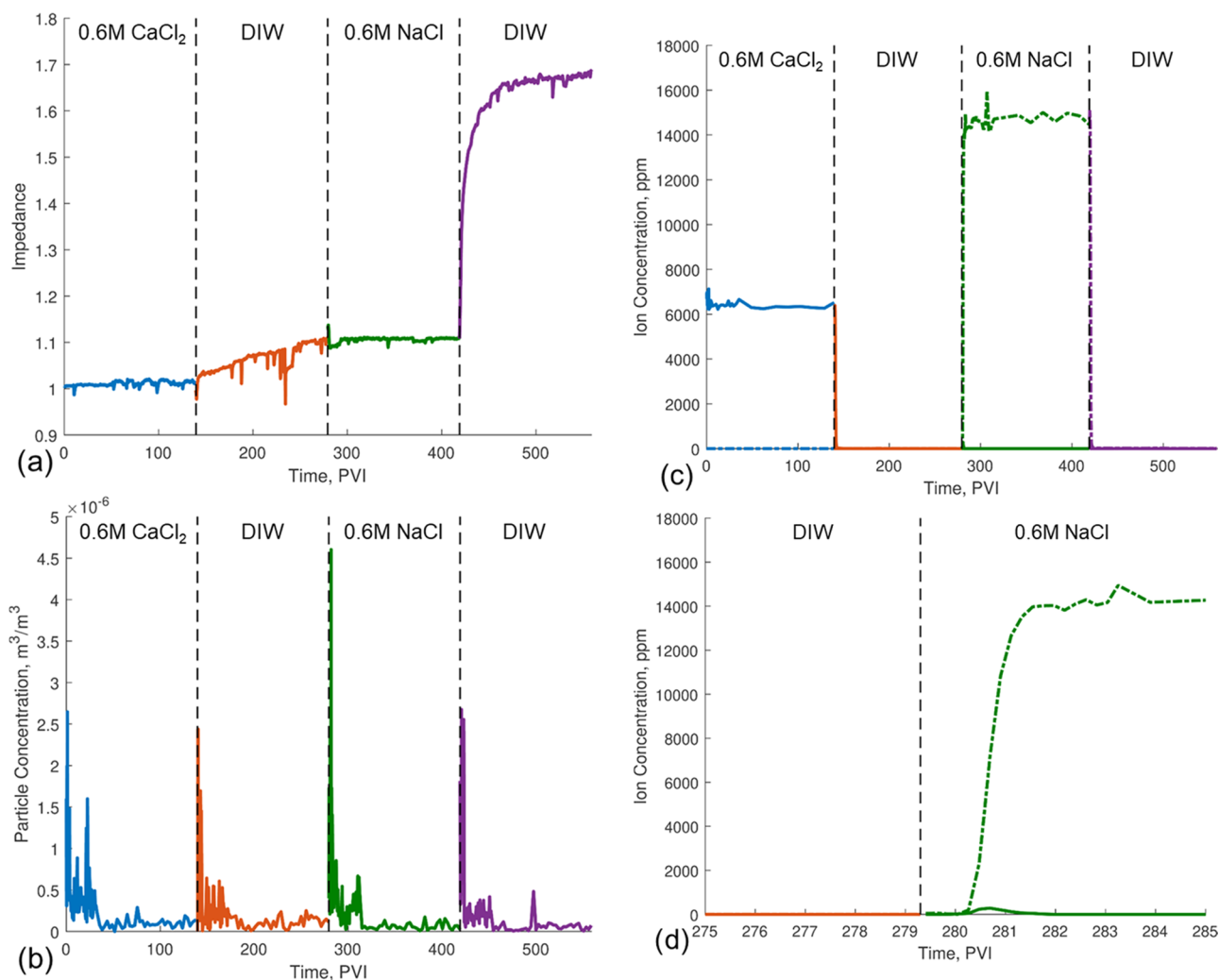


Figure 4. Single-phase test on unconsolidated sand-kaolinite core (5% kaolinite w/w, $k = 537$ mD): (a) normalized permeability, (b) outlet particle concentration, (c) outlet ion concentrations for sodium and calcium, (d) enlarged graph of outlet ion concentrations during the beginning of the injection of 0.6 M NaCl.

Table 2. Mineralogy of Berea 1 Determined Using XRD

mineral	weight %
quartz	84.6
K-feldspar (ordered microcline)	4.3
plagioclase (albite)	2.6
kaolinite (disordered)	2.3
illite	6.2

second DIW injection, approximately 15 times higher than the stabilized impedance during the CaCl_2 injection stages. Figure 7b shows that a substantial amount of clay particles was produced at the core outlet during the second DIW but not in any injection stages before that. This clearly demonstrates that fines migration occurred during the second DIW stage. This coincided with an increase in oil recovery such that the residual oil saturation decreased from 0.49 to 0.34.

Berea 3. Results similar to those of the Berea 2 test were observed in the Berea 3 coreflood. Figure 8a shows the pressure drop of the drainage displacements. In the first drainage, the pressure drop increased to 84 psi before breakthrough and stabilized at 58 psi after 5.5 PVI. In the second drainage, the pressure drop rose to ~95 psi before the breakthrough and then stabilized at ~63 psi after 8 PVI. The initial water saturations for the first and second drainage displacements are close, at 0.36 and 0.39, respectively, indicating a

reproducibility of the initial conditions. The oil end-point relative permeabilities of these drainages are 0.89 and 0.93, respectively.

Injecting low-salinity CaCl_2 in the secondary mode resulted in a slightly higher impedance (stabilized at ~1.5 after 8 PVI of LS CaCl_2 solution injection with an initial pressure drop of ~71 psi) compared to HSW (stabilized at ~1.3 after 8 PVI of HS CaCl_2 with an initial pressure drop of ~63 psi) as shown in Figure 8b. The residual oil saturations are 0.32 for the HSW and 0.24 for the LSW, which correspond to 0.32 and 0.38 PV of oil production, respectively, as illustrated in Figure 8b. Tertiary waterflooding of lower CaCl_2 salinities had almost no impact on the impedance (stable at ~2 with an initial pressure drop of ~71 psi) or oil production, as was seen in the Berea 2 test. However, injecting DIW after 0.05 M NaCl resulted in a significant rise in impedance (~11 times higher than the stabilized impedance during CaCl_2 LSW), fine particle production, and, hence, incremental oil recovery as shown in Figure 9a,b. The residual oil saturation decreased from 0.24 to 0.10.

For low permeability and HSW CaCl_2 , there is a particle production in two phase, which is permeability dependent. At the time of the 0.05 M CaCl_2 injection, the only aqueous solution that the cores had been exposed to was 0.6 M CaCl_2 . As a result, some Ca^{2+} can desorb during this injection, resulting in some particle detachment. The fact that it is more significant for the lower permeability core could be due to a higher clay content or due to a higher detaching force resulting from particles being situated in smaller pores.

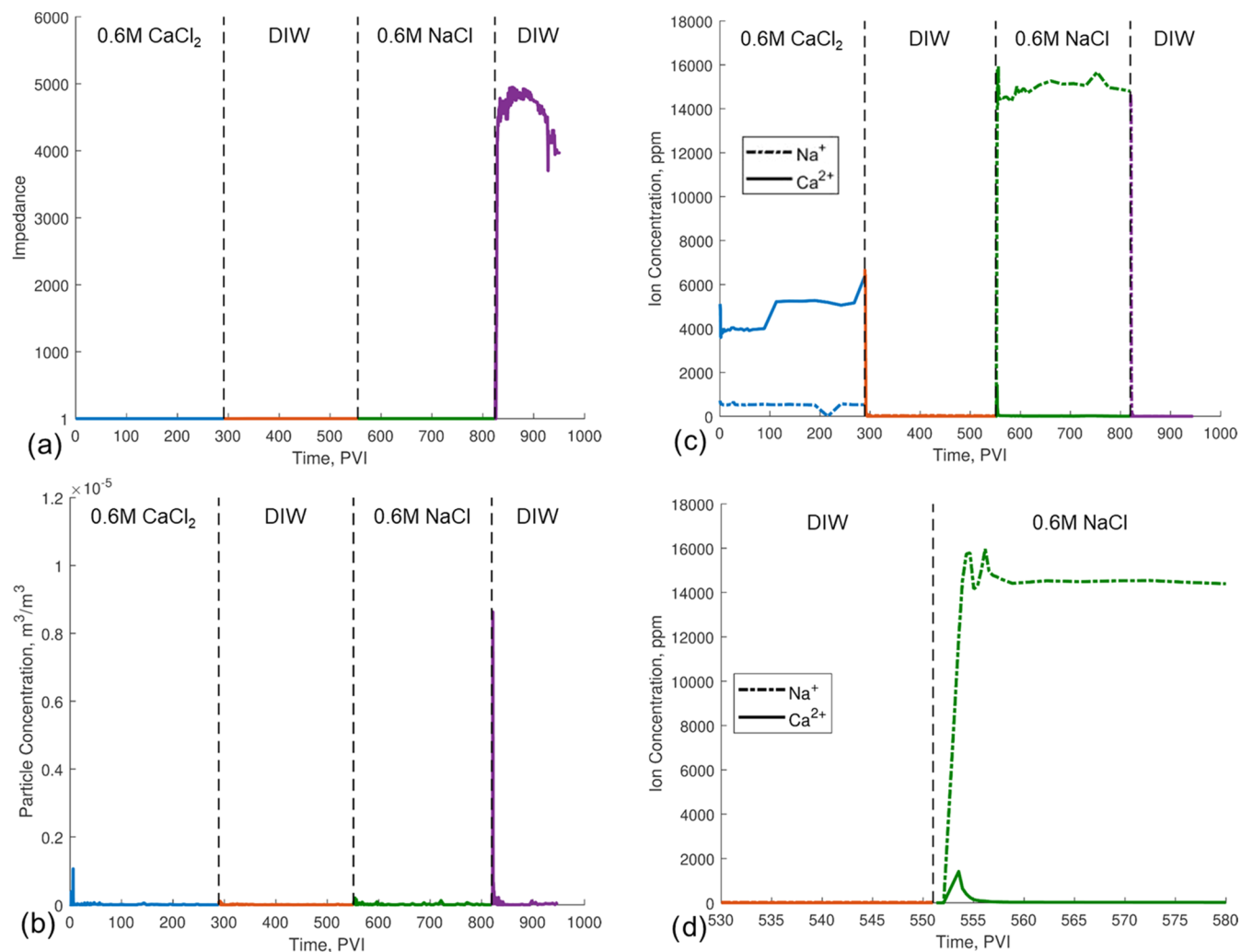


Figure 5. Single-phase test on Berea core 1 with $k = 120$ mD: (a) normalized permeability, (b) outlet particle concentration, (c) outlet ion concentrations for sodium and calcium, (d) enlarged graph of outlet ion concentrations during the beginning of the injection of 0.6 M NaCl.

DISCUSSION

Ion Sorption and Particle Detachment. The lack of particle detachment during CaCl_2 injections can be explained by the strong electrostatic force between the particles and rock surface due to the adsorbed calcium ions. The strong attraction arises from the suppression of the repulsive components of the electrostatic force by the adsorbed cations.⁵⁰ Following the injection of deionized water, neither the impedance nor outlet particle concentration showed any indications that particle detachment had occurred. In conjunction with the ion chromatography results, this suggests that the calcium ions were not fully desorbed during this injection cycle. The remaining calcium ions maintain a sufficiently large electrostatic force such that particles remain attached to the rock surface. The desorption of Ca^{2+} ions would in fact be an ion exchange process with the H^+ ions in solution. The experimental results suggest that this exchange has not resulted in the complete desorption of the calcium ions. During the NaCl injection, the high concentration of Na^+ ions present in solution resulted in at least a partial desorption of the remaining Ca^{2+} ions. The resulting adsorbed Na^+ ions can be readily desorbed during deionized water injection, resulting in the observed particle detachment.

This explanation is supported by the data presented on the outlet pH during the two-phase tests in Figures 7c and 9c. These graphs show that the pH is largely constant during all stages except the last, in which DIW is injected after 0.05 M NaCl. Changes to pH indicate that the hydrogen ions in solution are participating in the ion exchange. The lack of change during the first DIW injection supports the argument that very little Ca^{2+} ions are desorbed during this stage, as otherwise hydrogen ions would replace them on the clay surfaces, and a rise in pH would be observed at the outlet. This rise is observed, however, during the second DIW injection, where the Na^+ ions are replaced by the H^+ ions in solution. The lack of a change in pH during the NaCl injection indicates that the ion exchange occurring during this stage is primarily between the previously adsorbed Ca^{2+} ions and the Na^+ ions in solution.

Hysteresis of ionic sorption on clays has been widely reported in ion exchange in aquifers.⁵¹ In particular, Comans⁵² showed that the adsorption of cadmium ions onto illite will appear partially irreversible unless given up to 54 days for desorption. Gao et al.⁵³ showed that the sorption of cadmium and lead on soil samples showed significant hysteresis unless an acidic solution was used to desorb the ions.

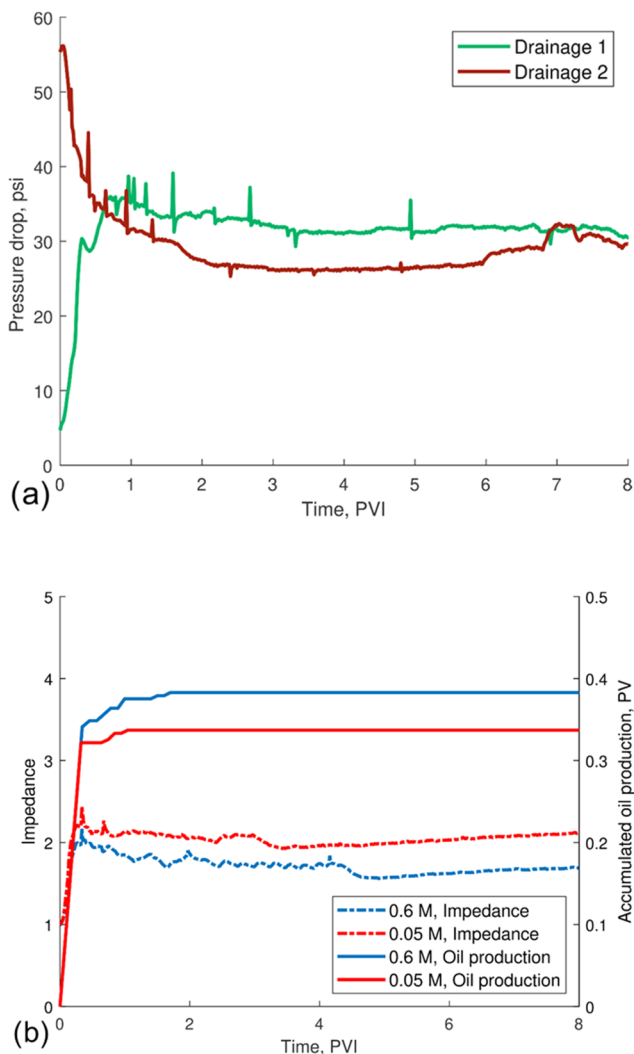


Figure 6. Berea 2 two-phase drainage and secondary displacements: (a) drainage pressure drop, (b) secondary waterflooding pressure drop and oil production.

Table 3. Saturations and End-Point Relative Permeabilities of the Two-phase Displacement Samples

	Berea 2	Berea 3
K_{rovi} (drainage 1)	0.97	0.89
S_{wi} (drainage 1)	0.16	0.36
K_{rWOR} (0.6 M CaCl_2)	0.02	0.03
S_{or} (0.6 M CaCl_2)	0.49	0.32
K_{rovi} (drainage 2)	0.88	0.93
S_{wi} (drainage 2)	0.21	0.39
K_{rWOR} (0.05 M CaCl_2)	0.02	0.02
S_{or} (0.05 M CaCl_2)	0.49	0.24
K_{rWOR} (0.025 M CaCl_2)	0.02	0.02
S_{or} (0.025 M CaCl_2)	0.49	0.24
K_{rWOR} (0.01 M CaCl_2)	0.02	0.02
S_{or} (0.01 M CaCl_2)	0.49	0.24
K_{rWOR} (DIW 1)	0.02	0.02
S_{or} (DIW 1)	0.49	0.24
K_{rWOR} (0.05 M NaCl)	0.01	0.01
S_{or} (0.05 M NaCl)	0.49	0.24
K_{rWOR} (DIW 2)	0.001	0.002
S_{or} (DIW 2)	0.34	0.10

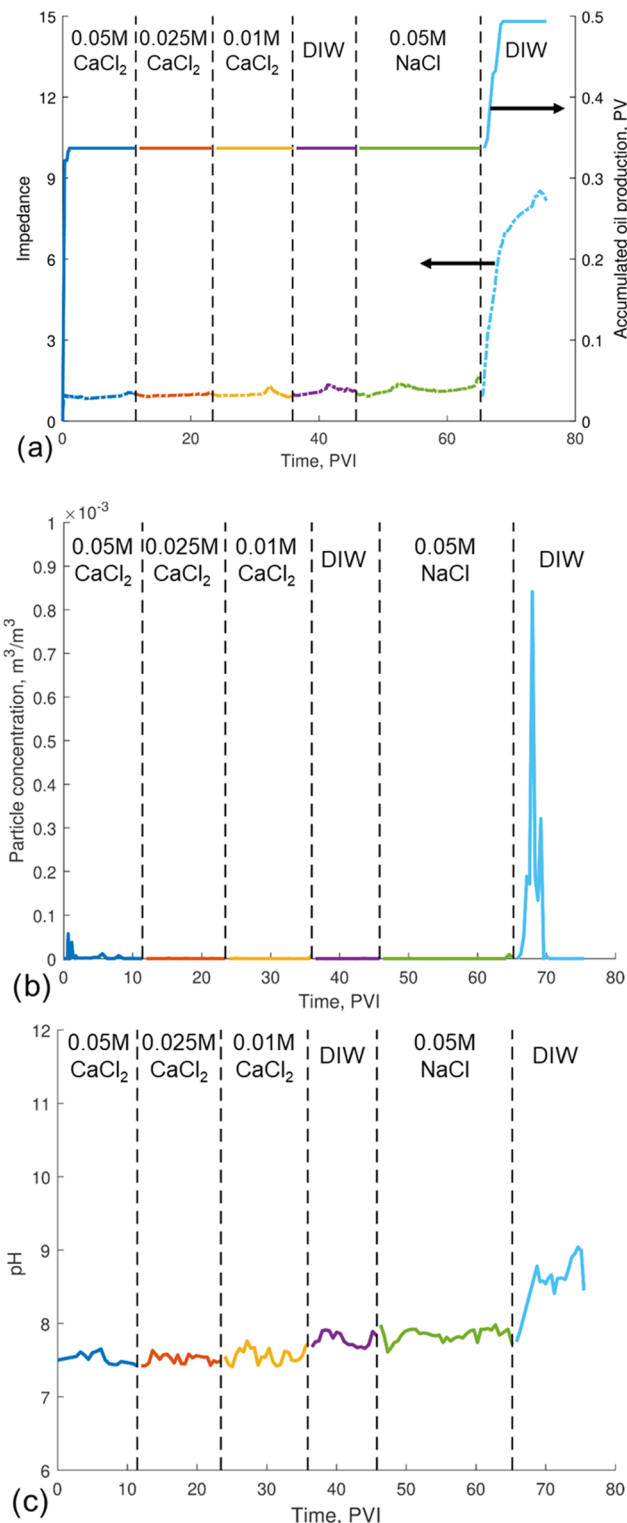


Figure 7. Two-phase tests on Berea core 2 with $k = 40$ mD: (a) pressure drop and oil production, (b) outlet particle concentration, (c) outlet pH.

This study similarly provides evidence of ion sorption hysteresis but provides little information on the physical basis and nature of the hysteresis. Of particular importance to practical applications is whether the hysteresis is permanent or is a result of ion desorption being substantially slower than adsorption. Strawn and Sparks⁵⁴ consider a multitude of existing laboratory tests and support the notion that the

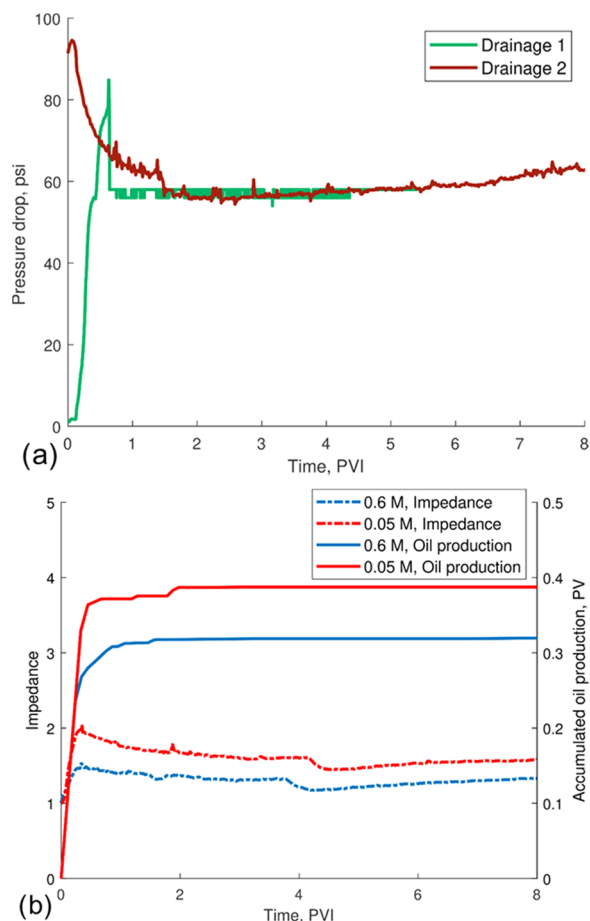


Figure 8. Berea 3 two-phase drainage and secondary displacements: (a) drainage pressure drop, (b) secondary waterflooding pressure drop and oil production.

apparent hysteresis is a result of slow desorption kinetics. A slow desorption phase could be a result of diffusive mass transfer into micropores followed by adsorption onto interior surfaces as was investigated quantitatively by Joekar-Niasar and Mahani⁵⁵ for the desorption of oil droplets from clays. An alternative explanation is that adsorbed ions transition between different adsorption mechanisms while adsorbed to the particle surface.⁵⁴ This conceptual model involves a transition from outer-sphere complexes, where adsorption is due to primarily electrostatic bonding, to inner-sphere complexes, where ionic or covalent bonding would provide a more stable ion-surface complex. Several molecular dynamics studies have confirmed the co-existence of multiple adsorption complexes on clays.^{56,57} Some authors have shown that while the total adsorbed ion concentration remains constant after some time, the fraction that can be desorbed increases as the clay is left in the saturating solution.^{58,59} This supports the notion of a transition between adsorption mechanisms. Given that rock saturation occurs over geological time periods in petroleum reservoirs, the ability to desorb certain ions may be overestimated by relatively short laboratory tests such as those presented in this study.

It should be noted that neither the complete desorption of adsorbed calcium by the NaCl injection nor the complete desorption of sodium during the second deionized water injection can be confirmed from these tests. The only inferences that can be made are that calcium sorption clearly

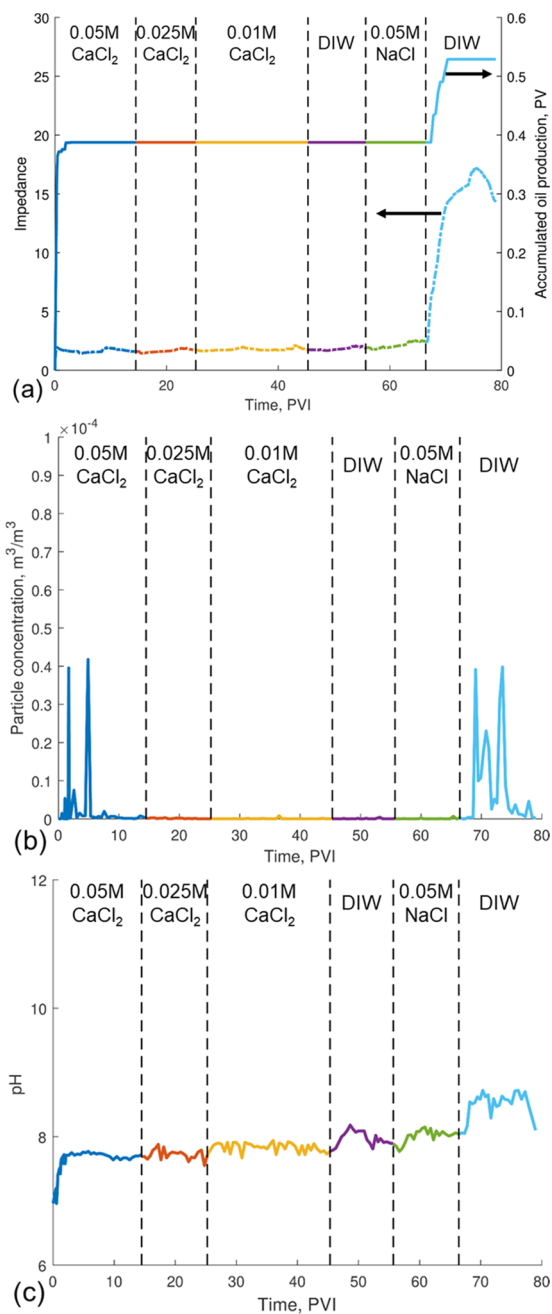


Figure 9. Two-phase tests on Berea core 3 with $k = 21$ mD: (a) pressure drop and oil production, (b) outlet particle concentration, (c) outlet pH.

demonstrates hysteretic behavior and that the adsorbed composition during the final deionized water injection favors particle detachment.

Impact on Oil Recovery. The use of nonpolar oil ensures that no wettability alteration takes place during low-salinity injection,^{25,26} and any extra oil production can be solely attributed to fines migration. The detachment of fine particles and their capture leads to microscopic flux diversion because the water flow is redirected away from blocked pores and into the thin pores where residual oil is trapped. This leads to the mobilization of oil ganglia and, therefore, a decrease in S_{or} . During redisplacement of the residual oil by the redirected water, the water–oil menisci will pass over a fraction of the rock surface. Attached particles on this surface will be exposed

to a capillary force acting to detach them. Such capillary forces are significantly higher than the electrostatic forces acting to keep the particles attached to the surface.^{60,61} Thus, oil mobilization can lead to further fines detachment and capture.

During both two-phase tests, injection of LS CaCl₂ brine resulted in almost no change in residual oil saturation compared to HSW. This is explained by a lack of particle detachment, evident from both the impedance and outlet particle concentration measurements (Figures 6b and 8b). This is consistent with the behavior described above, wherein hysteretic calcium sorption leads to a residual adsorbed concentration that is sufficient to inhibit particle detachment. Injection of NaCl results in ion exchange, favoring the adsorption of Na⁺ ions. During the deionized water injection, the desorption of these Na⁺ ions is sufficient to reduce the electrostatic forces and, hence, detach clay particles. This is reflected in an increase in the impedance and outlet fines concentration, as well as a decrease in the residual oil saturation.

It should be noted that in several tests, notably in the single-phase test of the 5% clay content unconsolidated core and in Berea 3, some evidence of fines migration is observed during the decrease in CaCl₂ salinity. This is evidence that while the residual adsorbed calcium ions substantially reduce the sensitivity of the cores to low-salinity water, they do not completely inhibit fines migration. Nonetheless, the increase in impedance is negligible compared to similar tests run with pure NaCl solutions for both single phase⁶² and two phase.⁴³

An understanding of the hysteretic nature of ion exchange and its relation to fines migration is critical in designing field-scale smart (low-salinity) water injection projects. This study demonstrates that the sensitivity of sandstone rocks to low-salinity water can be controlled by the type of ion in the saturating solution.

Formation damage due to fines migration in the vicinity of injection and production wells remains a major issue in waterflooding projects. Pretreating the near-wellbore region with a solution of high CaCl₂ concentration could be used to mitigate injectivity or productivity decline issues during low-salinity waterflooding projects by stabilizing fines. Conversely, far from injection and production wells, increases in macro- and microscale sweep efficiencies can make enhancing fines migration crucial to the success of a waterflood. In these cases, pretreating the rock with NaCl could enhance the sensitivity of the rock to low-salinity water, unlocking further potential for reducing the residual oil saturation.

While calcium and sodium are two of the most abundant cations found in most petroleum reservoirs, many other ions are typically present, and the potential for hysteretic sorption in more complex ionic solutions deserves proper investigation. Furthermore, a quantitative investigation of the hysteresis and potential long-term desorption kinetics would allow for more rigorous modeling of fines migration during low-salinity waterflooding.

Limitations of the Study. This study used both artificial and Berea cores. We use Berea cores as a means to extend the results of this study to petroleum reservoirs. However, the Berea cores are outcrop cores, which are subject to weathering, which might alter the detachment characteristics of the kaolinite particles.⁶³ This limitation does not prohibit studying the hysteresis of Na–Ca ion exchange and its impact on fines detachment, but it does limit the extension of these results to field-scale applications. A comparison of the results of this

study with results from reservoir cores is the subject of further work.

Additional limitations stem from differences between the conditions of the tests in this study and common reservoir conditions. These differences include the chemical composition of crude oil, which commonly includes polar components; high reservoir temperatures; more complex ionic compositions, including trivalent ions in the formation water; the presence of reactive minerals such as feldspars and evaporates; and additional clays not present in the cores used in this study (e.g., montmorillonite). These factors can significantly impact the detachment of fines. For example, the effectiveness of high temperatures in increasing particle detachment has been well studied.^{64,65} The application of fines migration coreflooding results to a particular reservoir requires careful replication of these important conditions in the laboratory.

Miscellaneous. Primary and secondary drainages have been performed to create identical oil–water–rock systems before HSW and LSW. Some hysteresis occurs between first and second drainage displacements; however, the values S_{wi} and $K_{r,owi}$ were close enough. The method can be improved by HSW injection after the second drainage displacement and then LSW.

CONCLUSIONS

In this study, we performed laboratory corefloods with variation in the sodium and calcium concentrations of the injected brine. Ion chromatography measurements allowed observation of the underlying ion exchange processes. Similar tests in the presence of residual oil were performed to investigate the impact this ion exchange might have on oil recovery. These tests allow concluding the following:

1. During the DIW injection that follows the CaCl₂ injection, the impedance remains constant and clay fines do not appear in the effluent. This indicates no fines detachment.
2. Further DIW injection that follows the NaCl injection exhibits a large increase in impedance and significant fines concentration in the effluent, suggesting that the permeability decline can be attributed to fines mobilization and capture.
3. Some Ca²⁺ ions have been released during the NaCl injection, suggesting competitive adsorption of Na⁺ and Ca²⁺ ions on the clay and residual adsorbed Ca²⁺ concentration after the DIW injection.
4. Adsorption of Ca ions on kaolinite clay exhibits a hysteretic behavior.
5. The same phenomena have been observed in the presence of residual oil.
6. Induced fines migration results in a decrease in residual oil.

AUTHOR INFORMATION

Corresponding Author

*Email: abdullah.sarihi@adelaide.edu.au

ORCID

A. Al-Sarihi: 0000-0001-7075-0526

A. Zeinijahromi: 0000-0002-3088-6952

Notes

The authors declare no competing financial interest.

ACKNOWLEDGMENTS

The authors would like to thank Drs. Alex Badalyan (Australian School of Petroleum, University of Adelaide), Luis Genolet, Aron Behr, and Patrick Kowollik (Wintershall Holding GmbH) for their fruitful discussions. The authors would also like to thank Dr. Tony Hall for performing the XRD study.

NOMENCLATURE

- J = impedance
 k = permeability
 $K_{r_{\text{owi}}}$ = oil relative permeability at initial water saturation
 $K_{r_{\text{wor}}}$ = water relative permeability at residual oil saturation
 S_{or} = residual oil saturation
 S_{wi} = initial water saturation
 Ca = calcium
 Ca^{2+} = calcium ions
 Na = sodium
 Na^+ = sodium ions

GREEK LETTERS

- Δp_0 = stabilized initial pressure drop
 Δp = stabilized pressure drop

ABBREVIATIONS

- DIW = deionized water
 HS = high salinity (0.6 M ionic strength)
 HSW = low-salinity waterflooding
 LS = low salinity (0.05 M ionic strength)
 LSW = low-salinity waterflooding
 M = molar
 PVI = pore volume injected

REFERENCES

- (1) Khilar, K. C.; Fogler, H. S. *Migrations of Fines in Porous Media*; Springer Science & Business Media, 1998; Vol. 12.
- (2) Fogden, A.; Kumar, M.; Morrow, N. R.; Buckley, J. S. Mobilization of Fine Particles during Flooding of Sandstones and Possible Relations to Enhanced Oil Recovery. *Energy Fuels* **2011**, *25*, 1605–1616.
- (3) Khilar, K. C.; Fogler, H. S. Water sensitivity of sandstones. *Soc. Pet. Eng. J.* **1983**, *23*, 55–64.
- (4) Qajar, J.; Arns, C. H. Characterization of reactive flow-induced evolution of carbonate rocks using digital core analysis-part 2: Calculation of the evolution of percolation and transport properties. *J. Contam. Hydrol.* **2017**, *204*, 11–27.
- (5) Yuan, H.; Shapiro, A. A. Induced migration of fines during waterflooding in communicating layer-cake reservoirs. *J. Pet. Sci. Eng.* **2011**, *78*, 618–626.
- (6) Zheng, X. L.; Shan, B. B.; Chen, L.; Sun, Y. W.; Zhang, S. H. Attachment-detachment dynamics of suspended particle in porous media: Experiment and modeling. *J. Hydrol.* **2014**, *511*, 199–204.
- (7) Kia, S.; Fogler, H. S.; Reed, M. Effect of pH on colloidal induced fines migration. *J. Colloid Interface Sci.* **1986**, *118*, 158–168.
- (8) Barkman, J.; Abrams, A.; Darley, H.; Hill, H. An Oil-Coating Process To Stabilize Clays in Fresh Waterflooding Operations (includes associated paper 6405). *J. Pet. Technol.* **1975**, *27*, 1053–1059.
- (9) Akhmetgareev, V.; Khisamov, R. In *40 Years of Low-Salinity Waterflooding in Pervomaiskoye Field, Russia: Incremental Oil*, SPE European Formation Damage Conference and Exhibition; Society of Petroleum Engineers, 2015.
- (10) Ezeukwu, T.; Thomas, R. L.; Gunnerod, T. In *Fines Migration Control in High-Water-Cut Nigerian Oil Wells: Problems and Solutions*, SPE International Symposium on Formation Damage Control; SPE: Lafayette, Louisiana, 1998.
- (11) Reinoso, W.; Torres, F.; Aldana, M.; Campo, P.; Alvarez, E.; Tovar, E. In *Removing Formation Damage from Fines Migration in the Putumayo Basin in Colombia: Challenges, Results, Lessons Learned, and New Opportunities after more than 100 Sandstone Acidizing Treatments*, SPE International Conference & Exhibition on Formation Damage Control; SPE: Lafayette, Louisiana, 2016.
- (12) Brady, P. V.; Morrow, N. R.; Fogden, A.; Deniz, V.; Loahardjo, N. Electrostatics and the low salinity effect in sandstone reservoirs. *Energy Fuel* **2015**, *29*, 666–677.
- (13) Qiao, C.; Johns, R.; Li, L. Modeling low-salinity waterflooding in chalk and limestone reservoirs. *Energy Fuels* **2016**, *30*, 884–895.
- (14) Aksulu, H.; Håmsø, D.; Strand, S.; Puntervold, T.; Austad, T. Evaluation of low-salinity enhanced oil recovery effects in sandstone: Effects of the temperature and pH gradient. *Energy Fuels* **2012**, *26*, 3497–3503.
- (15) Mahani, H.; Keya, A. L.; Berg, S.; Bartels, W.-B.; Nasralla, R.; Rossen, W. R. Insights into the mechanism of wettability alteration by low-salinity flooding (LSF) in carbonates. *Energy Fuels* **2015**, *29*, 1352–1367.
- (16) Mahani, H.; Menezes, R.; Berg, S.; Fadili, A.; Nasralla, R.; Voskov, D.; Joekar-Niasar, V. Insights into the impact of temperature on the wettability alteration by low salinity in carbonate rocks. *Energy Fuels* **2017**, *31*, 7839–7853.
- (17) Zahid, A.; Shapiro, A.; Stenby, E. H.; Yan, W. Managing injected water composition to improve oil recovery: A case study of North Sea chalk reservoirs. *Energy Fuels* **2012**, *26*, 3407–3415.
- (18) Bazyari, A.; Soulgani, B. S.; Jamialahmadi, M.; Dehghan Monfared, A.; Zeinijahromi, A. Performance of smart water in clay-rich sandstones: experimental and theoretical analysis. *Energy Fuels* **2018**, *32*, 10354–10366.
- (19) Puntervold, T.; Mamonov, A.; Aghaeifar, Z.; Frafjord, G. O.; Moldestad, G. M.; Strand, S.; Austad, T. Role of Kaolinite Clay Minerals in Enhanced Oil Recovery by Low Salinity Water Injection. *Energy Fuels* **2018**, *32*, 7374–7382.
- (20) Farajzadeh, R.; Guo, H.; van Winden, J.; Bruining, J. Cation exchange in the presence of oil in porous media. *ACS Earth Space Chem.* **2017**, *1*, 101–112.
- (21) RezaeiDoust, A.; Puntervold, T.; Austad, T. Chemical verification of the EOR mechanism by using low saline/smart water in sandstone. *Energy Fuel* **2011**, *25*, 2151–2162.
- (22) Torrijos, I. D. P.; Puntervold, T.; Strand, S.; Austad, T.; Abdullah, H. I.; Olsen, K. Experimental Study of the Response Time of the Low-Salinity Enhanced Oil Recovery Effect during Secondary and Tertiary Low-Salinity Waterflooding. *Energy Fuels* **2016**, *30*, 4733–4739.
- (23) Bartels, W.-B.; Mahani, H.; Berg, S.; Hassanizadeh, S. Literature review of low salinity waterflooding from a length and time scale perspective. *Fuel* **2019**, *236*, 338–353.
- (24) Nasralla, R. A.; Mahani, H.; van der Linde, H. A.; Marcellis, F. H.; Masalmeh, S. K.; Sergienko, E.; Brussee, N. J.; Pieterse, S. G.; Basu, S. Low Salinity Waterflooding for a carbonate reservoir: Experimental evaluation and numerical interpretation. *J. Pet. Sci. Eng.* **2018**, *164*, 640–654.
- (25) Hao, J.; Mohammadkhani, S.; Shahverdi, H.; Esfahany, M. N.; Shapiro, A. Mechanisms of smart waterflooding in carbonate oil reservoirs-A review. *J. Pet. Sci. Eng.* **2019**, No. 49.
- (26) Mohammadkhani, S.; Shahverdi, H.; Nielsen, S. M.; Esfahany, M. N.; Shapiro, A. Bicarbonate flooding of homogeneous and heterogeneous cores from a carbonaceous petroleum reservoir. *J. Pet. Sci. Eng.* **2019**, *178*, 251–261.
- (27) Li, Y. Oil recovery by low salinity water injection into a reservoir: A new study of tertiary oil recovery mechanism. *Trans. Porous Media* **2011**, *90*, 333–362.
- (28) Hussain, F.; Zeinijahromi, A.; Bedrikovetsky, P.; Badalyan, A.; Carageorgos, T.; Cinar, Y. An experimental study of improved oil recovery through fines-assisted waterflooding. *J. Pet. Sci. Eng.* **2013**, *109*, 187–197.

- (29) Zeinijahromi, A.; Farajzadeh, R.; Bruining, J. H.; Bedrikovetsky, P. Effect of fines migration on oil–water relative permeability during two-phase flow in porous media. *Fuel* **2016**, *176*, 222–236.
- (30) Civan, F. Reservoir Formation Damage: Fundamentals. In *Modeling, Assessment, and Mitigation*; Gulf Professional Publishing, 2007; Vol. 2.
- (31) Khilar, K. C.; Fogler, H. S.; Ahluwalia, J. Sandstone water sensitivity: existence of a critical rate of salinity decrease for particle capture. *Chem. Eng. Sci.* **1983**, *38*, 789–800.
- (32) Bedrikovetsky, P.; Siqueira, F. D.; Furtado, C. A.; Souza, A. L. S. Modified particle detachment model for colloidal transport in porous media. *Trans. Porous Med.* **2011**, *86*, 353–383.
- (33) Bedrikovetsky, P.; Zeinijahromi, A.; Siqueira, F. D.; Furtado, C. A.; de Souza, A. L. S. Particle detachment under velocity alternation during suspension transport in porous media. *Trans. Porous Med.* **2012**, *91*, 173–197.
- (34) Israelachvili, J. *Intermolecular and Surface Forces*; Academic Press: London, U.K, 1992; p 450.
- (35) Mohan, K. K.; Fogler, H. S.; Vaidya, R. N.; Reed, M. G. Water Sensitivity of Sandstones Containing Swelling and Non-swelling Clays. In *Colloids in the Aquatic Environment*; Elsevier, 1993; pp 237–254.
- (36) Schembre, J.; Tang, G.-Q.; Kovscek, A. Wettability alteration and oil recovery by water imbibition at elevated temperatures. *J. Petr. Sci. Eng.* **2006**, *52*, 131–148.
- (37) Sarkar, A. K.; Sharma, M. M. Fines migration in two-phase flow. *J. Pet. Technol.* **1990**, *42*, 646–652.
- (38) Scheuerman, R. F.; Bergersen, B. M. Injection-water salinity, formation pretreatment, and well-operations fluid-selection guidelines. *J. Pet. Technol.* **1990**, *42*, 836–845.
- (39) Lever, A.; Dawe, R. A. Water-sensitivity and migration of fines in the hopeman sandstone. *J. Pet. Geol.* **1984**, *7*, 97–107.
- (40) Muecke, T. W. Formation fines and factors controlling their movement in porous media. *J. Pet. Technol.* **1979**, *31*, 144–150.
- (41) You, Z.; Bedrikovetsky, P.; Badalyan, A.; Hand, M. Particle mobilization in porous media: Temperature effects on competing electrostatic and drag forces. *Geophys. Res. Lett.* **2015**, *42*, 2852–2860.
- (42) Yuan, B.; Wang, W. Using nanofluids to control fines migration for oil recovery: Nanofluids co-injection or nanofluids pre-flush?—A comprehensive answer. *Fuel* **2018**, *215*, 474–483.
- (43) Al-Sarhi, A.; Zeinijahromi, A.; Genolet, L.; Behr, A.; Kowollik, P.; Bedrikovetsky, P. Effects of fines migration on residual oil during low-salinity waterflooding. *Energy Fuels* **2018**, *32*, 8296–8309.
- (44) Zeinijahromi, A.; Nguyen, T. K. P.; Bedrikovetsky, P. Mathematical model for fines-migration-assisted waterflooding with induced formation damage. *SPE J.* **2013**, *18*, 518–533.
- (45) Zeinijahromi, A.; Al-Jassasi, H.; Begg, S.; Bedrikovetski, P. Improving sweep efficiency of edge-water drive reservoirs using induced formation damage. *J. Pet. Sci. Eng.* **2015**, *130*, 123–129.
- (46) Ahmetgareev, V.; Zeinijahromi, A.; Badalyan, A.; Khisamov, R.; Bedrikovetsky, P. Analysis of low salinity waterflooding in Bastrykskoye field. *Pet. Sci. Technol.* **2015**, *33*, 561–570.
- (47) Grolimund, D.; Borkovec, M. Release of colloidal particles in natural porous media by monovalent and divalent cations. *J. Contam. Hydrol.* **2006**, *87*, 155–175.
- (48) Bradford, S. A.; Kim, H. Implications of cation exchange on clay release and colloid-facilitated transport in porous media. *J. Environ. Qual.* **2010**, *39*, 2040–2046.
- (49) Kia, S.; Fogler, H. S.; Reed, M. *Effect of Salt Composition on Clay Release in Berea Sandstones*, SPE International Symposium on Oilfield Chemistry; Society of Petroleum Engineers, 1987.
- (50) Gregory, J. Interaction of unequal double layers at constant charge. *J. Colloid Interface Sci.* **1975**, *51*, 44–51.
- (51) Jenne, E. A. *Adsorption of Metals by Geomedia*; Elsevier, 1998.
- (52) Comans, R. N. J. Adsorption, Desorption and Isotopic Exchange of Cadmium on Illite - Evidence for Complete Reversibility. *Water Res.* **1987**, *21*, 1573–1576.
- (53) Gao, Y.; Kan, A. T.; Tomson, M. B. Critical evaluation of desorption phenomena of heavy metals from natural sediments. *Environ. Sci. Technol.* **2003**, *37*, 5566–5573.
- (54) Strawn, D. G.; Sparks, D. L. Sorption Kinetics of Trace Elements in Soils and Soil Materials. In *Fate and Transport of Heavy Metals in the Vadose Zone*; Selim, H. M., Iskandar, I. K., Eds.; CRC Press: Boca Raton, Florida, 1999.
- (55) Joekar-Niasar, V.; Mahani, H. Nonmonotonic Pressure Field Induced by Ionic Diffusion in Charged Thin Films. *Ind. Eng. Chem. Res.* **2016**, *55*, 6227–6235.
- (56) Vasconcelos, I. F.; Bunker, B. A.; Cygan, R. T. Molecular dynamics modeling of ion adsorption to the basal surfaces of kaolinite. *J. Phys. Chem. C* **2007**, *111*, 6753–6762.
- (57) Li, X.; Li, H.; Yang, G. Promoting the Adsorption of Metal Ions on Kaolinite by Defect Sites: A Molecular Dynamics Study. *Sci. Rep.* **2015**, *5*, No. 14377.
- (58) McLaren, R. G.; Lawson, D. M.; Swift, R. S. Sorption and Desorption of Cobalt by Soils and Soil Components. *J. Soil Sci.* **1986**, *37*, 413–426.
- (59) Kuo, S.; Mikkelsen, D. S. Kinetics of Zinc Desorption from Soils. *Plant Soil* **1980**, *56*, 355–364.
- (60) Lazouskaya, V.; Wang, L.-P.; Or, D.; Wang, G.; Caplan, J. L.; Jin, Y. Colloid mobilization by fluid displacement fronts in channels. *J. Colloid Interface Sci.* **2013**, *406*, 44–50.
- (61) Shang, J.; Flury, M.; Chen, G.; Zhuang, J. Impact of flow rate, water content, and capillary forces on in situ colloid mobilization during infiltration in unsaturated sediments. *Water Resour. Res.* **2008**, *44*, No. 516.
- (62) Russell, T.; Pham, D.; Neishaboor, M. T.; Badalyan, A.; Behr, A.; Genolet, L.; Kowollik, P.; Zeinijahromi, A.; Bedrikovetsky, P. Effects of kaolinite in rocks on fines migration. *J. Nat. Gas Sci. Eng.* **2017**, *45*, 243–255.
- (63) Brady, P. V.; Morrow, N. R.; Fogden, A.; Deniz, V.; Loahardjo, N. Winoto, Electrostatics and the Low Salinity Effect in Sandstone Reservoirs. *Energy Fuels* **2015**, *29*, 666–677.
- (64) You, Z. J.; Bedrikovetsky, P.; Badalyan, A.; Hand, M. Particle mobilization in porous media: Temperature effects on competing electrostatic and drag forces. *Geophys. Res. Lett.* **2015**, *42*, 2852–2860.
- (65) You, Z.; Badalyan, A.; Yang, Y.; Bedrikovetsky, P.; Hand, M. *Laboratory Study of Fines Migration in Geothermal Reservoirs*, Proceedings World Geothermal Congress, 2014.

6 Conclusions and Recommendations

This thesis presented new results on the effect of salt ion type and fines migration on oil recovery. New coreflood designing criteria were also introduced to aid modelling relative permeability of two-phase flow by Welge-JBN method, accounting for the capillary-viscous ratio to fulfil the large scale approximation.

Flux diversion caused by clay particles detachment and blockage during low salinity waterflooding yields reduction in residual oil saturation and enhancement of oil production. This was concluded from the stepwise decrease in the injected water salinity, which causes simultaneous fines production and water relative permeability decrease in a maintained water-wet system during all the waterflooding stages. This effect occurs because of the weakened fine-rock electrostatic attraction which caused the release of clay particles that block the water-filled pores and, hence, resulted in the flux diversion phenomenon. Improving the microscale sweep efficiency aids in controlling water front and decrease of water fingering which causes early breakthrough time.

The presence of clay content plays a major role in enhancing oil production by fines migration. In the case of zero clay content in the rock, no change in permeability or pressure drop was observed during low salinity waterflooding i.e. low salinity waterflooding yields the same oil recovery as high salinity (conventional) waterflooding. As the clay content increases, the impact of low salinity becomes more effective and the fines production rises significantly as seen in the results. Additionally, the higher the decrease in water salinity, the higher is the decline in water relative permeability and, therefore, more oil is mobilised and produced. Although this trend was observed in most of the tests performed in this study, there are, however, a few experiments that showed

notable fines production at the early stage of the low salinity waterflooding (0.05 and 0.025 M concentrations). That is because of the high clay content of those core samples which induces a large number of smaller size fine particles to be detached when low salinity water is injected. Pressure drop may not have a significant increase due to the passage of the small size particles through the pore throats where size exclusion (detached clay particles plugging thin pore throats) does not take place. In the case of low permeability rocks, size exclusion causes large pressure drop across the samples.

Injection of divalent ions solution such as calcium chloride into a porous media aids to strengthen the attachment of clay particles on the rock surface, as seen in the results of chapter four paper. Reducing the salinity of injected water does not cause any significant fines detachment and migration, even when the rock is flushed with deionised water. This indicates a strong affinity of calcium ions to the rock surface which leads to stabilisation of clay particles during low salinity waterflooding. Further injection with monovalent ions solution such as sodium chloride and then deionised water leads to significant clay particles production, accompanied by a drastic decrease in permeability. This suggests that there is a competitive adsorption between sodium and calcium on the clay and also that the adsorption of calcium on clay has a hysteretic behaviour. This phenomenon can be applied to stabilize fines production at the injector or producer wells during low salinity waterflooding to minimise formation damage.

Another new outcome presented in this thesis is the designing criteria for the coreflooding experiments of high and low salinity waterflooding schemes. Two theoretical criteria of capillary-viscous ratio and capillary number need to be fulfilled for the validity of the Welge-JBN method. Furthermore, four operational criteria which include pressure precision, water cut accuracy,

number of effluent samples, and minimum sampling period are introduced to provide accurate measurements to determine relative permeability during coreflooding. Euclidian 3D space of velocity and core length is used to graphically solve the proposed criteria (formed in inequalities) to determine the required minimum displacement rate and core length. Moreover, capillary-viscous ratio was determined to be below 0.5 to fulfil Buckley-Leverett solution that assumes negligible capillary pressure effect on relative permeability and fractional flow curves.

Recommendations and Future Work

The conclusions of this work draw the following recommendations for future work:

- Investigation of the effect of fines migration to enhance oil recovery on reservoir samples.
- Apply X-ray computer tomography to study the effect of heterogeneity on flux diversion not only on micro-scale level but on the core level.
- Study the effect of clay swelling (without fines production) to investigate its influence on oil recovery.
- More investigation of the kinetics of the effect of fines migration and ionic exchange in real time is recommended to observe how long these processes take to detach oil from the rock surface.
- More experimental work is recommended to qualitatively represent the impact of fines migration in LSW-EOR and to cover a wider range of parameters besides residual oil and relative permeability in order to combine them into an analytical formula.
- It is recommended that the mathematical formulas presented in section 3 is transformed in a capillary dependent relative permeability correlation (or a

different dimensionless parameter reflecting the reservoir flow dynamics) that is suitable for numerical simulation for field applications.

- Investigation of the phenomena presented in this thesis on carbonate rocks and how low salinity water can react with the carbonate rock surface that has a different mineralogy from sandstone rocks (where wettability and surface charge is different).
- The negative impact of formation damage due to fine migration particularly in tight formation competes with the positive Sor reduction from flux diversion as explained in this thesis. It is recommended more work of fines-assisted EOR is done on tight reservoirs.
- Investigation of the impact of high salinity and low salinity slugs size in an alternating sequence to achieve an optimised scheme of HSW/LSW sequence for maximum oil recovery.
- More studies should be done to understand the mobility change away from the injectors in the field during HSW/LSW which can assist the pressure downhole gauge and deconvolution surveillance techniques in order to aid in mitigation plans and recovery optimisation.

Appendix

The following conference paper is a complementary to the papers in chapter 4 and shows how sweep efficiency is improved by fines migration.

Fines Migration as an EOR Method During Low Salinity waterflooding

Al-Sarihi, A., Zeinjahromi, A., Genolet, L., Behr, A., Kowollik, P. and Bedrikovetsky, P., published 10/2018

Presented SPE Asia Pacific Oil and Gas Conference and Exhibition. Society of Petroleum Engineers

Statement of Authorship

Title of Paper	Fines migration as an EOR method during low salinity waterflooding
Publication Status	<input checked="" type="checkbox"/> Published <input type="checkbox"/> Accepted for Publication <input type="checkbox"/> Submitted for Publication <input type="checkbox"/> Unpublished and Unsubmitted work written in manuscript style
Publication Details	A. Al-Sarihi, A. Zeinjahromi, L. Genolet, A. Behr, P. Kowollik, and P. Bedrikovetsky, Fines migration as an EOR method during low salinity waterflooding, APOGCE Conference 2018

Principal Author

Name of Principal Author (Candidate)	Abdullah Al-Sarihi				
Contribution to the Paper	Literature review, experimental work, analysis of results, writing the manuscript.				
Overall percentage (%)	70%				
Certification:	This paper reports on original research I conducted during the period of my Higher Degree by Research candidature and is not subject to any obligations or contractual agreements with a third party that would constrain its inclusion in this thesis. I am the primary author of this paper.				
Signature	<table border="1" style="width: 100%;"> <tr> <td style="width: 80%;"></td> <td style="width: 20%;">Date</td> </tr> <tr> <td></td> <td>17/9/2019</td> </tr> </table>		Date		17/9/2019
	Date				
	17/9/2019				

Co-Author Contributions

By signing the Statement of Authorship, each author certifies that:

- i. the candidate's stated contribution to the publication is accurate (as detailed above);
- ii. permission is granted for the candidate to include the publication in the thesis; and
- iii. the sum of all co-author contributions is equal to 100% less the candidate's stated contribution.

Name of Co-Author	Abbas Zeinjahromi				
Contribution to the Paper	Support in analysis of results, methodology writing, review manuscript				
Signature	<table border="1" style="width: 100%;"> <tr> <td style="width: 80%;"></td> <td style="width: 20%;">Date</td> </tr> <tr> <td></td> <td>17/09/19</td> </tr> </table>		Date		17/09/19
	Date				
	17/09/19				

Name of Co-Author	Luis Genolet				
Contribution to the Paper	Support in analysis of results				
Signature	<table border="1" style="width: 100%;"> <tr> <td style="width: 80%;"></td> <td style="width: 20%;">Date</td> </tr> <tr> <td></td> <td>10.09.2019</td> </tr> </table>		Date		10.09.2019
	Date				
	10.09.2019				

Please cut and paste additional co-author panels here as required.

Name of Co-Author	Aron Behr		
Contribution to the Paper	Support in analysis of results		
Signature		Date	11/2/19

Name of Co-Author	Patrick Kowollik		
Contribution to the Paper	Support in analysis of results		
Signature		Date	10/9/19

Name of Co-Author	Pavel Bedrkiovetsky		
Contribution to the Paper	Support in analysis of results, literature review, review of manuscript		
Signature		Date	17/09/19



SPE-192070-MS

Fines Migration as an EOR Method During Low Salinity Waterflooding

Abdullah Al-Sarihi and Abbas Zeinijahromi, ASP, University of Adelaide; Luis Genolet, Aron Behr, and Patrick Kowollik, Wintershall Holding GmbH; Pavel Bedrikovetsky, ASP, University of Adelaide

Copyright 2018, Society of Petroleum Engineers

This paper was prepared for presentation at the SPE Asia Pacific Oil & Gas Conference and Exhibition held in Brisbane, Australia, 23–25 October 2018.

This paper was selected for presentation by an SPE program committee following review of information contained in an abstract submitted by the author(s). Contents of the paper have not been reviewed by the Society of Petroleum Engineers and are subject to correction by the author(s). The material does not necessarily reflect any position of the Society of Petroleum Engineers, its officers, or members. Electronic reproduction, distribution, or storage of any part of this paper without the written consent of the Society of Petroleum Engineers is prohibited. Permission to reproduce in print is restricted to an abstract of not more than 300 words; illustrations may not be copied. The abstract must contain conspicuous acknowledgment of SPE copyright.

Abstract

This study presents a novel mechanism of enhancing oil recovery by fines migration during low salinity waterflooding. Formation damage is isolated from other low salinity mechanisms in the experimental tests performed in this work. Therefore, the reduction in residual oil saturation is attributed to fines migration mechanism only that is caused by improved microscale sweep efficiency via water flux diversion due to fine particles straining. Corefloods were performed on Berea cores with high clay content, Bentheimer cores with low clay content, and artificial clean sand cores with no clay to investigate the effect of clay presence on residual oil saturation. HSW and LSW took place after drainage displacements that resulted in the same initial conditions of connate water saturation and oil relative permeability. Non-polar oil is used to ensure water-wetness in the cores and to avoid possible wettability alteration by low salinity waterflooding. Single phase corefloods were also performed to study the effect of piecewise decreasing salinity on permeability. The results show a permeability decline with low salinity water injection in the single phase tests of clay-rich cores accompanied by fine particles production and pH increase. The same effect is observed in the two phase tests. In addition, incremental oil production is observed along with the permeability decrease and fines production. This is due to detachment of clay particles by weakened attraction as a result of LSW, which leads to fines migration and straining in water filled pores. Therefore, water flux diversion into trapped oil pores takes place, which displaces the residual oil in these pores. A relationship between formation damage, $\beta\Delta\sigma$, and residual oil saturation has been introduced and it can be applied in reservoir simulation for LSW.

Introduction

Low salinity waterflooding (LSW) has received great attention in recent years due to its low-cost EOR potential. However, the mechanisms of LSW effect are still debatable (Tang and Morrow 1999, RezaeiDoust, Puntervold, and Austad 2011, Al Shalabi, Sepehrnoori, and Delshad 2014, Mahani et al. 2015b, Afekare and Radonjic 2017). These include, fines migration, ionic exchange, double layer expansion, and decrease of contact angle and interfacial tension (Lager et al. 2008, Austad, Rezaeidoust, and Puntervold 2010, Morrow and Buckley 2011, Zeinijahromi et al. 2016, Al-Shalabi and Sepehrnoori 2016, Farajzadeh et al. 2017). In this study we focus mainly on fines migration as an EOR mechanism. As fines migration has

not always been observed during LSW, we isolate this mechanism by performing experimental coreflooding tests that exclude other mechanisms of low salinity effect such as wettability alteration.

Fines migration occurs as the clay fines that are attached to the rock surface by electrostatic forces are mobilized by drag forces. The equilibrium of the electrostatic and drag torques is disturbed by decreasing salinity or increasing flow rate. Electrostatic forces are weakened when the water salinity is decreased and, hence, the clay particles are detached. The drag force caused by the flowing fluid aids mobilizing these fines. This leads to plugging of some pore throats in the rock which results in a significant decline in water relative permeability during LSW as shown in Fig. 1 (Muecke 1979, Fogden et al. 2011, Bedrikovetsky et al. 2012, Zeinijahromi, Nguyen, and Bedrikovetsky 2013). Sweep efficiency can be improved by this effect as mobility control takes place when high permeable water channels are blocked and the flow is diverted into inswept zones. Therefore, residual oil that is trapped in thin pores can then be produced (Sharma and Filoco 2000, Hussain et al. 2013).

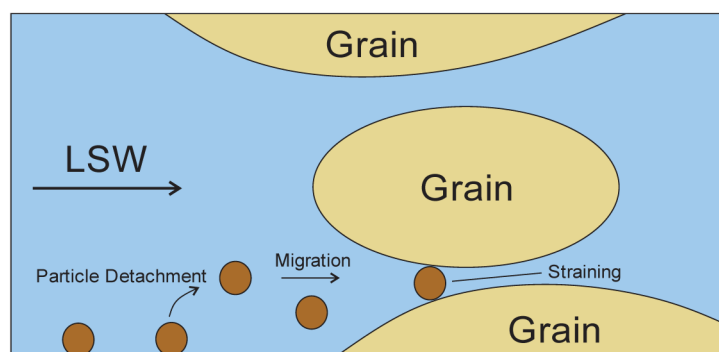


Figure 1—Fine particles detachment, migration and straining in thin pores.

The effect of ionic exchange and capillarity on reduction of residual oil during LSW has been shown by numerous authors (Morrow and Buckley 2011, Sheng 2014, Mahani et al. 2015a) but the effect of solely fines migration on residual oil has not. In this work we present a number of coreflood experiments performed on rock samples with a range of clay content as well as samples with no movable clay particles. A range of water salinities is used and non-polar oil is utilized as the non-wetting phase in the tests to avoid oil wettability and, hence, wettability alteration effect by LSW. The role of clay and fines migration is investigated to improve micro-scale sweep efficiency by flux diversion due to fines mobilization, migration and straining in the porous media.

Experimental Study

Rocks

Berea, Bentheimer, and artificial unconsolidated core samples were used in this study. One Berea and one Bentheimer were used for the single phase flow tests. Three Berea, one Bentheimer, and two artificial cores were used for two phase flow tests. The Berea cores have high clay content, whereas the Bentheimer sample has significantly low clay content and the artificial cores have none. The cores used for single phase tests are 6 cm long and 3.8 cm in diameter, whereas the cores used for two phase are 12 cm long and 3.8 cm in diameter. Mineralogy XRD analysis of the samples is summarized in table 1. The unconsolidated rock is made of silica grains that were sieved to grain size of 70-260 μm .

Table 1—XRD analysis of the consolidated core samples

	Berea A %(w/w)	Berea B %(w/w)	Bentheimer %(w/w)
Quartz	83.4	81.5	94
K-feldspar	5.5	5.4	2.8
Plagioclase	3.5	3.5	0
Kaolinite	3.6	3.8	1.7
Illite	4	5.8	1.6

Fluids

The injected synthetic brine has concentrations of 35,000 ppm, 17,500 ppm, 6,000 ppm, 3,000 ppm, 1,500 ppm, and 750 ppm. NaCl is dissolved in deionized water for each of the water salinity concentrations. Mineral Paraffin oil is used as non-polar oil to prevent oil wettability in the rock. The viscosity of the oil is 20 cp.

Method

Coreflooding and Amott tests were performed in this work. Coreflooding was run both as single phase and two phase flow modes. The aim of the single phase tests is to investigate the effect of salinity on fine particles detachment and mobilization. The two phase flow tests aim to study the effect of fines mobilization on residual oil saturation. Amott tests were run to measure the wettability of the Berea cores and to investigate whether wettability alteration occurs with LSW.

Single phase coreflood procedure:

1. The porosity of the cores is computed by measuring the pore volume based on the dry weight and the wet weight of the core after they are saturated with HS water (35,000 ppm) under vacuum.
2. The core is then inserted in a Viton rubber sleeve and installed in a Hassler core holder where overburden pressure of 500 psi more than the injection pressure is applied. Backpressure of 500 psi is also applied.
3. To identify the permeability of the cores, HS water is injected at a constant rate of 0.2 ml/min and the pressure drop is recorded as it stabilizes. Darcy law is used to calculate the permeability.
4. Step-wise decreasing water salinity is injected in the cores until pressure stabilizes.
5. Effluent samples undergo particle concentration, ionic strength and pH measurements.

Two phase coreflood procedure:

1. Steps 1-3 mentioned in single phase coreflood procedure are performed to measure porosity and permeability for the two phase experiments. All the following injections are performed at a constant rate of 0.2 ml/min.
2. Oil is injected to displace the HS water until no more water is produced and S_{wi} is achieved.
3. The core is then flooded with HS water to displace the oil until no more oil is produced in the effluent and S_{or} is achieved.
4. Oil is injected again until S_{wi} is reached as in step 2.
5. LS water (3,000 ppm) is injected to displace the oil until S_{or} is reached.
6. Tertiary LSW is performed afterwards with step-wise decreasing salinities of 1,500 ppm, 750 ppm and DI water to compare oil recovery between HSW and these salinities. The pressure drop needs to stabilize for each salinity injected.
7. Step 5 in the single phase coreflood procedure is also performed for these tests.

Amott Tests:

1. Berea cores are first saturated with 100% HS water and then drainage takes place by injecting oil into the samples to displace the HS water.
2. The sample is then removed from the core holder and inserted in an Amott cell filled with HS water for spontaneous imbibition. The volume of oil, V_{osp} , is recorded.
3. When oil production stops (about two weeks), the sample is installed in the core holder again and flushed with HS water for forced displacement. The volume of oil, $V_{o-forced}$, is recorded.
4. Spontaneous drainage is performed when the core is submerged in an Amott cell filled with the oil. The volume of water, V_{wsp} , is recorded.
5. Oil is then injected in the core for forced drainage and the volume of water, $V_{w-forced}$, is recorded.
6. Steps 1-5 are repeated for 3,000 ppm brine concentration and for DI water.
7. Wettability index is calculated for each brine salinity.

Results

Berea samples: the single phase test shows a reduction in permeability as salinity is decreased as presented in Fig. 2. Injection of HS water (35,000 ppm) decreased the initial permeability slightly from 40.8 to 35 mD. At salinity of 17,500 ppm, no significant change in permeability was noticed. However, injection of 6,000 ppm had a noticeable formation damage where the permeability decreased to 24 mD. At a salinity of 3,000 ppm, permeability decreased further to 20 mD. A dramatic decline in permeability was observed when the salinity was dropped to 750 ppm. The permeability stabilized at 0.14 mD. Fine particles production coincides with the permeability decline in each stage of injection as shown in the same figure. SEM-EDX analysis of the effluent samples was done to investigate the type of particles produced as illustrated in Fig. 3. The results show that kaolinite and illite were released from the core, which implies these clay particles had been detached, mobilized through the porous media, and produced in the effluent via the flowing water.

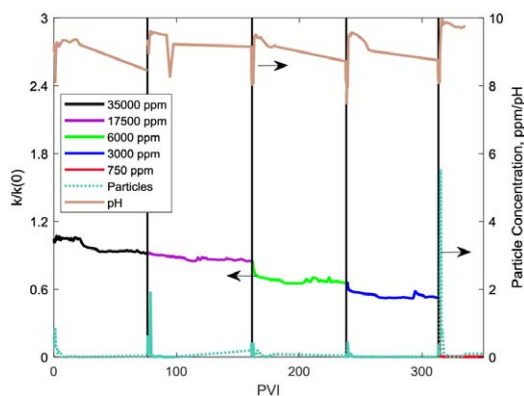


Figure 2—Single phase test on Berea sample with piecewise decreasing salinity: effect on permeability, fine particles production, and pH.

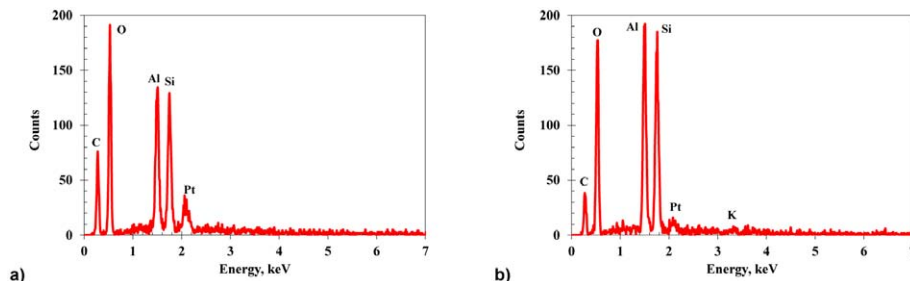


Figure 3—SEM-EDX analysis of the produced clay particles from the single phase test: a) kaolinite, b) illite.

Two phase coreflooding on Berea cores A, B, and C was performed to compare oil recovery when HS and LS water are injected. Double coreflooding took place by performing the drainage process twice before HSW and LSW, respectively. Achieving similar initial water saturation, S_{wi} , and end point relative permeability of oil, K_{rowi} , after both drainage displacements is key to compare residual oil saturation, S_{or} . The cores are bump flooded with a rate that is 10 times higher than the constant injection rate to produce trapped water due to capillary end effects. After the second drainage, 3,000 ppm NaCl brine was injected followed by tertiary lower salinity brines as mentioned in the Method section. Generally, the results show similar tendency of increasing pressure drop and declining water relative permeability with salinity decrease accompanied by fine particles production and reduction in S_{or} .

Fig. 4a shows the normalized pressure drop vs time (pore volume injected, PVI) of the first oil injection pressure drop, HSW pressure drop, and recovery factor for Berea A. The S_{wi} values are 0.14 and 0.15 for oil injection 1 and 2 respectively. The end point relative permeabilities of oil for both drainages are 0.69 and 0.62. S_{wi} and K_{rowi} values are close for both drainage displacements which implies the initial conditions are reached. The second oil injection pressure drop, LSW (3,000 ppm) pressure drop, and recovery factor are shown in Fig. 4b. Pressure drop during HSW increased before breakthrough, then dropped, and stabilized at 55 psi after ~ 10 PVI, whereas LSW resulted in an increasing pressure drop, which stabilized at 320 psi, approximately 6 times than that of HSW. Extra oil production was observed with LSW in secondary and tertiary modes as shown in Fig. 4d. Residual oil saturation decreased from 0.43 during HSW to 0.41 during 3,000 ppm, 0.39 during 1,500 ppm, 0.30 during 750 ppm and 0.25 during DI water injection. High pressure drop along with high fine particles production is observed in all stages of LSW in this test as shown in Fig. 4c. DI water shows the highest pressure drop due to the significant fines detachment and mobilization at this injection stage.

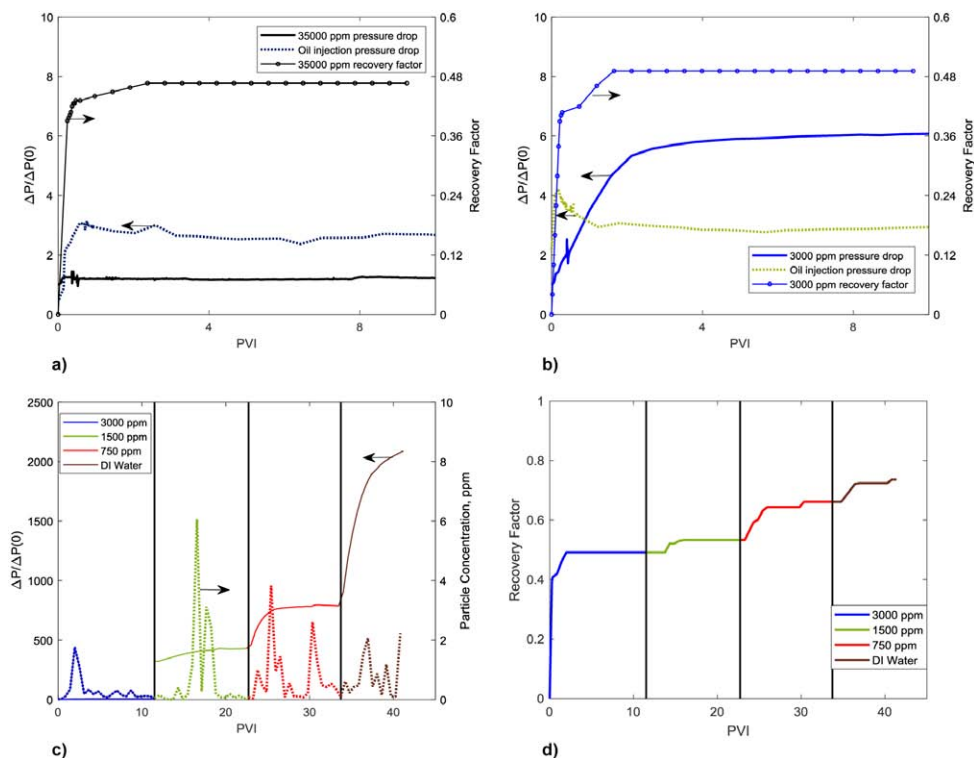


Figure 4—Berea A two phase coreflooding with piecewise decreasing salinity: a) HSW pressure drop and recovery factor, b) LSW pressure drop and recovery factor, c) tertiary LSW pressure drop and particle concentration, d) recovery factor during LSW.

Berea B and Berea C also showed restoration of initial conditions during both drainage processes as illustrated in Figs. 5 and 6. Berea B has S_{wi} of 0.08 for both the first and second drainages, respectively as the pressure drop stabilizes at 17 psi after 13 PVI. K_{rowi} is 0.94 for both displacements. Waterflooding of HS and LS to displace oil did not result in any difference in oil recovery (Figs. 5a and 5b), where S_{or} is 0.60 for each displacement. However, higher pressure drop is observed when injecting LS water due to detachment of clay particles. The pressure drop after injecting 3,000 ppm stabilizes at 155 psi which is 4 times higher than that of HSW. Tertiary LSW showed a reduction in S_{or} to 0.51 during DI water injection where the pressure drop is the highest due to the significant fines production.

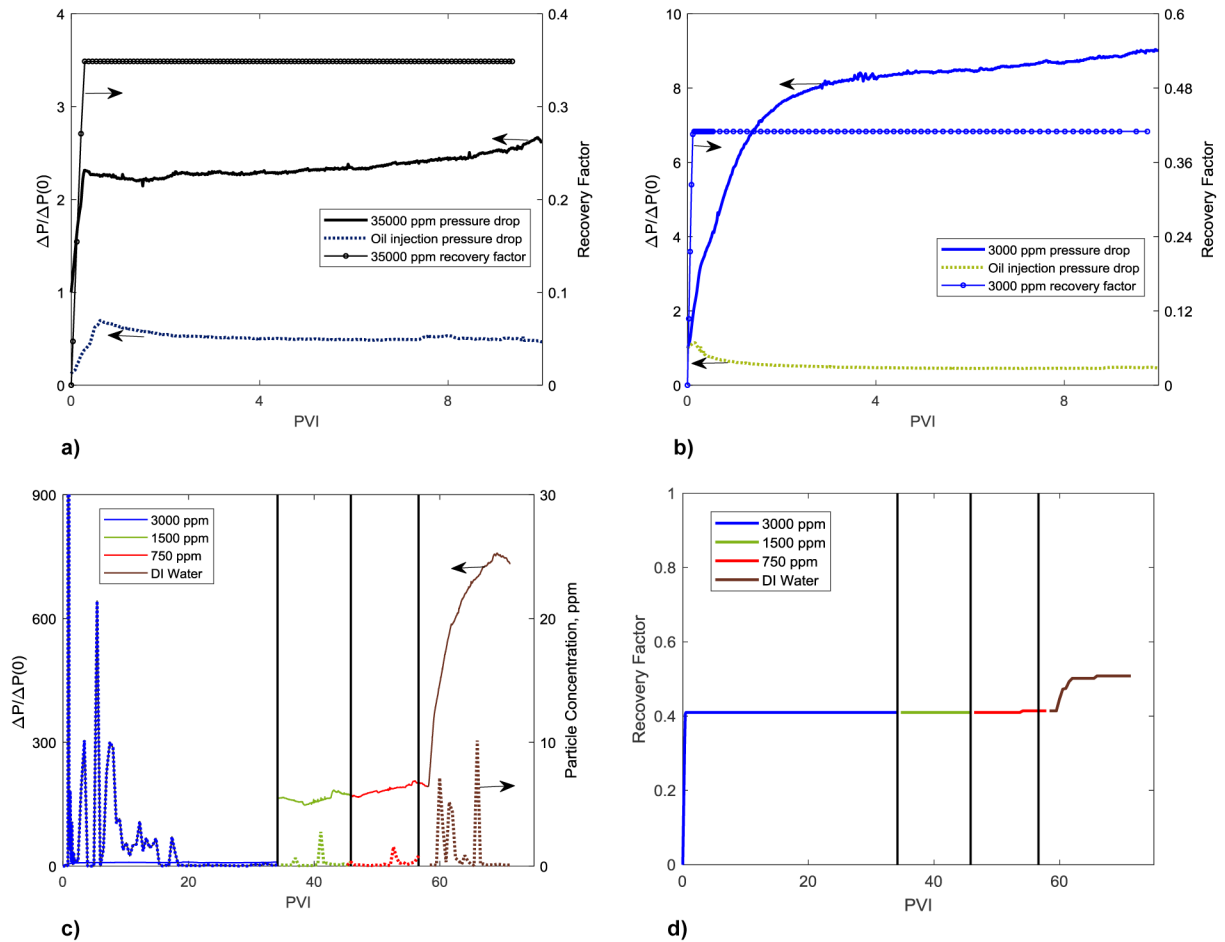


Figure 5—Berea B two phase coreflooding with piecewise decreasing salinity: a) HSW pressure drop and recovery factor, b) LSW pressure drop and recovery factor, c) tertiary LSW pressure drop and particle concentration, d) recovery factor during LSW.

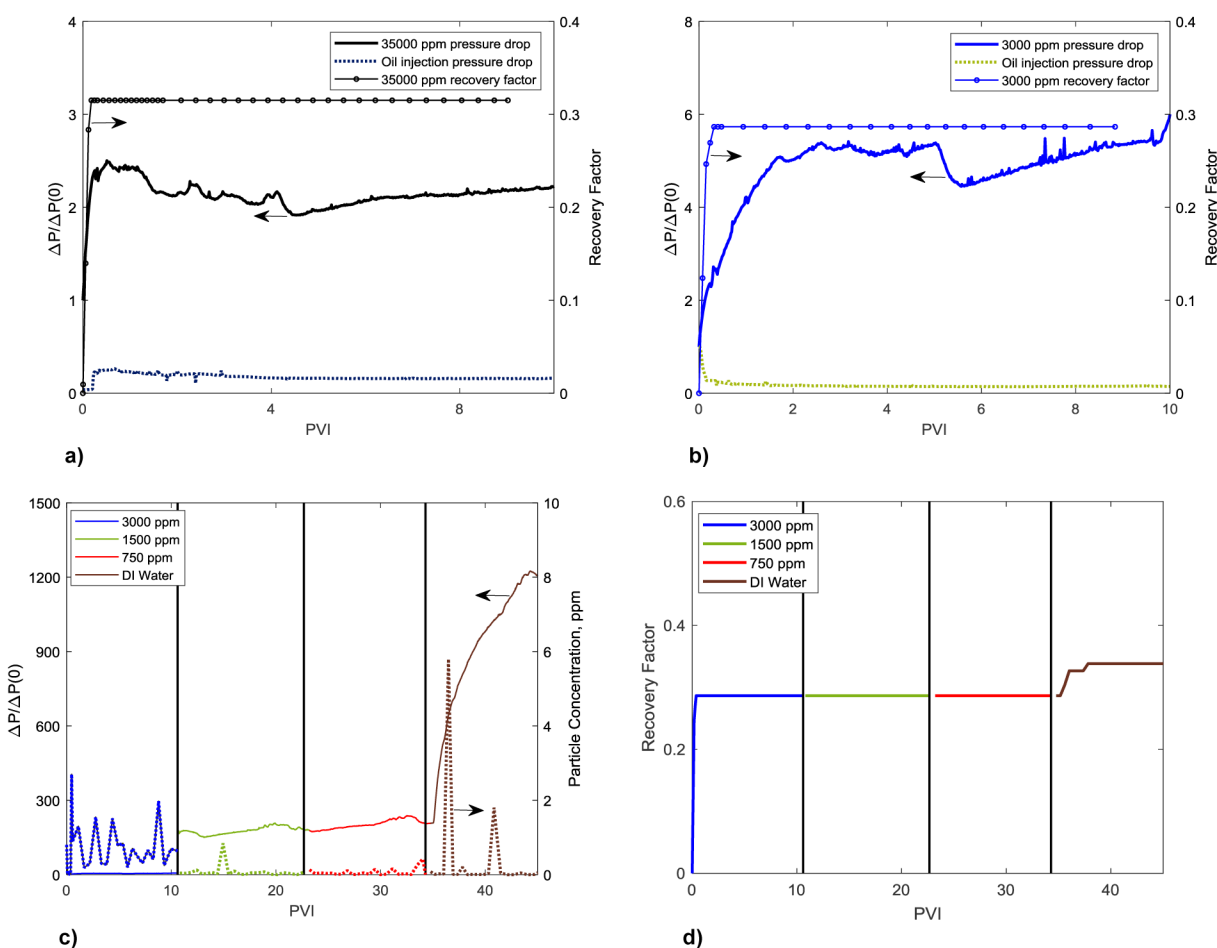


Figure 6—Berea C two phase coreflooding with piecewise decreasing salinity: a) HSW pressure drop and recovery factor, b) LSW pressure drop and recovery factor, c) tertiary LSW pressure drop and particle concentration, d) recovery factor during LSW.

Berea C shows similar results as sample Berea B. Drainage 1 and 2 have pressure stabilizes at ~ 9 psi, where S_{wi} is 0.23 and 0.22 for both displacements respectively. K_{rovi} is 0.27 and 0.30. HSW and LSW after drainage 1 and 2, respectively, show no change in oil recovery but a significant difference in pressure drop, as observed in Berea B results. The pressure drop stabilizes at 210 psi after 10 PVI during LSW, which is 3 times higher than that of HSW. Tertiary LSW shows higher pressure drop during all piecewise decreasing salinity stages. Fine particles are detected at the effluent samples of LSW which coincides with the high pressure drop. Extra oil production is also observed during DI water injection, where S_{or} decreased by 5 %.

Bentheimer samples: the single phase coreflood on the 6 cm Bentheimer core shows a stable permeability with HSW and all the LSW stages except DI water. The permeability decreased from 1,006 mD during HSW to 600 mD when the core was flooded with fresh water as shown in Fig. 7a. This reduction is ~ 200 times less than that observed in Berea cores. Table 1 shows that the clay concentration of kaolinite and illite in Bentheimer rocks is 1.7 and 1.8%, respectively, which is almost half the clay content of Berea rocks. The higher clay content in Berea samples caused more formation and permeability damage than in Bentheimer cores.

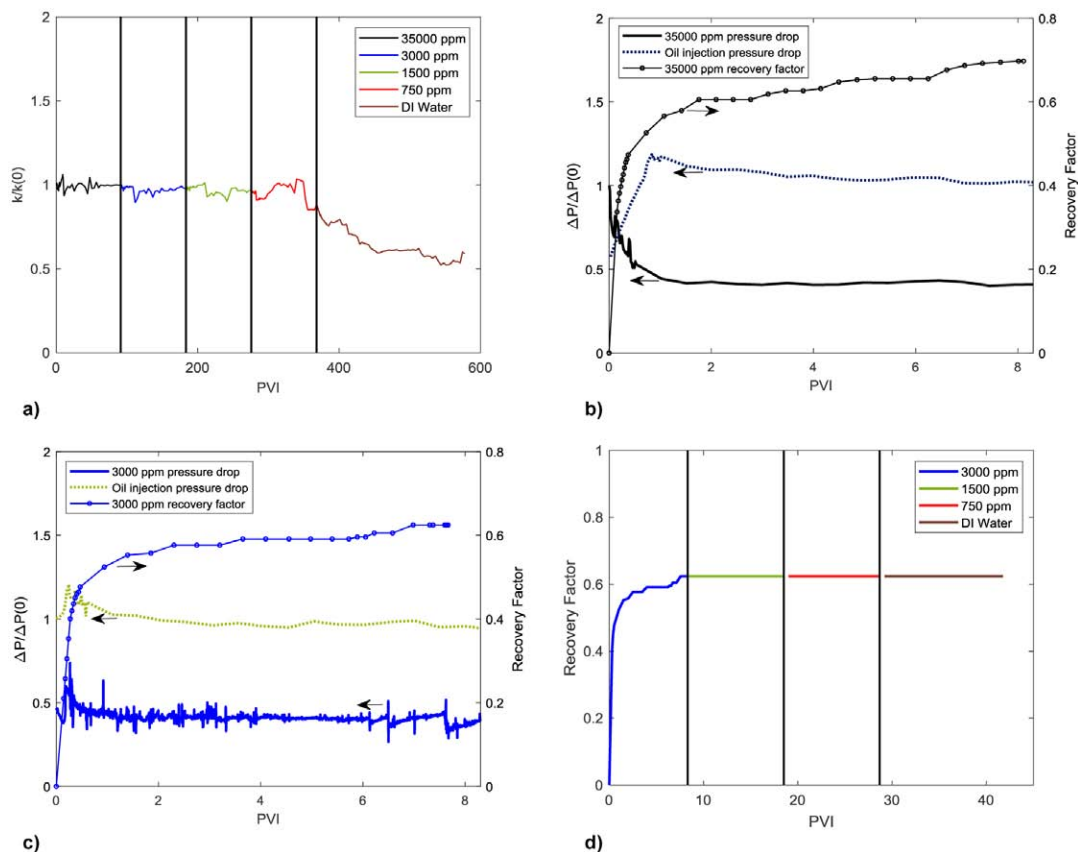


Figure 7—Bentheimer single and two phase corefloods with piecewise decreasing salinity: a) single phase permeability with HSW and LSW, b) HSW pressure drop and recovery factor, c) LSW pressure drop and recovery factor, d) recovery factor during LSW.

Table 2—Core samples' properties

	Berea A	Berea B	Berea C	Bentheimer
Permeability, mD	26	38.7	28	1,370
Porosity, %	18	18	18	23
K_{rwi} (1 st Drainage)	0.69	0.94	0.27	0.38
S_{wi} (1 st Drainage)	0.33	0.08	0.23	0.12
K_{ror} (0.6 M)	0.034	0.04	0.025	0.05
S_{or} (0.6 M)	0.43	0.60	0.56	0.41
K_{rwi} (2 nd Drainage)	0.62	0.94	0.30	0.39
S_{wi} (2 nd Drainage)	0.26	0.08	0.22	0.15
K_{ror} (0.05 M)	0.005	0.009	0.008	0.05
S_{or} (0.05 M)	0.41	0.60	0.55	0.38
K_{ror} (0.025 M)	0.004	0.008	0.009	0.05
S_{or} (0.025 M)	0.39	0.60	0.55	0.38
K_{ror} (0.01 M)	0.002	0.007	0.007	0.05
S_{or} (0.01 M)	0.30	0.60	0.55	0.38
K_{ror} (DI Water)	0.0009	0.002	0.001	0.05
S_{or} (DI Water)	0.25	0.51	0.51	0.38

Two phase coreflooding on the Bentheimer core shows no significant change in pressure drop nor oil production between HSW and all the stages of LSW as shown in Figs. 7b and 7c. Drainage 1 and 2 have similar initial water saturation of 0.12 and 0.15, respectively. The end point oil relative permeabilities are 0.38 and 0.39, respectively, where the pressure drop stabilized at ~ 2.5 psi. HSW and LSW have the same pressure behavior of increasing pressure drop before breakthrough and decreasing until stabilization after breakthrough. This shows no pressure increase during LSW as was observed in Berea samples due to fines migration. There is a small increase in oil recovery during LSW which is 3% more than that of HSW. This could be due to the low clay content in the core. The tertiary piecewise LSW shows no change in oil production and there is almost no change in pressure drop, unlike what was observed in Berea cores.

Clean sand samples: LSW was performed on the clay-free cores in two different sequential two-phase tests; stepwise decreasing salinity as in the Berea and Bentheimer cores as well as immediate DI water injection after the second drainage. HSW and LSW secondary imbibitions show no significant difference in oil production as shown in Fig. 8a. Tertiary LSW shows the same pressure drop for all salinities down to DI water and no extra oil has been detected (Fig. 8b).

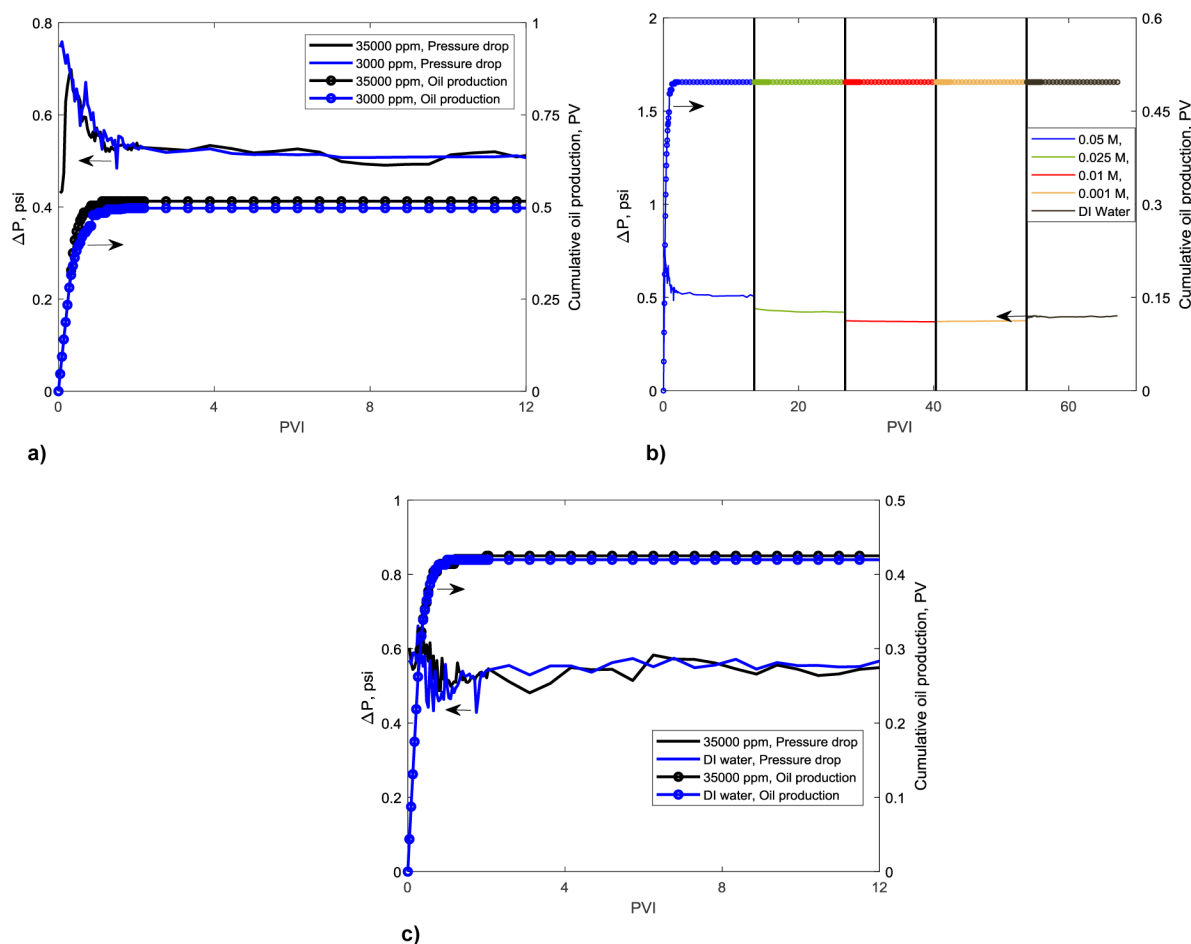


Figure 8—Unconsolidated cores two phase coreflooding with piecewise decreasing salinity: a) Unconsolidated core A secondary HSW and LSW pressure drop and oil production, b) Unconsolidated core A tertiary LSW pressure drop and oil production, c) Unconsolidated core B secondary HSW and DI water injection pressure drop and oil production.

Unconsolidated core B shows similar pressure drop behavior and no change in oil production for 35,000 ppm and DI water injections as presented in Fig. 8c. This shows that the presence of clay in the consolidated cores has a major role in fines migration and, hence, enhanced oil recovery.

Amott tests indicated that the Berea rocks are water-wet. The wettability index is calculated based on the following equation:

$$WI = \frac{V_{osp}}{V_{ot}} - \frac{V_{wsp}}{V_{wt}} \quad (1)$$

where V_{osp} is the volume of oil displaced spontaneously, V_{ot} is the total volume of oil displaced by imbibition and forced displacement, V_{wsp} is the volume of water displaced spontaneously, and V_{wt} is the total volume of water displaced by drainage and forced displacement. The WI is almost 1 for both HS and LS water tests (0.98 and 0.99, respectively), indicating the wettability had not changed in the cores during LS test due to the use of non-polar oil, which does not attach to the rock to create an oil-wet or mixed-wet surface.

Discussion

Microscopic flux diversion by size exclusion of mobilized particles during fines migration lead to residual oil saturation reduction. This effect can be observed as the permeability declines and fine particles are produced in the effluent when low salinity water is injected in the clay-rich cores. Therefore, the reduction in S_{or} seen in Berea core samples is due to microscopic flux diversion.

The single phase test on Berea shows a slow reduction of permeability with decreasing salinity from 35,000 ppm to 3,000 ppm as shown in Fig. 2a. Fines production is observed with the stepwise salinity decrease and it explains the permeability decline. When the core was flooded with 750 ppm, a drastic decrease in permeability is observed accompanied by significant particles production at the core outlet as shown in the high peak of particle production. The SEM-EDX analysis of the particles produced (Fig. 3) shows kaolinite and illite clays were produced from the core during low salinity waterflooding. This is due to the weakening of electrostatic attraction between clay particles and rock surface which leads to detachment and mobilization of the particles by the drag forces caused by the flowing water. The particles plug the thin pore throats (size exclusion) which reduces the permeability. The detachment of particles can cause permeability increase but the pore plugging has a tremendous effect to overcome this increase and hence results in reduction of permeability.

Fig. 2 also shows pH measurement for the single phase on the Berea core. The production of fines coincides with the change in pH and ionic strength. pH increases during 1 PVI for each low salinity brine concentration because Na^+ cations are desorbed from the negative clay sites and replaced with H^+ cations, which leads to abundance of OH^- anions and, therefore, pH rises. After 1 PVI, pH starts to drop due to the replacement of all the vacant negative clay sites by H^+ ions and also because of diffusion of connate water that has the low initial pH from dead-end pores. The detachment of clay particles exposes more negative sites for H^+ ions adsorption leading to an increase in pH.

The use of non-polar oil in the two phase tests ensures complete water-wetness of the rocks, which eliminates the possibility of wettability alteration mechanism to enhance oil recovery. The Amott tests confirm that by showing a wettability index close to 1 for all the salinity stages the experiments were performed on. Therefore, using non-polar oil separates the EOR fines migration mechanism from wettability alteration by capillary effects that can be seen when polar oil is used.

Two phase coreflooding in low-clay Bentheimer and clean sand cores prove the importance of the presence of clay to enhance oil recovery by fines migration. As the results of these tests show no change in pressure drop and, hence, no incremental oil recovery, microscopic flux diversion does not take place when low salinity water is injected. The change in residual oil vs salinity for consolidated cores is presented in Fig. 9a. It can be seen that as the salinity is reduced, S_{or} decreases. The low-clay Bentheimer core shows almost no change in S_{or} while the clay-rich cores show significant reduction in S_{or} with salinity drop. The water phase permeability decreases considerably as salinity is reduced and flux diverges to oil trapped thin pores. The water relative permeability for the Bentheimer core is similar for both HSW and LSW, unlike

for Berea cores. The reduction in permeability due to formation damage is given by the following formula (Bedrikovetsky et al. 2011, You et al. 2015):

$$k(\sigma) = \frac{k(0)}{1 + \beta\Delta\sigma} \tag{2}$$

where $k(\sigma)$ is the stabilized permeability due to formation damage by fines with concentration σ , $k(0)$ is the initial permeability, β is the formation damage coefficient, and $\Delta\sigma$ is the concentration of fine particles that are strained when salinity is dropped from high to lower salinities.

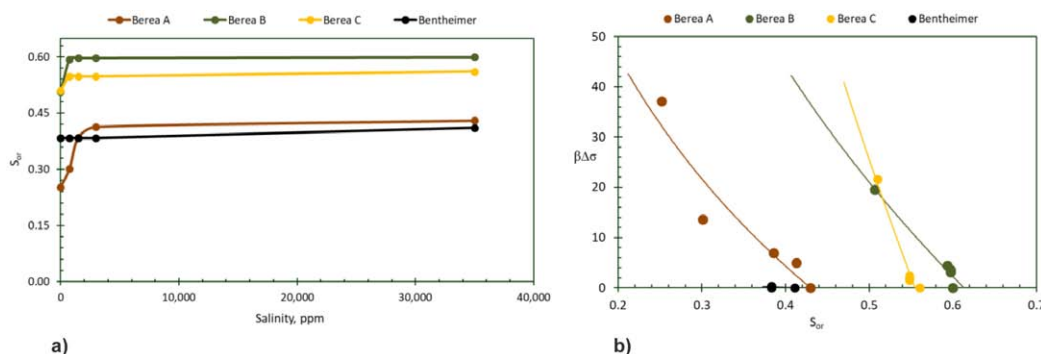


Figure 9—a) Effect of salinity on residual oil saturation, b) effect of formation damage on residual oil saturation.

From Fig. 9b, it can be seen that the higher the formation damage, $\beta\Delta\sigma$, the lower is the residual oil saturation. Higher formation damage means more fine particles are strained and, therefore, improved microscale sweep efficiency by flux diversion. Fig. 10 shows two cases in the porous media with HSW and LSW, where flux diversion takes place during low salinity brine injection. When the particles are still attached to the rock surface (HSW), the water flows through the preferential path (larger pore throat) as shown in Fig. 10a and oil droplets are trapped in thinner pores due to capillary forces. When the particles are detached and mobilized by the flowing water during LSW (Fig. 10b), they block the initial water channel forcing the flow to diverge to the thin pores where oil is trapped. As a result of viscous pressure exceeding capillary pressure, the residual oil droplet is displaced. Snap-off can also occur if the capillary forces are not overcome completely. The capillary number equation shows the ratio between viscous and capillary forces as following (Lake et al. 2014):

$$N_c = \frac{U\mu_w}{\sigma_{ow}} \tag{3}$$

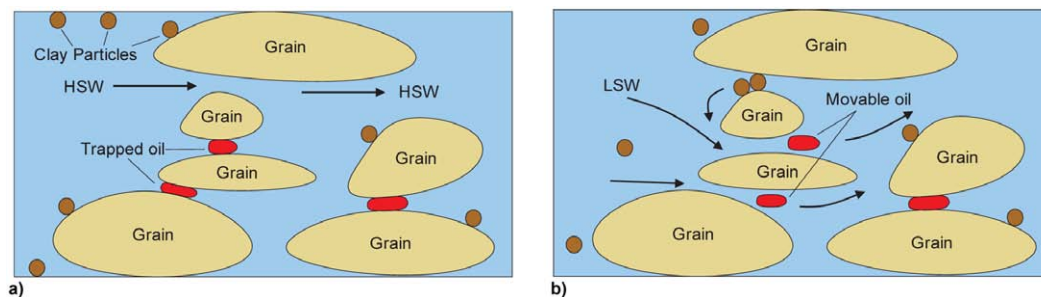


Figure 10—Microscopic flux diversion due to particles detachment: a) HSW, b) LSW.

Here U is flow velocity, μ_w is water viscosity, and σ_{ow} is the interfacial water between oil and water. Lake et al. (2014) shows that as the capillary number increases (increasing viscous forces), residual oil saturation

decreases in the capillary desaturation curve. The flux diversion seen in this study leads to higher viscous forces over capillary forces and, therefore, S_{or} decreases. The same mechanism is observed during polymer flooding, which is implemented to control water mobility (Wang et al. 2000, Hwang and Sharma 2018).

Conclusions

This paper presents a novel method of enhancing oil recovery by low salinity waterflooding via fines migration. Production of fine particles and permeability decline has shown to reduce residual oil saturation when the salinity of injection water is decreased in completely water wet cores. Separation of wettability alteration and fines migration as LSW mechanisms was successfully achieved in this study by the use of non-polar oil. This was determined by having the same wettability index of the rocks at different brine salinities.

Weakening of electrostatic forces caused by low salinity water injection leads to fines migration and straining in water flow pores, which promotes flux diversion at the micro-scale. This, in turn, results in the displacement of trapped oil ganglia, which enhances oil recovery. Water relative permeability decreases because of particle straining, which is the opposite of what has been observed in previous studies where no movable clay is present in the rock and the water relative permeability increases with low salinity waterflooding.

The clay content concentration is proportional to the reduction of residual oil saturation; the higher the movable clay content, the more oil is produced. This effect was proved by injecting low salinity water into low-clay and no-clay cores which showed no enhanced oil recovery.

Acknowledgments

The authors would like to thank Drs. Rouhi Farajzadeh and Hassan Mahani (Shell Research, Rijswijk) for the fruitful discussions about this work.

Nomenclature

k	permeability
$K_{r_{owi}}$	oil relative permeability at initial water saturation
$K_{r_{wor}}$	water relative permeability at residual oil saturation
S_{or}	residual oil saturation
S_{wc}	connate water saturation
S_{wi}	initial water saturation
V_{osp}	oil volume of spontaneous imbibition
$V_{o-forced}$	oil volume of forced imbibition
$V_{w-forced}$	water volume of forced drainage
V_{ot}	total oil volume of spontaneous and forced imbibition
V_{wsp}	water volume of spontaneous drainage
V_{wt}	total water volume of spontaneous and forced drainage

Greek letters

β	formation damage coefficient
σ	particle concentration
σ_{ow}	interfacial tension
$\Delta\sigma$	strained particles concentration

Abbreviations

DI	deionized water
----	-----------------

EOR	enhanced oil recovery
HS	high salinity water (35,000 ppm NaCl)
HSW	low salinity waterflooding
IS	ionic strength
LS	low salinity water (3,000 ppm NaCl)
LSW	low salinity waterflooding
PV	pore volume
PVI	pore volume injected
WI	wettability index

References

- Afekare, Dayo A., Mileva Radonjic. 2017. From Mineral Surfaces and Coreflood Experiments to Reservoir Implementations: Comprehensive Review of Low-Salinity Water Flooding (LSWF). *Energy & Fuels* **31** (12): 13043-13062.
- Al-Shalabi, Emad W., Kamy Sepehrnoori. 2016. A comprehensive review of low salinity/engineered water injections and their applications in sandstone and carbonate rocks. *Journal of Petroleum Science and Engineering* **139**: 137-161.
- Al Shalabi, Emad Waleed, Kamy Sepehrnoori, Mojdeh Delshad. 2014. Mechanisms behind low salinity water injection in carbonate reservoirs. *Fuel* **121**: 11-19.
- Austad, Tor, Alireza Rezaeidoust, Tina Puntervold. 2010. Chemical Mechanism of Low Salinity Water Flooding in Sandstone Reservoirs. Proc.
- Bedrikovetsky, Pavel, Fernando D Siqueira, Claudio A Furtado et al. 2011. Modified particle detachment model for colloidal transport in porous media. *Transport in porous media* **86** (2): 353-383.
- Bedrikovetsky, Pavel, Abbas Zeinijahromi, Fernando D Siqueira et al. 2012. Particle detachment under velocity alternation during suspension transport in porous media. *Transport in Porous Media* **91** (1): 173-197.
- Farajzadeh, Rouhi, Hua Guo, Julia van Winden et al. 2017. Cation exchange in the presence of oil in porous media. *ACS Earth and Space Chemistry* **1** (2): 101-112.
- Fogden, Andrew, Munish Kumar, Norman R. Morrow et al. 2011. Mobilization of Fine Particles during Flooding of Sandstones and Possible Relations to Enhanced Oil Recovery. *Energy & Fuels* **25** (4): 1605-1616.
- Hussain, F, A Zeinijahromi, P Bedrikovetsky et al. 2013. An experimental study of improved oil recovery through fines-assisted waterflooding. *Journal of Petroleum Science and Engineering* **109**: 187-197.
- Hwang, Jongsoo, Mukul M Sharma. 2018. Generation and filtration of O/W emulsions under near-wellbore flow conditions during produced water re-injection. *Journal of Petroleum Science and Engineering* **165**: 798-810.
- Lager, Arnaud, KJ Webb, CJJ Black et al. 2008. Low Salinity Oil Recovery-An Experimental Investigation. *Petrophysics* **49**.
- Lake, Larry W, Russell T Johns, William R Rossen et al. 2014. Fundamentals of enhanced oil recovery.
- Mahani, Hassan, Arsene L. Keya, Steffen Berg et al. 2015a. Driving Mechanism of Low Salinity Flooding in Carbonate Rocks. Proc.
- Mahani, Hassan, Arsene Levy Keya, Steffen Berg et al. 2015b. Insights into the Mechanism of Wettability Alteration by Low-Salinity Flooding (LSF) in Carbonates. *Energy & Fuels* **29** (3): 1352-1367.
- Morrow, Norman, Jill Buckley. 2011. Improved oil recovery by low-salinity waterflooding. *Journal of Petroleum Technology* **63** (05): 106-112.
- Muecke, Thomas W. 1979. Formation fines and factors controlling their movement in porous media. *Journal of petroleum technology* **31** (02): 144-150.
- Rezaei Doust, Alireza, Tina Puntervold, Tor Austad. 2011. Chemical Verification of the EOR Mechanism by Using Low Saline/Smart Water in Sandstone. *Energy & Fuels* **25** (5): 2151-2162.
- Sharma, MM, PR Filoco. 2000. Effect of brine salinity and crude-oil properties on oil recovery and residual saturations. *SPE Journal* **5** (03): 293-300.
- Sheng, J. J. 2014. Critical review of low-salinity waterflooding. *Journal of Petroleum Science and Engineering* **120**: 216-224.
- Tang, Guo-Qing, Norman R Morrow. 1999. Influence of brine composition and fines migration on crude oil/brine/rock interactions and oil recovery. *Journal of Petroleum Science and Engineering* **24** (2-4): 99-111.
- Wang, Demin, Jiecheng Cheng, Qingyan Yang et al. Viscous-elastic polymer can increase microscale displacement efficiency in cores. Society of Petroleum Engineers.
- You, Zhenjiang, Pavel Bedrikovetsky, Alexander Badalyan et al. 2015. Particle mobilization in porous media: temperature effects on competing electrostatic and drag forces. *Geophysical Research Letters* **42** (8): 2852-2860.

-
- Zeinjahromi, Abbas, Rouhi Farajzadeh, J Hans Bruining et al. 2016. Effect of fines migration on oil–water relative permeability during two-phase flow in porous media. *Fuel* **176**: 222-236.
- Zeinjahromi, Abbas, Thi Kim Phuong Nguyen, Pavel Bedrikovetsky. 2013. Mathematical model for fines-migration-assisted waterflooding with induced formation damage. *Spe Journal* **18** (03): 518-533.